Universita Karlova v Praze
Přírodovědecká fakulta

Studijní program: Imunologie

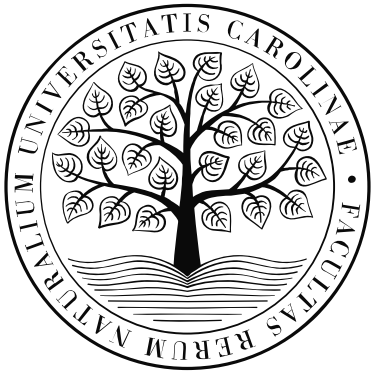

Mgr. Daniela Glatzová

The role of structural motifs in the localisation of T-cell plasma membrane proteins.

Vliv strukturních motivů na lokalizaci proteinů plazmatické membrány T lymfocytů.

Doktorská dizertační práce

Školitel:
Mgr. Marek Cebecauer, Ph.D.

Oddělení Biofyzikální chemie
Ústav fyzikální chemie, AV ČR

Praha, 2021

Prohlášení

Prohlašuji, že jsem dizertační práci vypracovala samostatně a že jsem uvedla všechny použité zdroje. Tuto práci, ani žádné její části, jsem nepoužila k získání jiného nebo stejného akademického titulu.

V Praze, dne 28.06.2021 Daniela Glatzová

Acknowledgement

I would like to thank to all the people who contributed to my Ph.D. I would like to acknowledge my supervisor Marek Cebecauer for supervising my work on the projects and the thesis. My special thanks also go to Tomáš Brdička, for his guidance and help and kind personal approach. Further, I would like to thank to my colleagues from both labs, especially Jarka Králová, Šimon Borna, Matěj Fabišík and Zuzka Kvíčalová for being also my very good friends and helping me to sail through my Ph.D. Last but not least I would like to thank to my friends and family for their support.

1. Contents

2. Abstract

Plasma membrane of T cells is abundant in diverse receptors and other molecules orchestrating immune responses. Numerous studies demonstrate that the localisation of proteins in the cell is non-random and that mislocalisation either in the context of plasma membrane at nanoscale or with respect to the cell interior can lead to the protein malfunction and subsequent aberrant T-cell response. In my first Ph.D. project we focused mainly on the role of the transmembrane domain length and amino acid composition, proximal sequences and the presence or absence of palmitoylation on the localisation of transmembrane adaptor proteins LAT, PAG and NTAL in T cells. We showed that plasma membrane localisation of PAG and NTAL is controlled by the amino acid composition of their TMD and is palmitoylation independent. We propose that NTAL localisation to the plasma membrane is, despite its suboptimal length, facilitated by the electrochemical asymmetry of its TMD. Among transmembrane adaptor proteins, LAT was the most interesting one. Dependency of LAT plasma membrane localisation on palmitoylation in combination with unusual amino acid composition of its TMD led us to investigate it in a separate project. My first author Ph.D. project was thus to elucidate the role of highly conserved helix-breaking amino acids, proline and glycine in the dynamics of LAT TMD and sorting to the plasma membrane. We found that the presence of central proline disrupts the α-helical structure of LAT TMD by inducing a kink and that the other proline and glycine amino acid residues have a role in overall helix properties. Exchange of helix-breaking amino acids for alanine or leucine led to the presence of these non-palmitoylatable LAT variants on the plasma membrane but surprisingly without capacity to support TCR-induced T-cell responses. Based on our data we hypothesised that palmitoylation of LAT is important for its proper nanoscopic localisation on the plasma membrane of T cells. Unfortunately, due to the changes in cellular morphology, we were unable to analyse the data from superresolution microscopy to further address this theory. The goal of my second co-author project was to investigate the importance of structural motifs for the proper membrane nanoscopic organisation of CD4 coreceptor. For the analysis of our superresolution data, we developed a model-free quantitative approach based on SOFI algorithm and discovered that plasma membrane organisation of CD4 relies on the presence of palmitoylation and its extracellular domain. This interested finding motivated us to further investigate the origin of those clusters. Using advanced algorithm which enabled us to map protein distribution in 3D nanometer resolution, we discovered, that CD4 coreceptor localizes to the tips of microvilli cells and that this localisation is driven by palmitoylation.

3. Abstrakt

Plasmatická membrána T buněk obsahuje různé druhy receptorů a dalších povrchových molekul nezbytných pro správnou imunitní odpověď. Mnoho studií ukázuje, že lokalizace proteinů v buňce není náhodná a jejich mislokalizace jak v rámci plasmatické mebrány, tak i v rámci nesprávného sortingu v rámci buňky, může vést ke špatné funkci proteinů a v důsledku tak i k nesprávné T buněčné odpovědi. V mém prvním Ph.D. projektu jsme se zaměřili na roli složení a délky transmembránové domény, jejích proximálních sekvencí a přítomnosti palmitoylace nebo extracelulární domény na lokalizaci transmembránových adaptorových molekul LAT, PAG a NTAL v T buňkách. Ukázali jsme, že v membránové lokalizaci PAGu a NTALu hraje roli jeho transmembránová doména a že je tato lokalizace nezávislá na palmitoylaci. Na základě našich pozorování tvrdíme, že je membránová lokalizace NTALu usnadněná asymetrií jeho transmembránové domény i přes to, že je její délka je suboptimální. Mezi zkoumanými adapterovými proteiny nás zaujal zejména LAT. Konkrétně kombinace závislosti jeho membánové lokalizace na přítomnosti palmitoylace s neobvyklým složením jeho transmembránové domény nás přivedla na myšlenku zpracovat toto téma v separátním projektu. Můj prvoautorský projekt se zabývá právě objasněním role vysoce konzervovaných prolinů a glycinu v transmembránové doméně LATu a jejich vlivu na helikální dynamiku a flexibilitu. Zjistili jsme, že centrální prolin způsobuje v α-helikální struktuře TMD LATu ohyb a také, že i zbývající prolin a také glycin mají roli v celkové dynamice TMD LATu. LAT mutovaný v těchto aminokyselinách byl schopný lokalizace na plasmatickou membránu T buněk i bez přítomnosti palmitoylace, mutantní proteiny však nedokázaly spustit aktivaci T buněk přes T receptor. Na základě těchto dat jsme došli k závěru, že palmitoylace je pravděpodobně důležitá pro lokalizování LATu do specifických membránových domén, nicméně jsme nebyli schopní tuto teorii ověřit. Cílem mého druhého Ph.D. projektu bylo ověřit důležitost strukturních motivů CD4 koreceptoru pro jeho nanoskopickou lokalizaci. Abychom byli schopní analysovat naše data, vyvinuli jsme robustní, na modelu nezávislý přístup založený na SOFI algoritmu. Zjistili jsme, že nativní nanoskopická lokalizace CD4 koreceptoru závisí především na jeho palmitoylačním stavu a také na přítomnosti jeho extracelulární domény. Tento jev jsme se rozhodli dále zkoumat pomocí pokročilého algoritmu, který je schopný mapovat distribuci proteinů v 3D rozlišení. Zjistili jsme, že CD4 lokalizuje na konce mikrovilů a že je tato lokalizace významně negativně ovlivněna absencí palmitoylace.

4. Introduction

Immune system protects organism from invading pathogens such as microbes and viruses. It also detects and eliminates damaged and tumour cells and distinguishes those from healthy cells and tissues to preserve the integrity of the body. The major cellular components of the immune response are leukocytes. The immune response is often a complex process involving several leukocyte subtypes, particularly granulocytes (neutrophils, eosinophils, and basophils), monocytes (macrophages and dendritic cells) and lymphocytes (T cells, B cells and NK cells). In general, the immune system can be divided into two basic categories, the innate immunity and the adaptive immunity. Innate immune system is immediate response to the pathogen or other non-physiological changes. It is non-specific and does not generate the long-term immunity. Adaptive immune system, on the other hand, provides organism with the capacity to recognize and remember specific pathogens throughout the life. This type of immunity is acquired through the life and it is highly specific to pathogens which has body encountered. It may take up to several days to its initiation. The adaptive immune response is also characterized by so-called immunological memory. B cells, important component of adaptive immunity, produce of antibodies, which bind to antigens and help to eliminate pathogens from the organism. The other important component of adaptive immunity are T cells. These cells are at the centre of my research and are, therefore, described in more detail in the following sections.

4.1. T cells

Lymphoid progenitors that develop from bone-marrow haematopoietic stem cells, migrate to the thymus to complete their maturation into functional T cells. The thymic microenvironment directs differentiation as well as positive and negative selection of thymocytes. Here, T cells develop their specific markers, including CD4/CD8 and other surface receptors and become antigen-specific. Each T cell clone has antigen-recognising T cell receptor (TCR) with unique specificity. Positive selection occurs when double positive ($CD4^+$ $CD8^+$) T cells bind cortical epithelial cells expressing class I or class II major histocompatibility complex (MHC) plus self-peptides with affinity high enough to initiate survival signal. Negative selection, on the other hand, occurs when double positive T cells bind to bone-marrow derived antigen presenting cells (APC) (macrophages and dendritic cells) expressing class I or class II MHC plus self-peptides with a high enough affinity to

receive an apoptotic signal. This process, called thymic T-cell development, gives rise to the peripheral pool of T cells, which mainly express αβ TCR. T cells expressing γδ TCR on their surface form only 1–10% of the pool and recognize non-peptidic antigens (Garcillan et al., 2015). The strength and quality of the signal transduced through the TCR has a key role in T cell development and differentiation since quantitative differences in antigen recognition can be translated into myriads of qualitative signalling responses. Moreover, each T cell clone is capable to recognize MHC containing an exogenous antigen in a pool of self-pMHCs with high specificity (Irvine et al., 2002; Singer et al., 2008).

4.2. TCR receptor triggering and downstream signalling

TCR is a polymorphic protein, the mature form of which is created by somatic DNA rearrangement and random chain pairing. TCRs are heterodimers formed by the subunits α and β joined by a disulphide bridge; each of them contains two extracellular immunoglobulin (Ig)-like domains, a single transmembrane domain (TMD) and a short intracellular tail that lacks any known structural or functional motifs. Matured αβ TCR on peripheral T-cells recognizes antigen in the form of a short peptide bound to MHC class I ($CD8^+$ T cells) or MHC class II molecules ($CD4^+$ T cells) on the surface of APCs. The αβ heterodimer forms a complex with the CD3 subunits (γ, δ, ε and ζ) for surface expression and function (Mariuzza et al., 2019). The intracellular tails of CD3 subunits contain 10 immunoreceptor tyrosine-based activation motifs (ITAMs) in total, which are involved in TCR-induced signalling. The TCR/CD3 complex lacks enzymatic activity. This distinguishes TCRs (and other immunoreceptors) from the receptors that directly stimulate downstream events upon binding to a ligand (e.g., receptor kinases). Although downstream signalling events are well studied, little is known about very early events, which are preceding CD3 phosphorylation. Besides ITAM motifs, cytoplasmic domains of CD3 molecules contain lipid-interacting basic rich sequences (CD3ε and CD3ζ) and a proline rich sequence (CD3ε). Mutation of basic-rich motif in CD3ε leads to impaired thymocyte differentiation and positive selection as well as limited peripheral T cell function, due to abnormal TCR surface level and signalling (Mingueneau et al., 2008; Martinez-Martin et al., 2009). It was shown previously that binding of TCR to the pMHC results in the exposure of cytoplasmic tails of CD3 molecules to the cytosol, most probably by their dissociation from the inner leaflet of the plasma membrane, making them accessible for phosphorylation (Aivazian et al., 2000; Xu et al., 2008; Guo et al., 2017; Shi et al., 2013; Gagnon et al., 2012).

Several mechanisms were proposed to explain the signal transduction through a plasma membrane (Mariuzza et al., 2019). Among these are force-induced conformational changes of TCR-CD3 complex (Das et al., 2015; Wu et al., 2019), pMHC-induced structural changes in the TMD of TCR (Lee et al., 2015; Brazin et al., 2018), pMHC-induced structural changes in CD3 cytoplasmic regions (Guo et al., 2017; Shi et al., 2013) and dynamically driven TCR allostery (Hawse et al., 2012). As these models are not mutually exclusive, it is probable that more of them act in synergy. During immune surveillance, T cells scan their environment, physically interact with and bind to many types of tissues, thus undergoing processes that can generate a wide range of mechanical stress over a wide range of forces (pN to nN). Presumably, αβ TCR acts as a mechanoreceptor where mechanical forces applied to TCR complex drive conformational change(s) in its structure and lead to a subsequent biochemical signalling. Direct evidence that the TCR acts as a mechanosensor was experimentally shown a decade ago with optical tweezer-based measurements that presented pMHC coated beads to TCRs on the surface of T cells. Simple binding without applying a force was insufficient for triggering, but tangential force led to T cell activation (Kim et al., 2009).

After antigen recognition by TCR, Src family kinase Lck is recruited by CD4/CD8 co-receptor to the proximity of TCR-CD3 complex to phosphorylate ITAM signalling motifs. Lck is anchored to the inner leaflet of the plasma membrane (PM) through myristoylation and palmitoylation (Palacios et al., 2004). CD45 is a pivotal phosphatase in TCR signalling that has an essential role in priming Lck for T cell activation (Koretzky et al., 1990). Phosphorylated ITAMs on CD3 chains function as docking sites for 70 kDa zeta-associated protein (ZAP-70), a Syk family kinase (Chan et al., 1992). For the full activation of ZAP-70, phosphorylation of a crucial tyrosine residue in the kinase domain is required. This phosphorylation event is probably catalysed by Lck and/or trans-auto-phosphorylation (Chan et al., 1995; Deindl et al., 2009). Activation of ZAP70 is followed by a cascade of phosphorylation events and subsequent T cell activation. Among the most important of the ZAP-70 targets are the transmembrane adapter protein linker for activation of T cells (LAT) and the cytosolic adapter protein src homology 2 (SH2) domain-containing leukocyte phosphoprotein of 76 kDa (SLP-76) (Zhang et al., 1998; Wardenburg et al., 1996). These two adapters form a core of a signalosome after TCR activation and are crucial for the organisation of downstream signalling (Figure 1.). Lack of SLP-76 leads to a near complete (SLP-76) and lack of LAT to a complete block of TCR signalling (Koretzky et al., 2006; Zhang et al., 1999). The proximal signalling complex results in the activation of several

signalling pathways including Ca2+ and DAG-induced responses, cytoskeletal rearrangements, and integrin activation. For example, processes associated with LAT signalosome lead to the activation of the small G protein Ras, through adaptors Grb2 and Sos. This event leads to activation of RAF/MAPK/ERK signalling followed by the activation of AP-1 transcription factor which contributes significantly to the regulation of interleukin-2 gene transcription during T-cell activation and may play a role in thymocyte development (Zhang et al., 1999). Another branch of this signalling pathway involves phospholipase-Cγ (PLCγ) activation by IL-2 inducible T-cell kinase (ITK) through GRB2-related adaptor protein (GADS). Activated PLCγ1 hydrolyses the membrane lipid PI(4,5)P2 (phosphatidylinositol 4,5 bisphosphate) to generate secondary messengers IP3 (inositol triphosphate) and DAG. These two messengers are essential for T cell function. IP3 induces intracellular calcium influx by opening calcium channels in the membrane of the endoplasmic reticulum (and subsequently calcium channels in the plasma membrane) (Lewis et al., 2001).

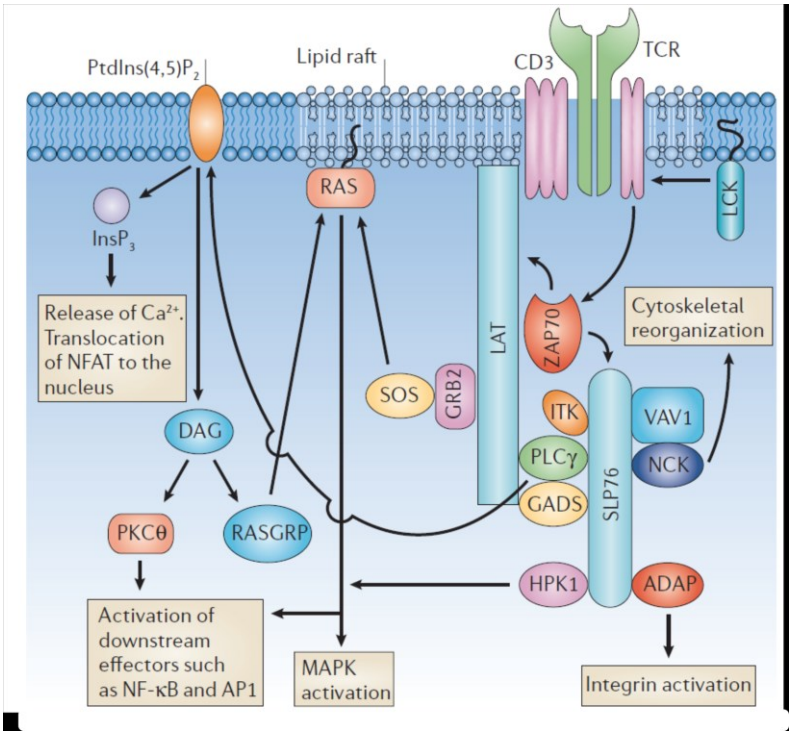

Increased intracellular calcium activates phosphatase calcineurin that dephosphorylates Nuclear factor of activated T cells (NF-AT) resulting in its nuclear translocation. NF-AT modulates T-cell immune response and synergizes with AP-1 transcription factor in regulation of transcription of several cytokine genes (Macian et al, 2005) (Figure 1.).

Figure 1. Basic scheme of TCR signalling. The scheme was adopted from (Koretzky et al., 2006)

4.3. Signalling molecules participating in T cell activation relevant for this Ph.D thesis

4.3.1. Co-receptors of TCR

The extracellular domains of both CD4 and CD8 interact with non-polymorphic parts of the MHC molecules (König et al. 1992; Salter et al., 1990). Due to sharing their ligand, CD4 and CD8 are often called as TCR co-receptors. They are essential for the proper T-cell development and thymic selection in vivo. These two co-receptors control the MHC specificity of selected thymocytes by limiting availability of Lck for TCR signalling in the absence of the ligand binding (Van Laethem et al. 2007, Van Laethem et al. 2013). In peripheral T cells, the expression of co-receptors is mutually exclusive. CD4+ T cells primarily provide help for B lymphocytes and innate immune cells during infections, whereas most CD8+ T cells exhibit cytotoxicity towards virally infected or tumour cells (Pennock et al. 2013). CD4 and CD8 co-receptors differ substantially in their structure. CD8 is an obligate dimer. It is homo- or heterodimeric type I transmembrane glycoprotein consisting of αα or αβ chains, which are covalently bound to each other (Terry et al., 1992; Gao et al. 1997). Both α and β chains are composed each of one N-terminal Ig-like domain connected by a long stalk to the TMD and a cytoplasmic tail. Lck binds to the CD8α cytoplasmic tail. Palmitoylation motif is in the juxtamembrane region on the CD8β chain (Leahy et al., 1995; Arcaro et al., 2001). CD8–MHC class I interactions have estimated K_Ds in a range from ∼10 μM (Wang et al., 2009) to ∼150 μM (Cole et al., 2008). In contrast to CD8 co-receptor, CD4 consist of single polypeptide chain with four extracellular Ig-like domains (D1-D4) connected to TMD and a cytoplasmic tail (Veillette et al., 1988; Yin et al., 2012). In the membrane-proximal part of the cytoplasmic domain, CD4 has a site for palmitoylation and, similarly to CD8α, there is a Lck-binding site in its cytoplasmic tail (Crise and Rose 1992; Fragoso et al., 2003). CD4 has also a binding site for IL-16 in the membrane-proximal D4 domain and a binding site for HIV envelope protein gp120 in the N-terminal D1 domain (Cruikshank et al., 1994; Wang et al., 2001). CD4 binds MHC class II with exceptionally low affinity compared to other leukocyte cell–cell recognition molecules. For the CD4–MHC classII interaction, *K*Ds have been estimated to range from ~200mM (for human CD4 binding to mouse MHC classII) to >2mM (for human CD4 binding to human MHC classII) (Xiong et al., 2001; Davis et al., 2003).

4.3.1.1. Role of CD4 co-receptor in T cell activation and function

As already mentioned, the first phosphorylation step of TCR-induced signal transduction is catalysed by Lck (and Fyn) kinase(s). One of the major roles of the CD4 co-receptor is to recruit Lck kinase to the TCR signalling complex. The interaction between CD4 and Lck regulates the sensitivity of T cells to the antigen (Erman et al., 2006, Stepanek et al., 2014), even though the interaction of TCRs with pMHCII is CD4-independent. In some cases, as in the presence of a very strong agonist or use of anti-TCR antibodies, T cells can be activated in the absence of CD4 (van der Merwe and Dushek 2011). However, CD4 is required for the recognition of most antigens in vivo (Vidal et al., 1999). The presence of the CD4 co-receptor enhances T cell sensitivity to antigens by 30- to 100-fold (Hampl et al. 1997; Madrenas et al. 1997) and reduces by approximately tenfold the number of antigenic peptides on APCs that are required for sustained TCR signalling (Li et al., 2004). CD4-TCR-pMCHII complex is usually depicted as one activation unit, yet its membrane organisation and the number of subunits being present at the beginning of the T cell activation is not yet known. Crystallographic studies of ternary complex of TCR, pMHCII and four extracellular domains of CD4 revealed a V-like arch formed when TCR and CD4 simultaneously bind the same pMHCII. This structure suggests that TCR binds to pMHCII as one arm of the arch and CD4 as the other one, while CD4-pMHCII form an apex of this structure (Yin et al., 2012). Two models of the CD4 co-receptor role in peripheral T cells seem to be relevant (reviewed in Glatzova and Cebecauer 2019). Firstly, CD4 interacts with its ligand in an antigen-independent manner so as to contribute to the contact between $CD4^+$ T cells and MHC class II-expressing cells (Janeway, 1992). Second, it interacts with pMHCII-TCR in an antigen-dependent manner so as to deliver Lck kinase to the complex and thus enhance T cell sensitivity (Artyomov et al., 2010). These two roles of CD4 do not have to be mutually exclusive. A direct role of CD4 in stabilising the TCR-pMHCII interaction is not supported by the community any longer.

4.3.2. Transmembrane adaptor proteins

Transmembrane adaptor proteins (TRAPs) are immune cell-specific adapters. They lack enzymatic activity and play a critical role in the signalosome assembly by connecting signal-transducing receptors with intracellular signalling pathways. TRAPs are usually single spanning membrane proteins with a short extracellular domain, a transmembrane segment followed by palmitoylation motif (CxxC) and a cytoplasmic tail containing several tyrosine

residues which can be phosphorylated by Src- or Syk-family kinases (Palacios et al., 2004). When phosphorylated, downstream signalling molecules (proteins with enzymatic activity or cytoplasmic adaptor proteins) bind to TRAPs and serve as docking sites for multiprotein complex assembly. TRAPs can be divided into three subgroups. First group include proteins directly associating with immunoreceptors like CD3 zeta chain linked to TCR, CD79 linked to BCR (B cell receptor) or DAP10 and DAP12 linked to the receptors involved in innate immunity (Weissman et al., 1986; Hombach et al., 1990; Lanier et al., 1998; role of DAP 10 and DAP12 reviewed in Lanier 2009). The three other TRAPs known to be involved in immunoreceptor signalling are TRIM (TCR-interacting molecule), SIT (SH2-domain-containing protein tyrosine phosphatase (SHP2)-interacting transmembrane adaptor protein) and LAX (linker for activation of X cells). They do not have the juxtamembrane palmitoylation motif. TRIM and SIT are structurally related transmembrane adaptors; both adapter proteins form disulphide-linked homodimers. It was found that they regulate TCR signalling and are influencing T-cell selection in the thymus (Kolsch et al., 2006; Simeoni et al., 2005; Kolsch et al., 2008). LAX on the other hand was identified as a negative regulator of T-cell signalling (Zhu et al., 2005). The role of these adapters in T-cell signalling was extensively reviewed in Horejsi et al., 2004. The last group comprise TRAPs, which do not associate directly with immunoreceptors. LIME (LCK-interacting membrane protein), PRR7 (proline rich 7), SCIMP (SLP adaptor and CSK interacting membrane protein) (Brdickova et al., 2003; Hrdinka et al., 2011; Draber et al., 2011), NTAL (non-T-cell activation linker), PAG (protein associated with glycosphingolipid-enriched microdomains) and LAT proteins belong to this group. NTAL is structurally and evolutionarily related to LAT but it is mainly expressed by B lymphocytes, natural killer (NK) cells, monocytes, and mast cells. It is palmitoylated on a juxtamembrane CxxC motif, contains eight conserved tyrosine-based signalling motifs but unlike LAT it cannot bind PLC-γ1 (Brdicka et al., 2002; Janssen et al., 2003). PAG is functionally distant from LAT and NTAL. Its tyrosine phosphorylation sites serve as a membrane anchor for Csk (C-terminal Src kinase) kinase, an important negative regulator of Src-family kinases. PAG thus acts as a negative regulator of immunoreceptor signalling (Brdicka et al., 2000).

4.3.2.1. Role of LAT in T-cell activation and function

LAT, as described previously, plays an essential role in the T-cell activation by providing a platform for signal transmission initiated by the TCR. Although LAT itself does not possess

any enzymatic activity, its role in TCR signal transduction is fundamental. Key molecules of the T-cell activation (e.g., Vav1, Sos, Grb2, PLCγ1) associate with phosphorylated tyrosine residues in its cytoplasmic tail in response to the TCR engagement (Zhang et al., 1998; Lin et al., 2001). Its role was firstly described in LAT-deficient Jurkat T cell line J.CaM2.5 (Finco et al., 1998). Crucial events necessary for T-cell activation were abolished, there was no calcium flux, ERK activation, AP-1/NFAT-directed gene transcription nor CD69 expression observed upon TCR stimulation (Finco et al., 1998; Zhang et al., 1999). Reintroduction of LAT to J.CaM2.5 cells rescued all these defects indicating that LAT is indispensable for T-cell activation via the TCR. Shortly after this discovery, targeted disruption of LAT gene in mice showed an early arrest in thymocyte development linked with a complete absence of mature peripheral αβ T cells (Finco et al., 1998; Zhang et al., 1999; Bacchelli et al., 2017).

4.3.3. CD45 phosphatase

CD45 is a tyrosine phosphatase expressed in all hematopoietic cells. It is characterized by expression of several isoforms, specific to a certain cell type and the developmental or activation status of the cell, generating the CD45RA, RB and RC isoforms, respectively (Oberdoerffer et al., 2008). Different CD45 isoforms vary in glycosylation patterns and size. CD45 molecule contains multiple sites for O-linked glycosylation close to the extracellular N-terminus and the reamining extracellular domain is heavily N-glycosylated. These complex N-glycans are necessary for CD45 stability and its transport to the cell surface (Pulido et al., 1992).

Intracellular domain of CD45 contains two tyrosine phosphatase domains (Stover et al., 1991; Desai et al., 1994). It is important for signal transduction through the T cell antigen receptor (TCR) by controlling the activation of the Src family protein-tyrosine kinase Lck. CD45 dephosphorylates Lck at its C-terminal negative regulatory tyrosine Y505, thereby inducing an opening conformation of the molecule and generating so-called ‘primed’ Lck (Koretzky et al., 1990; Sieh et al., 1993).

4.4. Spatiotemporal organization of signalling molecules on the surface of T cells

T cells are one of the most studied cell types regarding the role of membrane compartmentalisation. Plasma membrane of T cells is covered by signalling molecules

playing a role in their activation and their correct spatiotemporal localisation is thus crucial for correct immune response. Interaction between T cell and APC is organized in time and space by the formation of a specific structure called immune synapse (IS) where besides TCR-pMHC, numerous other co-receptor, co-stimulatory and inhibitory ligand pairs on both cell types are involved and unevenly distributed on the plasma membrane (Dustin et al., 2006). The classical definition of the IS is based on a cell-cell interface where a central supramolecular activation cluster (cSMAC) formed by TCR-pMHC is surrounded by a ring of adhesion molecules (LFA-1/ICAM-1) called a peripheral SMAC (pSMAC) (Monks et al., 1998; Grakoui et al., 1999). The formation of the cSMAC was first detected by live-cell imaging in T cell – APC conjugates (Monks et al., 1998). Later, Grakoui et al. used functionalised supported planar bilayers and shown that TCRs are engaged first in the periphery within 30 s from the first contact with a stimulatory surface and then these TCR clusters translocate to the centre of the IS to form the cSMAC within 5 min (Monks et al., 1998). The initial conception that the IS is formed as a stable structure to sustain signalling changed after the observation that a classical IS formation is missing when T cells are conjugated with dendritic cells loaded with physiological levels of antigen (Brossard et al., 2005). Moreover, the existence of TCR microclusters was revealed in stimulated T cells. Those microclusters were formed in the distal regions of the IS and moved centripetally to its centre. They represented the sites of signal initiation and were associated with essential signalling components such as Lck, Zap-70 and LAT and they excluded CD45 phosphatase (Yokosuka et al., 2005; Varma et al., 2006; Crites et al., 2014). Better understanding of spatio-temporal organisation of signalling events was achieved with new microscopy techniques (e.g. super-resolution imaging such as PALM (photoactivated localization microscopy) and STORM (stochastic optical reconstruction microscopy) (Betzig et al., 2006; Rust et al., 2006; Owen et al., 2010). Advances in microscopy techniques and image analysis in the last decade helped to reveal a complex spatiotemporal reorganisation of T-cell plasma membrane during the response to antigens. It was demonstrated that the TCR microclusters were pre-formed before the activation by an antigen, have an average size of tens of nanometres and that their numbers remain stable upon stimulation (Crites et al., 2014). For more details on advanced imaging see Methodological introduction

4.4.1. CD4 in the immunological synapse

Despite numerous studies, the role of CD4 in the IS formation and function was not resolved yet. Initial imaging experiments showed accumulation of CD4 in the cell-cell contact region between conjugated murine T-cell line and antigen presenting B-cell line (Kupfer et al., 1987). FRET analysis revealed that upon activation, CD4 was recruited to the IS, but not necessarily in an antigen-dependent manner (Zal et al., 2002). Their results suggested that it was the antigen-specific recruitment of the TCR and its close proximity to CD4 that initiated T cell activation, with CD4 playing a passive, supportive role instead of an active, dynamic role (Zal et al., 2002). Experiments in CD4 KO T cells showed delayed association of Lck with the synapse and reduced responsiveness of these cells to antigen (Holdorf et al., 2002). Live-cell imaging of conjugated cells uncovered that CD4 transiently accumulates in the centre of the IS but after a few minutes it moves to the periphery (Ehrlich et al., 2002). Moreover, it was shown that Lck kinase moves in a similar manner (Li et al., 2004). Co-clustering of CD4 and TCR was reported with the use of super-resolution microscopy. By dual-colour imaging, Roh and colleagues found that in unstimulated cells, CD4, TCR and Lck were localized in separate clusters with limited interactions at the interfaces. Upon T-cell activation, in both PALM and dSTORM experiments, they observed that TCR-CD3 and CD4 clusters remain segregated (Roh et al., 2015). Nevertheless, from published data we can conclude that CD4-Lck interactions play a significant role in the recruitment of Lck molecules into the IS between the T cell and APC to the proximity of TCR-CD3-MHCII complex, to enable its full activation and maximise the sensitivity of T cells towards weak antigens.

4.4.2. LAT in IS

Using PALM, the organization of the TCR and LAT was analysed in quiescent and activated native T cell plasma membrane sheets and live T cells. In quiescent T cells, both molecules existed in separate membrane domains and these domains concatenated after T cell activation (Lillemeier et al., 2010). Shermann and colleagues also observed separate pools of LAT and TCR. However, they identified mixed pools of LAT and TCR molecules prior to and following T cell activation (Shermann et al., 2011). They performed imaging of ZAP-70 with either TCRζ or LAT. They observed, that TCRζ and ZAP-70 showed very high colocalization consistent with the binding of ZAP-70 to phosphorylated TCRζ. In contrast, LAT and ZAP-70 were in spatially separated pools and they partially mixed with pools of LAT mixing with TCRζ. Shermann and colleagues called these intersections as „hot spots“ of activation, were

LAT is phosphorylated by ZAP-70 bound to TCRζ (Shermann et al., 2011). Interestingly, in their study, LAT clusters in activated cells were mixed with clusters of other TCR signalling proteins such as the PLCγ and the adaptors Grb2 and SLP-76. SLP-76 was arranged at the periphery of LAT clusters in an actin-dependent and LAT cluster size-dependent manner (Shermann et al., 2011). Recently, SMLM has been extended to 3D (Griffie et al., 2017). Interestingly it was shown that the increase in LAT clustering observed in 2D super-resolution imaging is partially from the recruitment of LAT vesicles to the IS from a deep intracellular pool, distinct from the membrane population (Griffie et al., 2017). This observation indicates importance of LAT vesicular trafficking in T cells. Trafficking of transmembrane proteins is tightly linked to their sorting in the intracellular membranes. As described in Results, I have studied structural elements, which affect LAT sorting in T cell membranes.

4.5. Determinants of protein sorting and localization within a cell

Eukaryotic cells are characteristic for their extensive intracellular membrane system which compartmentalizes diverse biochemical processes. Therefore, they need highly sophisticated system of sorting of proteins to their target membranes. Function of proteins is defined by their structure but their localisation within a cell is equally important. Protein mis-localisation can lead to a loss-of-function, resulting in cell malfunction and even development of diseases. Integral membrane proteins account for almost 30% of all proteins encoded by the human genome (Wallin et al., 1998; Fagerberg et al., 2010). They are synthesised at the endoplasmic reticulum (ER) and undergo sorting into target compartments such as the Golgi complex (GA), mitochondria or the plasma membrane to perform their function. The process is called membrane protein sorting. Number of determinants for intracellular targeting of membrane proteins have been identified. Short motifs within a primary sequence were found to firmly control sorting of proteins to some organelles. These include sequence motifs in cytosolic and luminal domains e.g. KDEL for the ER retainment (Munro et al., 1987), DxE for ER exit (Nishimura et al., 1997), YxxΦ motif to mediate sorting of transmembrane proteins to early endosomes (Sandoval et al., 1994) or nuclear export and import motifs NES and NLS (Wen et al., 1995; Gorlich et al., 1995). This wide variety of sorting signals is further extended by the fact that more than one determinant can define localisation of proteins in a cell. No universal signal or motif has been demonstrated for sorting of proteins to the plasma membrane. Nevertheless, it was published that post-translational protein modifications, such as N- and O-glycosylation of the extracellular domains of transmembrane proteins (Hendriks et al., 2004;

Xiang et al., 2013), ubiquitination (Azzo et al., 2005; Brignatz et al. 2005) and lipid modification like palmitoylation (Hundt et al., 2009; Chum et al. 2016; reviewed in Ernst et al., 2019) facilitate membrane transport of transmembrane proteins towards cell surface. There is also considerable interest in the possibility that local differences in the physical properties of membranes could contribute to the lateral segregation of proteins during sorting or signaling (Bretscher and Munro, 1993; Dukhovny et al., 2009; Ronchi et al., 2008; Simons and Ikonen, 1997). Recent paper published by Lorent et al., studied asymmetric lipid distribution between the bilayer leaflets. They showed that sfingomyelins were highly enriched on the outer leaflet, whereas most glycerophospholipids were exclusive to the cytoplasmic leaflet, excepting phosphatidylcholines, which were distributed equally between the two leaflets (Lorent et al., 2020). This assymmetry of PM is reflected in the assymmetry of the composition of most protein TMD (Sharpe et al., 2010). Moreover, it was published that physical properties such as the length and hydrophobicity of TMD can be important determinants for the plasma membrane sorting of many proteins due to the correlation between the length of their TMD and the thickness of the target membrane (Cosson et al., 2013; Sharpe et al., 2010).

4.5.1. Palmitoylation

Protein acylation regulates intracellular protein trafficking, subcellular organisation, protein-lipid and protein-protein interactions. These modifications, along with polybasic regions of the proteins, are known to be essential for their proper subcellular localization (reviewed in Resh 2006; Jack et al., 2009). Many proteins important for T-cell activation are modified by fatty acylation; for instance, TCR coreceptors CD4 and CD8, adapters LAT and PAG or Lck kinase (Resh, 2006; Bijlmakers, 2009). The latter is both myristoylated and palmitoylated but does not belong to transmembrane proteins. Acylation anchors Lck to the plasma membrane, which is indispensable for its proper function (Alland et al., 1994; Kabouridis et al., 1997; Yasuda et al., 2000). Myristoylation (N-myristoylation) and palmitoylation (S-acylation) are the most common types of fatty acylation. Protein N-myristoylation needs some kind of second signal to anchor protein stably to the membrane. It can be either second lipid modification, polybasic region or hydrophobic residues (Sigal et al., 1994; Hof and Resh, 1997; Williams 2003; Resh, 2006). Myristoylation of Fyn, another Src kinase important in T cell activation, is essential for its trafficking to plasma membrane and binding with ζ chain of TCR (Hof and Resh, 1999). Unlike myristoylation, palmitoylation is tightly regulated and reversible post-translational modification. Palmitoylation belongs to a subtype of fatty acid

modification called S-acylation, involving covalent attachment of 16-carbon palmitic acid to one or more cysteine residues of a protein through a thioester linkage. It was first identified by Schmidt and Schlesinger (Schmidt and Schlesinger 1979). The attached palmitate is removed when the thioester linkage is cleaved. Therefore, cycles of palmitoylation and de-palmitoylation can be precisely regulated and this reversibility allows dynamic regulation and fine-tuning of protein function and activities in leukocytes. It also promotes membrane-binding of cytosolic proteins and has a role in protein targeting, stability and activity (reviewed in Blaskovic et al., 2013). LAT mutant lacking palmitoylation is unable to sort to the plasma membrane and is retained in the intracellular compartments, mainly in the GA (Tanimura et al., 2006; Hundt et al., 2009). The recognition sequence for palmitoylation has not been defined yet. The sites of palmitoylation in transmembrane proteins are prevalently the cytosolic cysteine residues within CC or CxxC motifs adjacent to the transmembrane domain. Although more consensus sequences motifs were found in different types of proteins (Resh, 1996; Ren et al., 2008). It has been suggested that the anchors themselves contribute to the lateral organization of lipid-anchored proteins in the plasma membrane. Palmitoylation is also believed to target some transmembrane proteins to putative sphingolipid- and cholesterol-enriched membrane compartments called lipid rafts (Simons and Ikonen 1997; Zhang et al., 1998b; Melkonian et al., 1999; Canobbio et al., 2008; Lorent and Levental 2015). It was suggested that such membrane microdomains facilitate sequestering of signalling molecules and thus play a role in the activation of immunoreceptors (Yasuda et al., 2000; Shimada et al., 2005). However, the existence of such domains remains inconclusive (Sevcsik and Schutz 2015; Bernardino de la Serna et al., 2016).

4.5.2. Glycosylation

Glycosylation is the most common post-translational modification in eukaryotic cells and has been shown to play an important role in protein trafficking to specific membranes, prominently the apical membrane of epithelia (Vagin et al., 2008). It is a covalent attachment of glycans (carbohydrates) to proteins or lipids via nitrogen (N-glycosylation) or oxygen (O-glycosylation) linkages (Fiedler and Simons, 1995). Glycosylation enzymes operate predominantly in the ER and GA (Steen et al., 1998). N-linked glycans are attached to the majority of surface membrane proteins. They play a major role in protein folding and quality control of newly synthetized glycoproteins. They interact with the ER-resident lectins to ensure that only properly folded proteins exit the ER (Helenius, 1994; Bosques et al., 2004).

Glycosylation plays a role in the trafficking of proteins to membrane compartments. The lack of N-glycosylation could result in the ER retention and therefore trafficking to any cellular membrane (Duellman et al., 2015).

4.6. Methodological introduction

4.6.1. Super-resolution microscopy

A relative novelty of the super-resolution microscopy in biology inspired me to mention these methods, which were used in the two works described in Results. This is due to the fact that microclusters involved in T-cell activation are usually too small to be resolved by a conventional light microscopy. The invention of several super-resolution techniques surpassed the diffraction limit, improving spatial resolution in some cases by an order of magnitude. Application of these techniques in the field of plasma membrane biology and membrane microdomains shed a light on many biological processes and extended the study of membrane architecture to the nanometre scale (Huang et al., 2010). In these studies, mainly single-molecule localization microscopy (SMLM) techniques were used.

4.6.1.1. Single molecule-based localization microscopy

SMLM comprises methods that produce super-resolution images (maps) from locations of single molecules (Figure 2.). There are several methods based on temporal separation of fluorophore emission, e.g., by stochastic photoswitching as in PALM (Betzig et al., 2006), fluorescence PALM (FPALM) (Hess et al., 2006), STORM (Rust et al., 2006) and direct STORM (dSTORM) (Heilemann et al., 2009). SMLM techniques are performed with fluorophores that can be converted between a fluorescent (on state) and a dark (off state), that fluoresce at different wavelengths or use other tricks to control the molecule-of-interest between the fluorescence-accessible and inaccessible states. They share a strategy of imaging a limited number of isolated fluorescent molecules with a camera and fitting their images with the point spread function (PSF) to determine the precise localisation of the fluorophore (Patterson et al., 2010). The goal is to visualize a small number of well separated fluorophores in a single frame, however to collect a large number of frames for image reconstruction. One basic approach is that the fluorophores are kept in a non-fluorescent (dark) state most of the time using mild reducing buffer and are activated randomly with an excitation laser to become fluorescent. A readout laser stimulates fluorescence, which leads to photobleaching or the emitter photoswitches back to the dark state (Barr et al., 2017). Emitted photons are usually collected with an electron multiplying charge coupled device (EMCCD) or next-generation sCMOS (scientific complementary metal–oxide–semiconductor) cameras, which multiplies extremely weak signals, achieve high temporal resolution and fast signal acquisition with a

high signal-to-noise ratio to get the most information from the imaged sample (Long et al., 2012).

STORM was originally described as a method based on a Cy3-Cy5 pair of organic dyes, which are photoswitchable. With this setup a 633nm red laser was used to turn all Cy5 molecules to a dark (OFF) state. A 532nm green laser was then used to excite Cy3 dyes, which stochastically reactivated Cy5 molecules (Rust et al., 2006). Later, it was found that Cy5 dye can be photoswitched without an activator fluorophore and a variation of STORM, called dSTORM was proposed (Heilemann et al., 2008). Here, a fine oxidoreductive balance is used to keep the appropriate ratio of the fluorophores in the bright and dark states.

PALM is SMLM method, which uses the properties of photoactivatable (do not emit fluorescence without activation) or photoswitchable (after activation emit fluorescence with a different wavelength) fluorescent proteins for the localisation of individual molecules over many frames. These are expressed in the form of genetic fusion to a protein-of-interest

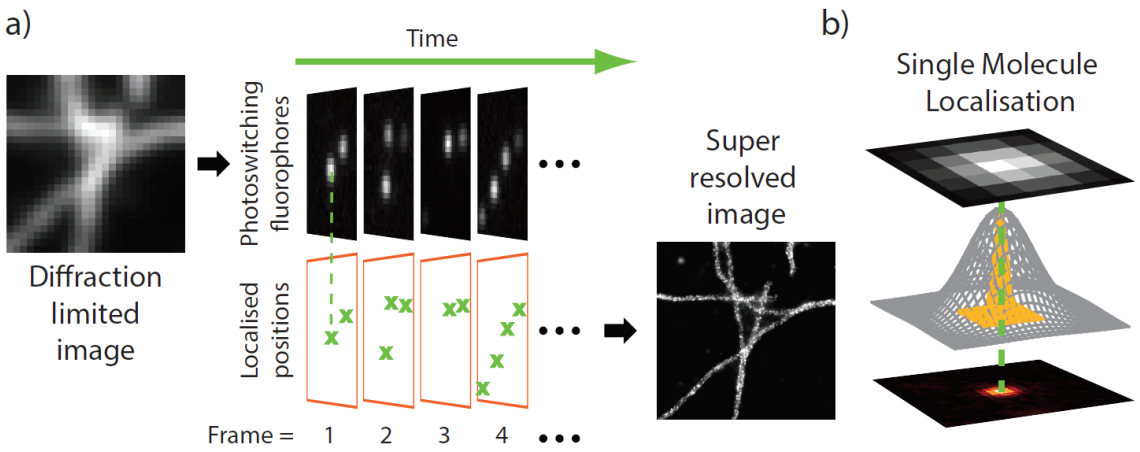

(Betzig et al., 2006).

Figure 2. Scheme of SMLM imaging. The scheme was adopted from (Patel et al., 2019)

4.6.1.2. Stochastic optical fluctuation imaging (SOFI)

SOFI also requires fluorophores that are cycling through two distinguishable states (organic dyes or fluorescent fusion proteins) (Dertinger et al., 2010). It is a post-processing method calculating super-resolved images from recorded image time series that is based on the temporal correlations of independently fluctuating fluorescent emitters. SOFI can be also used to analyse SMLM data, however, it performs better with much higher emitter densities, which means that it is a faster imaging method (Geissbuehler et al., 2011; Burgert et al, 2015).

4.6.1.3. Temporal, radial-aperture-based intensity estimation (TRABI)

TRABI a 3D SMLM method which can generate 3D localisation from acquired 2D microscopic data (Franke et al., 2016). This algorithm analyses emission pattern of a fluorophore and then extracts its z-dependent photometric parameters to improve axial localisation.

4.6.2. TIRF microscopy

The abovementioned methods are usually combined with total internal reflection (TIRF) microscopy when imaging structures and processes close to the plasma membrane) (van de Linde et al., 2011). In TIRF, the laser beam illuminates the sample under a high incident angle (called critical angle) that is completely reflected from the glass/water (sample) interface. It this setup, the reflection creates an evanescent wave that exponentially decreases with the depth of the sample and excites only fluorophores close to the optical interface (usually 100-200nm from the coverslip surface). It enables a significant reduction of the background fluorescence from the out-of-focus sample space (Axelrod, 1981).

5. Aims of the study

The aim of this Ph.D. thesis was to study the role of structural motifs on protein sorting, nanoscopic localisation and function.

- First project of my Ph.D. study was to characterize the impact of transmembrane domain (TMD) and proximal sequences on the localization and function of LAT and other transmembrane adaptor protein family members, PAG and NTAL, in T cells. We focused on how TMD length and amino acid composition impacts the requirement of palmitoylation for protein plasma membrane localisation.

- We based my first author project on the finding that only LAT surface expression depends on palmitoylation. We asked whether highly conserved helix-breaking amino acids, proline and glycine, modulate geometry and dynamics of the helical transmembrane segment of LAT and, thus, its sorting, nanoscopic plasma membrane organization and signalling capacity in T cells.

- In my side project, we investigated membrane organisation of CD4 at the surface of T cells at nanoscale and its dependence on diverse structural motifs found in this transmembrane receptor. The focus was on receptor microclusters and their origin in non-stimulated T cells.

- A part of this project was also to develop and experimentally evaluate robust, model-free and quantitative clustering and three-dimensional distribution algorithms using super-resolution microscopy techniques: super-resolution optical fluctuation imaging (SOFI) and single molecule localization microscopy (SMLM).

6. Results and discussion

6.1. Transmembrane domains in charge of protein sorting

Transmembrane adaptor proteins serve as plasma membrane docking sites for cytoplasmic signalling molecules, or as anchors of cytoskeletal components to the plasma membrane. TRAPs represent a group of TM proteins that are differentially expressed in a variety of hematopoietic cells and can influence immunoreceptor signalling either positively or negatively. For their function, they must be transported and localised to the plasma membrane (reviewed in Horejsi, 2004). Sorting of proteins to target membranes often involves the encoding of specific sequence motif in to the protein termed 'sorting signal'. Those are recognized by sorting machinery to compartmentalise proteins (Bonifacio et al., 2003). TRAPs are characterized by a short extracellular domain composed of only few amino acids, a single transmembrane domain and a cytoplasmic tail, which has no intrinsic enzymatic activity but possesses various tyrosine-containing motifs. Because TRAPs have no signal sequence nor extracellular domain, TMD length and amino acid composition is most likely a major factor regulating their sorting to the PM. In this study, we have investigated the impact of the TMD, its flanking sequences and palmitoylation on effective sorting of TRAP family proteins to the plasma membrane. We selected monomeric, single-spanning integral membrane proteins of TRAP family, namely LAT, PAG and NTAL. Using a panel of mutant proteins and quantitative live-cell imaging we revealed a complexity of determinants important for their plasma membrane sorting.

6.1.1. TM domain length as an important sorting determinant

Although cytosolic sorting determinants have received the most attention in the protein sorting field, there are numerous studies that have shown that TMDs also contribute to protein localisation and transport. In 1984, Mouritse and Bloom formulated the 'hydrophobic mismatch theory' which says that sorting is controlled by the correlation between the length of protein's TMD and the thickness of the target membrane (Mouritse and Bloom, 1984). They performed sequence analysis of transmembrane, Golgi resident proteins and realized that transmembrane domains of Golgi residents are on average 5 amino acid residues shorter than those of plasma membrane proteins (Bretscher and Munro, 1993). This theory was confirmed later in a bigger and more comprehensive study. Sharpe and colleagues analysed

the length of TMDs from all the major compartments of the eukaryotic secretory pathway and validated, that the TMD of plasma membrane proteins of both fungi and vertebrates are longer (usually 23 amino-acids long) than those from the proteins of internal membranes. Proteins with shorter TMDs remain in the Golgi apparatus or the ER (Sharpe et al., 2010). However, the applied algorithm which predicts localisation of membrane proteins based on amino acid sequence of their TMD (http://www.tmdsonline.org; page is not available anymore), predicted only three of our tested monomeric TRAPs to sort to the plasma membrane (LAT, PAG and SCIMP). The other three were predicted to localise in the ER (NTAL, LIME, PRR7) despite their known localisation to plasma membrane (Brdicka et al., 2002; Hur et al., 2003; Hrdinka et al., 2011). We selected three TRAPs (LAT, PAG and NTAL) for our study. These proteins can be palmitoylated. LAT and PAG have TMD of 23 amino acids. NTAL whasith suboptimal TMD composed of 19 amino acids (Fig. X). We confirmed their localisation at the plasma membrane by confocal microscopy. We assumed that other determinants, not considered by the prediction algorithm, might contribute to the plasma membrane localisation of these pTRAPs. It is worth to note, that this tool does not take post-translational modifications into account.

6.1.2. Palmitoylation is essential for plasma membrane localisation of LAT but not PAG and NTAL proteins.

Most proteins undergo chemical modification after their synthesis during their route through the intracellular processing machinery. As already described in the introductory part, one of those modifications, palmitoylation, is essential for TRAPs function (Stepanek et al., 2014) and is thought to be a targeting signal for sphingolipid- and cholesterol-enriched membrane microdomains called lipid rafts (Hořejší et al., 2010; Levental et al., 2010). Malfunction of unpalmitoylatable LAT was earlier demonstrated by immunofluorescence which revealed its mislocalisation to the intracellular membranes of human T cells (Hundt et al., 2009). We therefore decided to assess the importance of palmitoylation for the localisation of tested TRAPs. Colocalisation analysis with markers of the GA (Golgi7) and ER (Sec61) demonstrated that non-palmitoylated LAT remained localised to the GA membranes. Moreover, we treated LAT CS transfected cells with cycloheximide to determine whether reduced kinetics causes its mislocalisation. Instead of observing PM localisation after 4-6h of treatment, we rather observed degradation of the construct. LAT WT version PM localisation

was not affected by cycloheximide so we concluded that reduced kinetics was not the cause of LAT CS retention in intracellular membranes. We did not observe any effect of palmitoylation state on the localisation of NTAL despite its suboptimal TMD length. Sorting of unpalmitoylated PAG was also unaffected but we observed a lower viability of transfected cells. Cells transiently transfected with unpalmitoylated PAG tend to detach from the tissue culture plate and dye within a day post transfection. We did not observe such strongly reduced viability in Jurkat cells transfected with unpalmitoylated LAT (LAT CS) neither with unpalmitoylated NTAL (NTAL CS). To investigate the impact of TM domains and distinguish it from the other parts of proteins, we generated truncated versions of LAT (LAT dCT) and PAG (PAG dCT) missing the intracellular domain (LAT: Δ34−262 residues; PAG: Δ44–432 residues) both in palmitoylated and non-palmitoylated versions. We compared their cellular localisation to their WT counterparts. Localisation of mutant variants missing intracellular part showed that TMD itself with palmitoylation was sufficient for PM localisation. Plasma membrane localisation efficiency of non-palmitoylated LAT lacking the intracellular domain (LAT dCT CS) was comparable to the negative control represented by ER marker Sec61, it was retained in the ER membranes. PAG deprived of its intracellular domain (PAG dCT) unexpectedly sorted to the PM even though in reduced amount than its WT form. However, palmitoylated and non-palmitoylated variants of PAG dCT exhibited comparable distribution between the ER and plasma membrane, confirming that palmitoylation does not influence sorting of PAG to the plasma membrane and most probably, its TMD amino acid composition or/and its flanking sequences play an essential role in sorting of this protein.

6.1.2.1. Presence of CD4 extracellular domain reduces the impact of missing palmitoylation on LAT

Glycosylated extracellular domain is known to facilitate sorting of proteins to the PM (Böer et al., 2000; Hendricks et al., 2004). It was also shown that adding N-glycosylation motif to sequence of proteins, originally residing on the basolateral membrane caused its redistribution to the apical membrane in polarised cells (Benting et al., 1999; Bulbarelli et al., 2002). Because TRAPs belong to the group of membrane proteins which do not possess any glycosylated extracellular domain, we were speculating if its addition could promote PM localisation. We therefore fused LAT variants (lacking the palmitoylation motif and/or

cytoplasmic domain) to the large, strongly glycosylated extracellular domain of CD4 co-receptor, to verify the impact of glycosylation on TRAP protein sorting. With live-cell confocal imaging, we confirm that the attachment of the CD4 extracellular domain rescued localisation to the PM of both non-palmitoylatable LAT variants (CD4ex LATCS and CD4ex LAT dCT CS). These data demonstrate, that glycosylated extracellular domain is one of the dominant sorting signals and that it has a role in protein sorting not only in polarised cells.

6.1.3. Importance of TMD length and asymmetry for plasma membrane sorting of proteins

We wanted to further address the theory about the importance of TMD length and asymmetry for PM sorting of proteins proposed by the group of Prof. Sean Munro (Bretscher and Munro, 1993; Sharpe et al., 2010). In addition to statistical analysis of membrane proteins, Munro also performed several direct experiments. Replacing artificial TMD 23 amino acids long which localised to PM with TMD of 17 amino acids resulted in accumulation of the protein in the GA (Munro, 1995). He also shown earlier in his work with sialyl transferase, that it was retained in the Golgi apparatus even when its 17 residue TMD was replaced by 17 leucines. However, when he prolonged TMD to 23 leucines, it localised to PM (Munro, 1991). We unsuccessfully tried to simulate such experiment and rescue the plasma membrane sorting of LAT CS by expanding its TMD with six amino acids (six leucine residues or PILAML sequence), however we did not succeed. To test this hypothesis and further investigate the role of TMD flanking sequences in protein sorting, we decided to design model TRAP-like proteins containing artificial TMDs of differents length composed of leucines with tryptophans and lysines as flanking residues at the membrane-water interface and the intracellular domain (Figure 3.). We were inspired by TMD peptide LW21 used in vitro as a model transmembrane peptide in a number of biophysical studies (Fastenberg et al., 2003; Kaiser et al., 2011; Machan et al., 2014). Our TRAP-like designed proteins share overall topological similarity to the TRAP family proteins (very short extracellular domain, a single transmembrane domain and an intracellular domain lacking enzymatic function). We discovered that artificial TRAP-like LW25 with the optimal TMD length of 25 residues localised to the PM. Suboptimal TRAP LW19 version accumulated in GA and ER with no visible PM localisation. However, the sequence of TRAP LW19 was rather symmetric with lysine residues in both flanking sequences. It is known that TMDs of plasma membrane

proteins exhibit an asymmetric distribution of amino-acids along the α-helix, compared to the TMDs of ER proteins which do not display such asymmetry (Lorent et al., 2020). We therefore decided to generate asymmetric variant of LW19 (LW19asym) changing flanking lysine residues in the extracellular portion of TMD with glutamic acid. When we transiently transfected this variant to cells, we observed increase in the PM localisation of LW19(Asym). Interestingly, even when we deprived LW19asym version of the intracellular domain (LW19asym-ΔCT), it still exhibited detectable PM localisation in about 20% of inspected cells. Interestingly, incorporation of CVHC palmitoylation motif to the sequence of this mutant (LAT LW19asymCVHC ΔCT) improved its PM localisation to surface expression level comparable to native LAT. These data demonstrate the importance of electrostatic asymmetry for the PM sorting of proteins with suboptimal TMDs. Since TRAP-like LW19asym variant was able to sort to the PM, we tested whether this TMD could rescue PM targeting of non-palmitoylated LAT. Interestingly, the exchange of the TMD sequence of LAT protein for asymmetric LW19 sequence led to its sorting to the PM even in the absence

Protein	TMD sequence plus flanking residues*	Mean hydrophobicity‡
LAT	**EEAILVPCVLGLLLLPILAMLMALCVHCHRLP**	5
PAG	**GQMQITLWGSLAAVAIFFVITFLIFLCSSCDREK**	5
NTAL	**SSGTELLWPGAALLVLLGVAASLCVRCSRP**	4
LW19(Sym)	GLLDPKK**WWLLLLLLLLALLLLLLLL**KKFSRS	9
LW19(Asym)	GLLDPEE**WWLLLLLLLLALLLLLLLL**KKFSRS	9
LW21(Sym)	GLLDPKK**WWLLLLLLLLALLLLLLLLWW**KKFSRS	ND
LW25(Sym)	GLLDPKK**WWLLLLLLLLLLALLLLLLLLLLL**KKFSRS	9.3
LW25(Asym)	GLLDPEE**WWLLLLLLLLLLALLLLLLLLLLL**KKFSRS	9.3
LAT-LW19(Asym)	DLGTEE**WWLLLLLLLLLLALLLLLLLLLL**KKGSYD	9
LAT-LW19(Asym$_{CVHC}$)	DLGTEE**WWLLLLLLLLLLALLLLLLLLLL**CVHCHR	9
LAT-LW19(Asym$_{SVHS}$)	DLGTEE**WWLLLLLLLLLLALLLLLLLLLL**SVHSHR	9

*Hydrophobic stretch is highlighted in bold. Putative palmitoylation sites (cysteines) are underlined.
‡Mean hydrophobicity of the hydrophobic stretch (bold) was calculated using HydroMCalc algorithm (Tossi et al., 2002). Hydrophobicity scale is –10 to +10. An average value calculated for randomly selected 20 amino acids is ~–3. ND, not determined.

of the palmitoylation. In summary we observed that PM localisation of proteins is primarily determined by their TMD sequence and that additional signals, such as palmitoylation can increase sorting efficiency.

Figure 3. Sequences of TMDs of TRAP and TRAP-like proteins tested in this study

6.2. Unusual TMD of LAT

In previous paper, we demonstrated that the TMD of LAT determines its sorting to the plasma membrane (Chum et al., 2016). We therefore took a closer look on its amino acid composition. In vertebrates, the structure of TMD is almost exclusively formed by an α-helix with non-random position of amino acids. There are aliphatic amino acids (Leu, Val, Ala, Ile)

in the helix hydrophobic core (Sharpe et al., 2010). Distribution of charged amino acids (Lys, Arg, His) along the α-helix is asymmetric, occurring more frequently on the cytoplasmic end of the domain. This was defined as so called ‚positive-inside rule' (von Heijne 1992; Baker et al., 2017). LAT TMD contains two higly conserved prolines and one glycine residue with biophysical properties, which can affect the geometry and dynamics of TMDs.

6.2.1. Known role of proline and glycine residues in protein structure

Proline and glycine were reported as helix-breaking residues having important role in protein dynamics (Eilers et al., 2000). In LAT, one proline residue is positioned centrally (Pro^{17}) and the other one close to the luminal end of its TMD (Pro^{8}). Glycine (Gly^{12}) is also situated in the luminal part of the LAT TMD, in the position i + 4 with respect to Pro8 and i - 5 with respect to Pro^{17}. We therefore hypothesised that Pro^{8}, Gly^{12} and Pro^{17} residues can play a role in membrane stability and sorting of LAT to the PM. Proline has been found to occur with relatively high frequency in α-helical TM segments of many integral membrane proteins that function as receptor subunits or transporters (Brandl & Deber, 1986). The cyclic structure of proline makes it unique among the 20 natural amino acids because its amide group lacks the proton necessary for the hydrogen bond which is required for the stabilisation of the α-helix or the β-sheet structure (Polinski et al., 1992; Bywater et al., 2001). Bright & Sansom simulated 24 different sequence motifs involving proline and glycine pairings in a polyalanine backbone helix and they found that a proline is necessary to introduce pronounced bend/kink-swivel motions in the peptide, acting as an effective "molecular hinge" that decouples the upstream- and downstream-proline portions of the helix (Bright & Sansom, 2003). Glycine, due its size and torsional flexibility, is also believed to have a role in the flexibility of helices. These properties depend also on the local environment (Li & Deber, 1992). Glycine may also play an important role in the interhelical packing of membrane proteins (Javadpour et al., 1999; Eilers et al., 2000), it was reported that its positioning close to the proline (GxxP or GxP motifs) enhances local dynamics of the helix and can affect the function of transmembrane peptides or proteins (Jacob et al. 1999).

6.2.2. LAT TMD conformation in model lipid membrane

To investigate a potential existence of a kink in LAT TMD, we decided to perform all-atom molecular dynamics (MD) simulations in model lipid membranes. All-atom MD simulations allow to study a motion of a protein within a lipid bilayer in time and thus putative conformational changes can be uncovered. We were particularly interested in the impact of

Pro^{8}, Gly^{12} and Pro^{17} residues in LAT TMD structure. Interestingly, a kink could be observed in the central part of the α-helix of native LAT TMD around the position of Leu^{14}. This is in agreement with previously observed kinks induced by proline (or glycine) where maximal impact was reported for positions i – 3 or i-4 with respect to the proline residue (Kumar & Bansal 1998; Richardson et al., 1984). Another smaller deviation in the α-helical structure was observed near Pro^{8} residue. To reveal the origin of the kink and to characterise the behaviour of prolines and glycine, we separately simulated their mutated versions. Pro^{8} and Pro^{17} were changed to alanine (P8A and P17A, respectively) and Gly^{12} was changed to leucine (G12L). Mutation of glycine to leucine was chosen with respect to its surrounding environment by several leucine residues. P17A mutation led to complete disappearance of the kink for the full period of the simulation, which confirmed our assumption that Pro^{17} caused the helix distortion. No effect on the central kink was observed for the second proline mutant P8A as well as for the mutant G12L. Nevertheless, mutants P8A and G12L indicated shortening of the helical TM segment. The helix of P8A mutant was two residues shorter and helix of G12L mutant was 3 residues shorter compared to simulated LAT WT peptide. No such shortening was observed for P17A mutant. This result suggests that even though only Pro^{17} is critical for the formation of the kink in the LAT TMD, Pro^{8} and Gly^{12} influence its structure as well.

6.2.3. Mutations promote sorting of non-palmitoylated LAT to the PM

Imaging of proline and glycine mutants in LAT-deficient cells (J.Cam2.5) did not show any visible phenotype. All mutant proteins exhibited PM distribution with partial trapping in the GA which is comparable to the distribution native LAT protein (Bonello et al., 2004; Balagopalan et al., 2018). To investigate functional impact of LAT mutants, we analysed intracellular calcium mobilisation of transiently transfected J.Cam2.5 cells after activation with antibody. It is known, that LAT is indispensable in T cell activation through TCR (Zhang et al., 1998). We observed about three-fold increase in Ca^{2+} flux in LAT helix-breaking mutants one minute after the antibody stimulation which was comparable to the activation of J.Cam2.5 cells reconstituted with LAT WT. We thus concluded that mutation of helix breaking residues does not affect function of LAT in T cells. We were further interested if mutating helix-breaking amino acids will have an impact on the PM sorting of LAT in the absence of palmitoylation. Strikingly, mutation of helix-breaking amino acids to alanine or

leucine in unpalmitoylatable LAT (P8A CS, P17A CS and G12L CS) partially restored PM localisation in 30–50% of inspected cells. This effect was visible the most in P17A CS mutant. It is worth to note, that PM localisation of mutants was the strongest about 18h after transient transfection in all variants and continually decreased in time. The reason was probably instability or toxicity of the mutants at the PM because cells transfected with non-palmitoylatable LAT mutants showed decreased viability in comparison to their palmitoylated variants. Apart from PM localisation, all unpalmitoylatable helix breaker mutants were also observed to localise to the intracellular membrane compartments (mainly ER and GA), similarly to the LAT CS mutant. PM localisation of unpalmitoyatable mutants was particularly interesting finding because up to now it was assumed that the reason of unpalmitoylatable LAT malfunction is its separation from TCR signalling molecules due to its absence from PM. On that account we analysed the response of J.CaM2.5 cells expressing non-palmitoylatable mutants to TCR antibody stimulation in. Interestingly, regardless of the mutations in the LAT TM domain, no calcium mobilisation was observed. Those results indicate, that surface expression is not sufficient for LAT function in antibody-induced T-cell signalling.

It was published that T cells deficient in adaptor protein Gads (that links SLP-76 to LAT), exhibit suppressed PLC-γ1 mediated responses because of the deficient recruitment of PLC-γ1 to LAT microclusters (Bilal et al., 2015). Apparently, absence of palmitoylation targets LAT WT outside of signalling microdomains in the context of PM decreasing its accessibility for signalling molecules critical for TCR activation. To further examine this interesting observation, we transfected J.Cam2.5 with LAT and LAT CS mutant with attached CD4 extracellular domain (CD4ex-LAT and CD4ex-LAT-CS), which we found to localise to the PM (Chum et al., 2016) and tested the response of those mutants to antibody stimulation. Surprisingly, we observed a significant increase in calcium signalling in cells with non-palmitoylatable CD4ex-LAT-CS variant although the increase in calcium mobilisation was not full in comparison to the response of cells with palmitoylated LAT variants. We thus hypothesised, that CD4 extracellular domain localises LAT CS to membrane compartments where LAT is only partially accessible to signalling molecules and, therefore, we cannot see full cell activation. This theory was also supported by the fact that calcium signal induced in cells expressing both CD4ex-LAT CS and CD4ex-LAT variants was the same.

The cytoskeleton and plasma membrane are structurally and functionally coupled via membrane proteins that anchor the cytoskeleton or induce actin polymerization (reviewed in Kaizuka et al., 2020). Previous studies have suggested a role of the cytoskeleton in the organization of signalling molecules at the PM (Harwood and Batista, 2011). Since we hypothesised that plasma membrane nanoscopic organisation of LAT variants can be influenced by introduced mutations, we decided to characterise their nanoscopic organisation in T cells using PALM superresolution microscopy. LAT WT and proline mutants P17A and P8A exhibited very similar, random distribution at the surface of unstimulated T cells. Unfortunately, LAT CS version couldn't be imaged because of its total absence from PM. However, non-palmitoylatable mutant variants P8A CS and P17A CS showed irregular distribution. We observed reduced spreading and accumulation of the signal in plasma membrane ruffles. Interference reflection microscopy (IRM) which enables to detect the contact area of a cell with a glass coverslip additionally revealed that cells transiently transfected with P8A CS and P17A CS variants had difficulties with the attachment to the glass coverslip (Figure 4.). Since the ability of these cells to spread was heavily affected by the absence of LAT palmitoylation, we were unable to fully evaluate their nanoscopic localisation and compare it to their palmitoylated counterparts. Bunnel et al., showed that even though LAT-deficient cells produced actin-rich contacts with surface, they were less extensive, less well organized and shorter lived than those formed by LAT-reconstituted cells. As a consequence, it led to severe defects in the spreading of T cells (Bunnell et al., 2001). Since actin polymerization is needed for the changes in T-cell morphology and adhesion, it is possible that either the absence of LAT palmitoylation or a combination of changes in LAT TMD biophysical properties introduced by mutations plus absence of palmitoylation influenced the actin cytoskeleton organisation and therefore the ability of transfected cells to adhere and spread properly.

Figure 4. Super-resolution imaging of LAT variants on the surface of T cells. **(A)** PALM images of J.CaM2.5 cells transiently transfected with LAT WT, LAT P17A and LAT P17A CS **(B)** IRM images of J.CaM2.5 cells transiently transfected with LAT WT, LAT P17A and LAT P17A CS. Scale bars 5um.

6.3. Structural motifs of CD4 determine its organisation on the plasma membrane

In analogy to the works described above, which investigated determinants in protein sequence important for sorting of transmembrane adaptor proteins to the plasma membrane (Chum et al., 2016; Glatzová et al., 2021), we also studied a role of structural motifs in the plasma membrane organisation of CD4 on the surface of T cells. CD4 has several structural motifs that could potentially influence its localisation on the plasma membrane. These include four glycosylated immunoglobulin-like domains (D1-D4) at the N-terminus (Leahy, 1995), transmembrane segment of 22 amino acids followed by a short cytoplasmic tail with two cysteines for palmitoylation in the juxtamembrane region (Crise and Rose, 1992) and a basic-rich domain which was reported to play a role in CD4 localisation into lipid microdomains (Popik and Alce, 1994; Balamuth et al., 2004). There are also two cysteines close to the C-terminus of CD4 which promote its association with Lck kinase through Zn^{2+} bridge (Straus

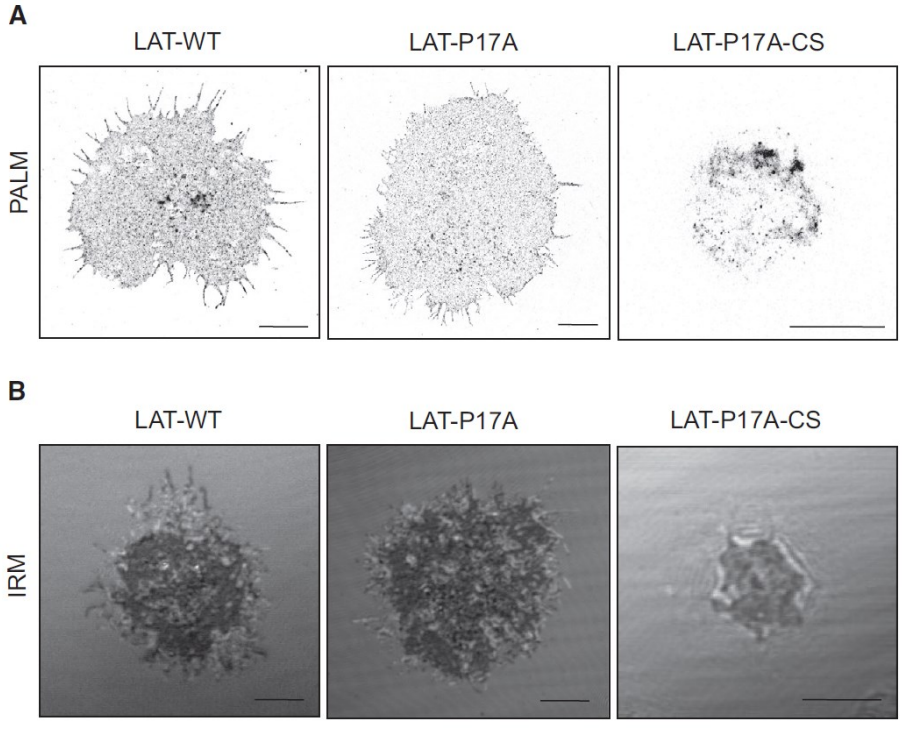

and Weis, 1992). This interaction has also a role in the stabilisation of CD4 at the surface of T cells (Laguette et al., 2009).

6.3.1. Differences in the distribution of CD4 mutants are beyond the resolution of confocal imaging

We first generated a panel of mutant variants to characterise the importance of selected structural motifs for CD4 localisation in T cells. Confocal microscopy analysis of GFP-fused mutants showed surface expression for all of them. We observed only minor changes in sorting of CD4 variants lacking cysteines for Lck-binding (CS2), basic-rich motif (RA5), intracellular domain (dCT) and extracellular domain deletion (dD1D4). We detected these variants also in the intracellular vesicles. This can be explained by already mentioned importance of CD4-Lck interaction for stable CD4 surface expression (this interaction is missing in CS2 and dCT mutants) (Laguette et al., 2009). Partial mislocalisation of dD1D4 mutant can be explained by protein misfolding due to the missing extracellular glycosylation (importance of glycosylation for proper protein folding reviewed in Helenius, 1994). Basic-rich motif (RCRHRRR in CD4) was reported to have a role in association with negatively charged inner leaflet phospholipids of the plasma membrane. DeFord-Watts et al., found that the substitution of arginine residues in the CD3 ζ basic-rich regions with alanines, glycines or valines completely eliminated its phospholipid binding (DeFord-Watts et al., 2011). We can speculate that this could lead to potential surface instability of RA5 CD4 variant in T cells. Even though there were no significant differences in sorting of our mutants, we hypothesized that there still can be a difference in their nanoscopic distribution on the plasma membrane unresolvable by standard microscopy techniques.

Because the size of membrane protein clusters is below the resolution limit of standard fluorescent microscopy, we have decided to employ SMLM technique PALM combined with TIRF microscopy to image CD4 variants fused to the photoswitchable fluorescent protein mEos2 at nanoscale. For the analysis, we chose four variants which exhibited the strongest surface expression (SMLM data analysis requires high density of emitters): WT, palmitoylation mutant (CS1), dCT and dD1D4. In contrast to confocal microscopy, PALM imaging uncovered two groups of CD4 variants with significantly altered surface distribution at the surface of resting T cells. CS1 and dD1D4 appeared to be distributed randomly at the plasma membrane surface. The other two variants, WT and dCT, formed a heterogeneous

network-like structures which gave rise to many obstacles during the quantitative analysis of acquired PALM data. We realized, that thanks to the irregular shape of studied clusters, standard Ripley's K and pair correlation analyses were not applicable. The application of more complex algorithms DBSCAN (Ester et al., 1996) and SR-Tesseler (Levet et al., 2015) did not lead to the satisfactory and reproducible results. We therefore decided to explore a different approach for quantitative image analysis of protein clustering in our samples and started a collaboration with prof. T. Lasser and his student T. Lukes (EPFL, Switzerland). Together, we developed a new method for nanoscopic cluster analysis of membrane proteins based on SOFI superresolution microscopy.

6.3.2. Molecular clustering analysis by bSOFI (Lukes at al. 2017)

In this work, we introduced a novel method for characterization of molecular organization and clustering of receptors on cellular surfaces. SMLM techniques like PALM are frequently used methods to characterize membrane protein assemblies. However, SMLM suffers from several weaknesses which can be caused by low excitation energy (Burgert et al., 2015) or, on the other hand, by high photoswitching rates in combination with high densities of fluorescent molecules in certain areas which can give rise to clustering artefacts (Annibale et al., 2011). In contrast to SMLM, SOFI is compatible with weakly emitting fluorophores and a wide range of blinking conditions. Big advantage of SOFI is also that it tolerates areas with higher emitter densities and overlapping emitters (Geissbuehler et al., 2011; Deschout et al., 2016). SOFI algorithm analyses localisations in the full image sequence, temporally cross-correlates neighbouring pixels and applies higher order statistics to separate point spread functions (Dertinger et al., 2010). Balanced SOFI (bSOFI) algorithm is an extended version of SOFI. It balances the image contrast (it linearizes the brightness and blinking) and can extract molecular parameters, such as distributions of fluorophores within biological samples (Geissbuehler et al., 2012). The advantage of our SOFI-based cluster analysis is that it does not need a manual selection of any parameters and it distinguishes between a random and a non-random distribution by continually increasing the threshold in a full spectrum of calculated densities to find an optimal density threshold. For each region of interest (ROI) and each density threshold it can calculate the average number and area of high density regions (HDRs) and the relative area occupied by HDRs. For the analysis, we combined SOFI image acquisition with TIRF imaging. Afterwards, we applied our modified bSOFI algorithm to the

stock of image frames and extracted molecular density maps, which were further analysed to extract clustering parameters for each of the tested CD4 variants.

6.3.3. CD4 nanoscale organization depends on its intact extracellular domain and palmitoylation

Our SOFI-based algorithm showed exceptional robustness despite the fact that imaged cells exhibited a high level of intercellular variability and diversity of HDRs. The use of mutant forms revealed that CD4 membrane distribution strongly depends on its intact extracellular domain and palmitoylation since these mutants lacking these parts (dD1D4 and CS1, respectively) showed rather small HDRs and mainly randomly distributed receptors. We observed accumulation of CD4 WT in HDRs covering a large part of the plasma membrane). The quantitative data on CD4 membrane organisation also revealed that truncated CD4 variant dCT showed an intermediate pattern. It formed fewer HDRs than WT but it was more heterogeneously distributed on the plasma membrane than CS1 variant with no palmitoylation. The difference in membrane organisation between dCT and CS1 mutants led us to the question of their palmitoylation state. To clarify this, I performed palmitoylation assay of our mutants in the laboratory of Prof. Ed Tate at Imperial College in London (unpublished data). Assay performed in his lab was based on metabolic labelling with acyl analogue (YnC15) combined with click-chemistry (described in Lanyon-Hogg et al., 2015). My results indicate that CD4 WT and dD1D4 are palmitoylated while CS1 mutant is not palmitoylated, as expected. Importanbtly, dCT mutant was also palmitoylated. The sequence of this truncated mutant is terminated after the first cysteine in the palmitoylation motif CxxC. Apparently, it can be palmitoylated even in the absence of the second cysteine in the motif. The lipid modification can influence CD4 nanoscopic localisation on the surface of T cells.

6.3.4. Palmitoylation locates CD4 to the tips of T cell microvilli

SMLM methods are usually used to generate 2D localization maps by projecting molecules from the plasma membrane to the 2D plane. However, the surface of T cells is not flat but covered with numerous membrane protrusions, ruffles and microvilli (Kim et al., 2018). Precise information about the axial position of surface molecules using standard SMLM methods is often missing and the interpretation of such data can potentially lead to misinterpretations. In our first study, we also used 2D projection and modified bSOFI algorithm to quantify lateral nanoscopic localisation of CD4 in unstimulated T cells. We

decided to extend our work on CD4 localization and wanted to elucidate the three-dimensional nature of CD4 receptor clusters.

To address this question, we started a collaboration with Sebastian van de Linde (University of Strathclyde, Glasgow, Scottland) and Christian Franke (University of Jena, Germany) and developed an advanced version of TRABI algorithm for quantitative processing of SMLM data (newly called directTRABI or dTRABI). In comparison to bSOFI imaging where we imaged CD4 variants genetically fused to photoswitchable fluorophores, dTRABI uses directly labelled antibodies to acquire higher photon counts. Applying our new algorithm, we were able to achieve 10-20nm resolution of images in 3D and therefore reveal precise surface morphology of CD4 and CD45 molecules on the surface of unstimulated T cells. It is known that CD45 molecules segregate from CD3ζ /TCR molecules which were reported to be localized at the tips of T-cell microvilli (Pageon et al., 2016; Jung et al., 2016; Razwag et al., 2018). Because localisation of CD4 to the proximity of TCR also depends on its interaction with Lck kinase (Foti et al., 2002) (one of the substrates of CD45 phosphatase (Sieh et al., 1993)), we were interested in relative 3D localisation of CD4 and CD45 molecules.

By applying dTRABI algorithm to the SMLM data from unstimulated T cells, we demonstrated that CD4 WT localizes preferentially to the tips of microvilli and that CD45, important regulator of T cell activation (Mustelin et al., 1989) segregates from CD4 and distributes mainly to the shaft and base of these membrane structures. Our data are in agreement with recently reported clustering of CD4 on the tips of T cell microvilli (Gosh et al., 2020) but in addition to this work, we revealed that palmitoylation as an important localisation determinant for CD4 co-receptor since palmitoylation mutant of CD4 (CS1) is distributed more randomly over the complex surface of T cells. A possible role of CD4 accumulation at the tips of T-cell microvilli is discussed in our recent review (Glatzova & Cebecauer, 2019).

7. Conclusions

In the presented work, I discuss three projects dealing with the importance of diverse structural motifs on protein sorting and/or localisation at the T-cell surface. Two projects focus on transmembrane adaptor proteins, including PAG, NTAL and LAT. In the first project, using a panel of mutants and live-cell confocal microscopy, we revealed the importance of palmitoylation, length and asymmetry of TMD for proper localisation of transmembrane adaptor proteins in T cells. In the second project, we specifically focused on LAT, the plasma membrane localisation of which depends on its palmitoylation. The unusual primary structure of its transmembrane domain is particularly interesting. We demonstrate that prolines and a glycine in the TMD of LAT influence its dynamics and flexibility. Abolition of kink drove sorting of mutants to the plasma membrane even in the absence of palmitoylation. The capability of those mutants to activate T cells was however impaired. Our data point to the possibility, that unpalmitoylated LAT, even though present on the plasma membrane, doesn't bridge TCR and its signalling molecules important for calcium release and T-cell activation. Third project I discuss in this thesis also deals with the importance of structural motifs, namely palmitoylation and the extracellular domain, on the proper nanoscopic organisation of CD4 co-receptor at the T-cell surface. Evaluation of superresolution data from this project required to develop modified SOFI algorithm which could deal with an irregular shape and high density of clusters observed on plasma membrane of T cells. We demonstrated the importance of palmitoylation for proper nanoscopic localisation of CD4 molecule. Furthermore, we adapted the recently reported TRABI method for precise 3D SMLM imaging of plasma membrane structures and showed, that palmitoylation is also important for localisation of CD4 molecule in 3D to the tips of microvilli.

8. Contributions

8.1. The role of palmitoylation and transmembrane domain in sorting of transmembrane adaptor proteins.

I prepared a part of the DNA constructs used in the study, I participated in microscopy analyses and I performed glycosylation assay with subsequent western blot analysis of mutant proteins. I participated in designing the experiments and writing the manuscript and I am listed as the second author on the publication.

8.2. The role of prolines and glycine in the transmembrane domain of LAT.

I independently wrote successful GA UK (The Charles University Grant Agency) application which resulted in this project. I designed and performed majority of experiments. I wrote the manuscript (with great help from my supervisor) and I am listed as the first author on the manuscript.

8.3. Quantifying protein densities on cell membranes using super-resolution optical fluctuation imaging.

I prepared all constructs used in the project and I performed SMLM imaging with subsequent ThunderSTORM data pre-processing. I am listed as a second author on the publication.

8.4. Unravelling nanotopography of cell surface receptors.

I prepared DNA constructs and stable Jurkat CD4KO cell line used in the project and performed calcium measurement experiments with subsequential data analysis.

Prohlášení o podílu studenta na výsledcích

Prohlašuji, že se Daniela Glatzová podílela na publikacích uvedených v této dizertační práci v rozsahu uvedeném v kapitole Contributions.

V Praze dne 28.6.2021 Mgr. Marek Cebecauer, Ph.D.

9. References

Aivazian D, Stern LJ, Phosphorylation of T cell receptor zeta is regulated by a lipid dependent folding transition. Nat Struct Biol, 2000 Nov;7(11):1023-6.

Alland L, Peseckis SM, Atherton RE, Berthiaume L, Resh MD, Dual myristylation and palmitylation of Src family member p59fyn affects subcellular localization, J Biol Chem 1994 Jun 17;269(24):16701-5.

Annibale P, Vanni S, Scarselli M, Rothlisberger U, Radenovic A, Identification of clustering artifacts in photoactivated localization microscopy, Nat Methods 2011 Jun 12;8(7):527-8.

Arcaro A, Grégoire C, Bakker TR, Baldi L, Jordan M, Goffin L, Boucheron N, Wurm F, van der Merwe PA, Malissen B, Luescher IF, CD8beta endows CD8 with efficient coreceptor function by coupling T cell receptor/CD3 to raft-associated CD8/p56(lck) complexes, J Exp Med 2001 Nov 19;194(10):1485-95.

Artyomov MN, Lis M, Devadas S, Davis MM, Chakraborty AK, CD4 and CD8 binding to MHC molecules primarily acts to enhance Lck delivery, Proc Natl Acad Sci U S A 2010 Sep 28;107(39):16916-21.

d'Azzo A, Bongiovanni A, Nastasi T, E3 ubiquitin ligases as regulators of membrane protein trafficking and degradation, Traffic 2005 Jun;6(6):429-41.

Axelrod D, Cell-substrate contacts illuminated by total internal reflection fluorescence, J Cell Biol 1981 Apr;89(1):141-5.

Bacchelli C, Moretti FA, Carmo M, Adams S, Stanescu HC, Pearce K, Madkaikar M, Gilmour KC, Nicholas AK, Woods CG, Kleta R, Beales PL, Qasim W, Gaspar HB, Mutations in linker for activation of T cells (LAT) lead to a novel form of severe combined immunodeficiency, J Allergy Clin Immunol 2017 Feb;139(2):634-642.e5.

Baeza-Delgado C, Marti-Renom MA, Mingarro I, Structure-based statistical analysis of transmembrane helices, Eur Biophys J 2013 Mar;42(2-3):199-207.

Baker JA, Wong W, Eisenhaber B, Warwicker J, Eisenhaber F, Charged residues next to transmembrane regions revisited: "Positive-inside rule" is complemented by the "negative inside depletion/outside enrichment rule", BMC Biol 2017 Jul 24;15(1):66.

Balagopalan L, Yi L, Nguyen T, McIntire KM, Harned AS, Narayan K, Samelson LE, Plasma membrane LAT activation precedes vesicular recruitment defining two phases of early T-cell activation, Nat Commun 2018 May 22;9(1):2013.

Balamuth F, Brogdon JL, Bottomly K, CD4 raft association and signaling regulate molecular clustering at the immunological synapse site, J Immunol 2004 May 15;172(10):5887-92

Barr VA, Yi J, Samelson LE, Super-resolution Analysis of TCR-Dependent Signaling: Single-Molecule Localization Microscopy, Methods Mol Biol 2017;1584:183-206.

Benting JH, Rietveld AG, Simons K, N-glycans mediate the apical sorting of a gpi-anchored, raft-associated protein in madin-darby canine kidney cells, J Cell Biol 1999 Jul 26;146(2):313-20.

Betzig E, Patterson GH, Sougrat R, Lindwasser OW, Olenych S, Bonifacino JS, Davidson MW, Lippincott-Schwartz J, Hess HF, Imaging intracellular fluorescent proteins at nanometer resolution, Science 2006 Sep 15;313(5793):1642-5.

Bernardino de la Serna J, Schütz GJ, Eggeling C, Cebecauer M, There Is No Simple Model of the Plasma Membrane Organization, Front Cell Dev Biol 2016 Sep 29;4:106.

Bijlmakers C, Protein acylation and localization in T cell signaling, Mol Membr Biol 2009 Jan;26(1):93-103.

Bilal MY, Zhang EY, Dinkel B, Hardy D, Yankee TM, Houtman JCD, GADS is required for TCR-mediated calcium influx and cytokine release, but not cellular adhesion, in human T cells, Cell Signal 2015 Apr;27(4):841-50.

Blaskovic S, Blanc M, van der Goot FG, What does S-palmitoylation do to membrane proteins?, FEBS J 2013 Jun;280(12):2766-74.

Böer U, Neuschäfer-Rube F, Möller U, Püschel GP, *Requirement of N-glycosylation of the prostaglandin E2 receptor EP3beta for correct sorting to the plasma membrane but not for correct folding*, Biochem J 2000 Sep 15;350 Pt 3(Pt 3):839-47.

Bonello G, Blanchard N, Montoya MC, Aguado E, Langlet C, He H, Nunez-Cruz S, Malissen M, Sanchez-Madrid F, Olive D, Hivroz C, Collette Y, Dynamic recruitment of the adaptor protein LAT: LAT exists in two distinct intracellular pools and controls its own recruitment, J Cell Sci 2004 Mar 1;117(Pt 7):1009-16.

Bonifacino JS, Traub LM, Signals for sorting of transmembrane proteins to endosomes and lysosomes, Annu Rev Biochem 2003;72:395-447.

Bosques CJ, Tschampel SM, Woods RJ, Imperiali B, Effects of glycosylation on peptide conformation: a synergistic experimental and computational study, J Am Chem Soc 2004 Jul 14;126(27):8421-5.

Brandl CJ, Deber CM, Hypothesis about the function of membrane-buried proline residues in transport proteins, Proc Natl Acad Sci U S A 1986 Feb;83(4):917-21.

Brazin KN, Mallis RJ, Boeszoermenyi A, Feng Y, Yoshizawa A, Reche PA, Kaur P, Bi K, Hussey RE, Duke-Cohan JS, Song L, Wagner G, Arthanari H, Lang MJ, Reinherz EL, The T Cell Antigen Receptor α Transmembrane Domain Coordinates Triggering through Regulation of Bilayer Immersion and CD3 Subunit Associations, Immunity 2018 Nov 20;49(5):829-841.e6.

Brdicka T, Imrich M, Angelisová P, Brdicková N, Horváth O, Spicka J, Hilgert I, Lusková P, Dráber P, Novák P, Engels N, Wienands J, Simeoni L, Osterreicher J, Aguado E, Malissen M,

Schraven B, Horejsí V, Non-T cell activation linker (NTAL): a transmembrane adaptor protein involved in immunoreceptor signaling, J Exp Med 2002 Dec 16;196(12):1617-26.

Brdicka T, Pavlistová D, Leo A, Bruyns E, Korínek V, Angelisová P, Scherer J, Shevchenko A, Hilgert I, Cerný J, Drbal K, Kuramitsu Y, Kornacker B, Horejsí V, Schraven B, Phosphoprotein associated with glycosphingolipid-enriched microdomains (PAG), a novel ubiquitously expressed transmembrane adaptor protein, binds the protein tyrosine kinase csk and is involved in regulation of T cell activation, J Exp Med 2000 May 1;191(9):1591-604.

Brdicková N, Brdicka T, Angelisová P, Horváth O, Spicka J, Hilgert I, Paces J, Simeoni L, Kliche S, Merten C, Schraven B, Horejsí V, LIME: a new membrane Raft-associated adaptor protein involved in CD4 and CD8 coreceptor signaling, J Exp Med 2003 Nov 17;198(10):1453-62.

Bretscher MS, Munro S, Cholesterol and the Golgi apparatus, Science 1993 Sep 3;261(5126):1280-1.

Brossard C, Feuillet V, Schmitt A, Randriamampita C, Romao M, Raposo G, Trautmann A, Multifocal structure of the T cell - dendritic cell synapse, Eur J Immunol 2005 Jun;35(6):1741-53.

Bright JN, Sansom MSP, The Flexing/Twirling Helix: Exploring the Flexibility about Molecular Hinges Formed by Proline and Glycine Motifs in Transmembrane Helices, Phys. Chem. B 2003, 107, 2, 627–636.

Brignatz C, Restouin A, Bonello G, Olive D, Collette Y, Evidences for ubiquitination and intracellular trafficking of LAT, the linker of activated T cells, Biochim Biophys Acta 2005 Dec 15;1746(2):108-15.

Bulbarelli A, Sprocati T, Barberi M, Pedrazzini E, Borgese N, Trafficking of tail-anchored proteins: transport from the endoplasmic reticulum to the plasma membrane and sorting between surface domains in polarised epithelial cells, J Cell Sci 2002 Apr 15;115(Pt 8):1689-702.

Bunnell SC, Kapoor V, Trible RP, Zhang W, Samelson LE, Dynamic actin polymerization drives T cell receptor-induced spreading: a role for the signal transduction adaptor LAT, Immunity 2001 Mar;14(3):315-29.

Bywater RP, Thomas D, Vriend G, A sequence and structural study of transmembrane helices, J Comput Aided Mol Des 2001 Jun;15(6):533-52.

Canobbio I, Trionfini P, Guidetti GF, Balduini C, Torti M, Targeting of the small GTPase Rap2b, but not Rap1b, to lipid rafts is promoted by palmitoylation at Cys176 and Cys177 and is required for efficient protein activation in human platelets, Cell Signal 2008 Sep;20(9):1662-70.

Burgert A, Letschert S, Doose S, Sauer M, Artifacts in single-molecule localization microscopy, Histochem Cell Biol 2015 Aug;144(2):123-31.

Chan AC, Dalton M, Johnson R, Kong GH, Wang T, Thoma R, Kurosaki T, Activation of ZAP-70 kinase activity by phosphorylation of tyrosine 493 is required for lymphocyte antigen receptor function, EMBO J 1995 Jun 1;14(11):2499-508.

Chan AC, Iwashima M, Turck CW, Weiss A, ZAP-70: a 70 kd protein-tyrosine kinase that associates with the TCR zeta chain, Cell 1992 Nov 13;71(4):649-62.

Chum T, Glatzová D, Kvíčalová Z, Malínský J, Brdička T, Cebecauer M, The role of palmitoylation and transmembrane domain in sorting of transmembrane adaptor proteins, J Cell Sci 2016 Aug 1;129(15):3053.

Cole DK, Dunn SM, Sami M, Boulter JM, Jakobsen BK, Sewell AK, T cell receptor engagement of peptide-major histocompatibility complex class I does not modify CD8 binding, Mol Immunol 2008 May;45(9):2700-9.

Cosson P, Perrin J, Bonifacino JS, Anchors aweigh: protein localization and transport mediated by transmembrane domains, Trends Cell Biol 2013 Oct;23(10):511-7.

Crise B, Rose JK, Human immunodeficiency virus type 1 glycoprotein precursor retains a CD4-p56lck complex in the endoplasmic reticulum, J Virol 1992 Apr;66(4):2296-301.

Crites TJ, Padhan K, Muller J, Krogsgaard M, Gudla PR, Lockett SJ, Varma R, TCR Microclusters pre-exist and contain molecules necessary for TCR signal transduction, J Immunol 2014 Jul 1;193(1):56-67.

Cruikshank WW, Center DM, Nisar N, Wu M, Natke B, Theodore AC, Kornfeld H, Molecular and functional analysis of a lymphocyte chemoattractant factor: association of biologic function with CD4 expression, Proc Natl Acad Sci U S A 1994 May 24;91(11):5109-13.

Das DK, Feng Y, Mallis RJ, Li X, Keskin DB, Hussey RE, Brady SK, Wang J, Wagner G, Reinherz EL, Lang MJ, Force-dependent transition in the T-cell receptor β-subunit allosterically regulates peptide discrimination and pMHC bond lifetime, Proc Natl Acad Sci U S A 2015 Feb 3;112(5):1517-22.

Davis SJ, Ikemizu S, Evans EJ, Fugger L, Bakker TR, van der Merwe PA, The nature of molecular recognition by T cells, Nat Immunol 2003 Mar;4(3):217-24.

DeFord-Watts LM, Dougall DS, Belkaya S, Johnson BA, Eitson JL, Roybal KT, Barylko B, Albanesi JP, Wülfing C, van Oers NSC, The CD3 zeta subunit contains a phosphoinositide-binding motif that is required for the stable accumulation of TCR-CD3 complex at the immunological synapse, J Immunol 2011 Jun 15;186(12):6839-47.

Deindl S, Kadlecek TA, Cao X, Kuriyan J, Weiss A, Stability of an autoinhibitory interface in the structure of the tyrosine kinase ZAP-70 impacts T cell receptor response, Proc Natl Acad Sci U S A 2009 Dec 8;106(49):20699-704.

Dertinger T, Heilemann M, Vogel R, Sauer M, Weiss S, Superresolution optical fluctuation imaging with organic dyes, Angew Chem Int Ed Engl 2010 Dec 3;49(49):9441-3.

Desai DM, Sap J, Silvennoinen O, Schlessinger J, Weiss A, The catalytic activity of the CD45 membrane-proximal phosphatase domain is required for TCR signaling and regulation, EMBO J 1994 Sep 1;13(17):4002-10.

Deschout H, Lukes T, Sharipov A, Szlag D, Feletti L, Vandenberg W, Dedecker P, Hofkens J, Leutenegger M, Lasser T, Radenovic A, Complementarity of PALM and SOFI for super-resolution live-cell imaging of focal adhesions, Nat Commun 2016 Dec 19;7:13693.

Draber P, Vonkova I, Stepanek S, Hrdinka M, Kucova M, Skopcova T, Otahal P, Angelisova P, Horejsi V, Yeung M, Weiss A, Brdicka T, SCIMP, a transmembrane adaptor protein involved in major histocompatibility complex class II signaling, Mol Cell Biol 2011 Nov;31(22):4550-62.

Duellman T, Burnett J, Yang J, Functional Roles of N-Linked Glycosylation of Human Matrix Metalloproteinase 9, Traffic 2015 Oct;16(10):1108-26.

Dukhovny A, Yaffe Y, Shepshelovitch J, Hirschberg K, The length of cargo-protein transmembrane segments drives secretory transport by facilitating cargo concentration in export domains, J Cell Sci 2009 Jun 1;122(Pt 11):1759-67.

Dustin MM, Impact of the immunological synapse on T cell signaling, Results Probl Cell Differ 2006;43:175-98.

Ehrlich LIR, Ebert PJR, Krummel MF, Weiss A, Davis MM, Dynamics of p56lck translocation to the T cell immunological synapse following agonist and antagonist stimulation, Immunity 2002 Dec;17(6):809-22.

Eilers M, Shekar SC, Shieh T, Smith SO, Fleming PJ, Internal packing of helical membrane proteins, Proc Natl Acad Sci U S A 2000 May 23;97(11):5796-801.

Erman B, Alag AS, Dahle O, van Laethem F, Sarafova SD, Guinter TI, Sharrow SO, Grinberg A, Love PE, Singer A, Coreceptor signal strength regulates positive selection but does not determine CD4/CD8 lineage choice in a physiologic in vivo model, J Immunol 2006 Nov 15;177(10):6613-25.

Ernst AM, Toomre D, Bogan JS, Acylation - A New Means to Control Traffic Through the Golgi, Front Cell Dev Biol 2019 Jun 12;7:109.

Ester M, Kriegel H, Sander J, Xu X, A Density-Based Algorithm for Discovering Clusters in Large Spatial Databases with Noise, 1996 Institute for Computer Science, University of Munich. Proceedings of 2nd International Conference on Knowledge Discovery and Data Mining (KDD-96)

Fagerberg L, Jonasson K, von Heijne G, Mathias Uhlén, Lisa Berglund, Prediction of the human membrane proteome, Proteomics 2010 Mar;10(6):1141-9.

Fastenberg ME, Shogomori H, Xu X, Brown DA, London E, Exclusion of a transmembrane-type peptide from ordered-lipid domains (rafts) detected by fluorescence quenching: extension

of quenching analysis to account for the effects of domain size and domain boundaries, Biochemistry 2003 Oct 28;42(42):12376-90.

Fiedler K, Simons K, The role of N-glycans in the secretory pathway, Cell 1995 May 5;81(3):309-12.

Finco TS, Kadlecek T, Zhang W, Samelson LE, Weiss A, LAT is required for TCR-mediated activation of PLCgamma1 and the Ras pathway, Immunity 1998 Nov;9(5):617-26.

Foti M, Phelouzat MA, Holm A, Rasmusson BJ, Carpentier JL, p56Lck anchors CD4 to distinct microdomains on microvilli, Proc Natl Acad Sci U S A 2002 Feb 19;99(4):2008-13.

Fragoso R, Ren D, Zhang X, Su MW, Burakoff SJ, Jin Y, Lipid raft distribution of CD4 depends on its palmitoylation and association with Lck, and evidence for CD4-induced lipid raft aggregation as an additional mechanism to enhance CD3 signaling, J Immunol 2003 Jan 15;170(2):913-21.

Franke C, Sauer M, van de Linde S, *Photometry unlocks 3D information from 2D localization microscopy data*, Nat Methods 2017 Jan;14(1):41-44.

Gagnon E, Schubert DA, Gordo S, Chu HH, Wucherpfennig KW, Local changes in lipid environment of TCR microclusters regulate membrane binding by the CD3ε cytoplasmic domain, J Exp Med 2012 Dec 17;209(13):2423-39.

Gao GF, Tormo J, Gerth UC, Wyer JR, McMichael AJ, Stuart DI, Bell JI, Jones EY, Jakobsen BK, Crystal structure of the complex between human CD8alpha(alpha) and HLA-A2, Nature 1997 Jun 5;387(6633):630-4.

Garcillán B, Marin A, Jiménez-Reinoso A, Briones AC, Muñoz-Ruiz M, García-León MJ, Gil J, Allende LM, Martínez-Naves E, Toribio ML, Regueiro JR, γδ T Lymphocytes in the Diagnosis of Human T Cell Receptor Immunodeficiencies. Front Immunol, 2015 Jan 29;6:20.

Geissbuehler S, Dellagiacoma C, Lasser T, Comparison between SOFI and STORM, Biomed Opt Express 2011 Jan 28;2(3):408-20.

Glatzová D, Cebecauer M, Dual Role of CD4 in Peripheral T Lymphocytes, Front Immunol. 2019 Apr 2;10:618.

Glatzová D, Mavila H, Saija MC, Chum T, Cwiklik L, Brdička T, Cebecauer M, *The role of prolines and glycine in the transmembrane domain of LAT*, FEBS J 2021 Jan 18 Online ahead of print.

Görlich D, Nuclear protein import, Curr Opin Cell Biol 1997 Jun;9(3):412-9.

Grakoui A, Bromley SK, Sumen C, Davis MM, Shaw AS, Allen PM, Dustin ML, The immunological synapse: a molecular machine controlling T cell activation, Science 1999 Jul 9;285(5425):221-7.

Griffié J, Shlomovich L, Williamson DJ, Shannon M, Aaron J, Khuon S, Burn GL, Boelen L, Peters R, Cope AP, Cohen EAK, Rubin-Delanchy P, Owen DM, 3D Bayesian cluster analysis of super-resolution data reveals LAT recruitment to the T cell synapse, Sci Rep 2017 Jun 22;7(1):4077.

Guo X, Yan C, Li H, Huang W, Shi X, Huang M, Wang Y, Pan W, Cai M, Li L, Wu W, Bai Y, Zhang C, Liu Z, Wang X, Zhang XF, Tang C, Wang H, Liu W, Ouyang B, Wong CC, Cao Y, Xu C, Lipid-dependent conformational dynamics underlie the functional versatility of T-cell receptor, Cell Res 2017 Apr;27(4):505-525.

Hampl J, Chien YH, Davis MM, CD4 augments the response of a T cell to agonist but not to antagonist ligands, Immunity 1997 Sep;7(3):379-85.

Harwood NE, Batista FD, The cytoskeleton coordinates the early events of B-cell activation, Cold Spring Harb Perspect Biol 2011 Feb 1;3(2):a002360.

Hawse WF, Champion MM, Joyce MV, Hellman LM, Hossain M, Ryan V, Pierce BG, Weng Z, Baker BM, Cutting edge: Evidence for a dynamically driven T cell signaling mechanism, J Immunol 2012 Jun 15;188(12):5819-23.

von Heijne G, *Membrane protein structure prediction. Hydrophobicity analysis and the positive-inside rule*, J Mol Biol 1992 May 20;225(2):487-94.

Heilemann M, van de Linde S, Schüttpelz M, Kasper S, Seefeldt B, Mukherjee A, Tinnefeld P, Sauer M, Subdiffraction-resolution fluorescence imaging with conventional fluorescent probes, Angew Chem Int Ed Engl 2008;47(33):6172-6.

Heilemann H, van de Linde S, Mukherjee A, Sauer M, Super-resolution imaging with small organic fluorophores, Angew Chem Int Ed Engl 2009;48(37):6903-8.

Helenius A, How N-linked oligosaccharides affect glycoprotein folding in the endoplasmic reticulum, Mol Biol Cell 1994 Mar;5(3):253-65.

Hendriks G, Koudijs M, van Balkom BWM, Oorschot V, Klumperman J, Deen PMT, van der Sluijs P, Glycosylation is important for cell surface expression of the water channel aquaporin-2 but is not essential for tetramerization in the endoplasmic reticulum, J Biol Chem 2004 Jan 23;279(4):2975-83.

Hess ST, Girirajan TPK, Mason MD, Ultra-high resolution imaging by fluorescence photoactivation localization microscopy, Biophys J 2006 Dec 1;91(11):4258-72.

van't Hof W, Resh MD, Rapid plasma membrane anchoring of newly synthesized p59fyn: selective requirement for NH2-terminal myristoylation and palmitoylation at cysteine-3, J Cell Biol 1997 Mar 10;136(5):1023-35.

van't Hof W, Resh MD, Dual fatty acylation of p59(Fyn) is required for association with the T cell receptor zeta chain through phosphotyrosine-Src homology domain-2 interactions, J Cell Biol 1999 Apr 19;145(2):377-89.

Holdorf AD, Lee K, Burack WR, Allen PM, Shaw AS, Regulation of Lck activity by CD4 and CD28 in the immunological synapse, Nat Immunol 2002 Mar;3(3):259-64.

Hombach J, Tsubata T, Leclercq L, Stappert H, Reth M, Molecular components of the B-cell antigen receptor complex of the IgM class, Nature 1990 Feb 22;343(6260):760-2.

Horejsí V, Otáhal P, Brdicka T, LAT--an important raft-associated transmembrane adaptor protein, FEBS J 2010 Nov;277(21):4383-97.

Horejsí V, Zhang W, Schraven B, Transmembrane adaptor proteins: organizers of immunoreceptor signalling, Nat Rev Immunol 2004 Aug;4(8):603-16.

Hrdinka M, Dráber P, Stepánek O, Ormsby T, Otáhal P, Angelisová P, Brdicka T, Paces J, Horejsí V, Drbal K, PRR7 is a transmembrane adaptor protein expressed in activated T cells involved in regulation of T cell receptor signaling and apoptosis, J Biol Chem 2011 Jun 3;286(22):19617-29.

Huang B, Babcock H, Zhuang X, Breaking the diffraction barrier: super-resolution imaging of cells, Cell 2010 Dec 23;143(7):1047-58.

Hundt M, Harada Y, Giorgio L, Tanimura N, Zhang W, Altman A, Palmitoylation-dependent plasma membrane transport but lipid raft-independent signaling by linker for activation of T cells, J Immunol 2009 Aug 1;183(3):1685-94.

Hur EM, Son m, Lee O, Choi YB, Park C, Lee H, Yun Y, LIME, a novel transmembrane adaptor protein, associates with p56lck and mediates T cell activation, J Exp Med 2003 Nov 17;198(10):1463-73.

Irvine DJ, Purbhoo MA, Krogsgaard M, Davis MM, Direct observation of ligand recognition by T cells. Nature. 2002 Oct 24;419(6909):845-9.

Jack ER, Madine J, Lian L, Middleton DA, Membrane interactions of peptides representing the polybasic regions of three Rho GTPases are sensitive to the distribution of arginine and lysine residues, Mol Membr Biol 2008 Jan;25(1):14-22.

Jacob J, Duclohier H, Cafiso DS, The role of proline and glycine in determining the backbone flexibility of a channel-forming peptide, Biophys J 1999 Mar;76(3):1367-76.

Janeway CA Jr, The T cell receptor as a multicomponent signalling machine: CD4/CD8 coreceptors and CD45 in T cell activation, Annu Rev Immunol 1992;10:645-74.

Janssen E, Zhu M, Zhang W, Koonpaew S, Zhang W, LAB: a new membrane-associated adaptor molecule in B cell activation, Nat Immunol 2003 Feb;4(2):117-23.

Javadpour MM, Eilers M, Groesbeek M, Smith SO, Helix packing in polytopic membrane proteins: role of glycine in transmembrane helix association, Biophys J 1999 Sep;77(3):1609-18.

Jung Y, Riven I, Feigelson SW, Kartvelishvily E, Tohya K, Miyasaka M, Alon R, Haran G, Three-dimensional localization of T-cell receptors in relation to microvilli using a combination of superresolution microscopies, Proc Natl Acad Sci U S A 2016 Oct 4;113(40):E5916-E5924.

Kabouridis PS, Magee AI, Ley SC, S-acylation of LCK protein tyrosine kinase is essential for its signalling function in T lymphocytes, EMBO J 1997 Aug 15;16(16):4983-98.

Kaiser H, Orłowski A, Róg T, Nyholm TKM, Chai W, Feizi T, Lingwood D, Vattulainen I, Simons K, Lateral sorting in model membranes by cholesterol-mediated hydrophobic matching, Proc Natl Acad Sci U S A 2011 Oct 4;108(40):16628-33.

Kaizuka Y, Regulations of T Cell Activation by Membrane and Cytoskeleton, Membranes (Basel) 2020 Dec 19;10(12):443.

Kim HR, Mun YV, Lee KS, Park YJ, Park JS, Park JH, Jeon BN, Kim CH, Jun Y, Hyun YM, Kim M, Lee SM, Park CS, Im SH, Jun CD, T cell microvilli constitute immunological synaptosomes that carry messages to antigen-presenting cells, Nat Commun 2018 Sep 7;9(1):3630.

Kim ST, Takeuchi K, Sun ZJ, Touma M, Castro CE, Fahmy A, Lang MJ, Wagner G, Reinherz EL, The alphabeta T cell receptor is an anisotropic mechanosensor, J Biol Chem 2009 Nov 6;284(45):31028-37.

Kölsch U, Arndt B, Reinhold D, Lindquist JA, Jüling N, Kliche S, Pfeffer K, Bruyns E, Schraven B, Simeoni L, Normal T-cell development and immune functions in TRIM-deficient mice, Mol Cell Biol 2006 May;26(9):3639-48.

Kölsch U, Schraven B, Simeoni L, SIT and TRIM determine T cell fate in the thymus, J Immunol 2008 Nov 1;181(9):5930-9.

König R, Huang LY, Germain RN, MHC class II interaction with CD4 mediated by a region analogous to the MHC class I binding site for CD8, Nature 1992 Apr 30;356(6372):796-8.

Koretzky GA, Abtahian F, Silverman MA, SLP76 and SLP65: complex regulation of signalling in lymphocytes and beyond, Nat Rev Immunol 2006 Jan;6(1):67-78.

Koretzky GA, Picus J, Thomas ML, Weiss A, Tyrosine phosphatase CD45 is essential for coupling T-cell antigen receptor to the phosphatidyl inositol pathway, Nature 1990 Jul 5;346(6279):66-8.

Kumar S, Bansal M, Geometrical and sequence characteristics of alpha-helices in globular proteins, Biophys J 1998 Oct;75(4):1935-44.

Kupfer A, Singer SJ, Janeway Jr CA, Swain SL, Coclustering of CD4 (L3T4) molecule with the T-cell receptor is induced by specific direct interaction of helper T cells and antigen-presenting cells, Proc Natl Acad Sci U S A 1987 Aug;84(16):5888-92.

Laguette N, Brégnard C, Bouchet J, Benmerah A, Benichou S, Basmaciogullari S, Nef-induced CD4 endocytosis in human immunodeficiency virus type 1 host cells: role of p56lck kinase, J Virol 2009 Jul;83(14):7117-28.

Lanier LL, DAP10- and DAP12-associated receptors in innate immunity, Immunol Rev 2009 Jan;227(1):150-60.

Lanier LL, Corliss BC, Wu J, Leong C, Phillips JH, Immunoreceptor DAP12 bearing a tyrosine-based activation motif is involved in activating NK cells, Nature 1998 Feb 12;391(6668):703-7.

Leahy DJ, A structural view of CD4 and CD8, FASEB J 1995 Jan;9(1):17-25.

van Laethem F, Sarafova SD, Park J, Tai X, Pobezinsky L, Guinter TI, Adoro S, Adams A, Sharrow SO, Feigenbaum L, Singer A, Deletion of CD4 and CD8 coreceptors permits generation of alphabetaT cells that recognize antigens independently of the MHC, Immunity 2007 Nov;27(5):735-50.

van Laethem F, Tikhonova AN, Pobezinsky LA, Tai X, Kimura MY, Saout CL, Guinter TI, Adams A, Sharrow SO, Bernhardt G, Feigenbaum L, Singer A, Lck availability during thymic selection determines the recognition specificity of the T cell repertoire, Cell 2013 Sep 12;154(6):1326-41.

Lanyon-Hogg T, Masumoto N, Bodakh G, Konitsiotis AD, Thinon E, RodgersUR, Owens RJ, Magee AI, Tate EW, Click chemistry armed enzyme-linked immunosorbent assay to measure palmitoylation by hedgehog acyltransferase, Anal Biochem 2015 Dec 1;490:66-72.

Leahy DJ, A structural view of CD4 and CD8, FASEB J 1995 Jan;9(1):17-25.

Lee SM, Glassman CR, Deshpande NR, Badgandi HB, Parrish HL, Uttamapinant C, Stawski PS, Ting AY, Kuhns MS, A Mechanical Switch Couples T Cell Receptor Triggering to the Cytoplasmic Juxtamembrane Regions of CD3ζζ, Immunity 2015 Aug 18;43(2):227-39.

Levental I, Lingwood D, Grzybek M, Coskun U, Simons K, Palmitoylation regulates raft affinity for the majority of integral raft proteins, Proc Natl Acad Sci U S A 2010 Dec 21;107(51):22050-4.

Levet F, Hosy E, Kechkar A, Butler C, Beghin A, Choquet D, Sibarita JB, SR-Tesseler: a method to segment and quantify localization-based super-resolution microscopy data, Nat Methods 2015 Nov;12(11):1065-71.

Lewis RS, Calcium signaling mechanisms in T lymphocytes, Annu Rev Immunol 2001;19:497-521.

Li SC, Deber CM, Influence of glycine residues on peptide conformation in membrane environments, Int J Pept Protein Res Sep-Oct 1992;40(3-4):243-8.

Li Q, Dinner AR, Qi S, Irvine DJ, Huppa JB, Davis MM, Chakraborty AK, CD4 enhances T cell sensitivity to antigen by coordinating Lck accumulation at the immunological synapse, Nat Immunol 2004 Aug;5(8):791-9.

Li SC, Goto NK, Williams KA, Deber CM, Alpha-helical, but not beta-sheet, propensity of proline is determined by peptide environment, Proc Natl Acad Sci U S A 1996 Jun 25;93(13):6676-81

Lillemeier BF, Mörtelmaier MA, Forstner MB, Huppa JB, Groves JT, Davis MM, TCR and Lat are expressed on separate protein islands on T cell membranes and concatenate during activation, Nat Immunol 2010 Jan;11(1):90-6.

Lin J, Weiss A, Identification of the minimal tyrosine residues required for linker for activation of T cell function, J Biol Chem 2001 Aug 3;276(31):29588-95.

van de Linde S, Löschberger A, Klein T, Heidbreder M, Wolter S, Heilemann M, Sauer M, Direct stochastic optical reconstruction microscopy with standard fluorescent probes, Nat Protoc 2011 Jun 16;6(7):991-1009.

Long F, Zeng S, Huang Z, Localization-based super-resolution microscopy with an sCMOS camera part II: experimental methodology for comparing sCMOS with EMCCD cameras, Opt Express 2012 Jul 30;20(16):17741-59.

Lorent JH, Levental KR, Structural determinants of protein partitioning into ordered membrane domains and lipid rafts, Chem Phys Lipids 2015 Nov;192:23-32.

Lorent JH, Levental KR, Ganesan L, Rivera-Longsworth G, Sezgin E, Doktorova M, Lyman E, Levental I, Plasma membranes are asymmetric in lipid unsaturation, packing and protein shape, Nat Chem Biol 2020 Jun;16(6):644-652.

Lukeš T, Glatzová D, Kvíčalová Z, Levet F, Benda A, Letschert S, Sauer M, Brdička T, Lasser T, Cebecauer M, Quantifying protein densities on cell membranes using super-resolution optical fluctuation imaging, Nat Commun 2017 Nov 23;8(1):1731.

Macháň R, Jurkiewicz P, Olżyńska A, Olšinová M, Cebecauer M, Marquette A, Bechinger B, Hof M, Peripheral and integral membrane binding of peptides characterized by time-dependent fluorescence shifts: focus on antimicrobial peptide LAH_4, Langmuir 2014 Jun 3;30(21):6171-9.

Macian F, NFAT proteins: key regulators of T-cell development and function, Nat Rev Immunol 2005 Jun;5(6):472-84

Madrenas J, Chau LA, Smith J, Bluestone JA, Germain JN, The efficiency of CD4 recruitment to ligand-engaged TCR controls the agonist/partial agonist properties of peptide-MHC molecule ligands, J Exp Med 1997 Jan 20;185(2):219-29.

Mariuzza RA, Agnihotri P, Orban J, The structural basis of T-cell receptor (TCR) activation: An enduring enigma. J Biol Chem., 2020 Jan 24;295(4):914-925.

Martínez-Martín N, Risueño RM, Morreale A, Zaldívar I, Fernández-Arenas E, Herranz F, Ortiz AR, Alarcón B, Cooperativity between T cell receptor complexes revealed by conformational mutants of CD3epsilon. Sci Signal, 2009 Aug 11;2(83):ra43.

Melkonian KA, Ostermeyer AG, Chen JZ, Roth MG, Brown DA, Role of lipid modifications in targeting proteins to detergent-resistant membrane rafts. Many raft proteins are acylated, while few are prenylated, J Biol Chem 1999 Feb 5;274(6):3910-7.

van der Merwe PA, Dushek O, Mechanisms for T cell receptor triggering, Nat Rev Immunol 2011 Jan;11(1):47-55.

Mingueneau M, Sansoni A, Grégoire C, Roncagalli R, Aguado E, Weiss A, Malissen M, Malissen B, The proline-rich sequence of CD3epsilon controls T cell antigen receptor expression on and signaling potency in preselection CD4+CD8+ thymocytes. Nat Immunol, 2008 May;9(5):522-32.

Monks CR, Freiberg BA, Kupfer H, Sciaky N, Kupfer A, Three-dimensional segregation of supramolecular activation clusters in T cells, Nature 1998 Sep 3;395(6697):82-6.

Munro S, Pelham HR, A C-terminal signal prevents secretion of luminal ER proteins, Cell 1987 Mar 13;48(5):899-907.

Munro S, Sequences within and adjacent to the transmembrane segment of alpha-2,6-sialyltransferase specify Golgi retention, EMBO J 1991 Dec;10(12):3577-88.

Mouritsen OG, Bloom M, *Mattress model of lipid–protein interactions in membranes*, Biophys J 1984 Aug;46(2):141-53.

Munro S, An investigation of the role of transmembrane domains in Golgi protein retention, EMBO J 1995 Oct 2;14(19):4695-704.

Mustelin T, Coggeshall KM, Altman A, Rapid activation of the T-cell tyrosine protein kinase pp56lck by the CD45 phosphotyrosine phosphatase, Proc Natl Acad Sci U S A 1989 Aug;86(16):6302-6.

Nishimura N, Balch WE, A di-acidic signal required for selective export from the endoplasmic reticulum, Science 1997 Jul 25;277(5325):556-8.

Oberdoerffer S, Moita SF, Neems T, Freitas RP, Hacohen N, Rao A, Regulation of CD45 alternative splicing by heterogeneous ribonucleoprotein, hnRNPLL, Science 2008 Aug 1;321(5889):686-91.

Owen DM, Gaus K, Magee AI, Cebecauer M, Dynamic organization of lymphocyte plasma membrane: lessons from advanced imaging methods, Immunology 2010 Sep;131(1):1-8.

Pageon SV, Tabarin T, Yamamoto Y, Ma Y, Nicovich PR, Bridgeman JS, Cohnen A, Benzing C, Gao Y, Crowther MD, Tungatt K, Dolton C, Sewell AK, Price DA, Acuto O, Parton RG, Gooding JJ, Rossy J, Rossjohn J, Gaus K, Functional role of T-cell receptor

nanoclusters in signal initiation and antigen discrimination, Proc Natl Acad Sci U S A 2016 Sep 13;113(37):E5454-63.

Palacios EH, Weiss A, Function of the Src-family kinases, Lck and Fyn, in T-cell development and activation, Oncogene 2004 Oct 18;23(48):7990-8000.

Patel P, Gustafsson N, Lin Y, Ober R, Henriques R, Cohen E, A hidden markov model approach to characterizing the photo-switching behavior of fluorophores, Ann Appl Stat 2019 Sep;13(3):1397-1429.

Patterson G, Davidson M, Manley S, Lippincott-Schwartz J, Superresolution imaging using single-molecule localization, Annu Rev Phys Chem 2010;61:345-67.

Pennock ND, White JT, Cross EW, Cheney EE, Tamburini BA, Kedl RM, T cell responses: naive to memory and everything in between, Adv Physiol Educ 2013 Dec;37(4):273-83.

Polinsky A, Goodman M, Williams KA, Deber CM, Minimum energy conformations of proline-containing helices, Biopolymers 1992 Apr;32(4):399-406.

Popik W, Alce TM, CD4 receptor localized to non-raft membrane microdomains supports HIV-1 entry. Identification of a novel raft localization marker in CD4, J Biol Chem 2004 Jan 2;279(1):704-12.

Pulido R, Sánchez-Madrid F, Glycosylation of CD45: carbohydrate processing through Golgi apparatus is required for cell surface expression and protein stability, Eur J Immunol 1992 Feb;22(2):463-8.

Razvag Y, Neve-Oz Y, Sajman J, Reches M, Sherman E, Nanoscale kinetic segregation of TCR and CD45 in engaged microvilli facilitates early T cell activation, Nat Commun 2018 Feb 21;9(1):732.

Ren J, Wen L, Gao X, Jin C, Xue Y, Yao X, CSS-Palm 2.0: an updated software for palmitoylation sites prediction, Protein Eng Des Sel 2008 Nov;21(11):639-44.

Resh MD, Regulation of cellular signalling by fatty acid acylation and prenylation of signal transduction proteins, Cell Signal 1996 Sep;8(6):403-12.

Resh MD, Trafficking and signaling by fatty-acylated and prenylated proteins, Nat Chem Biol 2006 Nov;2(11):584-90.

Richardson JS, Richardson DC, Amino acid preferences for specific locations at the ends of alpha helices, Science 1988 Jun 17;240(4859):1648-52.

Roh K, Lillemeier BF, Wang F, Davis MM, The coreceptor CD4 is expressed in distinct nanoclusters and does not colocalize with T-cell receptor and active protein tyrosine kinase p56lck, Proc Natl Acad Sci U S A 2015 Mar 31;112(13):E1604-13.

Ronchi P, Colombo S, Francolini M, Borgese N, Transmembrane domain-dependent partitioning of membrane proteins within the endoplasmic reticulum, J Cell Biol 2008 Apr 7;181(1):105-18.

Rust MJ, Bates M, Zhuang X, Sub-diffraction-limit imaging by stochastic optical reconstruction microscopy (STORM), Nat Methods 2006 Oct;3(10):793-5.

Salter RD, Benjamin RJ, Wesley PK, Buxton SE, Garrett TP, Clayberger C, Krensky AM, Norment AM, Littman DR, Parham P, A binding site for the T-cell co-receptor CD8 on the alpha 3 domain of HLA-A2, Nature 1990 May 3;345(6270):41-6.

Sandoval IV, Bakke O, Targeting of membrane proteins to endosomes and lysosomes, Trends Cell Biol 1994 Aug;4(8):292-7.

Schmidt MF, Schlesinger MJ, Fatty acid binding to vesicular stomatitis virus glycoprotein: a new type of post-translational modification of the viral glycoprotein, Cell 1979 Aug;17(4):813-9.

Senes A, Gerstein M, Engelman DM, Statistical analysis of amino acid patterns in transmembrane helices: the GxxxG motif occurs frequently and in association with beta-branched residues at neighboring positions, J Mol Biol 2000 Feb 25;296(3):921-36.

Sevcsik E, Schütz GJ, With or without rafts? Alternative views on cell membranes, Bioessays 2016 Feb;38(2):129-39.

Sharpe HJ, Stevens TJ, Munro S, A comprehensive comparison of transmembrane domains reveals organelle-specific properties, Cell 2010 Jul 9;142(1):158-69.

Sherman E, Barr V, Manley S, Patterson G, Balagopalan L, Akpan I, Regan CK, Merrill RK, Sommers CL, Lippincott-Schwartz J, Samelson LE, Functional nanoscale organization of signaling molecules downstream of the T cell antigen receptor, Immunity 2011 Nov 23;35(5):705-20.

Shi X, Bi Y, Yang W, Guo X, Jiang Y, Wan C, Li L, Bai Y, Guo J, Wang Y, Chen X, Wu B, Sun H, Liu W, Wang J, Xu C, Ca2+ regulates T-cell receptor activation by modulating the charge property of lipids, Nature 2013 Jan 3;493(7430):111-5.

Shimada Y, Inomata M, Suzuki H, Hayashi M, Waheed AA, Ohno-Iwashita Y, Separation of a cholesterol-enriched microdomain involved in T-cell signal transduction, FEBS J 2005 Nov;272(21):5454-63.

Sieh M, Bolen JB, Weiss A, CD45 specifically modulates binding of Lck to a phosphopeptide encompassing the negative regulatory tyrosine of Lck, EMBO J 1993 Jan;12(1):315-21.

Sigal CT, Zhou W, Buser CA, McLaughlin A, Resh MD, Amino-terminal basic residues of Src mediate membrane binding through electrostatic interaction with acidic phospholipids, Proc Natl Acad Sci U S A 1994 Dec 6;91(25):12253-7.

Simeoni L, Posevitz V, Kölsch U, Meinert I, Bruyns E, Pfeffer K, Reinhold D, Schraven B, The transmembrane adapter protein SIT regulates thymic development and peripheral T-cell functions, Mol Cell Biol 2005 Sep;25(17):7557-68.

Simons K, Ikonen E, Functional rafts in cell membranes, Nature 1997 Jun 5;387(6633):569-72.

Singer A, Adoro S, Park JH, Lineage fate and intense debate: myths, models and mechanisms of CD4- versus CD8-lineage choice. Nat Rev Immunol, 2008 Oct;8(10):788-801.

van den Steen P, Rudd PM, Dwek RA, Opdenakker G, Concepts and principles of O-linked glycosylation, Crit Rev Biochem Mol Biol 1998;33(3):151-208.

Stepanek O, Prabhakar AS, Osswald C, King CG, Bulek A, Naeher D, Beaufils-Hugot M, Abanto ML, Galati V, Hausmann B, Lang R, Cole DK, Huseby ES, Sewell AK, Chakraborty AK, Palmer E, Coreceptor scanning by the T cell receptor provides a mechanism for T cell tolerance, Cell 2014 Oct 9;159(2):333-45.

Stover DR, Charbonneau H, Tonks NK, Walsh KA, Protein-tyrosine-phosphatase CD45 is phosphorylated transiently on tyrosine upon activation of Jurkat T cells, Proc Natl Acad Sci U S A 1991 Sep 1;88(17):7704-7.

Straus DB, Weiss A, Genetic evidence for the involvement of the lck tyrosine kinase in signal transduction through the T cell antigen receptor, Cell 1992 Aug 21;70(4):585-93.

Tanimura N, Saitoh S, Kawano S, Kosugi A, Miyake K, Palmitoylation of LAT contributes to its subcellular localization and stability, Biochem Biophys Res Commun 2006 Mar 24;341(4):1177-83.

Terry LA, DiSanto JP, Small TN, Flomenberg N, Differential expression and regulation of the human CD8 alpha and CD8 beta chains, Tissue Antigens 1990 Feb;35(2):82-91.

Vagin O, Kraut JA, Sachs G, Role of N-glycosylation in trafficking of apical membrane proteins in epithelia, Am J Physiol Renal Physiol 2009 Mar;296(3):F459-69.

Varma R, Campi G, Yokosuka T, Saito T, Dustin ML, T cell receptor-proximal signals are sustained in peripheral microclusters and terminated in the central supramolecular activation cluster, Immunity 2006 Jul;25(1):117-27.

Veillette A, Bookman MA, Horak EM, Bolen JB, The CD4 and CD8 T cell surface antigens are associated with the internal membrane tyrosine-protein kinase p56lck, Cell 1988 Oct 21;55(2):301-8.

Vidal K, Daniel C, Hill M, Littman DR, Allen PM, Differential requirements for CD4 in TCR-ligand interactions, J Immunol 1999 Nov 1;163(9):4811-8.

Wallin E, von Heijne G, Genome-wide analysis of integral membrane proteins from eubacterial, archaean, and eukaryotic organisms, Protein Sci 1998 Apr;7(4):1029-38.

Wang JH, Meijers R, Xiong Y, Liu JH, Sakihama T, Zhang R, Joachimiak R, Reinherz EL, Crystal structure of the human CD4 N-terminal two-domain fragment complexed to a class II MHC molecule, Proc Natl Acad Sci U S A 2001 Sep 11;98(19):10799-804.

Wang R, Natarajan K, Margulies DH, Structural basis of the CD8 alpha beta/MHC class I interaction: focused recognition orients CD8 beta to a T cell proximal position, J Immunol 2009 Aug 15;183(4):2554-64.

Wardenburg JB, Fu C, Jackman JK, Flotow H, Wilkinson SE, Williams DH, Johnson R, Kong G, Chan AC, Findell PR, Phosphorylation of SLP-76 by the ZAP-70 protein-tyrosine kinase is required for T-cell receptor function, J Biol Chem. 1996 Aug 16;271(33):19641-4.

Weissman AM, Samelson LE, Klausner RD, A new subunit of the human T-cell antigen receptor complex, Nature 1986 Dec 4-10;324(6096):480-2.

Wen W, Meinkoth JL, Tsien RY, Taylor SS, Identification of a signal for rapid export of proteins from the nucleus, Cell 1995 Aug 11;82(3):463-73.

Williams CL, The polybasic region of Ras and Rho family small GTPases: a regulator of protein interactions and membrane association and a site of nuclear localization signal sequences, Cell Signal 2003 Dec;15(12):1071-80.

Wu P, Zhang T, Liu B, Fei P, Cui L, Qin R, Zhu H, Yao D, Martinez RJ, Hu W, An C, Zhang Y, Liu J, Shi J, Fan J, Yin W, Sun J, Zhou C, Zeng X, Xu C, Wang J, Evavold BD, Zhu C, Chen W, Lou J, Mechano-regulation of Peptide-MHC Class I Conformations Determines TCR Antigen Recognition, Mol Cell 2019 Mar 7;73(5):1015-1027.e7.

Xiang Y, Zhang X, Nix DB, Katoh T, Aoki K, Tiemeyer M, Wang Y, Regulation of protein glycosylation and sorting by the Golgi matrix proteins GRASP55/65, Nat Commun 2013;4:1659.

Xiong Y, Kern P, Chang H, Reinherz E, T Cell Receptor Binding to a pMHCII Ligand Is Kinetically Distinct from and Independent of CD4, J Biol Chem 2001 Feb 23;276(8):5659-67.

Xu C, Gagnon E, Call ME, Schnell JR, Schwieters CD, Carman CV, Chou JJ, Wucherpfennig KW, Regulation of T cell receptor activation by dynamic membrane binding of the CD3epsilon cytoplasmic tyrosine-based motif. Cell 2008 Nov 14;135(4):702-13.

Yasuda K, Kosugi A, Hayashi F, Saitoh S, Nagafuku M, Mori Y, Ogata M, Hamaoka T, Serine 6 of Lck tyrosine kinase: a critical site for Lck myristoylation, membrane localization, and function in T lymphocytes, J Immunol 2000 Sep 15;165(6):3226-31.

Yin Y, Wang XX, Mariuzza RA, Crystal structure of a complete ternary complex of T-cell receptor, peptide-MHC and CD4, Proc Natl Acad Sci U S A 2012 Apr 3;109(14):5405-10.

Yokosuka T, Sakata-Sogawa K, Kobayashi W, Hiroshima M, Hashimoto-Tane A, Tokunaga M, Dustin ML, Saito T, Newly generated T cell receptor microclusters initiate and sustain T cell activation by recruitment of Zap70 and SLP-76, Nat Immunol 2005 Dec;6(12):1253-62.

Zal T, Zal MA, Gascoigne NRJ, Inhibition of T cell receptor-coreceptor interactions by antagonist ligands visualized by live FRET imaging of the T-hybridoma immunological synapse, Immunity 2002 Apr;16(4):521-34.

Zhang W, Sloan-Lancaster J, Kitchen J, Trible RP, Samelson LE, LAT: the ZAP-70 tyrosine kinase substrate that links T cell receptor to cellular activation, Cell 1998 Jan 9;92(1):83-92.

Zhang W, Sommers CL, Burshtyn DN, Stebbins CC, DeJarnette JB, Trible RP, Grinberg A, Tsay HC, Jacobs HM, Kessler CM, Long EO, Love PE, Samelson LE, Essential role of LAT in T cell development, Immunity 1999 Mar;10(3):323-32.

Zhang W, Trible RP, Samelson LE, LAT palmitoylation: its essential role in membrane microdomain targeting and tyrosine phosphorylation during T cell activation, Immunity 1998 Aug;9(2):239-46.

Zhu M, Granillo O, Wen R, Yang K, Dai X, Wang D, Zhang W, Negative regulation of lymphocyte activation by the adaptor protein LAX, J Immunol 2005 May 1;174(9):5612-9.

10. Reprint of publications

Chum T, **Glatzová D**, Kvíčalová Z, Malínský J, Brdička T, Cebecauer M, *The role of palmitoylation and transmembrane domain in sorting of transmembrane adaptor proteins*, J Cell Sci 2016 Jan 1;129(1):95-107.

Glatzová D, Mavila H, Saija MC, Chum T, Cwiklik L, Brdička T, Cebecauer M, *The role of prolines and glycine in the transmembrane domain of LAT*, FEBS J 2021 Jan 18 Online ahead of print.

Lukeš T, **Glatzová D**, Kvíčalová Z, Levet F, Benda A, Letschert S, Sauer M, Brdička T, Lasser T, Cebecauer M, *Quantifying protein densities on cell membranes using super-resolution optical fluctuation imaging*, Nat Commun. 2017 Nov 23;8(1):1731.

Franke C, Chum T, Kvíčalová Z, **Glatzová D**, Rodriguez A, Helmerich D, Frank O, Brdička T, van de Linde S, Cebecauer M, *Unravelling nanotopography of cell surface receptors*, bioRxiv 2019.12.23.884460

© 2016. Published by The Company of Biologists Ltd | Journal of Cell Science (2016) 129, 95-107 doi:10.1242/jcs.175190

RESEARCH ARTICLE

The role of palmitoylation and transmembrane domain in sorting of transmembrane adaptor proteins

TomášChum[1], Daniela Glatzová[1,2], Zuzana Kvičalová[1],Jan Malınský[3], TomášBrdička[2] and Marek Cebecauer[1,*]

ABSTRACT

Plasma membrane proteins synthesised at the endoplasmic reticulum are delivered to the cell surface via sorting pathways. Hydrophobic mismatch theory based on the length of the transmembrane domain (TMD) dominates discussion about determinants required for protein sorting to the plasma membrane. Transmembrane adaptor proteins (TRAP) are involved in signalling events which take place at the plasma membrane. Members of this protein family have TMDs of varying length. We were interested in whether palmitoylation or other motifs contribute to the effective sorting of TRAP proteins. We found that palmitoylation is essential for some, but not all, TRAP proteins independent of their TMD length. We also provide evidence that palmitoylation and proximal sequences can modulate sorting of artificial proteins with TMDs of suboptimal length. Our observations point to a unique character of each TMD defined by its primary amino acid sequence and its impact on membrane protein localisation. We conclude that, in addition to the TMD length, secondary sorting determinants such as palmitoylation or flanking sequences have evolved for the localisation of membrane proteins.

KEY WORDS: LAT, PAG, Palmitoylation, Plasma membrane, Protein sorting, Transmembrane domain

INTRODUCTION

Integral membrane proteins of eukaryotic cells comprise almost 30% of all proteins encoded by the human genome (Almén et al., 2009). These undergo sorting into target compartments such as the endoplasmic reticulum (ER), Golgi complex, mitochondria or the plasma membrane to perform their function. Mis-localisation can lead to a loss-of-function of these proteins, resulting in cell malfunction and even development of diseases (Howell et al., 2006). Structural and sequence motifs responsible for protein sorting events have been studied for more than 30 years. During that time a number of determinants of specific membrane protein localisation have been identified. These include sequence motifs in cytosolic and lumenal domains (e.g. KDEL for the ER or YxxØ for clathrin-dependent processes; Traub, 2009), N- and O-glycosylation of the extracellular domains (Fiedler and Simons, 1995; Potter et al., 2006; Proszynski et al., 2004), and physical properties of the transmembrane domain (TMD) such as length and hydrophobicity (Cosson et al., 2013; Sharpe et al., 2010). This wide variety of sorting signals is further extended by the fact that more than one determinant can define the localisation of proteins in the cell (Alonso et al., 1997; Duffield et al., 2008). No universal signal or motif has been demonstrated for the sorting of proteins to the plasma membrane. Therefore, all parts of the protein need to be tested for their impact on the proper localisation when investigating protein function using various mutants.

Transmembrane adaptor proteins (TRAPs) are topologically related type I integral membrane proteins that enable the association of signalling effectors and other enzymes with the plasma membrane of eukaryotic cells. They contain only a short extracellular part, single TMD and the cytosolic domain with multiple protein-protein interaction motifs mediating their functions (Fig. 1A). TRAPs do not have any enzymatic activity. In mammalian white blood cells, they function as crucial check-points or regulators of the main signalling events defining the basic function of these cells by facilitating the assembly of signalling complexes at the plasma membrane (Horejšı et al., 2004). Three TRAP subfamilies were defined in these cells: (i) monomeric, palmitoylated TRAPs (pTRAPs), (ii) monomeric, non-palmitoylated TRAPs and (iii) dimeric TRAPs frequently associated with large multisubunit receptor complexes (Stepanek et al., 2014). The latter group represents a challenge when studying the impact of various motifs on protein localisation because of their dimeric character and strong association with other subunits of receptor complexes. For example, CD247 dimer (ζ chain) facilitates the surface expression of the multi-subunit TCR/CD3 complex in T lymphocytes (Weissman et al., 1989). Non-palmitoylated, monomeric TRAPs (LAX1 and SIT1) have an extracellular part of intermediate size (38–40 residues) with potential glycosylation sites. Their glycosylation status can influence the plasma membrane localisation as shown for a number of surface glycoproteins (Fiedler and Simons, 1995). On the contrary, none of the known pTRAPs [LAT, PAG1, NTAL (also known as LAT2), LIME1, PRR7, SCIMP] are likely to be glycosylated because of their very short extracellular part (3–20 amino acids) and lack of glycosylation sites. In addition, pTRAPs are missing a signal peptide and use their unique TMD for membrane insertion, similar to type II membrane proteins. It can be hypothesised that it is the TMD length or composition that defines the localisation of such proteins to the plasma membrane, as observed for type II proteins in the past (Munro, 1991).

Palmitoylation, a reversible post-translational modification of eukaryotic proteins (Bijlmakers, 2009), is another factor that can contribute to plasma membrane targeting of pTRAPs. In the process of palmitoylation, palmitoyl-CoA produced by fatty acid metabolism at the ER membrane is enzymatically reacted with cysteine residues in the cytoplasmic parts of target proteins by the DHHC family of proteins (Zeidman et al., 2009). No consensus palmitoylation motif has been found to date (Zeidman et al., 2009). In all pTRAPs, the palmitoylation sites are thought to be the cytosolic cysteine residues within CxxC or CxC motifs adjacent to

[1]Department of Biophysical Chemistry, J. Heyrovsky Institute of Physical Chemistry, Czech Academy of Sciences, Dolejskova 3, 18223 Prague, Czech Republic. [2]Laboratory of Leukocyte Signaling, Institute of Molecule Genetics, Czech Academy of Sciences, Videnska 1083, Prague, Czech Republic. [3]Microscopy Unit, Institute of Experimental Medicine, Czech Academy of Sciences, Videnska 1083, 14220 Prague, Czech Republic.

*Author for correspondence (marek.cebecauer@jh-inst.cas.cz)

Received 2 June 2015; Accepted 13 November 2015

Journal of Cell Science (2016) 129, 95-107 doi:10.1242/jcs.175190

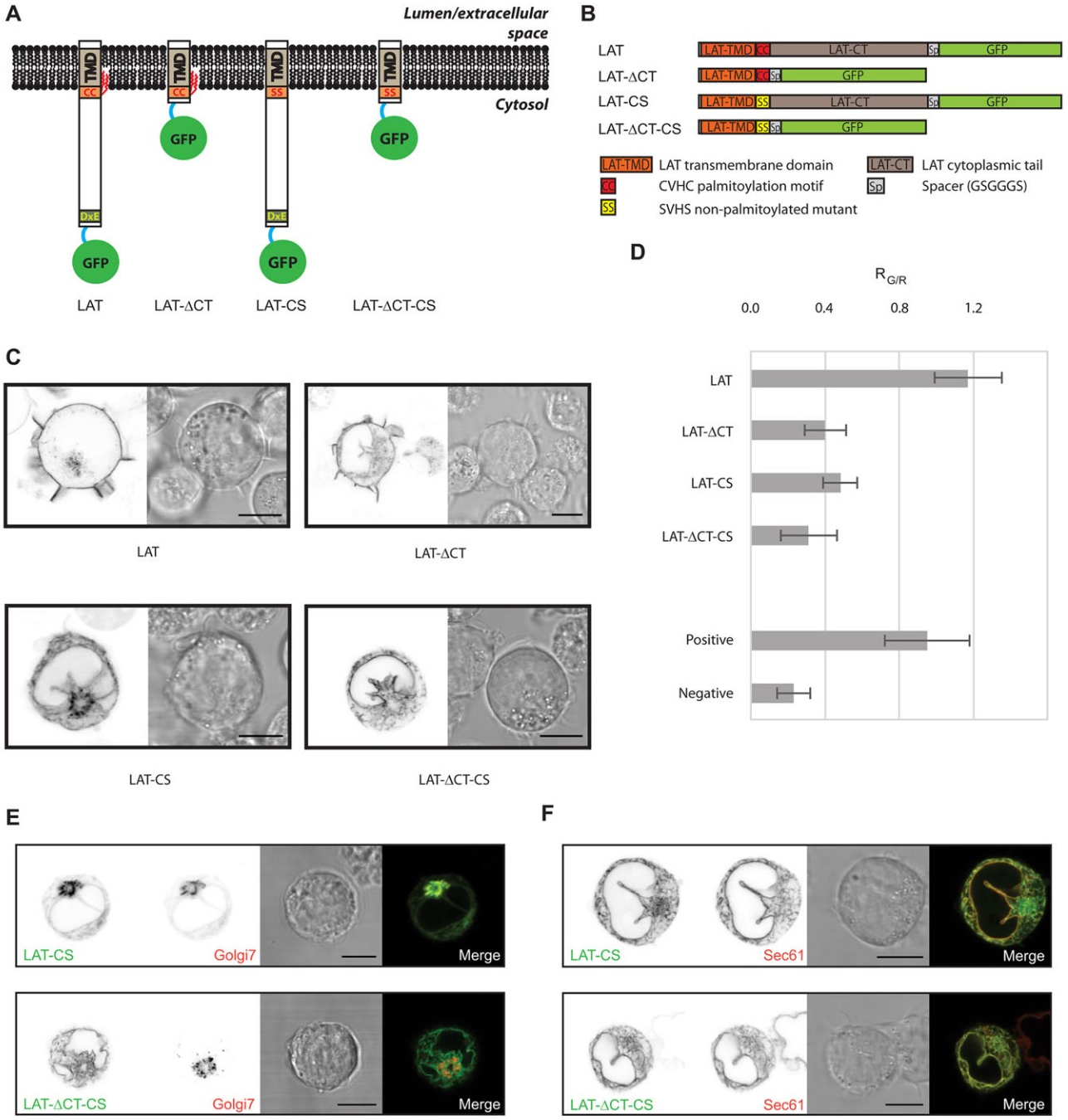

Fig. 1. Palmitoylation is essential for plasma membrane localisation of LAT. (A) Schematic illustration of LAT and its variants: lacking the intracellular domain (LAT- CT), with mutated palmitoylation site (LAT-CS), and non-palmitoylated variant lacking the intracellular domain (LAT- CT-CS). CC, CVHC motif for palmitoylation; SS, non-palmitoylatable SVHS motif; DxE, combined DxE/YxxΦ motif for the ER exit. (B) Schematic representation of wild-type LAT-GFP construct (LAT) and its variants: lacking the intracellular domain (LAT- CT); palmitoylation mutant (LAT-CS) and combined palmitoylation mutant lacking the intracellular domain (LAT- CT-CS). The lower part of the panel defines the colour coding for specific regions in LAT constructs. (C) Confocal images of live Jurkat T cells transfected with LAT (n=50), LAT- CT (n=47), LAT-CS (n=25) and LAT- CT-CS (n=26) GFP fusion proteins. The left side of each panel is a representative image acquired on the GFP channel, the right side is the corresponding bright-field image. (D) Quantitative plasma membrane localisation analysis of LAT variants in transfected Jurkat T cells (as in C). Relative values are shown where $R_{G/R}$~1 corresponds to plasma membrane localisation comparable to native LAT, $R_{G/R}$~0 indicates retention of proteins in the intracellular membranes. See Table 3 for details. Error bars represent s.d. For controls, Jurkat T cells were co-transfected with LAT-GFP/PAG-mCherry (Positive) or Sec61-GFP/LAT-mCherry (Negative). (E,F) Two-colour confocal images of LAT-CS (upper panel) and LAT- CT-CS (lower panel) GFP fusion proteins (green) and markers for the Golgi complex (E; Golgi7, red) or ER (F; Sec61, red). Images from left to right represent GFP channel, marker channel, corresponding bright-field and merged image of GFP and red channels. Scale bars: 5 µm.

the transmembrane domain, although for some family members it has not yet been proven experimentally. Palmitoylation stabilises the plasma membrane localisation of a number of myristoylated or farnesylated peripheral membrane proteins such as Ras or Src family proteins (Rocks et al., 2010). The importance of palmitoylation for plasma membrane localisation of LAT, a

Journal of Cell Science (2016) 129, 95-107 doi:10.1242/jcs.175190

member of the pTRAP subfamily, has also been reported (Hundt et al., 2009). Palmitoylation is also believed to target some pTRAPs to putative sphingolipid- and cholesterol-enriched membrane microdomains called lipid rafts (Horejšší et al., 2010; Levental et al., 2010). Levental and co-workers recently combined these two concepts and suggested that the capacity to associate with lipid rafts is a determinant of protein plasma membrane localisation (Diaz-Rohrer et al., 2014). In this study, we were interested in the impact of palmitoylation and TMD sequence (including adjacent sequences) on the plasma membrane localisation of pTRAP family proteins. Using a panel of mutant proteins and live cell imaging we reveal a complexity of determinants for plasma membrane targeting, specific for each individual membrane protein. Our data confirm the dominant impact of TMD length and/or hydrophobicity on plasma membrane localisation of proteins, but we also demonstrate that secondary sorting determinants such as palmitoylation, flanking sequences and the presence of the extracellular domain also contribute to plasma membrane localisation of proteins with suboptimal TMD length. We provide evidence that the intracellular domain (ER exit motifs) facilitates the flow of proteins towards the plasma membrane. The data indicate that more than one sorting determinant defines the dynamic localisation of proteins in cells.

RESULTS

Importance of palmitoylation and the intracellular domain for the plasma membrane localisation of LAT, PAG and NTAL proteins

The absence of a glycosylated extracellular domain suggests that TMD length and composition and/or other factors such as palmitoylation determine localisation of pTRAPs. The effect of TMD length and composition has recently been analysed by Munro and colleagues (Sharpe et al., 2010). They used a bioinformatics approach and found a strong correlation between the length and hydrophobicity of the TMD and the protein localisation. According to their results, TMDs of 22 residues and longer preferentially localise to the plasma membrane. In addition, specific distribution of side chain size and hydrophobicity throughout the TMD also correlated with protein subcellular distribution. Based on these data they created an algorithm (available online at www.tmdsonline.org as 'TMD organelle predictor') which predicts the localisation of membrane proteins in fungi and vertebrates to various cellular membranes (ER, Golgi complex and plasma membrane) based purely on the amino acid sequence. The algorithm has an overall success rate of 82% for prediction of plasma membrane localisation. However, analysis of all six human monomeric pTRAPs using this algorithm predicted the localisation of only three proteins to the plasma membrane, and localisation of the remaining three to the ER (Table 1). Five members of the pTRAP family have TMD lengths of 22–23 residues (Table 1) indicating that these proteins should be efficiently sorted to the plasma membrane. NTAL possesses a shorter TMD of 19 residues which falls outside of this range and was predicted to reside in the ER. LIME and PRR7, both with long TMDs, are also predicted to localise to the ER. As available data show that all these transmembrane adaptors are localised at the surface of human cells (Stepanek et al., 2014), we concluded that other determinants, not considered by the prediction algorithm, might contribute to the plasma membrane localisation of pTRAPs. It is worth noting that the bioinformatics tool 'TMD organelle predictor' was not designed for palmitoylated proteins.

In order to better characterise what determines plasma membrane localisation of these adaptors we selected three representative members of the pTRAP protein family: LAT, PAG and NTAL (Stepanek et al., 2014). To visualise sorting of these pTRAPs, green fluorescent protein (GFP) fusion variants (Fig 1A,B; Fig 2A; Fig. S1A) were expressed in a human T cell line (Jurkat, native environment) and cells of epithelial origin (HeLa, non-native environment) and imaged using live cell confocal microscopy. First, we verified the expression of wild-type variants of these fusion proteins and found that LAT, PAG and NTAL all almost exclusively localised in the plasma membrane of Jurkat (Fig 1C, Fig 2B; Fig. S1B) and HeLa cells (data not shown). Palmitoylation of pTRAPs is essential for their function (Stepanek et al., 2014) and is mainly thought to be a targeting signal for lipid rafts (Levental et al., 2010). Immunofluorescence of a non-palmitoylatable mutant of LAT revealed its mislocalisation to the intracellular membranes of human T cells (Hundt et al., 2009). We were, therefore, interested whether palmitoylation controls plasma membrane localisation of other pTRAPs, PAG and NTAL. pTRAPs are palmitoylated at the membrane proximal cysteines of the cytosolic tail (Fig. 1A). Transient expression of GFP fusion proteins with these cysteines mutated to serines (CS variants) demonstrated hindered plasma membrane localisation for non-palmitoylated LAT-CS (Fig. 1C,D, Table 3). Conversely, only a weak effect of Cys→Ser mutation was observed for PAG and NTAL proteins (Fig. 2B,C; Fig. S1B). Retention of LAT-CS in the Golgi complex was shown not to result from reduced kinetics of sorting; no plasma membrane localisation was observed in cells with blocked protein synthesis for 4–6 h (25 µg/ml cycloheximide; data not shown). Rather, LAT-CS mislocalisation led to its degradation. The surface expression of non-mutated LAT was unaffected in cyclohexamide-treated cells.

Changes in structure can cause re-orientation of proteins in membranes. Indeed, bioinformatics analysis (TMHMM 2.0; Krogh et al., 2001) suggests that non-palmitoylated LAT-CS is a type II membrane protein (cytosolic N-terminus). Native LAT protein is a type I protein (extracellular N-terminus). We, therefore, tested the orientation of LAT and LAT-CS proteins using a glycosylation assay (see Fig. S1C for more details) (van Geest and Lolkema, 2000). No difference in orientation between LAT and LAT-CS was observed (Fig. S1C).

Table 1. Predicted localisation of human pTRAP proteins

Protein name	UniProt* code	TMD length‡	Predicted localisation§	Prediction confidence§
LAT	O43561	23	Plasma membrane	Excellent
PAG	Q9NWQ8	23	Plasma membrane	Good
NTAL	Q9GZY6	19	Endoplasmic reticulum	Excellent
LIME	Q9H400	23	Endoplasmic reticulum	Excellent
PRR7	Q8TB68	22	Endoplasmic reticulum	Poor
SCIMP	Q6UWF3	23	Plasma membrane	Excellent

*UniProt database at http://www.uniprot.org/.

‡ TMD length determined using TMHMM 2.0 algorithm available at http://www.cbs.dtu.dk/services/TMHMM/; verified at http://www.tmdsonline.org/.

Journal of Cell Science (2016) 129, 95-107 doi:10.1242/jcs.175190

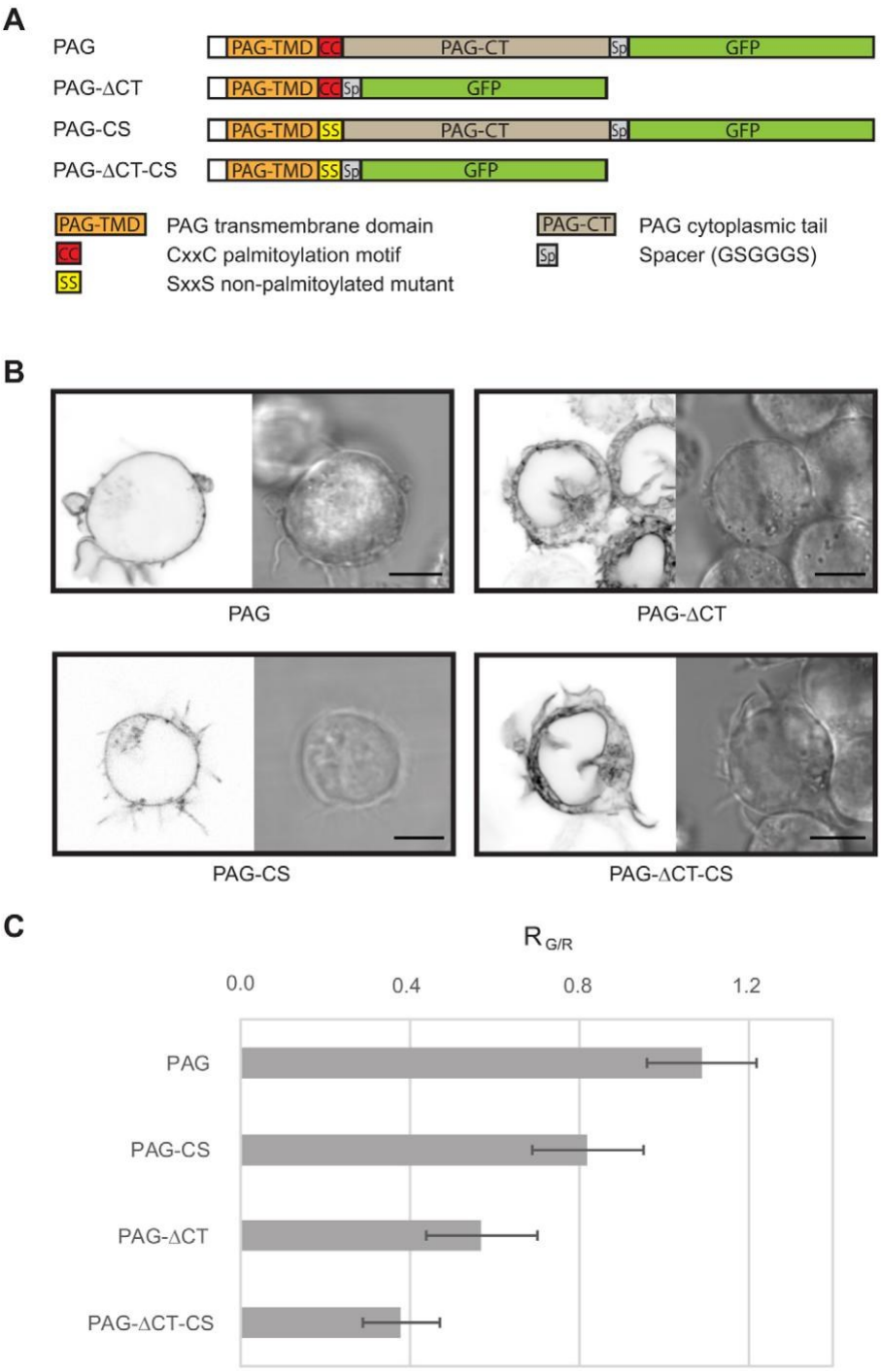

Fig. 2. PAG surface expression is independent of palmitoylation. (A) Schematic representation of wild-type PAG-GFP construct (PAG) and its variants: lacking the intracellular domain (PAG- CT); palmitoylation mutant (PAG-CS) and combined palmitoylation mutant lacking the intracellular domain (PAG- CT-CS). The lower part of the panel defines the colour coding for specific regions in PAG constructs. (B) Confocal images of live Jurkat T cells transfected with PAG (n=22), PAG- CT (n=26), PAG-CS (n=16) and PAG- CT-CS (n=24) GFP fusion proteins. The left side of each panel is a representative image acquired on the GFP channel, the right side is the corresponding bright-field image. Only cells with very low expression of PAG-CS mutants could be analysed because of a strong toxicity of these constructs in Jurkat T cells. Scale bars: 5 µm.
(C) Quantitative plasma membrane localisation analysis of PAG variants in transfected Jurkat T cells (as in B). Relative values are shown where $R_{G/R}$~1 corresponds to plasma membrane localisation comparable to native PAG, $R_{G/R}$~0 indicates retention of proteins in the intracellular membranes. See Table 3 for details. Error bars represent s.d.

We were further interested in whether TMD, together with palmitoylation, are sufficient for plasma membrane localisation and generated LAT and PAG mutants missing the intracellular domain (LAT: 34–262 residues; PAG: 44–432 residues). Both palmitoylated and non-palmitoylated versions of short variants were tested. Fig. 1C,D shows poor plasma membrane localisation of palmitoylated short LAT variant and retention of its non-palmitoylated counterpart in the ER. Similarly to LAT, removal of the intracellular domain of PAG reduced sorting to the plasma membrane. By contrast, its palmitoylated and non-palmitoylated variants exhibited comparable distribution between the ER and plasma membrane, confirming that palmitoylation does not influence sorting of PAG to the plasma membrane (Fig. 2B). Co-localisation analysis with markers of the Golgi complex (Golgi7) and ER (Sec61) demonstrated that non-palmitoylated LAT remained localised to the Golgi complex (Fig. 1E) whereas non-palmitoylated LAT missing the intracellular domain was retained in the ER (Fig. 1F). This was supported by quantitative analysis of plasma membrane localisation efficiency. Plasma membrane localisation efficiency of non-palmitoylated LAT lacking the intracellular domain was comparable to the negative control represented by ER marker Sec61 (Fig. 1D). In summary, we demonstrate here that palmitoylation is essential for plasma membrane localisation of LAT but not for PAG and NTAL and

Journal of Cell Science (2016) 129, 95-107 doi:10.1242/jcs.175190

that cytoplasmic domain of LAT and PAG also plays an important role in this process.

Addition of the extracellular glycosylated domain recovers plasma membrane localisation of non-palmitoylated LAT

The glycosylated extracellular domain of some proteins has been demonstrated to provide sufficient plasma membrane localisation signal (Potter et al., 2006; Proszynski et al., 2004). We were, therefore, interested in whether the lack of a large glycosylated extracellular domain in pTRAPs could be the reason for their increased dependence on palmitoylation and cytoplasmic sequences for plasma membrane localisation. To test the role of the extracellular domain on pTRAP localisation, we selected the extracellular region of T cell surface molecule CD4, which is relatively large, N-glycosylated and contains four immunoglobulin-like domains. In the native CD4 molecule it is followed by a transmembrane domain and a short cytoplasmic domain. The transmembrane domain is directly followed by a palmitoylation site (composed of two cysteine residues), which is very similar to the palmitoylation sites in pTRAPs. As shown in Fig. 3A, mutations of these cysteines did not have any effect on CD4 surface expression in human T cells. We fused the extracellular domain of CD4 (CD4ex) to the full coding sequence of LAT and its variants lacking the palmitoylation motif and/or cytoplasmic domain (Fig. 3B,C). The addition of the CD4 extracellular domain to the native LAT sequence (CD4ex-LAT) did not affect its surface expression in human T cells

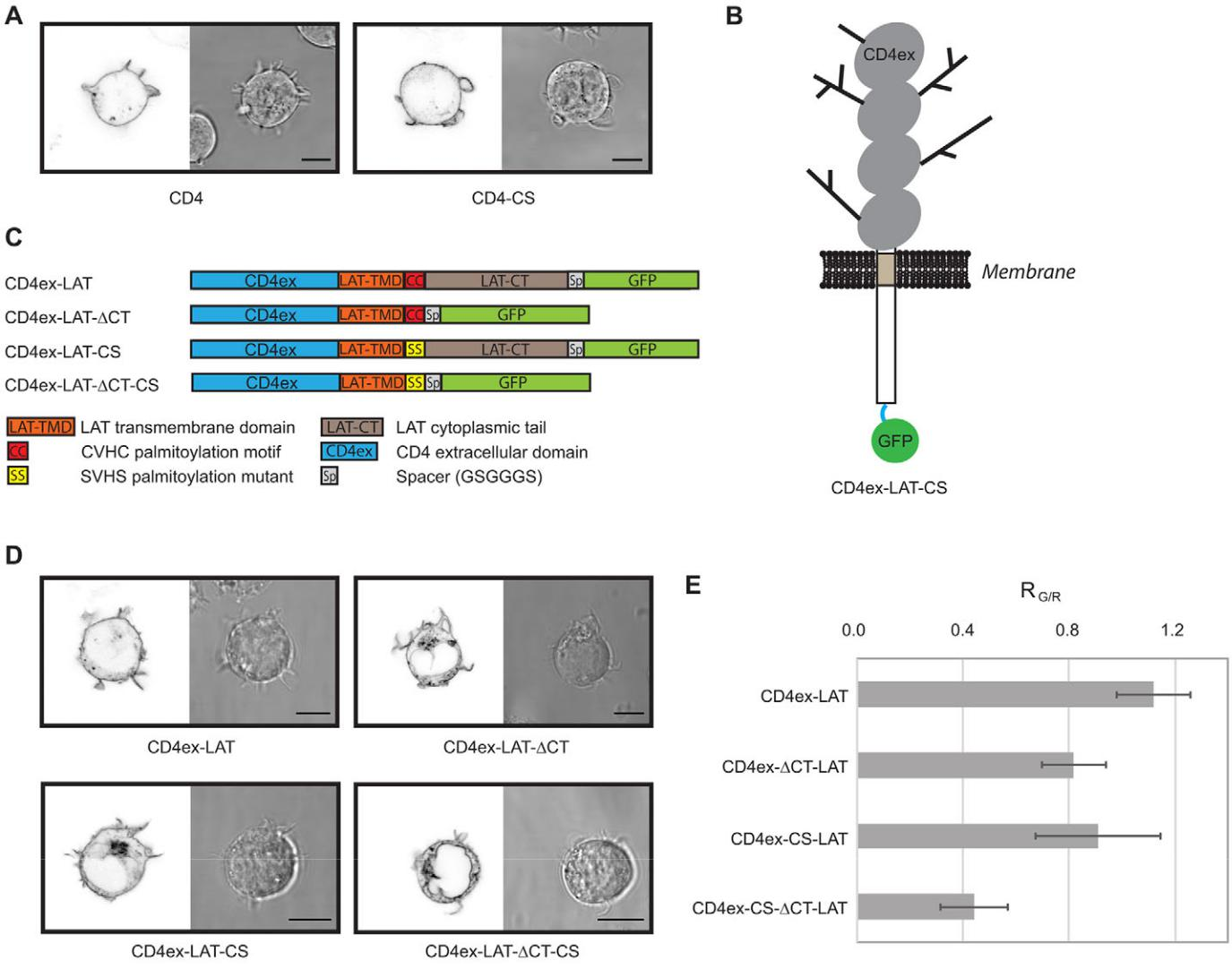

Fig. 3. Glycosylated extracellular domain facilitates sorting of LAT to the plasma membrane. (A) Confocal images of live Jurkat T cells transfected with GFP fusion proteins of wild-type human CD4 (n=15) and its palmitoylation mutant CD4-CS (n=12). The left side of each panel is a representative image acquired on the GFP channel, the right side is the corresponding bright-field image. (B) Schematic illustration of non-palmitoylated LAT mutant with added CD4 extracellular domain (CD4ex-LAT-CS; CD4ex, the extracellular domain of CD4). (C) Schematic representation of LAT-GFP variants: with added extracellular domain of human CD4 (CD4ex-LAT); with added extracellular domain of human CD4 but lacking the intracellular region of LAT (CD4ex-LAT- CT); with extracellular domain of human CD4 added to the LAT palmitoylation mutant (CD4ex-LAT-CS); and with extracellular domain of human CD4 added to the combined palmitoylation mutant lacking the intracellular region (CD4ex-LAT- CT-CS). The lower part of the panel defines the colour coding for specific regions in CD4ex-LAT constructs.
(D) Confocal images of live Jurkat T cells transfected with CD4ex-LAT (n=14), CD4ex-LAT- CT (n=18), CD4ex-LAT-CS (n=21) and CD4ex-LAT- CT-CS (n=22) GFP fusion proteins. The left side of each panel is a representative image acquired on the GFP channel, the right side is the corresponding bright-field image. Scale bars: 5 µm in A,D. (E) Quantitative plasma membrane localisation analysis of CD4ex-LAT variants in transfected Jurkat T cells (as in D). Relative values are shown where $R_{G/R}$~1 corresponds to plasma membrane localisation comparable to native LAT, $R_{G/R}$~0 indicates retention of proteins in the intracellular membranes. See Table 3 for details. Error bars represent s.d.

Journal of Cell Science (2016) 129, 95-107 doi:10.1242/jcs.175190

(Fig. 3D, upper left panel). Conversely, when this domain was attached to the non-palmitoylated LAT-CS mutant (CD4ex-LAT-CS), clear plasma membrane localisation was observed (Fig. 3D, lower left panel). This is in contrast to LAT-CS lacking the extracellular domain which exhibited no plasma membrane localisation (Fig. 1C). Similarly, the presence of the CD4 extracellular domain in the non-palmitoylatable CD4ex-LAT-

CT-CS variant missing the intracellular domain of LAT caused its weak but reproducible plasma membrane localisation (Fig. 3D, lower right panel). These data demonstrate the role of a glycosylated extracellular domain in plasma membrane localisation of proteins lacking other sorting determinants. Moreover, the additional effect of protein palmitoylation on the surface expression was reproduced by chimeric LAT proteins containing the extracellular domain of CD4.

Asymmetry of the artificial TMD augments plasma membrane localisation of TRAP-like proteins

Characterisation of chimeric and mutant LAT and PAG proteins suggests important roles for palmitoylation and both extra- and intracellular domains in protein sorting (Figs 1–3). To further address this effect we designed model TRAP-like proteins containing artificial TMDs followed by the intracellular domain of CD247, and transiently expressed these proteins in Jurkat cells. 'TRAP-like' here refers to an overall topological similarity to TRAP family proteins: monomers with a very short extracellular domain, a single transmembrane domain and an intracellular domain lacking enzymatic function. Our work was inspired by earlier findings that highly hydrophobic artificial sequences can provide a signal for membrane anchorage of model proteins (Munro, 1991, 1995). In these studies, the model TMDs were fused to the extracellular and intracellular domain of CD8α (UniProt ID P01732) and alpha-2,6-sialyltransferase (ST6GALNAC2), non-palmitoylated membrane proteins of type I and type II, respectively. The lengths of these TMDs were found to be important for protein sorting, with longer TMDs preferentially localising to the plasma membrane and shorter TMDs to the Golgi complex. Other parts of these proteins outside TMDs were also shown to play a role.

For our experiments we selected variants of peptide LW21 as an artificial transmembrane domain. LW21 has 21 hydrophobic residues and has been used *in vitro* as a model transmembrane peptide in a number of biophysical studies (Fastenberg et al., 2003; Kaiser et al., 2011; Machán˘ et al., 2014). The length of this peptide is close to the optimal TMD length for plasma membrane localisation of vertebrate membrane proteins (Sharpe et al., 2010).

We found TRAP-like proteins with LW21 to be expressed at the surface of transiently transfected Jurkat cells (data not shown), and subsequently designed a TMD of 19 hydrophobic residues to represent a suboptimal (short) plasma membrane localisation signal. LW19 TMD was obtained by modifying the LW21 sequence by removing two C-terminal tryptophan residues (Table 2). The remaining tryptophan residues at the extracellular end of the hydrophobic stretch mimic the TMDs of PAG and NTAL. We generated TRAP-like protein variants composed of LW19 TMD, the intracellular domain of CD247 and C-terminal GFP for visualisation. CD247 was selected to limit the impact of 'backbone' on plasma membrane localisation. A GFP fusion protein of CD247 is retained in the ER in the absence of remaining subunits of the TCR/CD3 complex (Fig. S2), suggesting that CD247 does not contain any dominant sorting sequence mediating its transport further down the exocytic pathway. In addition, CD247 is not palmitoylated. However, it shares a similar overall structure with other TRAP proteins such as LAT. Because the sequence of LW19 TMD is symmetric but the plasma membrane is asymmetric, we therefore generated two versions of LW19 TMD, one of which was made symmetric by adding 2 lysine residues at both ends of the hydrophobic core, and one of which was made asymmetric by adding 2 glutamic acid residues at the N-terminus (extracellular end) and 2 lysine residues at the C-terminus (intracellular end) of the hydrophobic core (Table 2; Fig. 4A,B). Designed model proteins [LW19(Sym)] maintained type I protein orientation in the membrane (Fig. S1C). Asymmetric TRAP-like protein LW19(Asym) localised at the plasma membrane and Golgi complex but not in the ER in Jurkat cells (Fig. 4C,D). By contrast, symmetric TRAP-like protein LW19(Sym) was largely maintained at the level of Golgi complex and ER (Fig. 4C,D). Weak surface expression was detected for this protein, but on very few cells (<10%). A less prominent difference in membrane distribution was observed for LW19 TRAP-like proteins lacking the intracellular domain (Fig. 4C–E). A small proportion (~20%) of cells expressing LW19- CT protein with the asymmetric TMD [LW19(Asym)-

CT] exhibited detectable sorting to the plasma membrane (Fig. 4E), but GA and ER localisation was observed in the remaining cells (Fig. 4C). However, no surface expression was observed for symmetric variant LW19(Sym)- CT even though >200 cells were inspected. These data experimentally demonstrate the importance of asymmetry for the plasma membrane protein sorting of proteins with suboptimal TMDs (Fig. 4C,D). However, a longer and highly hydrophobic asymmetric TMD was sufficient for plasma membrane localisation of TRAP-like proteins regardless of

Table 2. Sequences of TMDs of TRAP and TRAP-like proteins tested in this study

Protein	TMD sequence plus flanking residues*	Mean hydrophobicity‡
LAT	EEAILVPCVLGLLLLPILAMLMALCVHCHRLP	5
PAG	GQMQITLWGSLAAVAIFFVITFLIFLCSSCDREK	5
NTAL	SSGTELLWPGAALLVLLGVAASLCVRCSRP	4
LW19(Sym)	GLLDPKKWWLLLLLLLALLLLLLLLKKFSRS	9
LW19(Asym)	GLLDPEEWWLLLLLLLALLLLLLLLKKFSRS	9
LW21(Sym)	GLLDPKKWWLLLLLLLALLLLLLLLWWKKFSRS	ND
LW25(Sym)	GLLDPKKWWLLLLLLLLLLALLLLLLLLLLKKFSRS	9.3
LW25(Asym)	GLLDPEEWWLLLLLLLLLLALLLLLLLLLLKKFSRS	9.3
LAT-LW19(Asym)	DLGTEEWWLLLLLLLLLLALLLLLLLLLLKKGSYD	9
LAT-LW19(Asym$_{CVHC}$)	DLGTEEWWLLLLLLLLLLALLLLLLLLLLCVHCHR	9
LAT-LW19(Asym$_{SVHS}$)	DLGTEEWWLLLLLLLLLLALLLLLLLLLLSVHSHR	9

*Hydrophobic stretch is highlighted in bold. Putative palmitoylation sites (cysteines) are underlined.

‡Mean hydrophobicity of the hydrophobic stretch (bold) was calculated using HydroMCalc algorithm (Tossi et al., 2002). Hydrophobicity scale is −10 to +10. An average value calculated for randomly selected 20 amino acids is −3. ND, not determined.

Journal of Cell Science (2016) 129, 95-107 doi:10.1242/jcs.175190

Table 3. Quantitation of plasma membrane localisation

Protein variant (GFP fusion)	$R_{G/R}$	$\sigma_{R(G/R)}$	n (cells)	Plasma membrane GFP expression [%]*	$\sigma_{R(GFP)}$ [%]	Plasma membrane mCherry expression [%]‡	$\sigma_{R(mCherry)}$ [%]
LAT	1.17	0.18	15	32.5	12.0	27.6	9.4
LAT-CS	0.39	0.11	31	12.2	4.6	31.4	8.4
LAT- CT	0.48	0.09	10	13.1	3.8	27.5	8.0
LAT- CT-CS	0.31	0.15	17	8.4	5.2	27.2	7.6
PAG	1.09	0.13	18	39.2	13.8	35.8	11.9
PAG-CS	0.82	0.13	19	24.3	9.3	30.2	11.2
PAG- CT	0.57	0.13	12	15.9	6.1	28.2	10.4
PAG- CT-CS	0.38	0.09	20	10.3	3.1	27.1	5.1
CD4ex-LAT	1.12	0.14	19	31.4	5.9	28.2	4.7
CD4ex-LAT-CS	0.91	0.24	23	26.4	7.1	29.3	4.9
CD4ex-LAT- CT	0.82	0.12	22	20.9	3.7	26.0	5.5
CD4ex-LAT- CT-CS	0.44	0.13	18	12.3	3.8	29.0	7.8
CD4	1.32	0.18	16	30.5	8.5	23.4	6.8
CD4-CS	1.22	0.10	13	33.4	7.5	27.6	6.8
LW19(Sym)	0.75	0.33	25	15.3	6.8	21.5	5.9
LW19(Asym)	1.19	0.33	12	22.8	7.4	19.6	4.7
LW19(Sym)- CT	0.53	0.09	22	12.8	4.1	24.0	6.7
LW19(Asym)- CT	0.61	0.14	23	14.2	6.9	22.8	9.1
LW25(Sym)	1.18	0.23	17	34.1	10.1	29.4	8.8
LW25(Asym)	1.35	0.15	17	41.8	8.6	30.9	5.4
LW25(Sym)- CT	0.63	0.05	19	17.6	4.7	28.0	6.5
LW25(Asym)- CT	0.72	0.09	20	16.3	5.0	22.6	6.3
LAT-LW19(Asym)	1.30	0.14	16	38.5	5.9	29.7	3.8
LAT-LW19(Asym)- CT	0.59	0.10	41	14.7	4.2	25.1	6.5
LAT_LW19(Asym)$_{CVHC}$- CT	0.72	0.11	14	17.2	5.3	24.6	7.8
LAT_LW19(Asym)$_{SVHS}$- CT	0.36	0.10	15	8.3	2.1	25.1	10.5
Positive control	0.95	0.12	11	28.1	5.2	29.0	5.4
Negative control	0.23	0.09	6	5.5	2.8	25.0	6.6

*Percentage of GFP expressed at the plasma membrane, calculated as $R(GFP)=(I_{PM}(GFP)/I_{Cell}(GFP))$.

‡ PM Cell Percentage of mCherry expressed at the plasma membrane, calculated as R(mCherry)= [I (mCherry)/I (mCherry)].

whether symmetric and asymmetric versions of LW25 TRAP-like proteins were tested (Fig. 4D,F,G).

Plasma membrane localisation of palmitoylated TRAP-like proteins with the artificial TMD

Figs 1, 2 and Fig. S1 demonstrate the importance of palmitoylation for the plasma membrane sorting of LAT, but not of PAG and NTAL proteins. Because asymmetric LW19 TMD was able to mediate efficient sorting of our CD247-based artificial TRAP-like protein to the plasma membrane, we were interested in whether this TMD could rescue plasma membrane targeting of non-palmitoylated LAT. For this purpose, we replaced the TMD and palmitoylation motif in LAT with asymmetric LW19 TMD (Fig. 5A). Interestingly, the exchange of the TMD sequence of LAT protein for the highly hydrophobic, asymmetric LW19 sequence led to it sorting to the plasma membrane in the absence of palmitoylation (Fig. 5B). We did not observe any difference between asymmetric LW19 variants with CD247 or LAT 'backbones' (compare Fig. 4C with Fig. 5B). However, the absence of the intracellular domain again caused a reduction of LAT-LW19(Asym)- CT plasma membrane localisation (Fig. 5B,D). Thus, we next tested whether palmitoylation can improve plasma membrane localisation of this variant. For this experiment we inserted a LAT palmitoylation site (CVHC sequence) into LAT-LW19(Asym)- CT TRAP-like protein. Palmitoylation increased its plasma membrane localisation to almost complete surface expression level, comparable to native LAT (compare Fig. 1C with Fig. 5C). This effect was caused by the palmitoylation since the insertion of a non-palmitoylatable SVHS sequence had no impact (Fig. 5C,D). Our observations support the view that plasma membrane localisation of proteins is primarily determined by their TMD but supplementary signals, such as palmitoylation, can increase sorting efficiency.

DISCUSSION

In this study we have investigated the impact of the TMD, its flanking sequences and palmitoylation on the plasma membrane localisation of pTRAP family proteins. These proteins are essential for the proper function of various cells, facilitating signalling processes taking place at the plasma membrane. Their plasma membrane localisation is, therefore, a prerequisite for their function.

We studied the localisation of three pTRAP proteins: LAT, PAG and NTAL. Based on published data describing the correlation between TMD length and protein sorting to various cellular compartments (Sharpe et al., 2010), one would expect that in the absence of palmitoylation LAT and PAG, with TMDs of 23 residues, would localise to the plasma membrane, whereas NTAL, with a 19 amino acid TMD, would localise to the ER and Golgi complex. Intriguingly, our live cell imaging data showed that these predictions were valid only for PAG, whereas non-palmitoylated LAT was retained mainly in the Golgi complex, in agreement with data published by Hundt et al. (2009). Non-palmitoylated NTAL was sorted to the plasma membrane. Moreover, mislocalisation of LAT-CS to the Golgi complex caused its degradation. These experiments demonstrated that, in addition to TMD length, other sorting determinants such as palmitoylation also define the behaviour of pTRAPs in cell membranes.

Palmitoylation is essential for the proper function of LAT, PAG and NTAL (Brdicka et al., 2002, 2000; Posevitz-Fejfár et al., 2008; Zhang

Journal of Cell Science (2016) 129, 95-107 doi:10.1242/jcs.175190

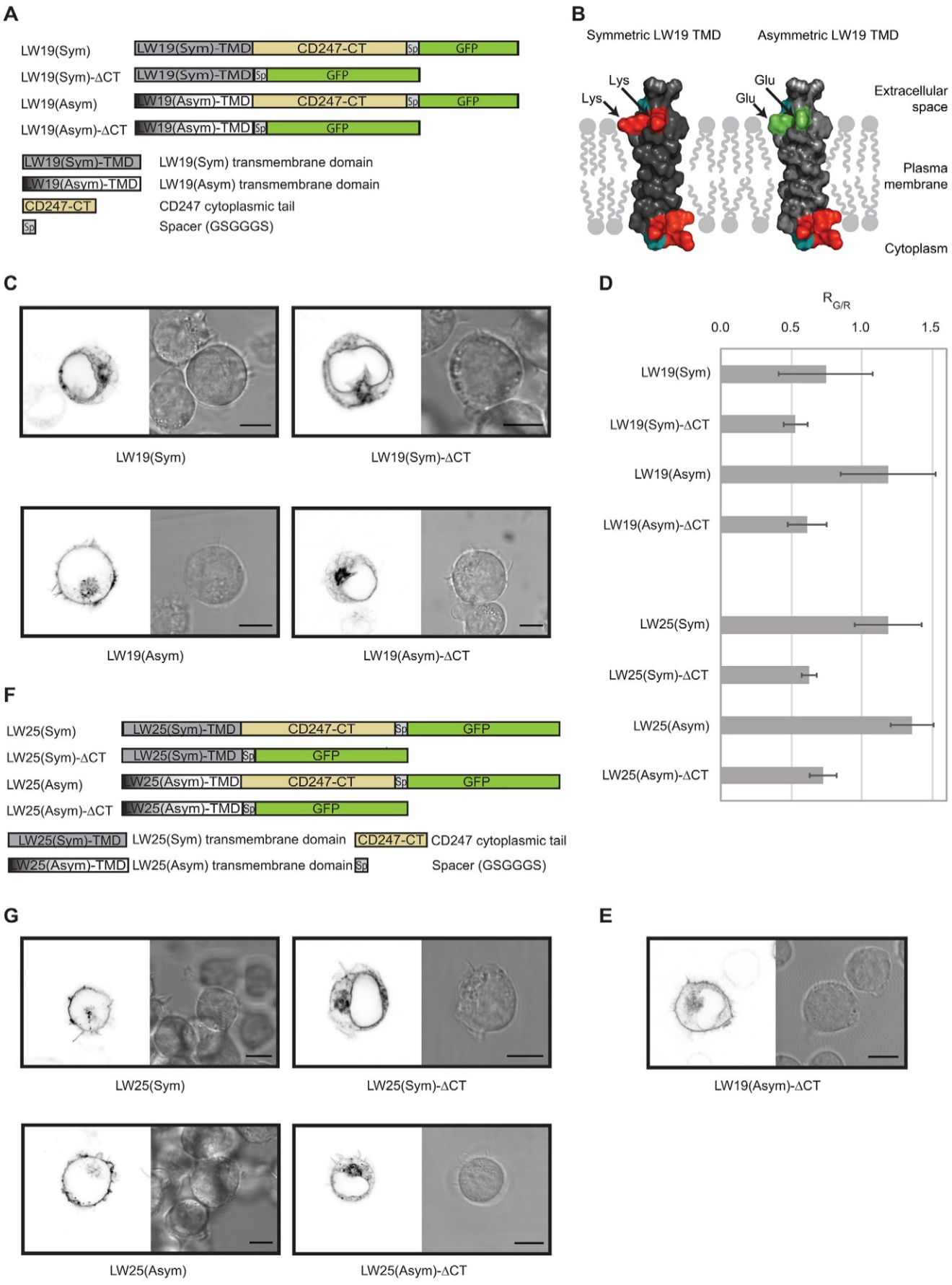

Fig. 4. See next page for legend.

Journal of Cell Science (2016) 129, 95-107 doi:10.1242/jcs.175190

Fig. 4. Asymmetry promotes plasma membrane localisation of TRAP-like proteins with a suboptimal TMD. (A) Schematic representation of model TRAP-like GFP fusion proteins: symmetric LW19 TMD with the intracellular part of CD247 [LW19(Sym)]; symmetric LW19 TMD missing the intracellular part of CD247 [LW19(Sym)- CT]; asymmetric LW19 TMD with the intracellular part of CD247 [LW19(Asym)]; and asymmetric LW19 TMD missing the intracellular part of CD247 [LW19(Asym)- CT]. All LW-based constructs contain a short extracellular domain (20 residues of c-Myc tag and CD247), a model TMD and C-terminal GFP fused to the protein via a short GSGGGS spacer (Fig. S2; Table 2). The lower part of the panel defines the colour coding for specific regions in TRAP-like protein variants. (B) Charged residues are evenly distributed in symmetric but not asymmetric LW19 TMDs. PyMOL models of α-helical TMD structures illustrate symmetric and asymmetric distribution of basic (red, Lys) and acidic (green, Glu) amino acid residues in LW19(Sym) and LW19(Asym) constructs, respectively. (C) Confocal images of live Jurkat T cells transfected with LW19(Sym) (n=63), LW19(Sym)- CT (n=56), LW19(Asym) (n=71) and LW19(Asym)- CT (n=58) GFP fusion proteins. The left side of each panel is a representative image acquired on the GFP channel, the right side is the corresponding brightfield image.

(D) Quantitative plasma membrane localisation analysis of TRAP-like proteins in transfected Jurkat T cells (as in C and G). Relative values are shown where $R_{G/R}$~1 corresponds to plasma membrane localisation comparable to native LAT, $R_{G/R}$~0 indicates retention of proteins in the intracellular membranes. See Table 3 for details. Error bars represent s.d. (E) Approximately one-fifth of cells expressing LW19(Asym)- CT variant showed surface expression (selected confocal image; as in panel C). (F) Schematic representation of model TRAP-like GFP fusion proteins: composed of a symmetric LW25 TMD and the intracellular region of CD247 [LW25(Sym)]; with a symmetric LW25 TMD lacking the intracellular region [LW25(Sym)- CT]; composed of an asymmetric LW25 TMD and the intracellular region of CD247 [LW25(Asym)]; with an asymmetric LW25 TMD lacking the intracellular region [LW25(Asym)- CT]. The lower part of the panel defines the colour coding for specific regions in TRAP-like protein constructs. (G) Confocal images of live Jurkat T cells transfected with LW25(Sym) (n=23), LW25(Sym)- CT (n=25), LW25(Asym) (n=18) and LW25(Asym)- CT (n=19) GFP fusion proteins. The left side of each panel is a representative image acquired on the GFP channel, the right side is the corresponding brightfield image. Scale bars: 5 µm in C,E,G.

et al., 1998). Here we demonstrated that non-palmitoylated PAG and NTAL showed unaltered sorting. These observations indicate that plasma membrane localisation is important but not sufficient for the function of pTRAPs in lymphocyte signalling. Super-resolution microscopy recently identified non-homogenous distribution of palmitoylated proteins in the plasma membrane (Fukata et al., 2013; Owen et al., 2010; Saka et al., 2014). This suggests that palmitoylation of PAG and NTAL, which is unresolvable using confocal microscopy, could determine their precise localisation at the plasma membrane. A loss of palmitoylation would then result in incorrect distribution of PAG and NTAL at the plasma membrane of Jurkat cells and consequently disrupt the spatio-temporal control required for their proper involvement in cell signalling (Cebecauer et al., 2010).

All LAT and PAG variants lacking the intracellular domain showed inefficient release from the ER. This was especially the case for non-palmitoylated LAT-CS- CT, which was almost exclusively resident in the ER (Fig. 1F). The data suggest that the intracellular domain encodes signals for ER exit whereas TMD and proximal sequences define the fate of membrane proteins further down the exocytic pathway. Both, LAT and PAG proteins contain DxE and YxxΦ motifs reported to provide signals for efficient exit of some proteins from the ER (Sevier et al., 2000). It was shown that mutation or deletion of a larger sequence containing these motifs, enables recycling of membrane proteins between the ER and Golgi complex and limits their sorting to the surface (Fossati et al., 2014). We speculate that by deletion of the entire intracellular domain, including combined DxE and YxxΦ motifs, we have reduced the ability of these variants to enter the later sorting machinery of the trans-Golgi/endosomal network.

We also designed artificial TRAP-like proteins containing a short model LW19 TMD and showed that, similarly to a previously used TMD composed of a stretch of 17 leucine residues (Munro, 1995), it was insufficient for sorting to the plasma membrane. Because the addition of two more hydrophobic residues in LW21 led to weak but detectable expression in the plasma membrane (data not shown), we concluded that LW19 is a suboptimal TMD for plasma membrane localisation, positioned at the borderline of the sorting length scale. This unique feature allowed us to investigate the impact of palmitoylation and proximal sequence(s) on sorting of TRAP-like proteins in more detail. For TMD proximal sequences, basic residues are enriched near the cytosolic end of the TMD of integral membrane proteins. These residues play a role during the insertion of the hydrophobic stretch of a nascent protein into the membrane (Andersson et al., 1992; Nilsson et al., 2005). By contrast, a slight increase in the presence of acidic residues near the extracellular end of the TMD was found in a comprehensive study with >700 vertebrate plasma membrane proteins analysed (Sharpe et al., 2010). Indeed, acidic amino acids are found close to the extracellular end of the TMD in some single-spanning membrane proteins of human lymphocytes (e.g. LAT, NTAL, CD8α, DAP-12). Interestingly, replacement of lysine residues with glutamic acid at the extracellular end of suboptimal LW19 TMD, and thereby generation of asymmetric LW19(Asym), led to an increase in plasma membrane localisation. Together with the preference of less voluminous hydrophobic amino acids for the exoplasmic half of the plasma membrane (Quiroga et al., 2013; Sharpe et al., 2010), these data support the importance of asymmetry in proteins with a suboptimal TMD. In addition, the increased surface localisation of palmitoylated LAT-LW19(Asym$_{CVHC}$)- CT compared with its non-palmitoylatable variant LAT-LW19(Asym$_{SVHS}$)- CT again supports the view that palmitoylation can facilitate protein sorting.

In this study we show the importance of the unique primary sequence of TMDs for the localisation of integral proteins in cell membranes. As such, we provide a novel standpoint for discussion on why so many TMDs have evolved when a handful would be sufficient for targeting membrane proteins to their proper cellular compartments (Spira et al., 2012). By contrast, no conclusive data were obtained to uncover the difference between LAT and PAG TMDs, which are formed of the same number of amino acids (23 residues). TMD sequence analysis shows that all tested TRAP proteins contain a similar number of hydrophobic (~80%) and no charged residues. No clear difference could be found by calculating mean hydrophobicity of their TMDs (Table 2) (Tossi et al., 2002). Further experiments are required to uncover the exclusive character of these TMDs, especially whether the limited presence of bulky amino acids in the hydrophobic core or the asymmetric distribution of charged residues flanking the TMD provide sufficient signal, comparable to asymmetric LW19 TRAP-like proteins tested herein. It would also be interesting to investigate how the exceptionally short 19 residue TMD of NTAL drives plasma membrane localisation in the absence of palmitoylation.

To summarise, we have confirmed the dominant impact of TMD length and hydrophobicity on plasma membrane localisation of proteins, but also provided evidence that secondary sorting determinants such as palmitoylation or flanking sequences have evolved for proteins with suboptimal TMD length. We additionally demonstrate that the presence of ER exit motifs in the intracellular domain further influences the transport of proteins towards the plasma membrane, supporting the view that more than one

Journal of Cell Science (2016) 129, 95-107 doi:10.1242/jcs.175190

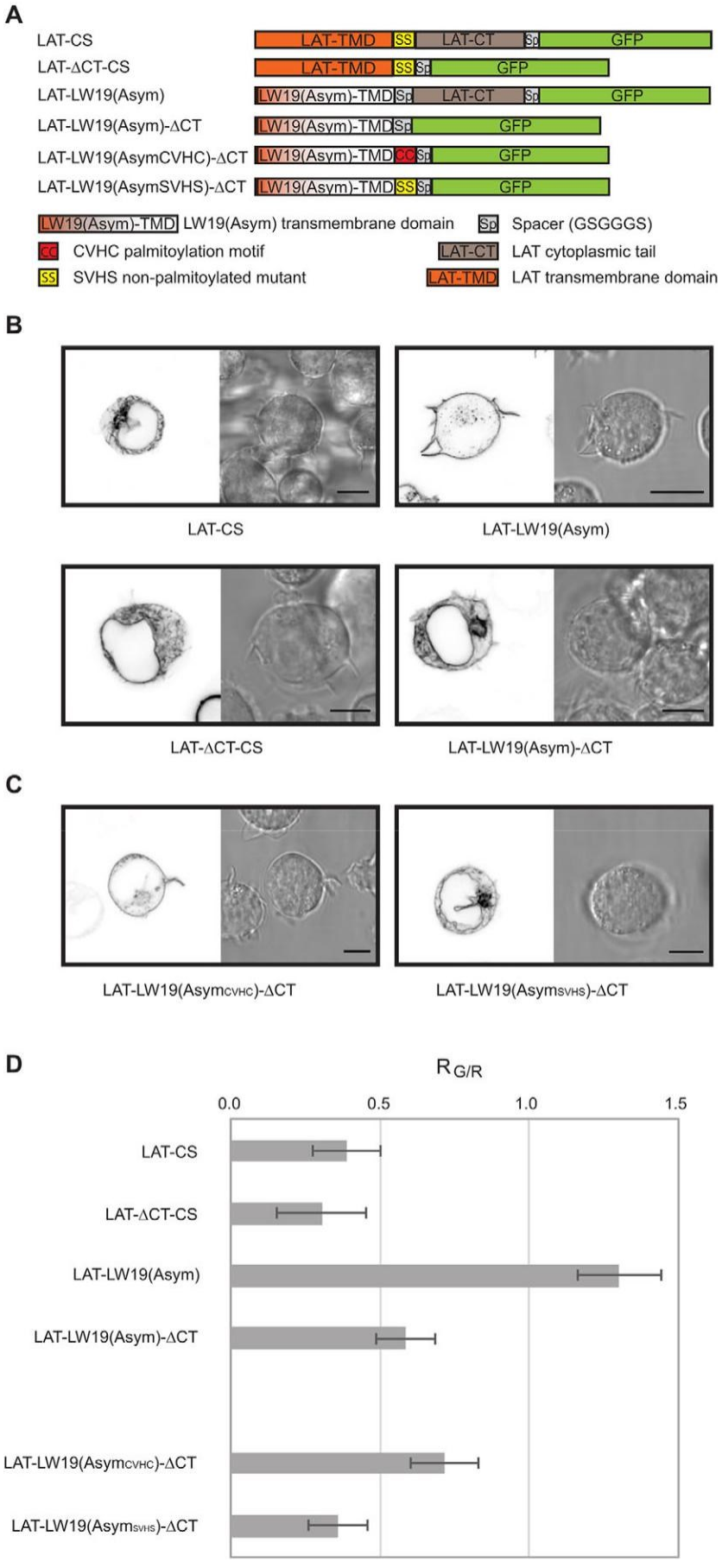

Fig. 5. Palmitoylation facilitates plasma membrane localisation of TRAP-like proteins. (A) Schematic representation of non-palmitoylated LAT variants (LAT-CS and LAT- CT-CS; as in Fig. 1B) and model TRAP-like GFP fusion proteins based on the LAT protein 'backbone'. LAT-LW19(Asym)LAT: TMD and palmitoylation site of LAT was replaced with asymmetric LW19 TMD; LAT-LW19(Asym)-CT: LAT-LW19(Asym) lacking the intracellular region; LAT-LW19(AsymCVHC)- CT: LAT-LW19(Asym)- CT with CVHC palmitoylation motif; LAT-LW19(AsymSVHS)- CT: LAT-LW19(Asym)- CT with non-palmitoylatable SVHS motif. All LW-based LAT 'backbone' constructs contain short extracellular domains (18 residues of c-Myc tag and LAT), a model TMD and C-terminal GFP fused to the protein via a short GSGGGS spacer (Fig. S3; Table 2). The lower part of the panel defines the colour coding for specific regions of TRAP-like protein constructs. (B) Confocal images of live Jurkat T cells transfected with LAT-CS (n=26), LAT- CT-CS (n=25), LAT-LW19(Asym) (n=13) and LAT-LW19(Asym)-CT (n=17) GFP fusion proteins. (C) Confocal images of live Jurkat T cells transfected with LAT-LW19(AsymCVHC)- CT (n=21) and LAT-LW19(AsymSVHS)- CT (n=19) GFP fusion proteins. The left side of each panel is a representative image acquired on the GFP channel, the right side is the corresponding bright-field image. Scale bars: 5 µm in B,C. (D) Quantitative plasma membrane localisation analysis of LAT mutants in transfected Jurkat T cells (as in B and C). Relative values are shown where $R_{G/R}$~1 corresponds to plasma membrane localisation comparable to native LAT, $R_{G/R}$~0 indicates retention of proteins in the intracellular membranes. See Table 3 for details. Error bars represent s.d.

Journal of Cell Science (2016) 129, 95-107 doi:10.1242/jcs.175190

determinant plays in concert to define the precise localisation of proteins in cells.

MATERIALS AND METHODS

Cell culture, transfection and biochemical procedures

Jurkat T and HeLa (or HEK293) cell lines were grown in RPMI-1640 and DMEM media, respectively (Sigma-Aldrich), supplemented with glutamine and 10% foetal calf serum (Life Technologies) at 37°C under 5% CO_2 in a humidified incubator. These cells originate from the cell bank of the Institute of Molecular Genetics in Prague, Czech Republic, are regularly tested for surface markers, morphology and contamination.

Jurkat cells were transiently transfected using Neon® transfection system (Life Technologies). According the manufacturer's instructions, 1 µg of vector DNA per shot per 50,000 cells was used. HeLa and HEK293 cells were grown at >50% confluency on clean coverslips for minimum of 18 h before transfection. For transfection, 500 ng of DNA was mixed with 1.5 µl of Fugene HD transfection reagent (Promega) in 25 µl OptiMEM, incubated for 20 min at ambient temperature and dispersed onto cultured cells in 24-well plates. Live cell imaging was performed 16–24 h after transfection.

To immunoprecipitate GFP-tagged proteins from the transfected cells, transfectants were lysed in lysis buffer [50 mM Tris pH 7.5, 150 mM NaCl, 1 mM AEBSF (Sigma-Aldrich)] containing 1% n-dodecyl-β-D-maltoside followed by immunoprecipitation with GFP-specific rabbit antisera (kind gift from Llewelyn Roderick, University of Wales). The immunoprecipitated proteins were detected by immunoblotting with the same anti-GFP antibody.

DNA cloning

Plasmid pXJ41-EGFP was prepared by PCR amplification of the EGFP sequence of vector pEGFP-N1 with a spacer (GSGGGS) attached to the N-terminus (primers T198 and T199; see list of all primers in Table S1) and sub-cloning into the BamHI and XhoI restriction sites of vector pXJ41 (Xiao et al., 1991). For further cloning, restriction sites KpnI and BglII in the pXJ41-EGFP construct were eliminated by mutation. We designed a modular system for cloning of pTRAP variants with or without the intracellular domain and with the possibility to exchange the sequence encoding the TMD and flanking 4–5 residues (Fig. S3A). A DNA fragment encoding the LAT sequence was synthesised by GeneArt (Invitrogen) and includes the 5′ UTR and leader sequence of human CD148, followed by a Myc-tag and the entire coding sequence of LAT without the ATG start codon. The Myc-tag sequence and the coding sequence of LAT were separated by a KpnI restriction site. A silent mutation was inserted into the LAT sequence (residues GGC→GGA) to introduce a BamHI restriction site between the TMD and the intracellular domain. Restriction sites NotI and BamHI (partial digestion) were used for sub-cloning and generation of a pXJ41-LAT-EGFP vector. A pXJ41-LAT- CT-EGFP variant was generated by deletion of the sequence encoding the intracellular domain using BamHI restriction sites and self-ligation. CS mutation was introduced into the pXJ41-LAT- CT-EGFP vector by amplification of its TMD sequence (using primers T255 and T256) and sub-cloning of the LAT-CS TMD sequence instead of the LAT TMD using KpnI and BamHI cloning sites. A full length version was generated by sub-cloning of the LAT intracellular sequence into pXJ41-LAT- CT-CS-EGFP using BamHI restriction sites.

A pXJ41-PAG- CT-EGFP vector was prepared by amplification of the PAG TMD sequence (using primers T257 and T258) from plasmid PAG/pEFIRES-N1 and sub-cloning it into vector pXJ41-LAT- CT-EGFP instead of the LAT TMD sequence using cloning sites KpnI and BamHI. The PAG intracellular region was amplified from PAG/pEFIRES-N1 (using primers T259 and T260) and sub-cloned into vector pXJ41-PAG- CT-EGFP using BamHI restriction sites to generate pXJ41-PAG-EGFP. A CS version of PAG- CT was prepared the same way except for the use of primer T263 instead of T258 to introduce the CS mutation. The PAG intracellular region amplified from plasmid PAG/pEFIRES-N1 was than sub-cloned into vector pXJ41-PAG- CT-CS-EGFP to generate pXJ41-PAG-CS-EGFP. Full-length LAT and PAG sequences were also cloned as fusions with mCherry fluorescent protein by replacing the EGFP sequence in pXJ41-LAT-EGFP and pPAG-EGFP with a sequence encoding mCherry from plasmid pcDNA3.1-mCherry (kind gift from Marco Purbhoo, Imperial College London).

The DNA sequence of the CD4 extracellular region was amplified (using primers T246 and T297) from plasmid CD4/pEGFP-N1 and sub-cloned into vectors pXJ41-LAT-EGFP, pXJ41-LAT-CS-EGFP, pXJ41-LAT- CT-EGFP and pXJ41-LAT- CT-CS-EGFP through EcoRI and KpnI restriction sites, to generate pXJ41-CD4ex-LAT-EGFP, pXJ41-CD4ex-LAT-CS-EGFP, pXJ41-CD4ex-LAT- CT-EGFP and pXJ41-CD4ex-LAT-CT-CS-EGFP constructs.

To generate pXJ41-LW19(Sym)-EGFP and pXJ41-LW19(Asym)-EGFP, DNA fragments encoding symmetric and asymmetric variants of LW19 fused to the CD247 intracellular domain were synthesised by GeneArt (Invitrogen) and sub-cloned into plasmid pXJ41-LAT-EGFP using restriction sites KpnI and BamHI, replacing the coding sequence of LAT. During the fragment synthesis, the native BamHI site in the CD247 sequence was removed and a BglII restriction site newly inserted into the CD247 sequence (AGGAGC→AGATCT) to separate the TMD and the intracellular domain. pXJ41-LW25(Sym)-EGFP and pXJ41-LW25(Asym)-EGFP constructs were generated from respective LW19 constructs by site-directed mutagenesis. To achieve this, from each template [pXJ41-LW19 (Sym)-EGFP or pXJ41-LW19(Asym)-EGFP], two separate overlapping cDNA fragments were synthesised by PCR with primer pairs T295/T292, and T291/T296. These fragments were then fused in a subsequent PCR reaction using flanking primers T295 and T296 and subcloned into the KpnI and BamHI sites of pXJ41-LAT-EGFP, replacing the coding sequence of LAT. CT variants of all these LW constructs were generated by deletion of the sequence encoding the intracellular domain using BglII and BamHI restriction and self-ligation for the generation of constructs pXJ41-LW19 (Sym)- CT-EGFP, pXJ41-LW19(Asym)- CT-EGFP, pXJ41-LW25 (Sym)- CT-EGFP and pXJ41-LW25(Asym)- CT-EGFP.

The asymmetric variant of LW19 in a LAT 'backbone' was amplified from the pXJ41-LW19(Asym)-EGFP construct (using primers T289 and T290) and sub-cloned into vectors pXJ41-LAT-EGFP and pXJ41-LAT-CT-EGFP using restriction sites EcoRI and BamHI to generate vectors LAT-LW19(Asym) and LW19(Asym)LAT- CT, respectively. To introduce the CVHC motif into the sequence of LAT-LW19(Asym)- CT construct we amplified its TMD sequence using primers T290 and T294, and then sub-cloned the mutated sequence into the pXJ41-LAT- CT-EGFP vector using EcoRI and BamHI restriction sites to generate the LAT-LW19(Asym$_{CVHC}$) LAT- CT construct. The cloning strategy for LAT-LW19(Asym$_{SVHS}$)LAT-CT construct was the same with the exception of using a different set of primers (T290, T298).

The pXJ41-NTAL-EGFP vector was generated by amplification of the NTAL coding sequence (using primers NTAL wt fwd EcoRI, NTAL rev BamHI) from the NTAL-pFLAG-CMV plasmid and sub-cloning into vector pXJ41-LAT-EGFP through EcoRI and BamHI restriction sites. We inserted the CS mutation in the NTAL sequence by linking PCR (using primers NTAL wt fwd EcoRI, NTAL rev BamHI, NTAL CS fwd, NTAL CS rev) using NTAL-pFLAG-CMV plasmid as a template. The PCR product was sub-cloned into vector pXJ41-LAT-EGFP through EcoRI and BamHI restriction sites to generate pXJ41-NTAL-CS-EGFP.

A version of pXJ41-LAT- CT-EGFP without the CD148 leader, c-Myc and 5′ UTR was generated by amplification of the LAT-EGFP sequence (using primers T287 and LAT BamHI rev) and sub-cloning into the former pXJ41-LAT- CT-EGFP vector using EcoRI and BamHI restriction sites. pXJ41-LAT- CT-CS-EGFP* without the CD148 leader, c-Myc and 5′ UTR was generated using the same cloning strategy (with use of primers T287 and T255). No difference between plasma membrane localisation of LAT variants with and without the CD148 leader, c-Myc and 5′ UTR was detected (Fig. S3B,C).

Live cell imaging and cyclohexamide treatment

Cells were imaged on poly-L-lysine-coated (to immobilise cells) glass-bottom 8-well chamber slides (Lab-Tek®, Thermo Scientific) supplemented with pre-heated, colour-free RPMI-1640 medium. Images were taken using a Leica SP5 TCS AOBS Tandem laser scanning confocal microscope equipped with Leica HyD hybrid detector, 63×1.3 NA glycerine immersion

Journal of Cell Science (2016) 129, 95-107 doi:10.1242/jcs.175190

objective (Leica PLAN APO) and live cell support chamber. LAS AF image software (Leica Microsystems) was used for acquisition. 3–4 sections were taken per cell, focused on the Golgi complex, ER and the plasma membrane. Minor contrast and/or level adjustments were applied and images were processed for publishing by Fiji/ImageJ (Schindelin et al., 2012).

For colocalisation studies, markers for the ER (Sec61-mCherry) and Golgi complex (Golgi 7-mApple) were co-transfected into Jurkat cells and imaged in parallel with GFP constructs using the TRIC channel setup (Leica Microsystems). mApple-Golgi-7 was a gift from Michael Davidson (Addgene plasmid #54907) and mCherry-Sec61 beta from Gia Voeltz (Addgene plasmid #49155).

Kinetic studies were performed using transiently transfected Jurkat T cells. After 16 h of culture, 25 µg/ml cyclohexamide was added to media and live cell imaging was performed after 0, 2, 4, 6 and 20 h.

Quantitative image analysis of plasma membrane localisation

In order to quantitate plasma membrane localisation, the proportion of plasma membrane signal on total cell fluorescence was calculated for each protein variant and compared with native LAT or PAG proteins (Fig. S4). Protein variants (with GFP) were transiently co-expressed with LAT-mCherry or PAG-mCherry in Jurkat T cells. Native LAT and PAG proteins were selected as positive controls as they reproducibly showed the most efficient plasma membrane localisation (Figs 1, 2). Sequential 2-colour live cell imaging was performed using a Zeiss LSM 510 laser scanning confocal microscope with a 100×1.4 NA PlanApochromat oil-immersion objective. Fluorescence signals of GFP and mCherry excited at 488 nm by Ar laser and 561 nm by DPSS laser were detected using the 505–550 nm band-pass and 580 nm long-pass emission filters, respectively. Acquired images were manually thresholded to remove signal noise detected outside of the cell. Then, total cell intensity (I_{Cell}) and plasma membrane signal (I_{PM}) were calculated in MATLAB by integration of fluorescence intensities in pixels of manually selected areas encompassing the whole cell body and the cell cortex, respectively. Relative plasma membrane localisation efficiency $R_{G/R}$ was calculated as

$$R_{G=R} = \frac{\delta I_{PM}\,\delta GFP\flat - I_{Cell}\,\delta GFP\flat\flat}{\delta I_{PM}\,\delta mCherry\flat - I_{Cell}\,\delta mCherry\flat\flat};$$

where mCherry-tagged proteins were treated as reference (positive control). Positive (PAG versus LAT) and negative (ER marker Sec61 versus LAT) controls of plasma membrane localisation generated $R_{G/R}$ values of 0.95± 0.12 and 0.23±0.09, respectively (Fig. 1D).

In silico analysis of TMD and protein properties

The hydrophobic core or TMD of all tested proteins (Table 2) were determined using the bioinformatics tool TMHMM 2.0 prediction of transmembrane helices in proteins (http://www.cbs.dtu.dk/services/TMHMM-2.0/) (Krogh et al., 2001). For in silico prediction of protein membrane compartmentalisation we employed http://www.tmdsonline.org/ predict.html#0 (Sharpe et al., 2010). Mean hydrophobicity of protein TMDs was calculated using HydroMCalc algorithm provided by A. Tossi (University of Trieste). No difference in mean hydrophobicity of TMDs was found when an alternative algorithm was used (Fauchere and Pliska, 1983).

Acknowledgements

We would like to thank Anthony I. Magee (Imperial College London) and Kvido Stříšovský (IOCB, Prague) for critical reading of the manuscript. We would also like to thank Radek Sachl' for help with MATLAB script development.

Competing interests

The authors declare no competing or financial interests.

Author contributions

T.B. and M.C. designed experiments; T.C., D.G., T.B. and M.C. performed experiments and data processing; T.C., Z.K. and J.M. performed quantitative image analysis; T.B. and M.C. wrote the paper.

Funding

This study received funding from the Czech Science Foundation [P305/11/0459] and Purkyne Fellowship to M.C.

Supplementary information

Supplementary information available online at http://jcs.biologists.org/lookup/suppl/doi:10.1242/jcs.175190/-/DC1

References

Almén, M. S., Nordström, K. J., Fredriksson, R. and Schiöth, H. B. (2009). Mapping the human membrane proteome: a majority of the human membrane proteins can be classified according to function and evolutionary origin. BMC Biol. 7, 50.

Alonso, M. A., Fan, L. and Alarcon, B. (1997). Multiple sorting signals determine apical localization of a nonglycosylated integral membrane protein. J. Biol. Chem. 272, 30748-30752.

Andersson, H., Bakker, E. and von Heijne, G. (1992). Different positively charged amino acids have similar effects on the topology of a polytopic transmembrane protein in Escherichia coli. J. Biol. Chem. 267, 1491-1495.

Bijlmakers, M.-J. (2009). Protein acylation and localization in T cell signaling (Review). Mol. Membr. Biol. 26, 93-103.

Brdicka, T., Pavlistova, D., Leo, A., Bruyns, E., Korinek, V., Angelisova, P., Scherer, J., Shevchenko, A., Hilgert, I., Cerny, J. et al. (2000). Phosphoprotein associated with glycosphingolipid-enriched microdomains (PAG), a novel ubiquitously expressed transmembrane adaptor protein, binds the protein tyrosine kinase csk and is involved in regulation of T cell activation. J. Exp. Med. 191, 1591-1604.

Brdicka, T., Imrich, M., Angelisova, P., Brdickova, N., Horvath, O., Spicka, J., Hilgert, I., Luskova, P., Draber, P., Novak, P. et al. (2002). Non-T cell activation linker (NTAL): a transmembrane adaptor protein involved in immunoreceptor signaling. J. Exp. Med. 196, 1617-1626.

Cebecauer, M., Spitaler, M., Serge, A. and Magee, A. I. (2010). Signalling complexes and clusters: functional advantages and methodological hurdles. J. Cell Sci. 123, 309-320.

Cosson, P., Perrin, J. and Bonifacino, J. S. (2013). Anchors aweigh: protein localization and transport mediated by transmembrane domains. Trends Cell Biol. 23, 511-517.

Diaz-Rohrer, B. B., Levental, K. R., Simons, K. and Levental, I. (2014). Membrane raft association is a determinant of plasma membrane localization. Proc. Natl. Acad. Sci. USA 111, 8500-8505.

Duffield, A., Caplan, M. J. and Muth, T. R. (2008). Protein trafficking in polarized cells. Int. Rev. Cell. Mol. Biol. 270, 145-179.

Fastenberg, M. E., Shogomori, H., Xu, X., Brown, D. A. and London, E. (2003). Exclusion of a transmembrane-type peptide from ordered-lipid domains (rafts) detected by fluorescence quenching: extension of quenching analysis to account for the effects of domain size and domain boundaries. Biochemistry 42, 12376-12390.

Fauchere, J. L. and Pliska, V. (1983). ProtScale tool. Amino acid scale: hydrophobicity scale (pi-r). Eur. J. Med. Chem. 18, 369-375.

Fiedler, K. and Simons, K. (1995). The role of N-glycans in the secretory pathway. Cell 81, 309-312.

Fossati, M., Colombo, S. F. and Borgese, N. (2014). A positive signal prevents secretory membrane cargo from recycling between the Golgi and the ER. EMBO J. 33, 2080-2097.

Fukata, Y., Dimitrov, A., Boncompain, G., Vielemeyer, O., Perez, F. and Fukata, M. (2013). Local palmitoylation cycles define activity-regulated postsynaptic subdomains. J. Cell Biol. 202, 145-161.

Horejší,V. V., Zhang, W. and Schraven, B. (2004). Transmembrane adaptor proteins: organizers of immunoreceptor signalling. Nat. Rev. Immunol. 4, 603-616.

Hořejší,V., Otáhal, P. and Brdička, T. (2010). LAT - an important raft-associated transmembrane adaptor protein. Delivered on 6 July 2009 at the 34th FEBS Congress in Prague, Czech Republic. FEBS J. 277, 4383-4397.

Howell, G. J., Holloway, Z. G., Cobbold, C., Monaco, A. P. and Ponnambalam, S. (2006). Cell biology of membrane trafficking in human disease. Int. Rev. Cytol. 252, 1-69.

Hundt, M., Harada, Y., De Giorgio, L., Tanimura, N., Zhang, W. and Altman, A. (2009). Palmitoylation-dependent plasma membrane transport but lipid raft-independent signaling by linker for activation of T cells. J. Immunol. 183, 1685-1694.

Kaiser, H.-J., Orlowski, A., Rog, T., Nyholm, T. K., Chai, W., Feizi, T., Lingwood, D., Vattulainen, I. and Simons, K. (2011). Lateral sorting in model membranes by cholesterol-mediated hydrophobic matching. Proc. Natl. Acad. Sci. USA 108, 16628-16633.

Krogh, A., Larsson, B., von Heijne, G. and Sonnhammer, E. L. L. (2001). Predicting transmembrane protein topology with a hidden Markov model: application to complete genomes. J. Mol. Biol. 305, 567-580.

Levental, I., Lingwood, D., Grzybek, M., Coskun, U. and Simons, K. (2010). Palmitoylation regulates raft affinity for the majority of integral raft proteins. Proc. Natl. Acad. Sci. USA 107, 22050-22054.
Machán˘, R., Jurkiewicz, P., Olz˙yńska, A., Olšinová,M., Cebecauer, M., Marquette, A., Bechinger, B. and Hof, M. (2014). Peripheral and integral membrane binding of peptides characterized by time-dependent fluorescence shifts: focus on antimicrobial peptide LAH(4). Langmuir 30, 6171-6179.
Munro, S. (1991). Sequences within and adjacent to the transmembrane segment of alpha-2,6-sialyltransferase specify Golgi retention. EMBO J. 10, 3577-3588.
Munro, S. (1995). An investigation of the role of transmembrane domains in Golgi protein retention. EMBO J. 14, 4695-4704.
Nilsson, J., Persson, B. and von Heijne, G. (2005). Comparative analysis of amino acid distributions in integral membrane proteins from 107 genomes. Proteins 60, 606-616.
Owen, D. M., Rentero, C., Rossy, J., Magenau, A., Williamson, D., Rodriguez, M. and Gaus, K. (2010). PALM imaging and cluster analysis of protein heterogeneity at the cell surface. J. Biophotonics 3, 6-454.
Posevitz-Fejfar, A., Sm̆ıda, M., Kliche, S., Hartig, R., Schraven, B. and Lindquist, J. A. (2008). A displaced PAG enhances proximal signaling and SDF-1-induced T cell migration. Eur. J. Immunol. 38, 250-259.
Potter, B. A., Hughey, R. P. and Weisz, O. A. (2006). Role of N- and O-glycans in polarized biosynthetic sorting. Am. J. Physiol. Cell Physiol. 290, C1-C10.
Proszynski, T. J., Simons, K. and Bagnat, M. (2004). O-glycosylation as a sorting determinant for cell surface delivery in yeast. Mol. Biol. Cell 15, 1533-1543.
Quiroga, R., Trenchi, A., Gonzalez Montoro, A., Valdez Taubas, J. and Maccioni, H. J. F. (2013). Short transmembrane domains with high-volume exoplasmic halves determine retention of Type II membrane proteins in the Golgi complex. J. Cell Sci. 126, 5344-5349.
Rocks, O., Gerauer, M., Vartak, N., Koch, S., Huang, Z.-P., Pechlivanis, M., Kuhlmann, J., Brunsveld, L., Chandra, A., Ellinger, B. et al. (2010). The palmitoylation machinery is a spatially organizing system for peripheral membrane proteins. Cell 141, 458-471.
Saka, S. K., Honigmann, A., Eggeling, C., Hell, S. W., Lang, T. and Rizzoli, S. O. (2014). Multi-protein assemblies underlie the mesoscale organization of the plasma membrane. Nat. Commun. 5, 4509.
Schindelin, J., Arganda-Carreras, I., Frise, E., Kaynig, V., Longair, M., Pietzsch, T., Preibisch, S., Rueden, C., Saalfeld, S., Schmid, B. et al. (2012). Fiji: an open-source platform for biological-image analysis. Nat. Methods 9, 676-682.
Sevier, C. S., Weisz, O. A., Davis, M. and Machamer, C. E. (2000). Efficient export of the vesicular stomatitis virus G protein from the endoplasmic reticulum requires a signal in the cytoplasmic tail that includes both tyrosine-based and di-acidic motifs. Mol. Biol. Cell 11, 13-22.
Sharpe, H. J., Stevens, T. J. and Munro, S. (2010). A comprehensive comparison of transmembrane domains reveals organelle-specific properties. Cell 142, 158-169.
Spira, F., Mueller, N. S., Beck, G., von Olshausen, P., Beig, J. and Wedlich-Söldner, R. (2012). Patchwork organization of the yeast plasma membrane into numerous coexisting domains. Nat. Cell Biol. 14, 640-648.
Stepanek, O., Draber, P. and Horejsi, V. (2014). Palmitoylated transmembrane adaptor proteins in leukocyte signaling. Cell Signal. 26, 895-902.
Tossi, A., Sandri, L. and Giangaspero, A. (2002). New consensus hydrophobicity scale extended to non-proteinogenic amino acids. In PEPTIDES 2002 (ed. E. Benedetti and C. Pedone). Napoli, Italy: Edizioni Ziino, 416-417.
Traub, L. M. (2009). Tickets to ride: selecting cargo for clathrin-regulated internalization. Nat. Rev. Mol. Cell Biol. 10, 583-596.
van Geest, M. and Lolkema, J. S. (2000). Membrane topology and insertion of membrane proteins: search for topogenic signals. Microbiol. Mol. Biol. Rev. 64, 13-33.
Weissman, A. M., Frank, S. J., Orloff, D. G., Mercep, M., Ashwell, J. D. and Klausner, R. D. (1989). Role of the zeta chain in the expression of the T cell antigen receptor: genetic reconstitution studies. EMBO J. 8, 3651-3656.
Xiao, J. H., Davidson, I., Matthes, H., Garnier, J.-M. and Chambon, P. (1991). Cloning, expression, and transcriptional properties of the human enhancer factor TEF-1. Cell 65, 551-568.
Zeidman, R., Jackson, C. S. and Magee, A. I. (2009). Protein acyl thioesterases (Review). Mol. Membr. Biol. 26, 32-41.
Zhang, W., Trible, R. P. and Samelson, L. E. (1998). LAT palmitoylation: its essential role in membrane microdomain targeting and tyrosine phosphorylation during T cell activation. Immunity 9, 239-246.

The FEBS Journal

FEBS PRESS science publishing by scientists

The role of prolines and glycine in the transmembrane domain of LAT

Daniela Glatzova[1,2,3], Harsha Mavila[1], Maria Chiara Saija[4], Tomas Chum[1], Lukasz Cwiklik[4], Tomas Brdicka[2] and Marek Cebecauer[1]

1 Department of Biophysical Chemistry, J. Heyrovsky Institute of Physical Chemistry, Czech Academy of Sciences, Prague, Czech Republic
2 Laboratory of Leukocyte Signaling, Institute of Molecule Genetics, Czech Academy of Sciences, Prague, Czech Republic
3 Faculty of Science, Charles University, Prague, Czech Republic
4 Department of Computational Chemistry, J. Heyrovsky Institute of Physical Chemistry, Czech Academy of Sciences, Prague, Czech Republic

Keywords

LAT; MD simulations; microscopy; T cells; transmembrane domain

Correspondence

M. Cebecauer, J. Heyrovsky Institute of Physical Chemistry, Czech Academy of Sciences, Dolejskova 3, Prague, Czech Republic
Tel: +420 6605 3733
E-mail: marek.cebecauer@jh-inst.cas.cz

(Received 18 September 2020, revised 15 December 2020, accepted 13 January 2021)

doi:10.1111/febs.15713

Linker for activation in T cells (LAT) is a critical regulator of T-cell development and function. It organises signalling events at the plasma mem-brane. However, the mechanism, which controls LAT localisation at the plasma membrane, is not fully understood. Here, we studied the impact of helix-breaking amino acids, two prolines and one glycine, in the transmem-brane segment on localisation and function of LAT. Using in silico analy-sis, confocal and super-resolution imaging and flow cytometry, we demonstrate that central proline residue destabilises transmembrane helix by inducing a kink. The helical structure and dynamics are further regu-lated by glycine and another proline residue in the luminal part of LAT transmembrane domain. Replacement of these residues with aliphatic amino acids reduces LAT dependence on palmitoylation for sorting to the plasma membrane. However, surface expression of these mutants is not sufficient to recover function of nonpalmitoylated LAT in stimulated T cells. These data indicate that geometry and dynamics of LAT transmem-brane segment regulate its localisation and function in immune cells.

Introduction

Function of proteins (e.g. enzymes or signal transduc-ers) is defined by their structure, but also localisation within a cell or an organism. Amino acid sequence, small molecule cofactors and interacting partners are primary determinants of the structure. however fea-tures defining protein localisation are less well under-stood. The process defining protein localisation is called sorting. Short motifs within a primary sequence were found to firmly control sorting of proteins to some organelles, for examples the endoplasmic reticu-lum (ER) retention (KDEL motif), the ER exit (DxE and YxxΦ coupled motifs) or transport to/from the nucleus (NES/NLS motifs) [1–3]. Trafficking of pro-teins to the plasma membrane (PM) appears to be controlled by several unrelated determinants. Post-translational modifications, such as glycosylation and palmitoylation, facilitate anterograde membrane trans-port of proteins to the cell surface [4–6]. In the oppo-site direction, ubiquitination regulates retrograde protein transport from the surface towards the cell interior [7]. However, the primary determinant of the PM sorting, at least for single-spanning membrane

Abbreviations

EGFP, enhanced GFP; ER, endoplasmic reticulum; FCS, foetal bovine serum; GA, Golgi apparatus; IRM, interference reflection microscopy; LAT, linker for activation in T cells; MD, molecular dynamics; PALM, photoactivation localisation microscopy; PM, plasma membrane; POPC, palmitoyl-oleoyl phosphatidylcholine; SR, super-resolution; TCR, T-cell receptor; TM, transmembrane; TMD, transmembrane domain; WT, wild-type.

proteins, is the length and amino acid composition of the transmembrane domain (TMD) [6,8]. A compre-hensive study demonstrated that, in vertebrates, pro-teins with TMDs of 22 residues or longer localise to the PM [9]. Those with shorter TMDs remain in the Golgi apparatus (GA) or the ER. The voluminous amino acids (Phe, Tyr, Trp) were found to accumulate in the cytosolic part of the TMD of the PM proteins. The position of other amino acids is also nonrandom [9,10]. These data indicate that physico-chemical prop-erties of TMDs strongly influence trafficking of pro-teins in cells.

In vertebrates, the structure of TMD is almost exclusively formed by an a-helix. The hydrophobic core is largely composed of aliphatic (Leu, Val, Ala, Ile) and aromatic amino acids (Phe, Tyr, Trp). Weakly polar amino acids (Ser, Thr, Met, Cys) are also common components of TMDs [10]. Cysteine residues due to their propensity to form disulphide bridges in the oxidative environment can force the protein to dimerise. Their presence is thus reduced in the exoplasmic part of the TMDs. Moreover, cys-teine residues at the cytosolic end of the TMD often represent palmitoylation sites [11]. Positively charged amino acids (Lys, Arg, His) can define the cytosolic end of TMDs (positive-inside rule; ref. [12]). In addi-tion, these residues form electrostatic bridges between the TMDs of multispanning or multicomponent membrane assemblies [13]. Interestingly, negatively charged amino acids (Asp, Glu) and their amido-derivatives (Asn, Gln) are almost absent from TMDs of vertebrate membrane proteins [10]. However, an increased representation of Asp and Glu has been observed in the membrane-adjacent sequence at the luminal side of the TMD [9,10]. Finally, proline and glycine are the two amino acids with physico-chemi-cal properties, which can affect the geometry of TMDs.

Proline and glycine were defined as typical 'helix-breakers' in soluble globular proteins. Indeed, they are virtually absent from the helical structures of such pro-teins [14]. However, proline is often present in the TMDs of integral membrane proteins, exhibiting the highest occupancy towards the ends but, with a lower frequency, also in the central parts of the a-helices [10,15,16]. The cyclic structure of proline makes it unique among the 20 natural amino acids because its amide group lacks the proton necessary for the hydro-gen bond stabilising the a-helix or the b-sheet structure [17]. Therefore, prolines in transmembrane (TM) helices are predicted to induce regions of helix distor-tions and/or dynamic flexibility (i.e. kinks, hinges, swi-vels; refs. [15,18]). Such structural distortions may play a role in the transmission of conformational changes along the helix, as well as establish crucial helix–helix packing interactions or geometries in polytopic pro-teins [15,19]. The presence of central proline can also lead to the change in the helix orientation [16]. Impor-tantly, prolines in TMDs are critical for the function of several proteins [19–21].

Glycine is also rather frequent in the TMDs of inte-gral membrane proteins [10]. In analogy to proline, glycine helix-affecting properties depend on the local environment [22,23]. No strong effect of a single gly-cine residue on basic structure of TM a-helices was found experimentally [22,23]. It functions primarily as an interface between individual helices of the polytopic membrane proteins and is involved in protein dimeri-sation [24,25]. However, when positioned close to the proline, it enhances local dynamics of the helix and, thus, can affect the function of TM peptides or pro-teins [26,27]. The complexity of proline and glycine environment-sensitive properties suggests that it is important to characterise their role in the TMD of individual proteins separately.

LAT, linker for activation in T cells, is 36 kDa pro-tein belonging to the family of TM adaptor proteins. It plays an important role in membrane immuno-receptor signalling pathways of T cells, NK cells, mast cells and platelets [28,29]. LAT is indispensable for the T-cell function and development [30]. It plays an essential role in T-cell activation by providing a platform for signal transmission initiated by the T-cell receptor (TCR) at the PM [29,31]. T cells lacking LAT, for example the Jurkat mutants J.CaM2.5, fail to mobilise calcium and promote other downstream effector events upon TCR stimulation (e.g. ERK phosphorylation or IL-2 production). Human LAT is a type III TM pro-tein, that is it is missing a signal peptide and, thus, uses its unique TMD for its membrane insertion. Its extra-cellular part has only three amino acids, the TMD is 24 residues long and the cytoplasmic tail (235 amino acids) contains nine conserved tyrosine residues involved in T-cell signalling. The cytoplasmic tail of LAT also possesses conserved juxtamembrane cysteines required for its palmitoylation (residues 26 and 29). Palmitoylation is mainly responsible for sorting of LAT to the PM [6,32,33].

In this study, we have investigated the impact of highly conserved proline and glycine residues of the LAT TMD on its PM localisation and function. We demonstrate that replacement of prolines and glycine with aliphatic amino acids (alanine or leucine) partially recovers the surface localisation of nonpalmitoylatable LAT mutant. However, such effect is not sufficient for restoration of its function. We also tested whether

nanoscopic surface organisation of LAT mutants is altered and, thus, leads to their malfunction in T cells.

Results

Atypical transmembrane domain of LAT contains highly conserved helix-breakers at positions 8, 12 and 17

We have previously shown that TMD controls sorting of LAT to the PM [6]. General PM sorting rules deter-mined for other proteins are not obeyed by LAT: (a) 24 residues long TMD should provide sufficient sort-ing signal but LAT, which lacks cysteines at the posi-tions 26 and 29 and, therefore, cannot be palmitoylated, remains trapped in the GA [6,9,32], and

(b) there are no voluminous amino acids in the exo-plasmic portion of the LAT TMD (Fig. 1A). It was previously reported that prolongation of the TMD leads to the PM localisation of the proteins, which normally reside in the GA [8]. Nevertheless, prolonga-tion of LAT TMD by six amino acids (six leucine resi-dues or PILAML sequence) did not overcome dependence of LAT surface expression on its palmitoy-lation (Fig. S1). We observed the accumulation of LAT with prolonged TMD in lysosomes and other unspecified intracellular vesicles (Fig. S1). These data indicate that LAT TMD contains residues, which con-trol its geometry or dynamics with respect to the lipid membranes of the secretory pathway.

The amino acid sequence of the LAT TMD exhibits high level of conservation with 48% identity in mam-mals (Fig. 1A). Among the conserved residues, there are two prolines, which were reported to introduce dis-tortions into the helical structure of TMDs in several proteins [15]. One proline is positioned centrally (Pro17) and one close to the luminal end of the LAT

TMD (Pro8). Moreover, the luminal part of LAT TMD contains glycine (Gly12) in the position i + 4

with respect to Pro8 and i 5 with respect to Pro17. The motif (PxxxG) was described to control the dynamics of pore-forming peptides and proteins [26]. Importantly, helix-breaking residues were shown to exhibit cumulative effect on the structure of TM helices [23]. We, therefore, hypothesised that Pro8, Gly12 and Pro17 residues play a role in membrane sta-bility and sorting of LAT to the PM.

All-atom MD simulations indicate kink formation in the helical structure of LAT TMD

We have first characterised the role of Pro8, Gly12 and Pro17 residues in LAT TMD structure using all-atom molecular dynamics (MD) simulations. Residues 2–33, EEAILVPCVLGLLLLPILAMLMALCVHCHRLP, which form the hydrophobic core and membrane prox-imal parts, were used to simulate human LAT TMD in a lipid membrane composed of 128 palmitoyl-oleoyl phosphatidylcholine (POPC) molecules for 1 μs. The peptide was first enforced to adapt a-helical structure and inserted into the membrane in a transbilayer orien-tation. Afterwards, the system was left to adjust its optimal conformation for 500 ns. The following 500 ns of the trajectory were used for the analysis of the pep-tide behaviour in a model membrane. The structure of LAT-wild-type (WT) peptide exhibited high level of helicity. However, a kink could be observed in the cen-tral part of the peptide at around the position of Leu14 (Fig. 1B,C). This nonhelical segment involving residues 13–15 is downstream of Gly12 (i + 2 for Leu14) and upstream of Pro17 (i 3 for Leu14). Such deviation within the a-helix is in agreement with previously observed kinks induced by proline and glycine residues in the TMDs of several membrane proteins (e.g. bacte-riorhodopsins, ref. [27]). The maximal impact was reported for positions i – 3 or i 4 with respect to the proline residue [34]. Maximal effect of glycine was observed for residues i + 1 and i + 2 [23]. Another deviation from the a-helical structure, even though much smaller compared to the central nonhelical seg-ment, could be observed near Pro8 residue (Fig. 1C).

We have further used MD simulations to characterise behaviour of LAT TMD mutants, in which helix-break-ing residues were replaced with alanine or leucine. Mutation of proline to alanine in the position 17 (P17A) led to complete disappearance of the kink for the full period of the simulation (Fig. 1B,C). A minor helix deviation near Pro8 was preserved in P17A mutant (Fig. 1C). On the contrary, no effect on the central kink was observed in the mutant P8A. Nevertheless, the mutant exhibited higher dynamics of the kink, as repre-sented by the analysis of the kink angles (Fig. S2) and shortening of the helical TM segment (Fig. 1C). The helix was two residues shorter compared to LAT-WT peptide. No such shortening was observed for P17A mutant (Fig. 1C). MD simulations of G12L mutant of LAT TMD peptide provided similar results as for LAT-WT peptide (Fig. 1C and Fig. S2). However, the helical TM segment was three residues shorter than in the LAT-WT peptide. The overall tilt angle of the peptides in the bilayer was similar for all variants except for the G12L mutant, probably caused by shortening of its heli-cal fragment (Fig. S3). The in silico data thus indicate that Pro17 is critical for the kink formation in the LAT TMD but Pro8 and Gly12 fine-tune the overall TMD structure and dynamics of the kink.

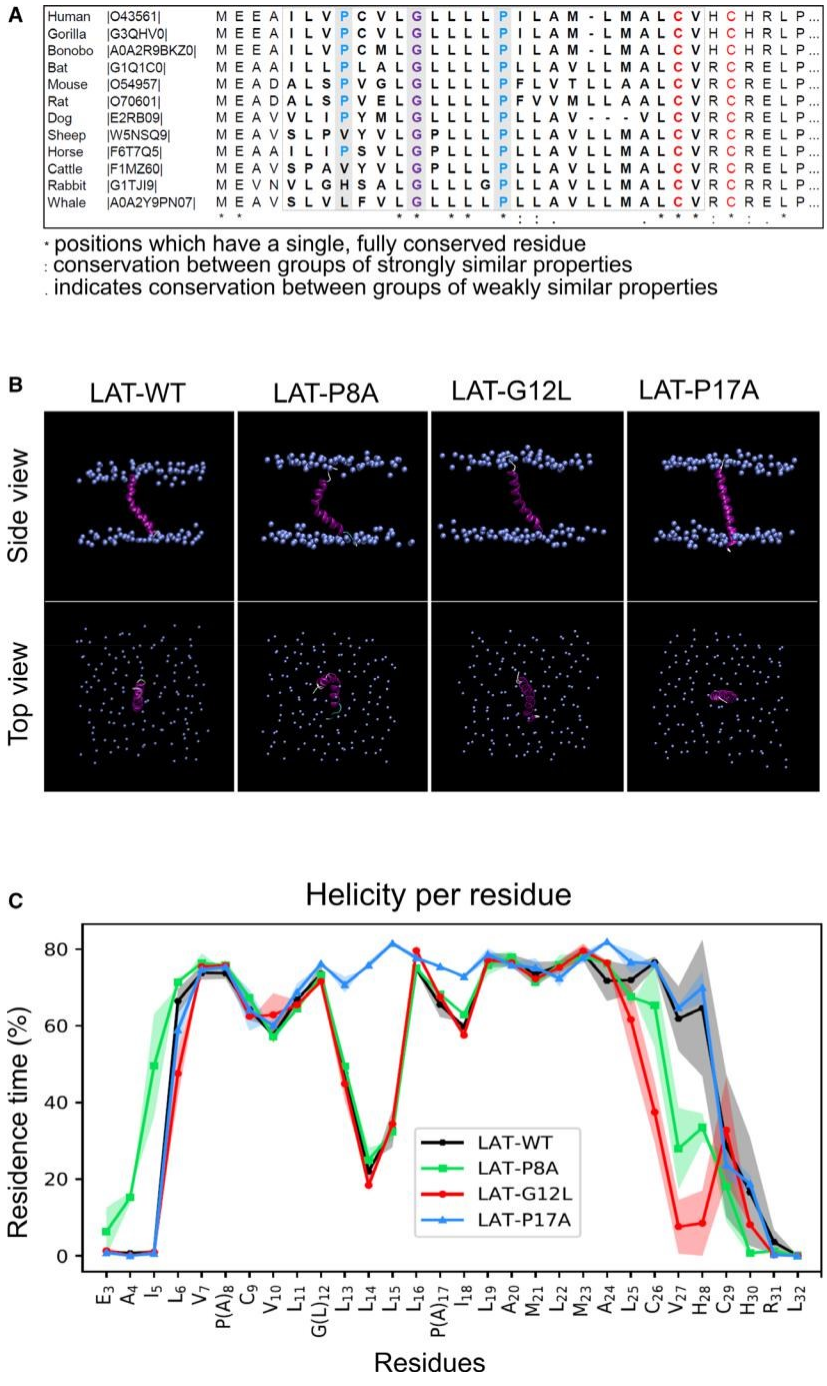

Fig. 1. Helix-breaking amino acids in the TM domain of LAT. (A) Sequence alignment of LAT TM segment and the adjacent parts (hydrophobic region in bold) showing conservation of amino acids among twelve mammalian species. Specific sequences are demarked by UNIPROT.org codes. Multiple sequence alignment was performed using CLUSTAL OMEGA (1.2.4, https://www.ebi.ac.uk/Tools/msa/clustalo/). (B) Representative snapshot from MD simulations of LAT TMD peptide and its variants in POPC bilayer. TM helix is shown in magenta, phospholipid headgroups are indicated with light blue spheres. (C) Helicity plot showing the propensity of individual amino acids in the LAT TMD peptide and its variants to accommodate helical geometry. Standard error is indicated as shadowing of the curves.

Mutation of helix-breaking amino acids promotes sorting of nonpalmitoylated LAT to the plasma membrane

We have therefore investigated the impact of Pro8, Gly12 and Pro17 on LAT sorting to the PM. The cod-ing DNA sequence was individually modified to replace Pro8 and Pro17 residues with alanine (Fig. 2A) and expressed as mutant LAT-GFP fusion proteins in LAT-deficient Jurkat T-cell line, J.CaM2.5. Gly12 resi-due was mutated to leucine to prevent the disruption of leucine-rich segment of the LAT TMD (Figs 1A and 2A). The cells were transiently transfected with the plasmid DNA and the expression was analysed 16–24 h later using confocal scanning microscopy. All mutant proteins exhibited a distribution, which was

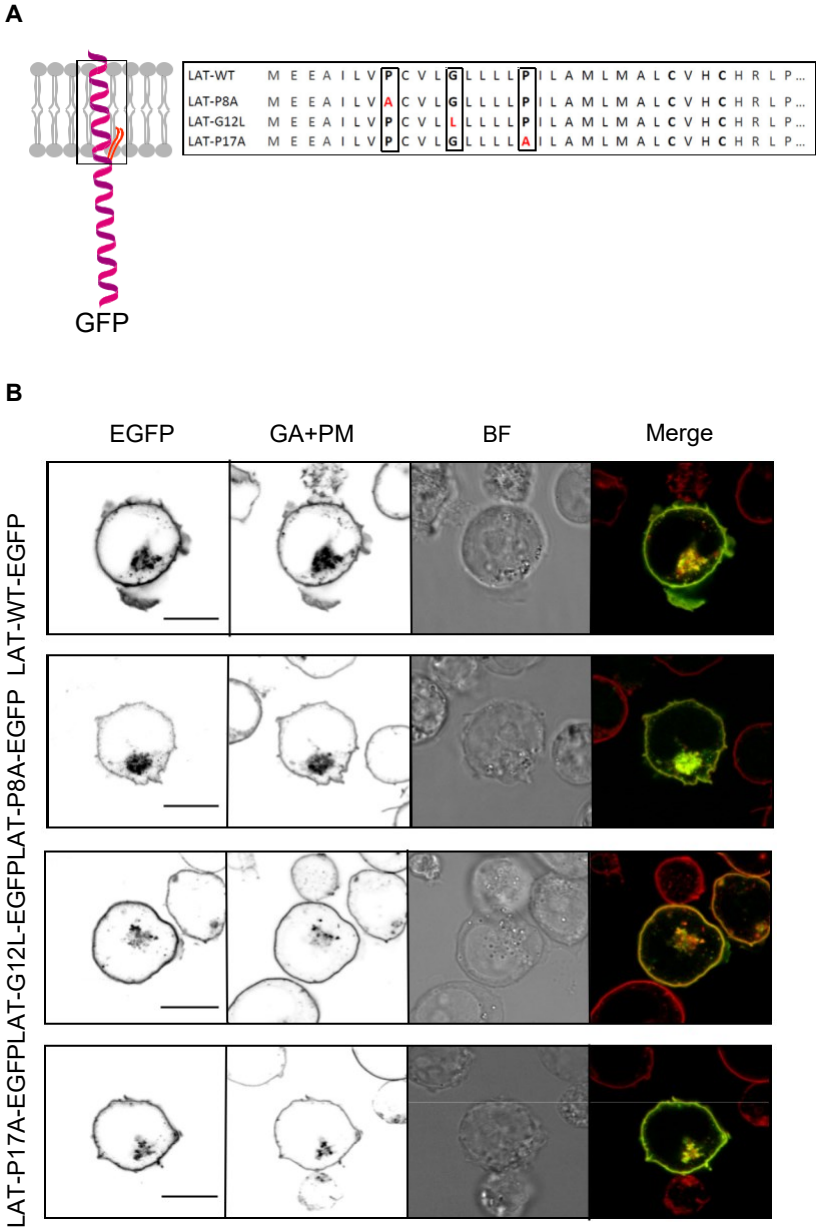

Fig. 2. Localisation of palmitoylated LAT variants in J.CaM2.5 cells. (A) Schematic representation of human LAT construct with attached EGFP and indicated TMD region with accompanied primary sequence. Amino acids mutated in tested LAT variants are highlighted in red. (B) Confocal microscopy of J.CaM2.5 cells expressing LAT-WT-EGFP, LAT-P8A-EGFP, LAT-G12L-EGFP and LAT-P17A-EGFP stained with the PM and GA marker lectin-HPA AF647. Single-channel (EGFP and GA + PM marker) or two-channel overlay images (merge; EGFP – green, GA + PM – red, overlay – yellow) are shown together with a brightfield image (BF). Scale bars, 10 μm. More examples in Figs S4–S7. Representative images of three measurement days are shown.

comparable to the native LAT protein. The proteins prevalently localised to the PM of transfected J.CaM2.5 cells (Fig. 2B). A partial trapping of the proteins in the GA could also be observed. This obser-vation is in agreement with previous findings that T cells express two pools of LAT, one localised in the PM and the other in the GA [35]. However, no exten-sive accumulation of the mutant LAT proteins in intracellular membranes, for example the ER, was visi-ble. These results indicate that mutating individual 'he-lix-breaking residues' of the LAT TMD to alanine (or leucine) does not substantially destabilise LAT protein.

As mentioned above, LAT requires palmitoylation of its membrane proximal cysteines 26 and 29 for its localisation to the PM and function. We were, thus, interested whether a kink in the helix of the TMD determined using MD simulations can influence PM sorting of LAT in the absence of its palmitoylation. We prepared LAT-GFP variants (Fig. 3A), which combined alanine mutants of Pro8 and Pro17 (or leu-cine mutant of Gly12) with cysteines 26 and 29 replaced for serines as described before [6]. The mutant proteins were transiently expressed in J.CaM2.5 cells and analysed by confocal microscopy

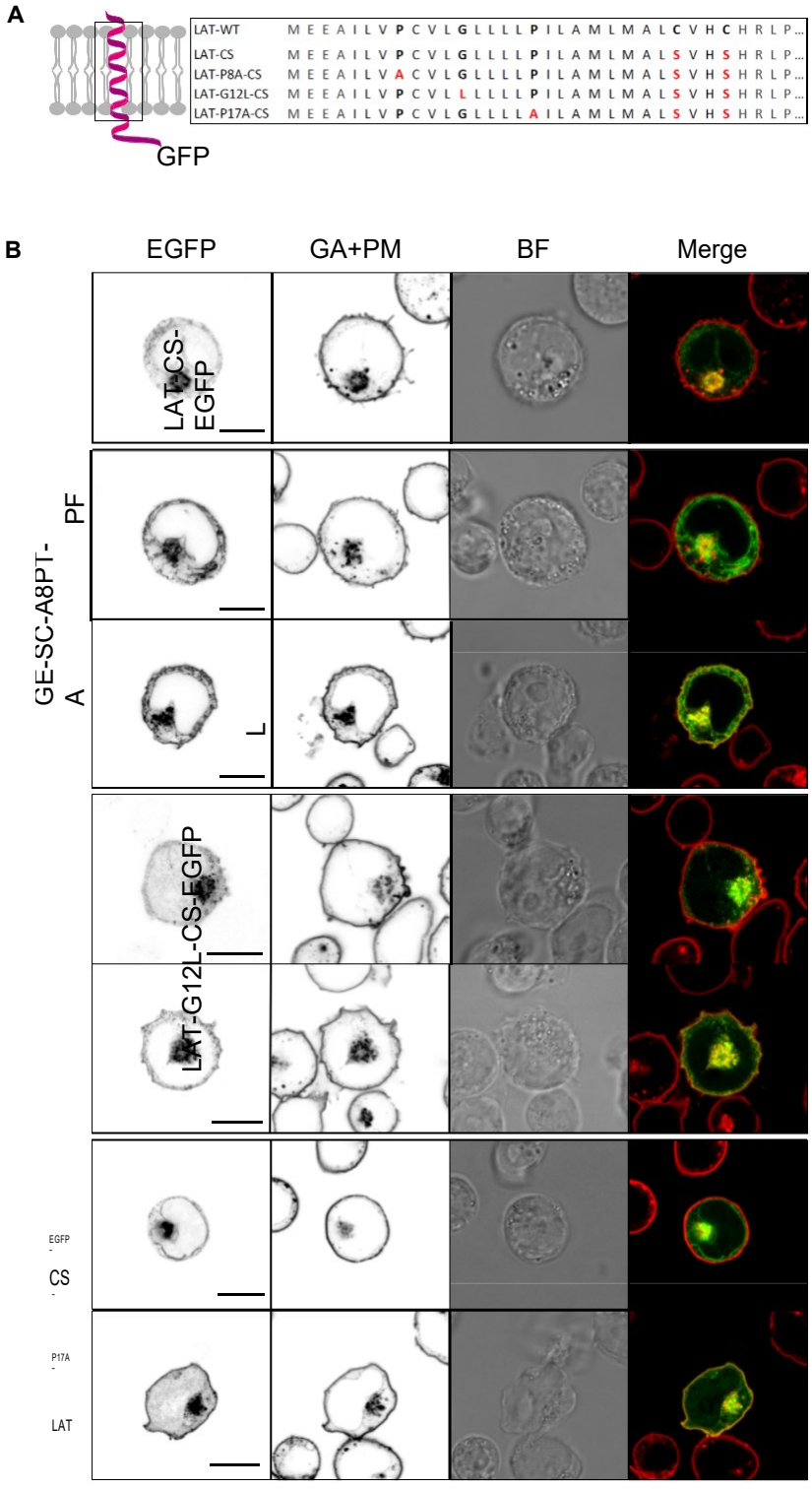

Fig. 3. Localisation of nonpalmitoylated LAT variants in J.CaM2.5 cells line. (A) Schematic representation of human nonpalmitoylated LAT construct with attached EGFP and indicated TMD region with accompanied primary sequence. Amino acids mutated in tested LAT-CS variants are highlighted in red. (B) Confocal microscopy of J.CaM2.5 cells expressing LAT-CS-EGFP, LAT-P8A-CS-EGFP, LAT-G12L-CS-EGFP and LAT-P17A-CS-EGFP stained with the PM and GA marker lectin-HPA AF647. Single-channel (EGFP and GA + PM marker) or two-channel overlay images (merge; EGFP – green, GA + PM – red, overlay – yellow) are shown together with a brightfield image (BF). Scale bars, 10 μm. More examples in Figs. S4-S7. Representative images of three measurement days are shown.

16–24 h post-transfection. Strikingly, mutation of helix-breaking amino acids in the TMD to alanine or leucine partially restored the PM localisation of non-palmitoylatable LAT in 30–50% of cells (Fig. 3B and Figs S4–S7). Compared to LAT-P8A-CS, slightly stronger surface signal was observed at the PM in cells expressing LAT-G12L-CS and LAT-P17A-CS (Fig. 3B and Figs S5–S7). Nevertheless, LAT-P8A-

CS, LAT-P17A-CS and LAT-G12L-CS were also found in the intracellular membranes, mainly GA and the ER. Such intracellular trapping is similar to LAT-CS mutant with preserved kink-forming amino acids (Fig. 3B and Fig. S4).

Mutation of helix-breaking amino acids cannot rescue signalling defect caused by the absence of LAT palmitoylation

Next, we analysed the effects of Pro?Ala or Gly? Leu mutations on LAT function in T cells. It was shown previously that antigen response of T cells is LAT-dependent process. Intracellular calcium mobili-sation is a key part of this process and is abrogated in the absence of LAT [36]. Reconstitution of LAT-defi-cient J.CaM2.5 cells with low expression of LAT-WT resulted in high level of cytosolic calcium mobilisation after stimulation with anti-TCR antibody as measured by flow cytometry (Fig. 4A and Fig. S8; see also Materials and methods). A threefold signal increase was observed less than a minute after stimulation, as detected by changes in fluorescence properties of the calcium-sensitive probe Fura Red (Fig. 4B). Similarly, stimulation of cells expressing LAT-P8A, LAT-G12L or LAT-P17A variants was associated with a rapid, strong and sustained calcium response (Fig. 4B). Together, these data indicate that mutation of helix-breaking residues does not affect function of LAT in

T cells.

Interestingly, when analysing response to TCR antibody stimulation in J.CaM2.5 cells expressing any of the nonpalmitoylated LAT-CS variants, no calcium mobilisation was observed regardless of the mutations in the LAT TM domain (Fig. 4B). Surface expression is thus not sufficient for LAT function in antigen-in-duced T-cell signalling. Previously, we demonstrated that addition of the CD4 extracellular domain to LAT-CS rescued PM sorting of CD4ex-LAT-CS vari-ant ([6] and Fig. S9). Importantly, robust calcium mobilisation is induced by antibody stimulation in J.CaM2.5 cells expressing CD4ex-LAT or its non-palmitoylatable variant – CD4ex-LAT-CS (Fig. 4B). CD4ex-LAT and CD4ex-LAT-CS contain intact LAT TMD (apart from cysteine residues 26 and 29 in the CS variant). These data indicate that replacement of helix-breaking amino acids in the TMD with helix sup-porting ones partially rescues LAT sorting to the PM, but such surface LAT molecules remain inaccessible for early T-cell signalling molecules (e.g. Lck and ZAP-70; ref. [31]).

Nanoscopic organisation of LAT mutants on the surface of T cells

We were thus interested whether this is due to the different nanoscopic organisation of LAT-WT and the mutants, which cannot be visualised by standard con-focal microscopy. We employed super-resolution (SR) microscopy called photoactivation localisation micro-scopy (PALM) to image nanoscopic organisation of the variants LAT-WT, LAT-P17A and LAT-P17A-CS at the surface of transiently transfected J.CaM2.5 cells. For this purpose, GFP tag was replaced with mEos2, which exhibits photoconvertible behaviour essential for PALM imaging [37]. Transfected cells were immo-bilised on glycine-coated coverslips to avoid artificial stretching of T cells caused by poly-L-lysine-coated surfaces [38]. As shown in Fig. 5A, LAT-WT exhibits a random distribution over the surface of unstimulated T cells. LAT-P17A variant, which generates similar calcium response in antibody-stimulated T cells, is also randomly distributed (Fig. 5A, middle panel). For J.CaM2.5 cells expressing the LAT-P17A-CS variant, which do not respond to antibody stimulation, irregu-lar distribution of molecules was observed using PALM (Fig. 5A, right panel). This is probably caused by reduced spreading of LAT-P17A-CS-transfected cells on glycine-coated coverslips as represented by a cell footprint on the optical surface analysed using interference reflection microscopy (IRM; Fig. 5B, right panel). The IRM images of these cells are highly non-homogenous indicating an extensive three-dimensional surface structure probably caused by the accumulation of microvilli or membrane ruffles at the contact site. Intensive spreading was observed for cells expressing LAT-WT and LAT-P17A (Fig. 5B). Similar protein distributions were detected for palmitoylated and non-palmitoylated LAT-P8A variants (Fig. S10). These data indicate that mutations to Pro8 and Pro17 of the TMD do not produce alterations in the observable nanoscopic organisation of LAT at the T-cell surface. However, the ability of T cells to spread on nonstimu-lating surface is affected by the palmitoylation state of LAT.

Discussion

In this work, we demonstrate the impact of helix-breaking residues on dynamic geometry of LAT TMD and localisation of LAT in T-cell membranes. Using MD simulations, we uncovered the presence of a kink in the TMD of human LAT. The in silico and live-cell imaging data indicate that the kink is primarily caused

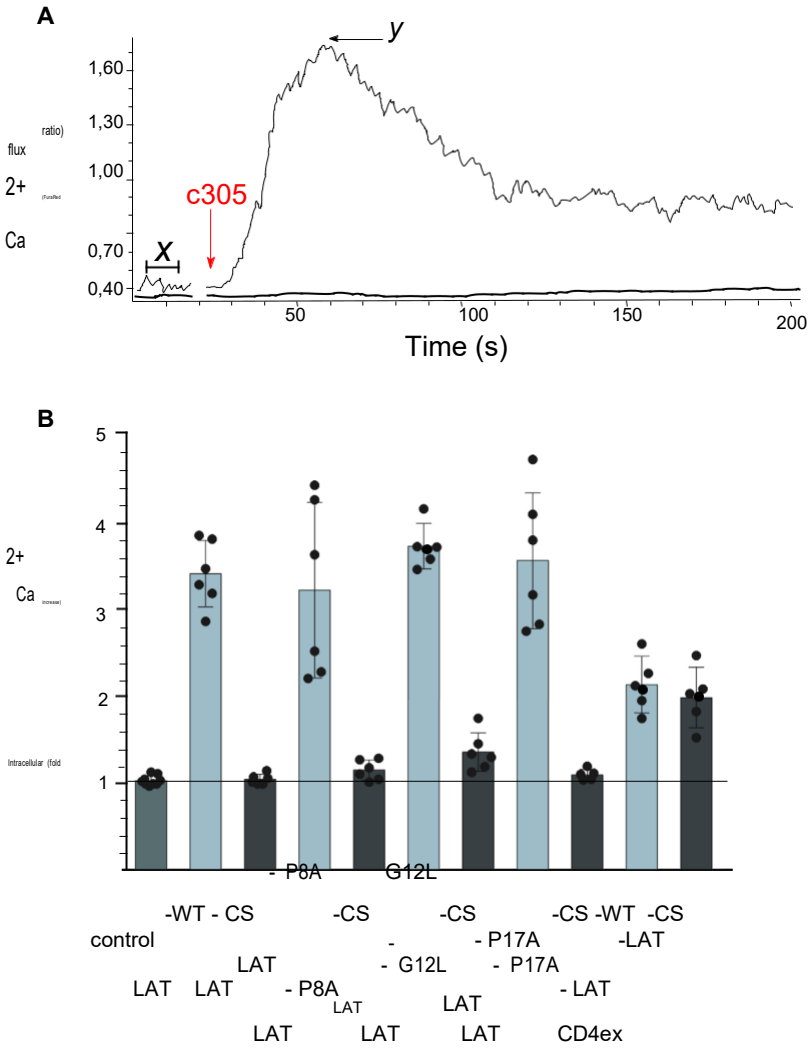

Fig. 4. TCR-mediated calcium response of J.CaM2.5 cells expressing LAT variants. (A) Representative plot of calcium mobilisation (FuraRed Ex405/Ex488) in the presence (full line) or absence (dotted line) of stimulating antibody recorded between 0 and 200 s in transiently transfected J.CaM2.5 cells cells by flow cytometry. Transfected cells were stained with FuraRed and stimulated by the addition of c305 antibody 25 s after the beginning of the measurement (indicated by red arrow; x – mean of the nonspecific calcium flux without stimulation, y – maximum peak response). For the analysis, transfected cells were selected using gating for GFP signal (see Supplementary Fig. S8). (B) A bar graph showing increased intracellular calcium levels after TCR antibody stimulation in J.CaM2.5 cells expressing indicated LAT variants (palmitoylatable LAT variants – dark grey bars; nonpalmitoylatable LAT variants – light grey bars). Increase in the intracellular calcium was calculated as y/x, where x and y values represent a baseline and a maximum response, respectively, as indicated in A. Analysed cells were gated for low expression of LAT(-EGFP) variants (Fig. S8). Error bars indicate standard deviation of the mean, black puncta represent individual experiments. The data show measurements for six independent measurement days.

by the presence of proline residue in the central seg-ment of the TMD. Replacement of this residue with alanine (P17A mutant) completely removed the kink in the LAT TMD structure. Moreover, nonpalmitoylated LAT-P17A mutant localised to the PM in approxi-mately half of the cells. No such localisation was observed for nonpalmitoylated LAT with native TMD sequence, thus, indicating that Pro17 is critical for the dependence of LAT surface expression on palmitoyla-tion. This is probably caused by a highly dynamic cen-tral region of native TMD. Indeed, similar helix destabilisation was observed in other TM peptides with centrally positioned proline residue [18]. In oligo-meric and multispanning (polytopic) proteins, central prolines were found to facilitate tight packing of TMDs and to function as transmission elements of conformational changes required for a rapid response to external stimuli (e.g. ligands, photons or electro-chemical fluctuations; refs. [19–21,39]). Potentially, such kinked TMD can affect the stability of single-spanning protein such as LAT in membranes. We did not observe cytosolic expression of native and mutant LAT protein, independent of its palmitoylation state.

Transmembrane domain kinks caused by centrally positioned prolines are controlled by neighbouring amino acids [20,21]. Our live-cell imaging data indicate such role for glycine positioned five residues upstream of the central proline. However, no effect on the kink and its dynamics was observed in MD simulations. This may be caused by a subtle effect of glycine resi-due on TMD dynamics, which is more pronounced in the complex lipid mixture of cell membranes. Glycine was found to enhance the helix-destabilising effect of proline in channel-forming peptide alamethicin [26]. On its own, it destabilises helical structure of down-stream residues, especially in the presence of additional helix-breaking residues in the TM segment [23]. The observed kink of LAT TMD spreads over three

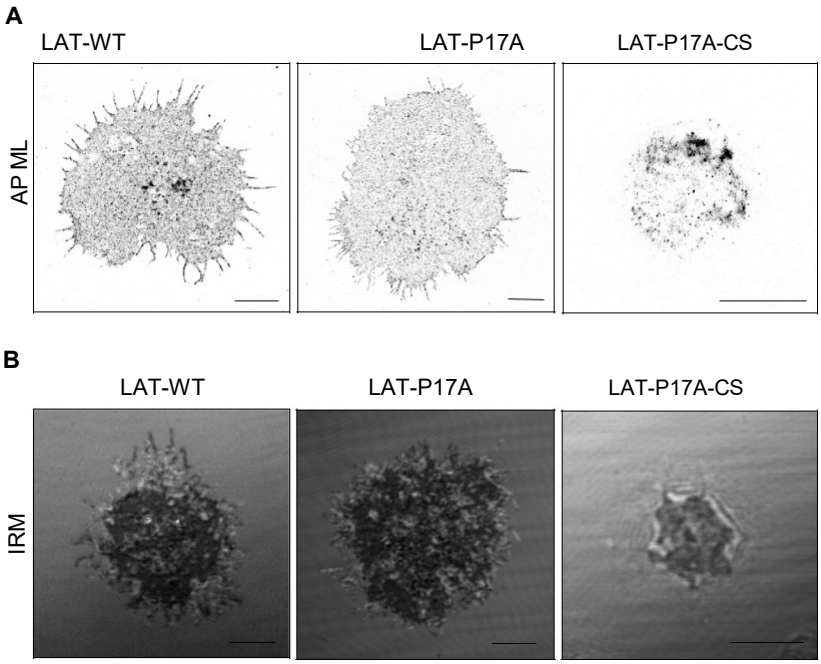

Fig. 5. SR imaging of LAT variants on the surface of T cells. (A) SR images of LAT-WT, LAT-P17A and LAT-P17A-CS in transiently transfected J.CaM2.5 cells imaged by PALM of mEos2 fusion proteins. The images represent a footprint of fixed cells on glycine-coated coverslips. (B) IRM images of living J.CaM2.5 cells transiently transfected with LAT-WT, LAT-P17A and LAT-P17A-CS. Dark areas represent a cell contact with the optical surface. Light grey diffraction rings indicate complex surface morphology of an imaged cell. Scale bars, 5 lm. Representative images from two measurement days. At least 10 cells were analysed for each LAT variant.

residues downstream of Gly12 and positions i 2 to i 4 with respect to Pro17. This is in agreement with reported destabilising effect of glycine and proline downstream and upstream, respectively, of their posi-tion in the helix [23,34].

Interestingly, as demonstrated by MD simulations, replacement of Pro8 in the luminal part of LAT TMD for alanine increased dynamics of the kink in the cen-tral part. Moreover, nonpalmitoylated LAT-P8A mutant localised to the T-cell surface in a similar pro-portion of cells as observed for the LAT-P17A mutant. A minor reduction of the helicity of native LAT TMD was observed around Pro8 residue. However, similar instability was detected for all tested peptides, includ-ing P8A variant. This minor helical instability is prob-ably not caused solely by Pro8. Von Heijne and Deber groups reported significant impact of prolines localised at the TMD ends on protein (peptide) function and structure [40,41]. On the contrary, no effect of central proline on TM helix was found using protein topol-ogy-sensitive glycosylation assay [40]. We have observed a strong impact of central proline and only a minor, if any, of proline present in the first loop of the helix. We speculate that local lipid environment and overall structure of the TM segment modulate impact of TM prolines on membrane proteins.

Cellular membranes can have diverse lipid composi-tion, which, among other things, determines their thickness [42]. Hydrophobic segment of human LAT TMD is rather long (24 residues, or 23 residues as reported in uniprot.org) but the protein requires palmitoylation for its sorting to the thicker bilayer of the PM [6,32,33]. This contradicts previous observa-tions that, in vertebrates, TMDs with > 22 residues are sufficient for protein sorting to the PM [8,9]. It is therefore possible that the kink modulates the appar-ent ‘length’ of LAT TMD by adapting the helix fold to the local lipid environment.

Recently, Levental and colleagues reported the role of TMD asymmetry in protein sorting to the PM [43]. Using bioinformatic approach, they found that proteins at the PM have smaller surface area in the luminal (exoplasmic) half of their TMD compared to the cytosolic half. This is in agreement with previ-ously reported accumulation of voluminous amino acids in the cytosolic part of the TMD of the PM proteins [9,10]. The authors argue that chemical asymmetry of the PM, which exhibits higher rigidity in its outer leaflet compared to the inner leaflet, selects proteins with asymmetric TMD in terms of surface area [43]. Voluminous amino acids are ran-domly distributed over the sequence of LAT TMD. LAT TM segment thus does not exhibit asymmetry with respect to the surface area. We have previously shown that voluminous, nonaromatic amino acids form a rough surface of TM segments and can locally rigidify membranes [44]. Strong presence of voluminous, nonaromatic amino acids in LAT TMD (14 out of 24 residues) and their distribution may, thus, require increased flexibility of this segment to

avoid interference with the PM function, which exhi-bits lipid composition prone to rigidify.

Indeed, LAT is one of very few integral membrane proteins, which segregate into more ordered parts of membranes, at least in giant PM vesicles [45]. Even though membrane domains with similar properties have not been indisputably proven in cells yet, their existence is supported by extensive indirect evidence [42,46]. The ability of LAT TMD to rapidly change geometry (intrahelically) may represent an advantage for its inclusion into membrane areas with more rigid organisation. Stabilisation of such membrane domains is predicted to involve curvature [47]. The kink in LAT TMD can help to localise the protein into mem-branes with complex molecular arrangement.

In summary, we demonstrate the existence of kink in LAT TMD, which controls LAT sorting to the PM. The kink is induced by centrally positioned proline but is further modulated by neighbouring glycine and pro-line. Replacement of these residues with helix-stabilis-ing amino acids partially recovers LAT sorting to the PM but not the function of this signalling adapter. These data indicate a complex control of LAT func-tion by highly dynamic structure of its TMD.

Materials and methods

Cell culture and transfection

LAT-negative Jurkat T-cell variant (J.CaM2.5) [48], kindly provided by Art Weiss (University of California San Fran-cisco), was cultured in RPMI-1640 media (Sigma-Aldrich, Merck KGaA, Darmstadt, Germany), complemented with 10% fetal bovine serum (FCS; Life Technologies, Thermo Fisher Scientific, Waltham, MA, USA) in a humidified incubator (Eppendorf) under controlled conditions of 37 °C and 5% CO_2. The cells were transiently transfected using the Neon transfection system (Life Technologies) according to the manufacturer's instructions. One micro-gram of vector DNA was used per shot (three pulses of 1325 V for 10 ms) per 500 000 cells, which were then incu-bated in 0.5 mL of media. Cells were analysed 16–20 h post-transfection.

DNA cloning

To generate LAT P8A and G12L mutants, LAT TMD coding sequence was modified using PCR and the primers with the appropriate mutations (Table S1) and cloned into pXJ41-LAT-enhanced GFP (EGFP) plasmid (or its non-palmitoylatable CS mutant) using EcoRI and BamHI restriction sites. The variants without the CD148 leader, c-Myc and 5^0 UTR were used [6]. LAT-P17A variants were prepared by annealing the appropriate oligonucleotides (Table S1) and subcloning as described above. For SR microscopy, the EGFP coding sequence was changed to mEos2 using BamHI and XhoI restriction sites.

Live-cell confocal microscopy

Cells transiently transfected with GFP variants of LAT in preheated, colour-free RPMI-1640 medium supple-mented with 10% FCS were placed on 1% gelatine-coated Ibidi l-Slide eight-well chambers (Ibidi, bidi GmbH Lochhame, Gr€afelfing, Germany) and imaged using a Leica TCS SP8 laser scanning confocal micro-scope equipped with sensitive hybrid detectors (HyD), 488 nm (20 mW) and 638 nm (30 mW) lasers and a 63 9 1.4 NA oil-immersion objective. Five to 10% laser power and 10% gain were used for image acquisition. Acquired images were manually thresholded to remove signal noise detected outside of the cell using IMAGEJ soft-ware package [49].

Two-colour confocal microscopy of fixed cells

Cells were immobilised on poly-L-lysine-coated Ibidi l-Slide eight-well chambers for 5 min, fixed with 4% paraformaldehyde in PBS for 20 min at room temperature and subsequently washed with PBS. Cells were perme-abilised for 40 min using 109 Permeabilisation Buffer (eBioscience, Thermo Fisher Scientific) diluted in water, washed with PBS and subsequently blocked with 5% BSA. PM and GA of transfected cells were stained with 0.5 lg mL^{-1} lectin-HPA conjugated to Alexa Fluor 647 in PBS supplemented with 1% BSA (Life Technologies) and washed twice with PBS prior imaging. Images were taken using a Leica TCS SP8 laser scanning confocal microscope equipped with a 639 1.4 NA oil-immersion objective. Minor contrast and/or brightness level adjustments were applied, and images were processed for publishing by IM-AGEJ software.

Photoactivation localisation microscopy

Sample preparation

Round 25 mm coverslips (No 1.5H, High precision; Marienfeld, Paul Marienfeld GmbH & Co. KG, Lauda-Konigshofen,€ Germany) cleaned with Helmanex III solu-tion were coated with 500 µL of 2 M glycine solution in ultrapure water for 30 min at room temperature. Prior to landing of the cells, coated coverslips were washed with Mili Q water once (Merck Millipore, Paul Marienfeld GmbH & Co. KG). Transfected cells were harvested (3 min at 300 rcf), transferred into PBS prewarmed to 37 °C and added to the coated coverslips. Cell immobili-sation was achieved by incubation at 37 °C for 10 min.

Afterwards, cells were fixed for 1 h at room temperature with 4% paraformaldehyde (Electron Microscopy Sciences, Hatfield, PA, USA) in PBS containing 2% sucrose (Sigma-Aldrich). Fixation was stopped with 50 mM NH_4Cl in PBS followed by three rounds of wash-ing with PBS. Coverslips with cells were transferred into ChamLide holder (Live Cell Instruments, Namyangju-si, Republic of Korea). Two hundred nanometer gold beads (fiducial markers; BBI Solutions, Crumlin, UK) were loaded to the sample in 0.9% NaCl for 5 min. Imaging was performed in PBS.

Microscope setup and measurements

Photoactivation localisation microscopy measurements were performed on a home-built microscope (IX71 body; Olym-pus, Olympus Czech Group, Prague, Czech Republic) equipped with 150 mW 405 nm (Cube; Coherent) and 150 mW 561 nm (Sapphire; Coherent) lasers, 1009 1.49 NA objective (UApoN; Olympus), EMCCD camera (iXon DU-897; Andor, Belfast, UK) and manual TIRF tilting mechanism (Thorlabs, Newton, NJ, USA). Synchronisation of laser switching and camera recording was performed with two acousto-optic tuneable filters (AOTF; AOTFnC-400.650-TN; AA Optoelectronics, Orsay, France) and a home written acquisition software (LabView, National Instruments Corporation, Austin, TX, USA). To turn the fluorophores into the dark state, fast epifluorescence irradi-ation with 561 nm laser was applied. Data were acquired using the highly inclined and laminated optical sheet (HILO) illumination mode with 50 ms per frame collection time. The power of activation laser (405 nm) was increased gradually to collect 10 000–15 000 frames with a uniform emitter signal.

Data analysis

To generate SR maps of LAT localisations, data were anal-ysed using ThunderSTORM plugin of the ImageJ/Fiji soft-ware package [49].

Interference reflection microscopy

Interference reflection microscopy of living cells immo-bilised on glycine-coated coverslips was recorded on a mod-ified Olympus Fluoview 1000 setup equipped with 609 1.2 NA water immersion objective (UPlanSApo; Olympus). GFP signal was excited with 20 mW 488 nm laser (Sap-phire; Coherent) and recorded on a single-channel PMT detector equipped with a selective dichroic mirror (DM488/ 543/633; Olympus). For acquisition and system control, the FluoView 1000 software package (Olympus) was used. The images were processed using ImageJ/Fiji software package [49].

Calcium measurements by flow cytometry

Cells resuspended at 10^6 cells mL^{-1} in prewarmed PBS containing 1 lM Fura Red AM (Invitrogen, Thermo Fisher Scientific) were incubated at 37 °C under 5% CO_2 in a humidified incubator for 30 min. Cells were then washed twice with PBS, resuspended in RPMI-1640 (Sigma-Aldrich) supplemented with 10% FCS (Life Technologies) and kept on ice. Prior to measurement, cells were equili-brated to 37 °C for 4 min in a water bath.

All measurements were performed on an LSRII flow cytometer (BD Bioscience, San Jose, CA, USA). A steady-state (background) signal was recorded for 25 s. After-wards, the cells were stimulated with an antibody: pre-warmed RPMI (Sigma-Aldrich) supplemented with 10% foetal bovine serum (Life Technologies) containing anti-TCR antibody C305 (home-produced supernatant, 10 μg mL^{-1}) was added in 1 : 1 ratio. Changes in calcium level were recorded continuously for over 200 s. Trans-fected cells were gated for EGFP positivity (see Supplemen-tary Fig. S8). The relative calcium concentration was measured as a ratio of the Fura Red fluorescence intensity elicited by the excitation at 405 nm (emission measured at 635–720 nm) and 488 nm (emission measured at 655–695 nm). The calcium values were calculated as the increasing signal stimulated by the 405 nm laser over the decreasing signal stimulated by the 488 nm laser using the Kinetics tool in FlowJo software version 10.6.1 (BD Biosciences, Inc.). The fold increase in signal was calculated as a ratio between maximum peak response and a mean of the steady-state signal recorded without stimulation, as indicated in Fig. 4.

All-atom MD simulations

For atomistic MD simulations, the amino acid sequence of WT LAT (EEAILVPCVLGLLLLPILAMLMALCVH CHRLP) was used to construct a fully helical model of the peptide employing the Protein Builder of the Molefacture plugin in the VMD software [50]. The standard GRO-MACS tool (pdb2gmx) was used to apply the fully atomis-tic AMBER99SB-ILDN force field for the peptide [51,52]. A lipid membrane consisting of 128 POPC molecules (64 in each leaflet) was hydrated with ~ 5000 water molecules and pre-equilibrated. The Slipid force field was used for phos-pholipids and TIP3P model was employed for water [53–55]. Then, the method of Javanainen was employed to insert the LAT peptide into the membrane in a transmem-brane orientation [56]. The overall 1 charge of LAT was neutralised by inserting one Na^+ cation into the water phase. The standard Dang's force field parameters were used for the sodium cation [57]. The membrane with LAT was then simulated using GROMACS software [51]. The same protocol of system preparation and simulations was used for the three LAT mutants considered in MD.

In simulations, fully periodic boundary conditions were used. The simulations were performed at the temperature of 310 K controlled by Nose–Hoover thermostat with the time constant 1.0 ps [58]. Pressure of 1 bar was controlled employ-ing the semi-isotropic Parrinello–Rahman barostat with the time constant of 5 ps and compressibility of 4.5 9 10 ^{5} per bar (ref. [59]). The Particle Mesh Ewald algorithm was used for accounting for long-range electrostatic interactions with the real-space cut-off set to 1.2 nm [60]. For long-range non-bonded interactions, 1.2 nm cut-off was used, switched at the distance of 1.0 nm. All covalent bonds were constrained by LINCS algorithm, and water molecules were constrained by SETTLE method [61,62]. The equations of motion were inte-grated with 2 fs time step. All simulations were performed for 1000 ns. Stabilisation of the root mean square displacement and peptide–lipid contacts was used as an equilibration crite-rion. The initial 500 ns were treated as equilibration period while the final 500 ns were used for the analysis.

The analysis of the simulated trajectories was performed using standard GROMACS tools combined with in house Python scripts. In the case of the helix tilt angle and bend-ing, the method of Bansal et al. implemented in the HELA-NAL Python library was applied [63]. The numerical data were presented using Matplotlib Python library and MATLAB [64]. Molecular visualisation was performed with the VMD software [50].

Acknowledgements

The work was supported by Charles University Grant Agency (GAUK; project number 298216) and Czech Science Foundation (19-26854X). It also received institutional funding from IMG CAS, Prague, Czech Republic (RVO 68378050). We acknowledge Light Microscopy Core Facility, IMG CAS supported by MEYS (LM2015062, CZ.02.1.01/0.0/0.0/16_013/0001775), OPPK (CZ.2.16/3.1.00/21547) and MEYS (LO1419).

Conflict of interest

The authors declare no conflict of interest.

Author contributions

MC, TB and LC designed the study. DG, HM and MCS performed the experiments. DG, HM, TC and MCS analysed the data. DG, MC and LC written the manuscript. All coauthors contributed to the final ver-sion of the manuscript.

Peer Review

The peer review history for this article is available at https://publons.com/publon/10.1111/febs.15713.

References

1 Munro S & Pelham HR (1987) A C-terminal signal prevents secretion of luminal ER proteins. Cell 48, 899– 907.

2 Nishimura N & Balch WE (1997) A di-acidic signal required for selective export from the endoplasmic reticulum. Science 277, 556–558.

3 Sandoval IV & Bakke O (1994) Targeting of membrane proteins to endosomes and lysosomes. Trends Cell Biol 4, 292–297.

4 Xiang Y, Zhang X, Nix DB, Katoh T, Aoki K, Tiemeyer M & Wang Y (2013) Regulation of protein glycosylation and sorting by the Golgi matrix proteins GRASP55/65. Nat Commun 4, 1659.

5 Diaz-Rohrer BB, Levental KR, Simons K & Levental I (2014) Membrane raft association is a determinant of plasma membrane localization. Proc Natl Acad Sci USA 111, 8500–8505.

6 Chum T, Glatzova D, Kvicalova Z, Malinsky J, Brdicka T & Cebecauer M (2016) The role of palmitoylation and transmembrane domain in sorting of transmembrane adaptor proteins. J Cell Sci 129, 95–107.

7 Smith CJ & McGlade CJ (2014) The ubiquitin ligase RNF126 regulates the retrograde sorting of the cation-independent mannose 6-phosphate receptor. Exp Cell Res 320, 219–232.

8 Munro S (1991) Sequences within and adjacent to the transmembrane segment of alpha-2,6-sialyltransferase specify Golgi retention. EMBO J 10, 3577–3588.

9 Sharpe HJ, Stevens TJ & Munro S (2010) A comprehensive comparison of transmembrane domains reveals organelle-specific properties. Cell 142, 158–169.

10 Baker JA, Wong WC, Eisenhaber B, Warwicker J & Eisenhaber F (2017) Charged residues next to transmembrane regions revisited: "Positive-inside rule" is complemented by the "negative inside depletion/ outside enrichment rule". BMC Biol 15, 66.

11 Blaskovic S, Blanc M & van der Goot FG (2013) What does S-palmitoylation do to membrane proteins? FEBS J 280, 2766–2774.

12 von Heijne G (1989) Control of topology and mode of assembly of a polytopic membrane-protein by positively charged residues. Nature 341, 456–458.

13 Fink A, Sal-Man N, Gerber D & Shai Y (2012) Transmembrane domains interactions within the membrane milieu: principles, advances and challenges. Biochim Biophys Acta 1818, 974–983.

14 Levitt M (1978) Conformational preferences of amino acids in globular proteins. Biochemistry 17, 4277–4285.

15 Sansom MS & Weinstein H (2000) Hinges, swivels and switches: the role of prolines in signalling via transmembrane alpha-helices. Trends Pharmacol Sci 21, 445–451.

16 Cordes FS, Bright JN & Sansom MS (2002) Proline-induced distortions of transmembrane helices. J Mol Biol 323, 951–960.

17 Bywater RP, Thomas D & Vriend G (2001) A sequence and structural study of transmembrane helices. J Comput Aided Mol Des 15, 533–552.

18 Thomas R, Vostrikov VV, Greathouse DV & Koeppe RE 2nd (2009) Influence of proline upon the folding and geometry of the WALP19 transmembrane peptide. Biochemistry 48, 11883–11891.

19 Peralvarez-Marin A, Bourdelande JL, Querol E & Padros E (2006) The role of proline residues in the dynamics of transmembrane helices: the case of bacteriorhodopsin. Mol Membr Biol 23, 127–135.

20 Konopka JB, Margarit SM & Dube P (1996) Mutation of Pro-258 in transmembrane domain 6 constitutively activates the G protein-coupled alpha-factor receptor. Proc Natl Acad Sci USA 93, 6764–6769.

21 Weber M, Tome L, Otzen D & Schneider D (2012) A Ser residue influences the structure and stability of a Pro-kinked transmembrane helix dimer. Biochim Biophys Acta 1818, 2103–2107.

22 Li SC & Deber CM (1992) Glycine and beta-branched residues support and modulate peptide helicity in membrane environments. FEBS Lett 311, 217–220.

23 Hogel P, Gotz A, Kuhne F, Ebert M, Stelzer W, Rand KD, Scharnagl C & Langosch D (2018) Glycine perturbs local and global conformational flexibility of a transmembrane helix. Biochemistry 57, 1326–1337.

24 Lemmon MA, Treutlein HR, Adams PD, Brunger AT & Engelman DM (1994) A dimerization motif for transmembrane alpha-helices. Nat Struct Biol 1, 157– 163.

25 Javadpour MM, Eilers M, Groesbeek M & Smith SO (1999) Helix packing in polytopic membrane proteins: role of glycine in transmembrane helix association. Biophys J 77, 1609–1618.

26 Jacob J, Duclohier H & Cafiso DS (1999) The role of proline and glycine in determining the backbone flexibility of a channel-forming peptide. Biophys J 76, 1367–1376.

27 Kumar S & Bansal M (1998) Geometrical and sequence characteristics of alpha-helices in globular proteins. Biophys J 75, 1935–1944.

28 Horejsi V, Zhang W & Schraven B (2004) Transmembrane adaptor proteins: organizers of immunoreceptor signalling. Nat Rev Immunol 4, 603–616.

29 Zhang W, Trible RP & Samelson LE (1998) LAT palmitoylation: its essential role in membrane microdomain targeting and tyrosine phosphorylation during T cell activation. Immunity 9, 239–246.

30 Zhang W, Sommers CL, Burshtyn DN, Stebbins CC, DeJarnette JB, Trible RP, Grinberg A, Tsay HC, Jacobs HM, Kessler CM et al. (1999) Essential role of LAT in T cell development. Immunity 10, 323–332.

31 Lin J & Weiss A (2001) Identification of the minimal tyrosine residues required for linker for activation of T cell function. J Biol Chem 276, 29588–29595.

32 Tanimura N, Saitoh S, Kawano S, Kosugi A & Miyake K (2006) Palmitoylation of LAT contributes to its subcellular localization and stability. Biochem Biophys Res Commun 341, 1177–1183.

33 Hundt M, Harada Y, De Giorgio L, Tanimura N, Zhang W & Altman A (2009) Palmitoylation-dependent plasma membrane transport but lipid raft-independent signaling by linker for activation of T cells. J Immunol 183, 1685–1694.

34 Richardson JS (1981) The anatomy and taxonomy of protein structure. Adv Protein Chem 34, 167–339.

35 Bonello G, Blanchard N, Montoya MC, Aguado E, Langlet C, He HT, Nunez-Cruz S, Malissen M, Sanchez-Madrid F, Olive D et al. (2004) Dynamic recruitment of the adaptor protein LAT: LAT exists in two distinct intracellular pools and controls its own recruitment. J Cell Sci 117, 1009–1016.

36 Zhang W, Sloan-Lancaster J, Kitchen J, Trible RP & Samelson LE (1998) LAT: the ZAP-70 tyrosine kinase substrate that links T cell receptor to cellular activation. Cell 92, 83–92.

37 McKinney SA, Murphy CS, Hazelwood KL, Davidson MW & Looger LL (2009) A bright and photostable photoconvertible fluorescent protein. Nat Methods 6, 131–133.

38 Franke C, Chum T, Kvıcalova Z, Glatzova D, Rodriguez A, Helmerich DA, Frank O, Brdicka T, van de Linde S & Cebecauer M (2019) Unraveling nanotopography of cell surface receptors. biorxiv [PREPRINT] https://doi.org/10.1101/2020.08.10.244251

39 Senes A, Engel DE & DeGrado WF (2004) Folding of helical membrane proteins: the role of polar, GxxxG-like and proline motifs. Curr Opin Struct Biol 14, 465–479.

40 Nilsson I, Saaf A, Whitley P, Gafvelin G, Waller C & von Heijne G (1998) Proline-induced disruption of a transmembrane alpha-helix in its natural environment. J Mol Biol 284, 1165–1175.

41 Li SC, Goto NK, Williams KA & Deber CM (1996) Alpha-helical, but not beta-sheet, propensity of proline is determined by peptide environment. Proc Natl Acad Sci USA 93, 6676–6681.

42 Bernardino de la Serna J, Schutz GJ, Eggeling C & Cebecauer M (2016) There is no simple model of the plasma membrane organization. Front Cell Dev Biol 4, 106.

43 Lorent JH, Levental KR, Ganesan L, Rivera-Longsworth G, Sezgin E, Doktorova M, Lyman E & Levental I (2020) Plasma membranes are asymmetric in lipid unsaturation, packing and protein shape. Nat Chem Biol 16, 644–652.

44 Olsinova M, Jurkiewicz P, Kishko I, Sykora J, Sabo J, Hof M, Cwiklik L & Cebecauer M (2018) Roughness

of transmembrane helices reduces lipid membrane dynamics. iScience 10, 87–97.

45 Levental I, Lingwood D, Grzybek M, Coskun U & Simons K (2010) Palmitoylation regulates raft affinity for the majority of integral raft proteins. Proc Natl Acad Sci USA 107, 22050–22054.

46 Sezgin E, Levental I, Mayor S & Eggeling C (2017) The mystery of membrane organization: composition, regulation and roles of lipid rafts. Nat Rev Mol Cell Biol 18, 361–374.

47 Cebecauer M, Amaro M, Jurkiewicz P, Sarmento MJ, Sachl R, Cwiklik L & Hof M (2018) Membrane lipid nanodomains. Chem Rev 118, 11259–11297.

48 Finco TS, Kadlecek T, Zhang W, Samelson LE & Weiss A (1998) LAT is required for TCR-mediated activation of PLCgamma1 and the Ras pathway. Immunity 9, 617–626.

49 Schindelin J, Arganda-Carreras I, Frise E, Kaynig V, Longair M, Pietzsch T, Preibisch S, Rueden C, Saalfeld S, Schmid B et al. (2012) Fiji: an open-source platform for biological-image analysis. Nat Methods 9, 676–682.

50 Humphrey W, Dalke A & Schulten K (1996) VMD: Visual molecular dynamics. J Mol Graph Model 14, 33– 38.

51 Abraham M, Murtola T, Schultz R, Pall S, Smith J, Hess B & Lindahl E (2015) GROMACS: high performance molecular simulations through multi-level parallelism from laptops to supercomputers. SoftwareX 1, 19–25.

52 Lindorff-Larsen K, Piana S, Palmo K, Maragakis P, Klepeis JL, Dror RO & Shaw DE (2010) Improved side-chain torsion potentials for the Amber ff99SB protein force field. Proteins 78, 1950–1958.

53 Jambeck JP & Lyubartsev AP (2012) An extension and further validation of an all-atomistic force field for biological membranes. J Chem Theory Comput 8, 2938– 2948.

54 Jambeck JPM & Lyubartsev AP (2012) Derivation and systematic validation of a refined all-atom force field for phosphatidylcholine lipids. J Phys Chem B 116, 3164–3179.

55 Chen F & Smith PE (2007) Simulated surface tensions of common water models. J Chem Phys 126, 221101.

56 Javanainen M & Martinez-Seara H (2016) Efficient preparation and analysis of membrane and membrane protein systems. Biochim Biophys Acta 1858, 2468– 2482.

57 Dang LX, Schenter GK, Glezakou VA & Fulton JL (2006) Molecular simulation analysis and X-ray absorption measurement of Ca2+, K+ and Cl- ions in solution. J Phys Chem B 110, 23644–23654.

58 Nose S (1984) A molecular-dynamics method for simulations in the canonical ensemble. Mol Phys 52, 255–268.

59 Bussi G, Donadio D & Parrinello M (2007) Canonical sampling through velocity rescaling. J Chem Phys 126, 014101.

60 Essmann U, Perera L, Berkowitz ML, Darden T, Lee H & Pedersen LG (1995) A smooth particle mesh ewald method. J Chem Phys 103, 8577–8593.

61 Hess B, Bekker H, Berendsen HJC & Fraaije JGEM (1997) LINCS: a linear constraint solver for molecular simulations. J Comput Chem 18, 1463–1472.

62 Hockney RW, Goel SP & Eastwood JW (1974) Quiet high-resolution computer models of a plasma. J Comput Phys 14, 148–158.

63 Bansal M, Kumar S & Velavan R (2000) HELANAL: a program to characterize helix geometry in proteins. J Biomol Struct Dyn 17, 811–819.

64 Hunter JD (2007) Matplotlib: A 2D graphics environment. Comput Sci Eng 9, 90–95.

Supporting information

Additional supporting information may be found online in the Supporting Information section at the end of the article.

Fig. S1. Localisation of LAT variants with prolonged TMD in J.CaM2.5T cell line.

Fig. S2. Angles formed by kinked helix of LAT pep-tides in POPC membrane – MD simulation data.

Fig. S3. Tilt angles of LAT peptides in POPC mem-brane – MD simulation data.

Fig. S4. Localisation of LAT-WT-EGFP and its non-palmitoylatable variant LAT-CS-EGFP.

Fig. S5. Localisation of LAT-P8A-EGFP and its non-palmitoylatable variant LAT-P8A-CS-EGFP.

Fig. S6. Localisation of LAT-G12L-EGFP and its nonpalmitoylatable variant LAT-G12L-CS-EGFP. Fig. S7. Localisation of LAT-P17A-EGFP and its nonpalmitoylatable variant LAT-P17A-CS-EGFP. Fig. S8. Gating for low expression of LAT variants in transiently transfected J.CaM2.5T cells for the analysis of antibody-stimulated intracellular calcium response. Fig. S9. Localisation of LAT variants containing the extracellular domain of CD4 in J.CaM2.5T cell line. Fig. S10. Super-resolution imaging of LAT variants on the surface of T cells.

Table S1. List of PCR primers.Movie S1. The last 500 ns of the 1 μs-long MD simulation of the LAT-WT peptide in POPC bilayer.Movie S2. The last 500 ns of the 1 μs-long MD simulation of the LAT P8A peptide in POPC bilayer.Movie S3. The last 500 ns of the 1 μs-long MD simulation of the LAT G12L peptide in POPC bilayer.Movie S4. The last 500 ns of the 1 μs-long MD simulation of the LAT P17A peptide in POPC bilayer.

nature COMMUNICATIONS

ARTICLE

DOI: 10.1038/s41467-017-01857-x OPEN

Quantifying protein densities on cell membranes using super-resolution optical fluctuation imaging

Tomáš Lukeš[1,2], Daniela Glatzová[3,4], Zuzana Kvíčalová[3], Florian Levet[5,6], Aleš Benda[3,7], Sebastian Letschert[8], Markus Sauer[8], Tomáš Brdička[4], Theo Lasser[1] & Marek Cebecauer[3]

Quantitative approaches for characterizing molecular organization of cell membrane molecules under physiological and pathological conditions profit from recently developed super-resolution imaging techniques. Current tools employ statistical algorithms to determine clusters of molecules based on single-molecule localization microscopy (SMLM) data. These approaches are limited by the ability of SMLM techniques to identify and localize molecules in densely populated areas and experimental conditions of sample preparation and image acquisition. We have developed a robust, model-free, quantitative clustering analysis to determine the distribution of membrane molecules that excels in densely labeled areas and is tolerant to various experimental conditions, i.e. multiple-blinking or high blinking rates. The method is based on a TIRF microscope followed by a super-resolution optical fluctuation imaging (SOFI) analysis. The effectiveness and robustness of the method is validated using simulated and experimental data investigating nanoscale distribution of CD4 glycoprotein mutants in the plasma membrane of T cells.

[1] Laboratoire d'Optique Biomédicale École Polytechnique Fédérale de Lausanne, STI-IBI, CH-1015 Lausanne, Switzerland. [2] Department of Radioelectronics, FEE, Czech Technical University in Prague, 166 27 Prague, Czech Republic. [3] Department of Biophysical Chemistry, J. Heyrovsky Institute of Physical Chemistry, Czech Academy of Sciences, 182 23 Prague, Czech Republic. [4] Laboratory of Leukocyte Signalling, Institute of Molecular Genetics, Czech Academy of Sciences, 142 20 Prague, Czech Republic. [5] Interdisciplinary Institute for Neuroscience UMR 5297 CNRS Université de Bordeaux, 33077 Bordeaux, France. [6] Bordeaux Imaging Center, UMS 3420 CNRS Université de Bordeaux US4 INSERM, 33077 Bordeaux, France. [7] Imaging Methods Core Facility BIOCEV, 252 50 Vestec u Prahy, Czech Republic. [8] Department of Biotechnology and Biophysics, Biocenter, University of Wuerzburg, D-97074 Wuerzburg, Germany. Correspondence and requests for materials should be addressed to T.L. (email: theo.lasser@epfl.ch) or to M.C. (email: marek.cebecauer@jh-inst.cas.cz)

Surface molecules influence vital functions of living cells. Proteins form the largest pool among these essential molecules. A growing body of evidence supports the hypothesis that proteins are not distributed homogeneously but rather in complexes, clusters and other higher-order patterns in membranes of cells and organisms[1–4]. It has been experimentally demonstrated that these protein clusters are involved in the regulation of signal transduction and other vital cell processes[5]. It is therefore important to monitor heterogeneous distribution of membrane proteins at nanoscale and with quantitative approa-ches[6]. The efficiency of currently available tools for cluster ana-lysis is limited in high-density regions by the ability to identify and localize individual molecules in raw images, as well as the blinking properties of the emitters[7, 8]. This has motivated us to develop a robust method for investigation of molecular organi-zation of cell membranes that tolerates diverse experimental conditions.

The size of membrane protein assemblies varies and is frequently smaller than 200 nm, which is below the resolution limit of classical fluorescence microscopy. During the last two decades, super-resolution techniques have been developed that overcome the diffraction limit[9, 10] and provide a detailed view of structures smaller than 200 nm. Single-molecule localization microscopy (SMLM) has been frequently used to characterize membrane protein assemblies[11–14]. SMLM techniques such as (fluorescence) photoactivated localization microscopy (PALM, FPALM)[15, 16] and (direct) stochastic optical reconstruction microscopy (STORM, dSTORM)[17–20] rely on temporal discrimination of otherwise spatially overlapping fluorophore images. In sequences of at least several thousand images, the position of fluorescent molecules is determined by fitting a model function to the imaged point spread functions (PSFs). In high-density regions this fitting procedure may meet its limit, leading to under-counting errors with significant localization errors for overlapping molecules[7]. The stochastic blinking behavior of fluorophores may result in multiple localizations from single molecules[8]. It was previously reported that high photoswitching rates in combination with high emitter densities can give rise to the appearance of artificial clusters[7]. These limitations may compromise the quantification of densely packed proteins in membrane clusters. Characterization of such protein clusters becomes a challenge because current methods for cluster analysis[12–14, 21–25] rely both on difficult-to-model photophysical properties and on acquisition parameters of the SMLM data. In this work, we readdress these problems with an approach based on SOFI and present an innovative and general method to study molecular distribution on cell membranes that overcomes the aforementioned limitations.

SOFI is an optical super-resolution technique that exploits the spatio-temporal photon traces created by stochastically blinking fluorophores. SOFI disentangles the overlapping PSFs by employing higher-order statistics. The strong temporal cross-correlation over several neighboring pixels is the underlying cause of SOFI super-resolution[26, 27]. The achieved resolution improvement results from the properties of spatio-temporal cross-cumulants calculated from the entire image sequence of 2D[26] or 3D[28] images. SOFI can be used to analyze SMLM data, but tolerates much higher emitter densities[29, 30]. Balanced SOFI (bSOFI) combines the information content of several cumulant orders in a system of linear equations, allowing to extract physical meaningful parameters such as brightness, emitter density and the on-time ratio of the blinking emitters[31]. Molecular density is a calculated parameter based on the full image sequence and not on individual localizations acquired in frame-by-frame data post-processing. In bSOFI multiple blinking of individual emitters improves the bSOFI signal and, therefore, the accuracy of these statistically estimated parameters.

SOFI used for estimation of molecular parameters shows some similarities in its mathematical formulation with image correla-tion spectroscopy (ICS) and related methods such as spatio-temporal ICS, raster ICS, and k-Space ICS[32–34]. All these methods exploit temporal correlations over a sequence of images. How-ever, SOFI relies on higher-order cumulants for super-resolution imaging. The molecular parameter maps, resulting from bSOFI, are calculated with increased spatial resolution, but compared to ICS on generally longer time intervals. bSOFI assumes the sample to be stationary during the image acquisition, where the fluc-tuations in intensity arise mostly from the blinking behavior of observed emitters. In contrast, ICS intends to measure fast molecular processes such as diffusion or number of molecules, but does not provide super-resolution.

Previously, we demonstrated the potential of bSOFI for molecular density estimation. The investigated samples have been tubulin meshworks[31] or dense protein structures such as focal adhesions labeled with fluorescent proteins[30].

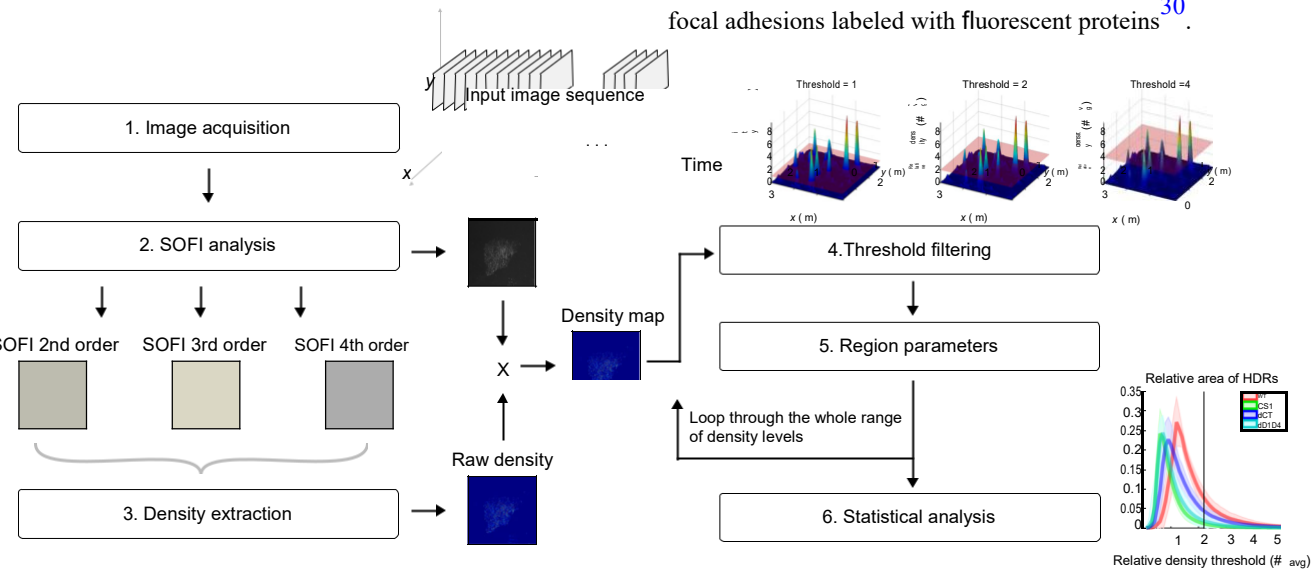

Fig. 1 The workflow of SOFI-based molecular density analysis. SOFI images of different cumulant orders were calculated and used to extract molecular densities. The background was removed using the bSOFI image as a transparency mask. High-density regions (HDRs) were segmented by varying the threshold parameter over the whole range of available density levels. For each threshold, the area, equivalent diameter, and number of HDRs were extracted and plotted as a function of the density threshold (Fig. 3). The procedure is then repeated for each sample and ROI

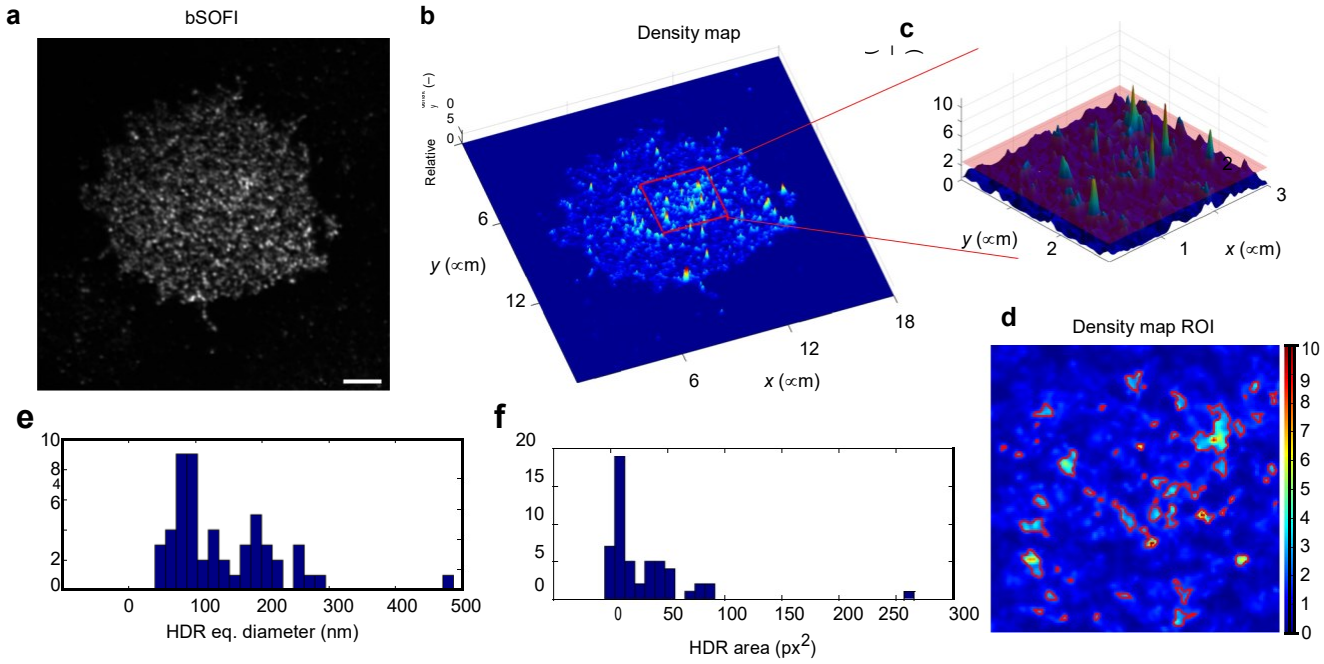

Fig. 2 Example of data processing for a single cell expressing wild-type CD4-mEos2 fusion protein. First, bSOFI image a is generated and a molecular density map b is calculated. Segmentation of clusters in the 3 × 3 µm region of interest (ROI) as indicated in b is performed for each molecular density by monotonically increasing the threshold (an example is shown for a relative density threshold equal to 2.2 times the mean density (c, d). For each threshold, a histogram of equivalent diameters (e), i.e. diameter of a circle of the same area as the non-circular region, and a histogram of the measured area (px^2; f) of high-density regions (HDRs) in the ROI shown in d are presented

Here we extend this preliminary work substantially for a quantitative and user-independent analysis of protein densities on cell membranes. We present a full framework of a SOFI-based clustering analysis for quantitative assessment of heterogenous protein distributions. By an automatic analysis of the bSOFI density maps, our method quantifies molecular clustering beha-vior and allows direct comparison of different membrane mole-cules, their mutant variants or membrane organization at altered experimental conditions (e.g. the effect of inhibitors or drugs).

Results

Molecular density clustering analysis. For quantifying the protein distribution in the plasma membrane of T cells, we acquired image sequences with a total internal reflection fluorescence (TIRF) microscope equipped with an EMCCD camera to detect the fluorescence originating from individual fluorescent emitters (see Methods). The proteins of interest were labelled with adequate blinking fluorophores, i.e. emitters cycling between dark/bright states.

The algorithm work flow is shown in Fig. 1. All acquired image sequences are first drift-corrected with sub-pixel precision. Using ThunderSTORM[35], we measured lateral drift using fluorescent beads (fiducial markers) present in the images. These drift-corrected image sequences were then processed by the bSOFI algorithm using second, third and fourth-order cumulant analysis (see Methods). We extracted molecular density maps by combining the cumulant images in a system of linear equations (see Methods). As shown previously[30], the accuracy of the density calculation is mainly determined by the size of the input image sequence. We acquired image sequences of 5000 frames for each dataset, optimizing the number of frames by analyzing the signal to noise ratio (SNR)[30]. The density maps were further analyzed to extract molecular density and clustering parameters for a direct comparison of tested molecules (see Methods). Figure 2 shows a data-processing example for a single cell.

Instead of setting the threshold by the examiner, our SOFI-based clustering analysis evaluates the density maps by monotonically increasing the threshold in a full spectrum of calculated densities (see Methods). Starting with a low threshold, large regions with a low average density are segmented. Increasing the threshold step by step allows precise density quantification (Supplementary Fig. 1). The algorithm analyzes each region of interest (ROI) by calculating, for each density threshold, the average number and area of HDRs, as well as the relative area occupied by the HDRs. The averaged data across all cells for each protein variant over the range of density thresholds are shown in Fig. 3a–c. This analysis provides an overview of HDR parameters in relation to the density threshold, unraveling the overall clustering behavior of the samples under study. Inset images in Fig. 3a and Supplementary Fig. 1 indicate how the density threshold affects the detection of HDRs. Detailed statistics of the quantitative molecular density data can be further presented for the optimal density threshold (Fig. 3d) or any other threshold selected, for example, based on biological reasoning. The optimal density threshold shown in Fig. 3a–c is determined automatically by the algorithm (Supplementary Fig. 2) to distinguish between clustering that corresponds to a random distribution of proteins and the non-random behavior of proteins that creates larger HDRs. This fully automated algorithm does not require manual selection of this important parameter by the user. When calculating the fourth-order SOFI image, the pixel size of the resulting SOFI density map is 26.25 nm. According to the Shannon-Nyquist sampling theorem, the smallest detectable HDR would have a diameter of 52.5 nm. The density analysis can distinguish differences in HDR diameters in increments of 26.25 nm. Higher resolution could be possible with higher-order SOFI images at the expense of more input images, i.e. longer acquisition times. To verify our approach in membrane areas with different molecular densities, we performed simulations that indicate good reliability of the analysis across a broad range of HDR densities (500–3000 mol/µm^2) and HDR to background

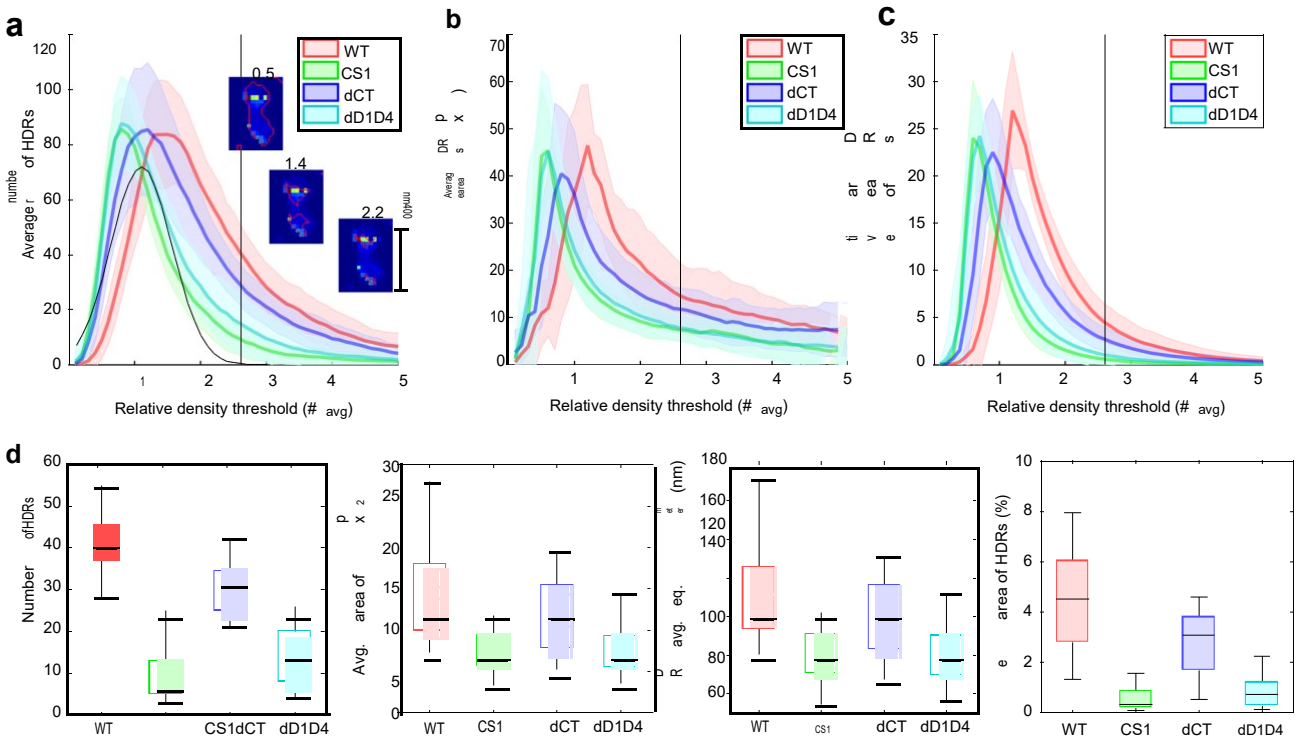

Fig. 3 SOFI analysis of four CD4 protein variants in resting T cells immobilized on poly-L-lysine-coated coverslips. Native CD4 (WT), palmitoylation mutant (CS1) and variants lacking the extracellular (dD1D4) and cytosolic parts (dCT) were tested (n = 20 per variant). a Number of high-density regions (HDRs) averaged over all samples for each CD4 variant. Density thresholds are related to the mean density calculated over the 3 × 3 µm ROIs of all samples. The inset images show examples of the segmented HDRs for various thresholds indicated above the image. b HDR area averaged over all samples for each CD4 variant in px^2, where pixel size is 25 nm. c Relative area occupied by HDRs related to the total area of the ROI. d Box plots of the properties of HDRs for a threshold equal to 2.6 δ_{avg} (marked by the vertical dash dot line). The chosen threshold is the value, where Gaussian function of a random distribution (marked in a by the dashed line) falls below 1 (Supplementary Fig. 2). Semi-transparent color areas in a–c represent standard deviation. In each box plot in d, the box represents the interquartile range (IQR), the central mark is the median, and the whiskers extend to the most extreme data points. Each box plot was calculated over 20 samples

ratios (20–100). The accuracy of HDR detection increases with increasing HDR to background ratio, which was sufficiently high for all conditions in our real cell experimental data (see Methods and Supplementary Fig. 3).

Protein nanoscale organization. In order to validate our approach, we expressed four different mutant variants of mEOS2-labeled CD4 and analyzed individual protein distributions on the plasma membrane of resting T cells immobilized on poly-L-lysine-coated glass coverslips. Using TIRF microscopy, we imaged 20 cells for each CD4 variant (i.e. 80 in total), acquiring 5000 frames per cell. Tested mutants were native CD4 protein (WT), palmitoylation mutant (CS1), and truncated variants lacking the extracellular (dD1D4) and cytoplasmic (dCT) domains (Supple-mentary Fig. 4).

Segmentation of SMLM data acquired for CD4(WT)-mEos2 indicated the accumulation of native CD4 in HDRs with irregular shape, frequently forming networks (Fig. 2 and Supplementary Fig. 5). SMLM-based cluster analysis of these localization data would be a challenge due to the limitations discussed above and in Supplementary Fig. 5. Moreover, we compared our SOFI-based approach with the state-of-the-art clustering analysis based on SMLM data and showed that SOFI exhibited a consistent performance across a whole range of tested conditions with no cluster-like artifacts (Supplementary Figs 6 and 7). On the contrary, SMLM-based clustering analysis is prone to artifacts if the optimal conditions are not met (i.e. in the case of low irradiation intensity, short off times of fluorophores, high molecular density per frame). SOFI-based clustering analysis achieved an unbiased robust performance and comparable results under different experimental conditions, which underlines the "quantitativeness" of our approach (Supplementary Figs 6 and 7).

Thus, we used our SOFI-based clustering analysis to quantify distribution of CD4 variants on the surface of resting T cells. To minimize cell-size dependency and aiming for a true comparative protein density analysis among different CD4 variants, we selected a 3 × 3 µm ROI in each cell. All CD4 variants exhibited comparable protein expression levels (Supplementary Fig. 8). Figure 3 summarizes the quantitative data on CD4 membrane organization and indicates significant differences between the tested protein variants at the cell surface of resting T cells. As shown in Fig. 3d, native (WT) CD4 are organized in HDRs covering a large part of the plasma membrane as indicated in Roh et al.[36]. Such arrangements depend on the intact extracellular domain and palmitoylation of CD4 since mutants lacking these structures exhibit more random distribution with rare accumula-tion in rather small HDRs (Fig. 3d). This observation is also supported by the truncation variant, which lacks the cytoplasmic part (dCT) but contains a single cysteine residue for palmitoyla-tion. Reversibility of this protein lipid modification can lead to a more rapid depalmitoylation of dCT variant compared to native CD4 with two membrane-proximal cysteine residues (Supple-mentary Fig. 4). Indeed, dCT variant forms fewer HDRs than native CD4, but is more heterogeneously distributed compared to a non-palmitoylatable mutant (CS1).

The results presented in Fig. 3 strongly indicate the ability of our new method to identify HDRs with irregular shape and varying densities. The imaged cells also exhibited a high level of

intercellular variability, especially in case of the intermediate phenotype (dCT), and heterogeneity between HDRs identified within ROIs (Supplementary Fig. 9). The presented results of clustering analysis performed under diverse (real) conditions emphasize the robustness of our method.

Discussion

In this work, we introduced a novel method for the character-ization of molecular organization and clustering on cellular sur-faces. The method shows an unbiased performance over a broad spectrum of non-ideal experimental conditions, which are com-mon in single-molecule localization microscopy and microscopy in general. Our fully-automated quantitative clustering analysis is based on SOFI, which provides several distinct advantages over SMLM-based approaches: (i) applicability to densely populated regions (overlapping fluorescence emitters) without a need to adapt specific imaging conditions[37], which are not always accessible; (ii) no need for multiple blinking corrections[38, 39] or other specialized approaches for circumventing the problem of cluster artifacts generated by overcounting of blinking fluor-ophores[11, 40], and (iii) inherent access to molecular density without a priori assumptions about the clustered molecules. Our approach does not require molecular localization coordinates to calculate clustering properties of proteins (or other molecules) on the cell surface. Importantly, the algorithm provides quantitative molecular density analysis of protein distributions independent of any user-defined parameters. The optimal density threshold to distinguish a random distribution of proteins from clustering is automatically determined for a tested dataset. We demonstrated the applicability of the proposed method by analyzing the surface distribution of CD4 glycoprotein, which forms large, dense, and interconnected regions on human T cells. Our molecular density analysis indicates the importance of the extracellular domain and of receptor palmitoylation for the organization of CD4 on the plasma membrane. This key conclusion is based on the analysis quantifying the clustering behavior of proteins across all density levels available in the sample with no need of an arbitrary threshold specified by the user (Fig. 3a). The fully automated approach opens widely the door for the identification of mole-cules, variants, or experimental conditions where diverse supra-molecular structures are formed at different densities. These would be more difficult in a cluster analysis depending on the manual threshold selection.

We believe that the presented method represents an innovative and universal tool to study molecular distribution on cell mem-branes. It bears the potential to be extended to any surface molecules accessible for fluorescent labeling under physiological, pathological, or pharmacological conditions.

Methods

Microscope setup. A customized setup built on an inverted optical microscope (IX71, Olympus) was used for cell imaging. A 150 mW 561 nm laser (Sapphire, Coherent) and a 100 mW 405 nm laser (Cube, Coherent) provided the excitation and activation, respectively. An acousto-optic tunable filter (AOTFnC-400.650-TN, AA Optoelectronics) provided fast switching of the laser sources. Both lasers were combined and focused into the back focal plane of an objective (UApoN 100x, NA = 1.49, Olympus). Total internal reflection was achieved with a commercial TIRF module (IX2-RFAEVA-2, Olympus) and the fluorescence emission was detected by an EMCCD camera (iXon DU-897, Andor).

Generation of CD4 mutant variants. pXJ41-mEOS2 plasmid was prepared by cloning the full mEOS2 sequence[41] (kind gift of Sean A. McKinney; Janelia Farm, Ashburn, VA) to the pXJ41 vector. The pXJ41-mEOS2 plasmid includes 5′UTR and the leader sequence of human CD148 with c-Myc tag for better protein expression in Jurkat T cells and immunolabeling.

The coding sequence of native CD4 and its non-palmitoylatable variant (CS1; mutations C419S and C421S) was a kind gift of W. Popik (Meharry Medical College, Nashville, TN;[42]). cDNA was amplified using primers TATGGTACCAAG AAAGTGGTGCTGGGCAAAAAA and GGATCCAATGGGGCTACATGTCTTC TGAAACC and sub-cloned into pXJ41-mEOS2 vector. Primers TATGGTACCA AGAAAGTGGTGCTGGGCAAAAAA and GGATCCACAGAAGAAGATGCC TAGCCCAAT were used to generate $CD4_{1-419}$ variant lacking the intracellular part (dCT), and GATCCGGAGGTGGATCTAGTGCGATTAAGCCAGACATGAAG and CTCGAGTTATCGTCTGGCATTGTCAGGCAATC for $CD4_{387-458}$ variant lacking the extracellular part (dD1D4). The products were subcloned into pXJ41-mEOS2 using KpnI and BamHI restriction sites.

Sample preparation. Jurkat T cells in RPMI-1640 media (Sigma-Aldrich), com-plemented with glutamine and 10% fetal calf serum (Life Technologies), were grown in an incubator under controlled conditions of 37°C, 5% CO_2, and 100% humidity. The cells were transiently transfected using the Neon® transfection system (Life Technologies). One microgram of vector DNA per shot (3 pulses of 1325 V lasting for 10 ms) per 200,000 cells was used (see manufacturer's instruc-tions). Twenty-five-millimeter diameter microscope coverslips were cleaned by incubation with 2% Hellmanex (Sigma-Aldrich) overnight at 42˚C and subse-quently washed with MiliQ water. Prior to use, the coverslips were coated with poly-L-lysine (Sigma-Aldrich). Twenty hours after transfection, the cells were washed with PBS, resuspended in phenol red-free RPMI-1640 media (Sigma-Aldrich), seeded on the poly-L-lysine-coated coverslips, and incubated for 5 min at 37°C under 5% CO_2. After a quick PBS wash the cells were fixed using 4% par-aformaldehyde in PBS at 37°C for 10 min. After removal of excess liquid, the fixation was stopped with 0.1 M NH_4Cl in PBS and the cells were washed with PBS. Finally, the coverslip was placed into a ChamLide holder for imaging (Live Cell Instruments).

Imaging. Fixed cells were imaged in a PBS solution at room temperature. For monitoring drift, 200 nm gold beads (BBI international) were added to the sample. The mEos2 fluorophore was excited at 561 nm with a maximum power of ~ 30 mW and activated by a 405 nm laser with a maximum power of ~ 0.3 mW (both measured at the sample plane). Cells were imaged with an EMCCD camera using an EM gain of 300 and an exposure time of 32 ms.

SOFI molecular density analysis. SOFI needs the sample to be immobile during image acquisition, and imaging beyond the diffraction limit demands drift cor-rection. Tracking the positions of gold nanoparticles provides translational motion vectors in between consecutive frames. Registering consecutive frames with sub-pixel precision using bilinear interpolation was used for drift correction.

The drift-corrected image sequence was sub-divided into sub-sequences of 500 frames each. These sub-sequences were chosen sufficiently short in order to minimize the influence of photobleaching[22, 24]. In each subsequence, SOFI images of second, third and fourth-order were calculated. These SOFI images were then averaged across all sub-sequences.

The SOFI-based molecular density analysis was programmed in MATLAB taking into account a linearization procedure as described in ref. [24]. Combining SOFI images of different orders allows one to extract density maps (Supplementary Note 1).

Molecular density (i.e. number of emitters per pixel area) at pixel position r is given as

$$N(r) = \frac{g_2(r)}{\mu_2\left(\frac{1}{2} - \frac{1}{2\sqrt{3K_1^2 - 2K_2}}\right)\left(\frac{1}{2} + \frac{1}{2\sqrt{3K_1^2 - 2K_2}}\right)};\text{where } K_1(r) = \frac{\mu_3 g_2(r)}{\mu_2 g_3(r)},$$

$K_2(r) = \frac{\mu_2 g_4(r)}{\mu_4 g_2(r)}$, g_2; g_3; g_4 represents cumulant images of second, third and fourth-order, respectively. $\mu_n = E_V\{U^n(r)\}$, where $E_V\{U^n(r)\}$ is the expectation value of the PSF ($U^n(r)$) of the n^{th}-order cumulant image. For more details, see Supplementary Note 1.

Areas containing only background are removed using the bSOFI image as a mask. The threshold filtering procedure is described in more detail in Supplementary Fig. 1. The algorithm loops through a whole range of density levels presented in the sample, starting with a threshold equal to zero and increasing the threshold step by step in each iteration. For each threshold, the data are further processed to acquire quantitative parameters describing regions with local protein density above the threshold, i.e. high-density regions (HDRs). The algorithm calculates the area, equivalent diameter, number of HDRs, and the proportion of the total area of the ROI covered with HDRs. As a result, we obtain a graph that describes the dependence of HDR parameters on the molecular density and reveals the overall clustering behavior of the sample under study. The reliability of the algorithm was investigated under a broad range of simulations (Supplementary Fig. 3).

The absolute values of SOFI molecular density map depend on expression of the fluorescent markers and parameters of the microscope (particularly excitation intensity and a camera gain). Therefore, we use relative densities and investigate relative changes of local density. For simulations, the molecular density maps were normalized by the mean density calculated over all ROIs. For the experimental data, samples were split into four groups according to four CD4 variants. In each group, the group mean density was calculated across ROIs of 20 samples. ROI of each sample was first normalized to the same mean within the group and then by the maximum of all group means. This normalization procedure largely removes

the expression dependence in between the experiments while preserving the differences in relative density in between the CD4 variants. Therefore, normalized SOFI density values can be compared across experiments, as long as the parameters of image acquisition remain the same.

Simulations. The simulation assumed photokinetics as known for fluorescent proteins in PALM experiments[24]. A photon time trace for each fluorophore was simulated providing the number of emitted photons over time. The pixel intensity at a given time point corresponds to the integration over the brightness originating from fluorophores in the conjugated object localizations. The number of converted photo-electrons was estimated by a Poisson distributed random distribution. The average value was taken as a pixel value multiplied by the detection efficiency. Additive noise corresponding to thermal noise, read-out noise, and gain variations was added as a Gaussian noise contribution. Optical system and camera parameters are matched to the microscope system settings (NA, wavelength, magnification, pixel size etc.).

The ground truth object is composed of 10 HDRs randomly distributed over an area of 3 × 3 μm. The diameter of generated HDRs varies over the range 60–180 nm, whereas the molecular density in HDRs varies over the range 500–3000 molecules/μm^2. In between the HDRs, individual molecules were randomly distributed such that the HDR to background ratio was {20, 50, 100}. For each test scenario, we simulated a random distribution of labeled molecules, including no clusters as a control. In total, we generated and analyzed 720 simulated image sequences (Supplementary Fig. 3). The simulation proves that the algorithm performs well under a broad range of conditions.

Data availability. All data and code are available from the corresponding authors upon request.

Received: 30 April 2017 Accepted: 20 October 2017
Published online: 23 November 2017

References

1. Malinsky, J., Opekarová, M., Grossmann, G. & Tanner, W. Membrane Microdomains, Rafts, and Detergent-Resistant Membranes in Plants and Fungi. Annu. Rev. Plant Biol. 64, 501–529 (2013).
2. Saka, S. K. et al. Multi-protein assemblies underlie the mesoscale organization of the plasma membrane. Nat. Commun. 5, 4509 (2014).
3. Ames, P., Studdert, C. a., Reiser, R. H. & Parkinson, J. S. Collaborative signaling by mixed chemoreceptor teams in Escherichia coli. Proc. Natl Acad. Sci. USA 99, 7060–7065 (2002).
4. Cebecauer, M., Spitaler, M., Sergé, A. & Magee, A. I. Signalling complexes and clusters: functional advantages and methodological hurdles. J. Cell Sci. 123, 309–320 (2010).
5. Prior, I. A., Muncke, C., Parton, R. G. & Hancock, J. F. Direct visualization of ras proteins in spatially distinct cell surface microdomains. J. Cell Biol. 160, 165–170 (2003).
6. Owen, D. M., Gaus, K., Magee, A. I. & Cebecauer, M. Dynamic organization of lymphocyte plasma membrane: Lessons from advanced imaging methods. Immunology. 131, 1–8 (2010).
7. Burgert, A., Letschert, S., Doose, S. & Sauer, M. Artifacts in single-molecule localization microscopy. Histochem. Cell Biol. 144, 123–131 (2015).
8. Annibale, P., Vanni, S., Scarselli, M., Rothlisberger, U. & Radenovic, A. Identification of clustering artifacts in photoactivated localization microscopy. Nat. Methods 8, 527–528 (2011).
9. Vandenberg, W., Leutenegger, M., Lasser, T., Hofkens, J. & Dedecker, P. Diffraction-unlimited imaging: from pretty pictures to hard numbers. Cell Tissue Res. 360, 151–178 (2015).
10. Huang, B., Bates, M. & Zhuang, X. Super-resolution fluorescence microscopy. Annu. Rev. Biochem. 78, 993–1016 (2009).
11. Baumgart, F. et al. Varying label density allows artifact-free analysis of membrane-protein nanoclusters. Nat. Methods 13, 661–664 (2016).
12. Rubin-Delanchy, P. et al. Bayesian cluster identification in single-molecule localization microscopy data. Nat. Methods 12, 1072–1076 (2015).
13. Sengupta, P. et al. Probing protein heterogeneity in the plasma membrane using PALM and pair correlation analysis. Nat. Methods 8, 969–975 (2011).
14. Levet, F. et al. SR-Tesseler: a method to segment and quantify localization-based super-resolution microscopy data. Nat. Methods 12, 1065–1071 (2015).
15. Betzig, E. et al. Imaging intracellular fluorescent proteins at nanometer resolution. Science 313, 1642–1645 (2006).
16. Hess, S. T., Girirajan, T. P. K. & Mason, M. D. Ultra-high resolution imaging by fluorescence photoactivation localization microscopy. Biophys. J. 91, 4258–4272 (2006).
17. Rust, M. J., Bates, M. & Zhuang, X. Sub-diffraction-limit imaging by stochastic optical reconstruction microscopy (STORM). Nat. Methods 3, 793–795 (2006).
18. Huang, B., Wang, W., Bates, M. & Zhuang, X. Three-dimensional super-resolution imaging by stochastic optical reconstruction microscopy. Science 319, 810–813 (2008).
19. Heilemann, M. et al. Subdiffraction-resolution fluorescence imaging with conventional fluorescent probes. Angew. Chemie Int. Ed. 47, (6172–6176 (2008).
20. Van de Linde, S. et al. Direct stochastic optical reconstruction microscopy with standard fluorescent probes. Nat. Protoc. 6, 991–1009 (2011).
21. Owen, D. M. et al. PALM imaging and cluster analysis of protein heterogeneity at the cell surface. J. Biophotonics 3, 446–454 (2010).
22. Ester, M., Kriegel, H.-P., Sander, J. & Xu, X. A. A density-based algorithm for discovering clusters in large spatial databases with noise. KDD 96, 226–231 (1996).
23. Ankerst, M., Breunig, M., Kriegel, H. & Sander, J. OPTICS: ordering points to identify the clustering structure. ACM SIGMOD Int. Conf. Manag. Data 28, 49–60 (1999).
24. Mazouchi, A. & Milstein, J. N. Fast Optimized Cluster Algorithm for Localizations (FOCAL): A spatial cluster analysis for super-resolved microscopy. Bioinformatics 32, 747–754 (2015).
25. Andronov, L., Lutz, Y., Vonesch, J. L. & Klaholz, B. P. SharpViSu: Integrated analysis and segmentation of super-resolution microscopy data. Bioinformatics 32, 2239–2241 (2016).
26. Dertinger, T., Colyer, R., Iyer, G., Weiss, S. & Enderlein, J. Fast, background-free, 3D super-resolution optical fluctuation imaging (SOFI). Proc. Natl Acad. Sci. USA 106, 22287–22292 (2009).
27. Dertinger, T., Colyer, R., Vogel, R., Enderlein, J. & Weiss, S. Achieving increased resolution and more pixels with Superresolution Optical Fluctuation Imaging (SOFI). Opt. Express 18, 18875–18885 (2010).
28. Geissbuehler, S. et al. Live-cell multiplane three-dimensional super-resolution optical fluctuation imaging. Nat. Commun. 5, 5830 (2014).
29. Geissbuehler, S., Dellagiacoma, C. & Lasser, T. Comparison between SOFI and STORM. Biomed. Opt. Express 2, 408–420 (2011).
30. Deschout, H. et al. Complementarity of PALM and SOFI for super-resolution live-cell imaging of focal adhesions. Nat. Commun. 7, 13693 (2016).
31. Geissbuehler, S. et al. Mapping molecular statistics with balanced super-resolution optical fluctuation imaging (bSOFI). Opt. Nanoscopy 1, 4 (2012).
32. Petersen, N. O., Hoddelius, P. L., Wiseman, P. W., Seger, O. & Magnusson, K.-E. Quantitation of membrane receptor distributions by image correlation spectroscopy: concept and application. Biophys. J. 65, 1135–1146 (1993).
33. Hebert, B., Costantino, S. & Wiseman, P. W. Spatiotemporal image correlation spectroscopy (STICS) theory, verification, and application to protein velocity mapping in living CHO cells. Biophys. J. 88, 3601–3614 (2005).
34. Brown, C. M. et al. Raster image correlation spectroscopy (RICS) for measuring fast protein dynamics and concentrations with a commercial laser scanning confocal microscope. J. Microsc. 229, 78–91 (2008).
35. Ovesný, M., Křížek, P., Borkovec, J., Švindrych, Z. & Hagen, G. M. ThunderSTORM: a comprehensive imageJ plug-in for PALM and STORM data analysis and super-resolution imaging. Bioinformatics 30, 2389–2390 (2014).
36. Roh, K.-H., Lillemeier, B. F., Wang, F. & Davis, M. M. The coreceptor CD4 is expressed in distinct nanoclusters and does not colocalize with T-cell receptor and active protein tyrosine kinase p56lck. Proc. Natl Acad. Sci. USA 112, E1604–E1613 (2015).
37. Rossy, J., Owen, D. M., Williamson, D. J., Yang, Z. & Gaus, K. Conformational states of the kinase Lck regulate clustering in early T cell signaling. Nat. Immunol. 14, 82–89 (2012).
38. Annibale, P., Vanni, S., Scarselli, M., Rothlisberger, U. & Radenovic, A. Quantitative photo activated localization microscopy: unraveling the effects of photoblinking. PLoS ONE 6, e22678 (2011).
39. Lee, S.-H., Shin, J. Y., Lee, A. & Bustamante, C. Counting single photoactivatable fluorescent molecules by photoactivated localization microscopy (PALM). Proc. Natl Acad. Sci. USA 109, 17436–17441 (2012).
40. Spahn, C., Herrmannsdörfer, F., Kuner, T. & Heilemann, M. Temporal accumulation analysis provides simplified artifact-free analysis of membrane-protein nanoclusters. Nat. Methods 13, 963–964 (2016).
41. McKinney, S. A., Murphy, C. S., Hazelwood, K. L., Davidson, M. W. & Looger, L. L. A bright and photostable photoconvertible fluorescent protein. Nat. Methods 6, 131–133 (2009).
42. Popik, W. & Alce, T. M. CD4 receptor localized to non-raft membrane microdomains supports HIV-1 entry. Identification of a novel raft localization marker in CD4. J. Biol. Chem. 279, 704–712 (2004).

Acknowledgements

We would like to thank Guy Hagen for his helpful remarks and comments. We acknowledge Peter Kapusta for technical assistance and professional advice. This work was funded by Czech Science Foundation (M.C.: 15–06989S; https://gacr.cz/en/). T.La. acknowledges the partly funding of the Horizon 2020 project AD-gut (SEFRI 16.0047, H2020-NMP-2015-two-stage – GA 686271), FP7-HEALTH-2013-INNOVA-TION-1 (HEALTH-E2-2014-602812) and the Swiss National Science Foundation (SNSF,

http://www.snf.ch/) under grants 200020-159945 and 205321-138305. T.Lu. acknowl-edges a SCIEX scholarship (13.183) and a CTU student grant (SGS16/167/OHK3/2T/13).

Author contributions

T.Lu., T.La. and M.C. conceived the study. T.Lu. and T.La. developed the molecular density analysis. D.G. and Z.K. prepared the samples. D.G. and T.Lu. performed the experiments, T.Lu., F.L., Z.K. and S.L. analyzed the data. A.B. made the microscope setup. A.B., T.B. and M.S. provided research advice. T.Lu., T.La. and M.C. wrote the paper. All authors reviewed and approved the manuscript.

Additional information

Supplementary Information accompanies this paper at doi:10.1038/s41467-017-01857-x.

Competing interests: The authors declare no competing financial interests.

Reprints and permission information is available online at http://npg.nature.com/reprintsandpermissions/

Publisher's note: Springer Nature remains neutral with regard to jurisdictional claims in published maps and institutional affiliations.

Unraveling nanotopography of cell surface receptors

Christian Franke[1,6,*], Tomáš Chum[2,6], Zuzana Kvíčalová[2], Daniela Glatzová[2,3], Alvaro Rodriguez[4], Dominic Helmerich[5], Otakar Frank[4], Tomáš Brdička[3], Sebastian van de Linde[6,8,*] and Marek Cebecauer[2,8,*]

[1] Max Planck Institute of Molecular Cell Biology and Genetics, Dresden, Germany

[2] Department of Biophysical Chemistry, J. Heyrovsky Institute of Physical Chemistry, Czech Academy of Sciences, Prague, Czech Republic

[3] Laboratory of Leukocyte Signalling, Department of Institute of Molecular Genetics, Czech Academy of Sciences, Prague, Czech Republic

[4] Department of Electrochemical Materials, J. Heyrovsky Institute of Physical Chemistry, Czech Academy of Sciences, Prague, Czech Republic

[5] Department of Biotechnology and Biophysics, Biocenter, University of Würzburg, D-97074, Würzburg, Germany

[6] Department of Physics, SUPA, University of Strathclyde, Glasgow, United Kingdom

[7] These authors contributed equally: Christian Franke and Tomáš Chum.

[8] These authors contributed equally: Sebastian van de Linde and Marek Cebecauer.

* Corresponding authors: Ch.F. cfranke@mpi-cbg.de, S.v.d.L. s.vandelinde@strath.ac.uk and M.C. marel.cebecauer@jh-inst.cas.cz

ABSTRACT

Cells communicate with the surrounding environment via receptors on their surface. However, it remains unclear how are receptors organized with respect to the complex cell surface morphology. This is mainly due to a lack of accessible, robust and high-resolution methods. Here, we present an approach for mapping the topography of receptors at the cell surface with nanometer precision. The method includes coating of glass coverslips with a glycine hydrogel which preserves the fine membrane morphology while it allows positioning of immobilized cells close to the optical surface. We further developed an advanced and simplified algorithm for the analysis of single molecule localization data acquired in a biplane detection scheme. These advancements enable direct and quantitative mapping of protein distribution on ruffled plasma membrane with near isotropic 3D nanometer resolution. By using CD4 clusters on unstimulated T cells as an example, we demonstrate that nanoclusters observed by 2D restricted methods represent accumulation of this receptor at the tips of membrane protrusions. On the contrary, CD45, which was shown to segregate from T cell nanoclusters, localizes to the membrane basis, thus, avoiding contact with CD4 on the tips. In summary, we provide a simple and straightforward workflow to study molecules and their relations at the complex surface nanomorphology of differentiated metazoan cells.

INTRODUCTION

Supramolecular complexes drive numerous vital processes in cells, such as gene expression, molecular transport or signal transduction. Cellular membranes provide an excellent platform to assemble molecules into complex structures. Indeed, membrane-associated molecules, including surface receptors, were found to form clusters with nanometric dimensions.[1, 2, 3, 4, 5] Lateral interactions and/or actin-cytoskeleton anchorage drive clustering of some receptors (e.g. tetraspanin platforms, focal adhesion complexes). However, the mechanism of cluster assembly for other receptors remains unknown and often controversial (e.g. receptor microclusters on lymphocytes). Indeed, receptor clustering is the subject of intense debate.[6, 7, 8] Several works provided the evidence about the monomeric character of receptors, which were shown to cluster using different experimental setups.[9, 10, 11] Thus, understanding their origins can help to unravel the very existence of receptor clusters. In this work we focus on receptor clustering on the plasma membrane of lymphocytes, but the method and general principles discussed herein apply to the surface of any cell, including those of prokaryotes.

A common feature of supramolecular structures, including membrane receptor clusters, is their small size (< 200 nm), which falls in a range inaccessible by standard light microscopy. Therefore, molecular assemblies in cells are often studied indirectly. For example, total internal reflection fluorescence (TIRF) microscopy enabled to visualize dynamic receptor microclusters in B and T cells.[12, 13] It was the lateral mobility of these entities, which indicated the very existence of clusters in these cells. The size and shape of the observed clusters were irresolvable because the spatial resolution of TIRF microscopy is diffraction limited. Later, super-resolution (SR) microscopy techniques were developed to overpass the diffraction limit and offered a more detailed insight into the architecture of cell receptor clusters (for example refs: [5, 14, 15, 16]).

Currently, single-molecule localization microscopy (SMLM) is the method of choice to study organization of membrane receptors due to its ability to localize emitters (i.e. labelled receptors) with nanometer precision and its potential for quantitative assessments of protein distribution and number.[17, 18, 19, 20] SMLM-based studies confirmed the earlier observations of TIRF microscopy that receptors and associated signaling molecules can cluster in non-stimulated and stimulated immune cells.[21, 22, 23, 24, 25] However, there is an intense discussion about the feasibility of SMLM for the cluster analysis of membrane molecules.[26, 27, 28] Recently, procedures aiming to minimize the impact of methodological artefacts on the SMLM results were developed.[29, 30, 31]

In most of these studies, the SMLM methods were used to generate localization maps by projecting the presumably three-dimensional receptor distribution onto a two-dimensional plane. The precise information about the axial position of emitters (e.g. receptors), and therefore their distribution, is missing. This was an accepted trade-off due to the limited axial resolution of the applied SR methods (including STED and SIM; ref. [32]). Moreover, the plasma membrane is routinely depicted as a rather featureless structure (for example: refs. [33, 34]). Yet differentiated cells of vertebrates are densely covered with membrane protrusions and

invaginations, thus, resulting in a highly three-dimensional nature of their surface.[35] Scanning electron microscopy micrographs demonstrated that finger-like membrane protrusions reminiscent of microvilli dominate the surface of immune cells.[36, 37, 38] Microvilli are dynamic structures with ~100 nm diameter and varying length between 0.5-5 µm.[39] Although less well comprehended on immune cells, tips of microvilli have a potential to accumulate membrane receptors in domains with a diameter ~100 nm in analogy to signaling receptors and channels on epithelial and sensory cells.[40]

Electron microscopy (EM), with its ability to provide information about ultrastructural details, was the key method for characterization of microvilli in the pioneering works.[41] However, EM cannot visualize specific proteins efficiently, since the labelling densities are limited by ligand/antigen accessibility, steric hindrance and electron repulsion.[42, 43, 44] A rapid development of SR light microscopy techniques enabled the visualization of three-dimensional objects with high precision, with the use of highly specific and frequently efficient labelling methods and on living cells (e.g. refs. [45, 46]). However, to characterize receptor distribution on nanometric membrane structures such as microvilli, it is important to develop three-dimensional SR techniques with axial resolution well below 50 nm. Several SMLM based methods were suggested,[47] such as astigmatism,[48] multiplane[46] or biplane imaging,[49, 50] double-helix point spread function[51] or interferometric PALM.[52]

Whereas microscopy techniques with dramatically improved spatial resolution recently became a reality, the (cell) sample preparation for SR imaging still suffers from several caveats. The spatial resolution offered by SMLM comes with the trade of time resolution since thousands of camera frames are needed to render a map, sufficiently representing, for example, a receptor distribution on a cell.[53] Thus, the movement of imaged objects (e.g. proteins) has to be minimized. This is usually accomplished by fixation of cells prior to imaging. Importantly, cells grown or isolated initially in suspension must be attached to the optical surface (e.g. coverslips). Poly-*L*-lysine (PLL; or its isomer poly-*D*-lysine) is used for immobilization of suspension cells in standard protocols.[54] However, attachment to a surface via interaction with PLL leads to the deformation of cells.[55] Similarly, the flattening of cell surfaces is observed when positioning immune cells on adhesion molecules (e.g. ICAMs) directly coated on coverslips or linked to a supported planar lipid bilayer.[56, 57] The use of hydrogel or Matrigel enables to stabilize cells for imaging without observable morphological changes.[58, 59] However, these materials submerge cells into a 3D matrix which leads to their random axial distribution. Single-molecule fluorescence microscopy techniques (including SMLM) depend on an efficient transmission of photons from emitters and, thus, provide the best results for molecules close to the optical surface.[47] Currently, none of the available methods can immobilize cells close to the optical surface without interfering with their complex surface morphology.

CD4 is a surface glycoprotein involved in T cell development and function. It is associated with Lck kinase which drives antigen-specific T cell activation.[60, 61] CD4 also mediates T cell adhesion to the cells which express major histocompatibility complex class II (MHCII) proteins

on their surface. We have recently shown that CD4 accumulates in clusters on the surface of non-stimulated T cells in a palmitoylation-dependent manner.[28] The origin of these CD4 clusters remains unknown. CD45, another glycoprotein that is three times larger than CD4, is expressed at the surface of all lymphocytes.[62] Its intracellular phosphatase domain regulates Lck kinase activity. CD45 was found to segregate from signaling molecules in activated T cells, as predicted by the kinetic segregation model of T cell activation.[63, 64] However, the mechanism responsible for such segregation is incompletely understood due to a lack of information about its precise localization at the surface of immune cells.

Here, we describe a new method for mapping receptors at the nano-topography of the plasma membrane with near isotropic three-dimensional resolution. The workflow involves a newly developed, optimized coating of glass coverslips which preserves the complex morphology of a cell surface while it allows for the positioning of immobilized cells close to the optical surface. Moreover, we adapted the recently reported TRABI method[65] for nanometer precise three-dimensional SMLM imaging to improve data acquisition, processing and drift correction, as well as the integrity of the three-dimensional SMLM data set. This allowed us to employ a straightforward quantitative assessment of the axial distributions of selected cell surface receptors at the nanoscale. We applied this method to reveal the three-dimensional nature of CD4 receptor clusters in non-stimulated T cells. We further uncovered the importance of membrane protrusions for the segregation of CD45 phosphatase from CD4 involved in T cell signaling. The presented method enables molecular studies of cell surface nano-morphology but also of other fluorescent nanoscopic structures.

RESULTS

Preservation of membrane morphology during cell immobilization on coverslips

In order to map receptor distribution at the complex surface of cells and at the nanoscale, the experimental setup must include quantitative labelling of target molecules, an appropriate sample preparation and a nanometer precise three-dimensional imaging method. In this work, labelling of surface receptors was performed by standard immunofluorescence protocols using directly labelled, highly specific antibodies.[66, 67]

Cells grown or isolated in suspension, e.g. T cells, must be immobilized on the optical surface (e.g. coverslips; Fig. 1a-b) in order to facilitate imaging approaches, which require long acquisition times. This is true for most SMLM techniques.[68] Commonly, poly-*L*-lysine (PLL; or poly-*D*-lysine) coating of glass coverslips is used to adhere suspension cells to the optical surface.[55] Negatively charged biomolecules at the cell surface electrostatically interact with the polycationic layer formed by PLL on coverslips.[69, 70] However, such electrostatic interaction can deform the cell surface (Fig. 1a; ref. [55]). Indeed, we have observed a rapid flattening of a T cell surface upon settling to the PLL-coated coverslip, visualized by TIRF microscopy of CD4-GFP fusion protein (Fig. 1c). With small exceptions (red arrowhead), a homogenous distribution of CD4-GFP signal dominated the attached T cell surface already 60

seconds after the first detectable contact with the optical surface (blue arrowheads; and Supplementary Fig. S1a). This is even more pronounced in cells observed 2 and 4 minutes after the first contact. Continuous and homogenous fluorescence signal of CD4-GFP indicates a lack of membrane accumulation in protrusions and invaginations. These data indicate that immobilization on PLL-coated coverslips is responsible for flattening of the T cell surface and, probably, for the variation in the number and size of CD4 clusters detected in our previous work.[28] Moreover, when analyzed by SMLM, diverse distribution patterns of CD4 can be found on T cells immobilized on PLL-coated coverslips. Only few cells have CD4 accumulated in high density regions (Supplementary Fig. S2a), a majority of cells exhibits a random distribution of this receptor (Supplementary Fig. S2b). We hypothesize that the pattern of CD4 distribution in these cells is defined by the time since their first contact with the PLL-coated surface. Of note, during the sample preparation, cells cannot be synchronized with respect to their first contact with the coverslip.

Since, in this work, we were interested in the origin of CD4 clusters on a rough T cell surface, we required an alternative method for coating of coverslips which better preserves their cellular morphology. Coating of an optical surface with glycine was previously used to minimize non-specific background signal in single-molecule fluorescence imaging.[71, 72] However, when applied without prior PLL treatment, glycine forms a hydrogel-like layer on a glass surface (Supplementary Fig. S3a). Our atomic force microscopy (AFM) measurements indicated a continuous surface coating with glycine (Supplementary Fig. S3b). However, the AFM measurements were limited by the softness of the glycine layer and a tendency of this material to adhere to the AFM tip. We were thus unable to determine the exact thickness and stiffness of the glycine layer. The few deformations observed in the tested samples indicated that the average thickness of glycine layer is at least 15 nm (Supplementary Fig. S3c). We further observed crystals on coverslips coated with glycine that were subsequently dried, which supports the notion of a glycine hydrogel. On the contrary, no such precipitate was observed on dried PLL-coated coverslips (Supplementary Fig. S3d). We thus conclude that glycine forms a gel-like structure on the glass surface, which functions as a semi-soft cushion upon cell landing.

To demonstrate the impact of glycine coating on cellular morphology, we imaged T cells, expressing CD4-GFP, during landing on coverslips using TIRF microscopy. In contrast to the PLL-coated samples, highly heterogeneous CD4-GFP signal was detected in cells immobilized on glycine-coated coverslips (Fig. 1d). Intensity line profiles measured across the surface of such T cells exhibit large deviations 1, 2 and 4 minutes after their first detectable contact with a coated coverslip (Supplementary Fig. S1b). These data clearly indicate that glycine-coating allows immobilization of cells close to the optical surface and improves the preservation of cellular morphology when compared to PLL-coating (Fig. 1a).

We further examined the impact of the newly developed coating method on the resting state and viability of immobilized T cells. PLL was reported to induce calcium response in cells attached to the coated surface.[73] Our measurements confirmed that PLL induces calcium

mobilization in unstimulated T cells, albeit much lower compared to antigenic stimulation mimicked by the coverslip coated with specific antibodies (anti-CD3ε) (Fig. 1e and Supplementary Fig. S4). In turn, the immobilization of T cells on glycine-coated coverslips stimulated only a negligible calcium response (Fig. 1e and Supplementary Fig. S4). Similarly, longer cultivation (> 20 min) of T cells on PLL-coated coverslips negatively influenced their viability (Fig. 1f). During the incubation of T cells on the glycine-coated coverslips, we observed much lower effect on the viability of cells compared to the sample on PLL. In summary, our findings indicate that coating of optical surfaces with glycine reduces the stress generated by the charged surface of, for example, PLL-coated coverslips. Moreover, the gel-like structure of the glycine coating preserves the surface morphology of immobilized cells as demonstrated using TIRF (Fig. 1c,d) and allows studying the three-dimensional receptor distribution on the surface of resting T cells with SMLM.

The three-dimensional SMLM method.

In order to capture the entire nanoscopic three-dimensional organization of receptors at the cell surface, we acquired image sequences with a highly inclined and laminated optical sheet (HILO) illumination, which enables single-molecule detection in cells much deeper than in TIRF microscopy (Fig. 2a). At the same time, it restricts the out-of-focus fluorescence from the remaining parts of a cell, thus improving the local signal-to-noise ratio.[74] Prior to the acquisition, we briefly irradiated the whole cell in epifluorescence to further minimize out-of-focus contributions (see **Methods**).

Intensity based biplane SMLM imaging - dTRABI. Previously, we reported the temporal, radial-aperture-based intensity estimation (TRABI) method in combination with a biplane emission detection mode as a powerful three-dimensional imaging tool with nanometer precision.[65, 75] In short, TRABI comprised fitting single-molecule spots by a Gaussian function with an invariant width, a subsequent independent photometric analysis of these spots and a final allocation of the axial coordinate based on a calibration curve. The photometric value was determined from the intensity obtained by the established Gaussian fitting procedure (I_{Fit}) and background-subtracted reference intensity of the spot (I_R), with $I_{Fit} < I_R$.

Here, we used a simplified but superior version of TRABI method where solely the intensity information obtained by the Gaussian fit (I_{Fit}) was used as metric for both channels in a biplane imaging scheme. Synchronized image stacks of the two channels (transmitted and reflected), generated by dividing the emitted fluorescence equally with a 50/50 beam-splitter, were analyzed by the same Gaussian function with an invariant width for every spot. Spots in the reflected channel were mapped to the corresponding spots in the transmitted channel by the nearest neighbor algorithm (Fig. 2b, see **Methods**). By omitting the standard, photometric analysis,[65] the computation time was reduced and the allowed number of localizations per frame was significantly increased. We therefore reckon, that we achieve an improved structural resolution while maintaining the same axial localization precision as the original

TRABI approach (Supplementary Fig. S5). We subsequently called the new method dTRABI (for *direct* TRABI; Fig. 2c).

Fiducial-free drift and tilt correction. In order to ensure optimal axial localization over an extended imaging time as well as accounting for subtle sample drift, we developed a fiducial free approach for its correction (see **Methods**). In short, the axial footprint of the entire structure is tracked over time, resulting in a spatio-temporal drift trace (Fig. 3). This trace is fitted with a high-order polynomial, which serves as the correction term for the raw localizations by linearization. We reckon that in a thin sample layer like the plasma membrane the spatio-temporal distribution of active photo-switches that reside in their on-state is constant over time. The selection of appropriate regions in axially more extended samples can include structures, where the local z-dimension is restricted. Most data sets that were used to conclude the results in the following paragraphs showed axial drift with different orders of magnitude and non-linearity, which could be accounted for by the described correction approach. However, an additional linear axial tilt was observable in some data sets, most likely due to minor imperfections of the sample rest. Since we assume the layer closest to the coverslip to be axially flat on the whole-cell scale, we fitted a three-dimensional plane to the raw image, thereby determining its gradient and thus enabling the linearization of the raw localization data (see **Methods** and Fig. 3).

Quantitative axial localization analysis. For the analysis of the axial receptor distribution, localization files were loaded and processed in Fiji with custom written scripts (see **Methods**).[76, 77] The analysis comprised three steps: generation of quantitative image stacks, segmentation in regions of interest (ROIs) and axial quantification of individual ROIs. (i) A quantitative 3D image stack (z-stack) was generated with 20 nm voxel size in *x*, *y* and *z*. (ii) These stacks were then segmented by automatically generating multiple region of interests (ROIs) with an area of 4 µm² within the interior of the cell (Supplementary Fig. S6). (iii) Then the axial distribution of localizations was analyzed, by counting all localizations per ROI along the z-stack. For each ROI the resulting distribution was fitted to a superposition of two Gaussians (Supplementary Fig. S6). By analyzing properties of these fits, we acquired parameters which provide quantitative information about the axial distribution of surface receptors (see **Methods**).

Imaging CD45 nano-topography using the dTRABI approach

To demonstrate the applicability of dTRABI, we labelled CD45 receptors, which are highly expressed on the surface of T cells (> 100.000 copies/cell; ref. [78]) with Alexa Fluor 647-conjugated antibody (MEM-28) and imaged as described above. Cells were immobilized on glycine-coated coverslips to preserve cell surface morphology. Resulting three-dimensional images with color-coded z-axis represent a footprint of a cell on a coverslip (Fig. 4a). The apparent optical depth, which varies between cells (300-650 nm), depends on the available structure in the individual field of view. CD45-labelled cells exhibited a variety of features that

can extend far away from the coverslip. However, the entire extent of the basal membrane resting on the surface was captured in all displayed and analyzed cells. Fig. 4b shows the three-dimensional image of CD45 which indicates a complex morphology of the cell surface. Magnified images and the corresponding *xz*-projections (Fig. 4c) demonstrate the ability of dTRABI to visualize large membrane protrusions at the edge of the cell (ROIs 1 and 3; blue arrowheads), as well as more subtle membrane extensions towards the exterior (ROIs 1-4; red arrowheads) and interior (ROIs 3 and 5; green arrowheads) of the cell.

The origin of CD4 nanoclusters on the surface of unstimulated T cells

Next, we examined the origin of previously reported receptor (signaling) microclusters.[1, 4, 5] Using two-dimensional SR imaging, we recently showed that CD4 receptors accumulate in high density regions on unstimulated T cells.[28] The three-dimensional organization of these clusters remained unresolved. In this work, we employed our new coverslip coating strategy and dTRABI to study CD4 clusters with near isotropic three-dimensional resolution in immobilized cell with preserved surface nanotopography. To verify the specificity of these structures, we also imaged CD45, which was reported to distribute on the surface of non-stimulated T cells more evenly.[79] To avoid visualization of intracellular molecules, fixed T cells were labelled with specific antibodies in the absence of membrane permeabilization.

First, we confirmed that CD4 accumulates in high density regions in palmitoylation-dependent manner using 2D *d*STORM with high lateral resolution (Supplementary Fig. S7). Next, three-dimensional high-resolution maps of the CD4 surface distribution were acquired by analyzing the same data sets with the dTRABI approach (Fig. 5a). These results provide detailed information about the nanotopography of CD4 at the surface of unstimulated T cells with axial localization precision of 10-20 nm (Supplementary Fig. S5). The nanoscopic three-dimensional view of wild-type CD4 indicates that the receptor is preferentially localized to one topographical level and is clustered (Fig. 5a). Plotting a relative z-position of CD4 molecules in the central area, which avoids cell edges, indicates the accumulation of wild-type CD4 in a narrow space near the coverslip (Fig. 5b and Supplementary Fig. S8). On the contrary, a broad surface distribution is evident from the three-dimensional view of a CD4 variant which cannot be palmitoylated and was previously shown to exhibit random distribution in such unstimulated T cells (CD4 CS1; Fig. 5c; ref. [28]). Our quantitative analysis demonstrates a less constrained distribution of receptor z-positions (Fig. 5d). The plot of averaged z-positions over all tested cells (21 CD4 WT and 18 CD4 CS1 cells) confirms the different axial distribution of the two CD4 variants on T cells (Supplementary Fig. S8). However, the contrast between the two variants is strongly reduced due to a variation in surface complexity of individual cells and distinct regions of the basal membrane. Therefore, the propensity of CD4 molecules to accumulate at the specific topographical levels was first analyzed in square regions of interest (ROIs) of 2×2 μm^2 selected to cover the cell-coverslip contact area over all tested cells (846 CD4 WT ROIs and 1044 CD4 CS1 ROIs in total; Supplementary Fig. S6). As mentioned above, for quantitative analysis, relative z-positions for the localizations in ROIs were fitted with a

sum of two Gaussians (Fig. 5e). From these fits, three parameters were derived, i.e. the spread of the two Gaussians termed z-distribution width (Fig. 5f-g), the peak-to-peak distance (Supplementary Fig. S9) and the width difference of the two Gaussians (Supplementary Fig. S10). These parameters better describe the axial distribution of receptors compared to the plots with the averaged relative z-positions of localizations. Indeed, a very narrow z-distribution width in the range of 90 – 150 nm in all segments demonstrated strong tendency of wild-type CD4 to accumulate at the specific topographical level in resting T cells (Fig. 4f-g). On the contrary, a lack of palmitoylation in CD4 CS1 variant caused much broader distribution of this receptor on T cell surface, exhibiting a z-distribution width predominantly in the range of 110 – 170 nm and with a substantial fraction between 150 and 340 nm. The difference between the widths of the two Gaussians is also more pronounced for CD4 CS1 (80 nm instead of 50 nm for CD4 WT) (Supplementary Fig. S9c).

The specificity of CD4 receptor clusters was further emphasized by a less constrained lateral and axial distribution of CD45 in T cells imaged using dTRABI (Fig. 5h,i; 13 cells and 305 ROIs were analyzed). Quantitative analyses performed consistent with the CD4 variants demonstrated a broader axial distribution of CD45 receptor compared to CD4 WT (Fig. 5f-g). We found the range of z-distribution widths to be similar around 90 and 150 nm, but in contrast to CD4 WT, CD45 has an additional large fraction between 150 and 400 nm. This broad CD45 distribution is particularly noticeable when analyzing the peak-to-peak distance of the fitted bimodal distribution to the relative z-position of the receptor (Supplementary Fig. S9b, see **Methods**). The obtained peak-to-peak distances were exponentially distributed and the mean values for CD4 WT and CS1 were 23 and 36 nm, respectively, whereas CD45 was more broadly distributed around 120 nm. More examples of 3D dTRABI images and their quantitative analysis for all three receptors are shown in Supplementary Fig. S10 and Supplementary Fig. S6, respectively.

Segregation of CD45 from CD4 clusters in non-stimulated T cells

When analyzing dTRABI images, we noted areas with a very low number of CD45 localizations (Fig. 6a; yellow arrowheads). Similarly, CD45 exclusion zones were detectable in 2D SOFI images of antibody-labeled T cells (Fig. 6b). The narrow shape of these exclusion zones was reminiscent of CD4 clusters observed on T cells imaged by dTRABI approach (Fig. 5a and Supplementary Fig. S10). We thus wondered whether the CD45 exclusion zones represent areas with CD4 accumulation. T cells expressing CD4 WT fused to photo-switchable protein mEos2 (ref. [28]) were labelled with specific anti-CD45 antibodies and analyzed using two-color SMLM. The data indicates that CD4 and CD45 essentially segregate into two separate zones on the surface of non-stimulated T cells immobilized on glycine-coated coverslips (Fig. 7a,b). Since CD4 clusters to one topographical level near the T cell-coverslip contact sites (Fig. 5a,b,f), we reckon that CD4 preferentially accumulates at the tips of membrane protrusions (e.g. microvilli) and CD45 to the shaft of these structures and their base at the plasma membrane (Fig. 7c). Indeed, we observed the accumulation of CD4 at the tips of large T cell

membrane protrusions in several cells (Fig. 7d,e). In turn, the shaft of protrusions was extensively covered with CD45 signal. Often, CD45 was essentially segregated from CD4 in these nanoscopic membrane structures (Fig. 7e).

Having established a new method which preserves the surface morphology and a resting state of immobilized cells, we analyzed segregation of CD4 and CD45 in living T cells forming contact with the glycine-coated coverslips using confocal microscopy (Fig. 8). Large scale (microscopic) segregation of CD4 and CD45 was observed in membranes forming contact with coverslips (Fig. 8; middle and lower panels). No such segregation was detectable in free-standing areas of the plasma membrane. Nevertheless, our two-color SMLM data indicate that CD4 and CD45 segregate on such membranes, however, at the nanoscopic scale (Fig. 7). In summary, our data suggest that CD4 and CD45 largely segregate on non-stimulated, cultured T cells which is most likely caused by their different preference for specific areas on the complex three-dimensional surface of these cells.

DISCUSSION

In this work, we have introduced a new approach for molecular mapping of the membrane receptor topography with nanometer precision. The method combines the use of glycine-coated optical surfaces which preserve membrane morphology of immobilized cells with an advanced and simplified dTRABI algorithm for quantitative, near isotropic three-dimensional SMLM imaging. Using directly labelled antibodies and dTRABI processing of biplane SMLM data, we achieved 10-20 nm localization precision in all spatial directions. This enabled us to reveal the origin of CD4 clusters and the involvement of cell surface morphology in CD45 segregation from signaling receptor clusters.

Our principal task was to preserve fine structures on the surface of T cells and to analyze the distribution of signaling receptors therein. Even though flat in most common illustrations, the plasma membrane of differentiated metazoan cells is a three-dimensional structure which is densely covered with finger-like protrusions (microvilli, filopodia), ruffles and invaginations (endocytic cavities and podosomes).[40] Its imaging with two-dimensional methods thus leads to simplifications and, potentially, misinterpretations. The availability of SR microscopy capable to resolve nanoscopic three-dimensional structures is currently limited to specialized nanophotonics laboratories. Nevertheless, standard methods of sample preparation for imaging (e.g. on PLL-coated coverslips) systematically damage the fragile surface morphology of studied cells, as indicated also by our data showing that the T cell surface complexity is diminished within few minutes since the first contact with a PLL-coated coverslip (Fig. 1c and Supplementary Fig. S2).

Several materials were previously developed to prevent cell deformation during their immobilization in a three-dimensional space, for example, Matrigel and synthetic hydrogels. Matrigel enables three-dimensional cell cultures but it is derived from the extracellular matrix of mouse tumors and exhibits autofluorescence. On the contrary, fluorescence properties of

synthetic hydrogels (e.g. CyGEL Sustain) can be controlled and the cells prepared in hydrogels display numerous protrusions on their surface, including nanoscopic structures which require SR microscopy for their detection.[58] However, TIRF and HILO sample illumination techniques which can reduce the out-of-focus background signal and, thus, improve the quality of SMLM images, enable fluorescence signal detection solely in the vicinity of the optical surface.[74, 80] Hydrogels do not allow efficient positioning of immobilized cells at the optical glass.

Here, we developed and analyzed glycine coating of coverslips which preserves cell membrane morphology. We observed a complex membrane morphology over 10 mins after the first contact of a cell with the optical surface (Fig. 1d). Moreover, a coating of coverslips with a narrow layer of glycine-hydrogel facilitates positioning of immobilized cells close to the optical surface. Importantly, cells immobilized on glycine exhibit improved viability and reduced non-specific stimulation compared to PLL-immobilized cells. Of note, the preparation of glycine-coated coverslips is straightforward, fast (<30 min) and inexpensive. All these properties qualify glycine-coating of coverslips for the advanced imaging of cells, including high-resolution three-dimensional dTRABI mapping of cell surface molecules.

We have also developed the dTRABI algorithm to allow for faster and computationally cheaper processing of SMLM data when compared to our original TRABI approach. It is built for a quantitative analysis of axial distribution of fluorescent molecules. Importantly, dTRABI can be used with any localization software that supports fixed Gaussian fitting in combination with a biplane detection scheme. In contrast to a classical biplane imaging that compares the width of spots evaluated by free Gaussian PSF fitting, which facilitates an improved localization precision. The ability of dTRABI to visualize fluorescent molecules on complex, irregular, three-dimensional cellular structures can be highlighted on a T cell which was not included in the quantitative analysis of a receptor axial distribution (Supplementary Fig. S11). Complex membrane structures formed by this dying cell were effectively labeled and visualized using dTRABI approach.

Importantly, dTRABI offers a tool for mapping localization of molecules within 1000 nm from the optical surface. Such working-space provides a sufficient axial signal penetration to visualize the eukaryotic plasma membrane with its nanotopography. Under the conditions used in our experiments, the plasma membrane protrusions were positioned 100-400 nm from the optical surface (Fig. 5). Thus, molecules which do not localize to the protrusions can be monitored as well. This was facilitated by folding of membrane protrusions, the length of which often exceeds the axial depth of our method, under the cell body (Fig. 4 and 9a,b). Evidently, a partial loss of molecular localizations in the areas where the basis of the plasma membrane is positioned outside of the optical limit of this method is caused by a diverse positioning of cells and intensive bending of cell-glass contacts (Fig. 9c,d and Supplementary Fig. S10).

A quantitative character of dTRABI data also enabled detailed analysis of receptor axial distribution. We modelled the axial receptor distribution by fitting a sum of two Gaussian functions (double Gaussian) to the data. Although CD4 distribution can be modelled by a

single Gaussian to a high degree of confidence, a double Gaussian is even more accurate and accounts for a slight asymmetric organization of receptors. In contrast, non-palmitoylatable CD4 CS1 mutant does not follow a mono Gaussian distribution and the superposition of two Gaussians is essential. The analysis allowed us to derive quantitative parameters describing axial receptor distribution in detail, i.e. z-distribution width, peak-to-peak distance and width difference. All these analytical approaches emphasized narrow and symmetrical distribution of CD4 (z-distribution width ~110 nm, peak-to-peak distance < 25 nm), while CD4 CS1 and CD45 show broader distributions.

After implementing our new imaging approach, we focused on two important biological questions: i) what is the origin of receptor microclusters in T cells, and ii) how membrane morphology affects segregation of signaling receptors into different areas of the plasma membrane. Both questions cannot be studied by previously reported protocols. Using quantitative SOFI analysis, we have previously shown that CD4 accumulates in high density regions (clusters) in non-stimulated T cells by a process which depends on its post-translational lipid modification, palmitoylation.[28] However, as in many other cases, these data represented two-dimensional projections of receptor localizations on the complex T cell surface. Using dTRABI imaging of non-stimulated T cells immobilized on glycine-coated coverslips, we demonstrate that CD4 accumulates on the tips of membrane protrusions reminiscent of microvilli. Thus, CD4 clusters, and potentially other clusters, represent receptors (or other molecules) trapped at the tips of membrane protrusions, stressing, that intact cell surface morphology is essential for the proper organization of signaling molecules. Importantly, the mutant CD4 CS1 variant which cannot be palmitoylated, distributed more randomly over the complex surface of T cells. This is in agreement with our previous observation that CD4 CS1 does not accumulate in detectable structures on these cells.[28] Targeting to or stabilizing proteins on membrane protrusions thus may be another, previously unreported role of protein palmitoylation.[81]

The best described function of CD4 is to deliver critical Lck kinase to the proximity of T cell receptor for a rapid response to antigens.[60] TCR was recently reported to accumulate in T cell microvilli by projecting a two-dimensional SMLM image onto the morphological map generated by varying-angle TIRF microscopy (VA-TIRFM) of a membrane dye.[82] VA-TIRFM is diffraction-limited and, therefore, does not provide a high-resolution map of cell surface nanotopography. However, the data indicated the accumulation of TCR in domains formed by or dependent on membrane morphology. We thus speculate that CD4 and TCR localize to the protrusions, the tips of which can represent membrane areas with concentrated signaling molecules arranged to rapidly respond to appropriate signals (Fig. 7c). How these molecules accumulate in these structures and whether the tips of protrusions undergo a further compartmentalization remains unclear. In future ventures, we will establish a robust workflow consisting of a reliable sample preparation, labelling and multi-color dTRABI analysis, in order to investigate multi-molecular architecture of these structures. Our current

approach already provides a good basis for such advancement and is adaptable to further questions.

As discussed earlier, CD4 accumulates in clusters at the tips of membrane protrusions. However, several molecules, including CD45, were shown to segregate from signaling microclusters (e.g. refs. [63, 83]). Using dTRABI and glycine-coated coverslips, we demonstrate that CD45 distributes over a broader axial spectrum compared to CD4. Since CD45 segregates from CD4 in non-stimulated T cells under the experimental conditions used in this study, we conclude that CD45 segregates from signaling molecules by localizing to the basis of the plasma membrane and by avoiding highly curved membranes of the protrusions (Fig. 7c). The molecular mechanism of such segregation remains unknown. Even though listed in a high-throughput study of palmitoylated proteins,[84] a direct experimental proof of CD45 palmitoylation is missing. Since non-palmitoylated CD4 CS1 variant exhibits a more random distribution compared to its native variant, we speculate that the lack of CD45 palmitoylation contributes to its preference for the basis of the plasma membrane. We also demonstrate that CD45 microscopically segregates from the contact site of non-stimulated T cells with a glycine-coated surface. No such segregation is observed for CD4. This suggests that CD45 reacts to mechanical forces by segregating into membranes areas unaffected by force. Nevertheless, nanoscopic segregation caused by complex membrane morphology was observed also in membranes unaffected by cell attachment to the optical surface.

In summary, we provide a new and undemanding workflow to study nanotopography of receptors at the cell surface. We highlight the importance of appropriate sample preparation for the imaging of three-dimensional structures. The improved algorithm of dTRABI exemplifies an easy to implement and high-quality method to generate three-dimensional SMLM data. Finally, we demonstrate the applicability of the workflow by answering two important questions related to the localization and function of surface receptors on lymphocytes. Even though used here for human receptors, the method can be implemented for characterization of molecules on the surface of other organisms (e.g. yeast, plants) but also for complex nanomaterials which do not exceed the current axial penetration of dTRABI (~ 1000 nm).

METHODS

Cell culture and transfection

Jurkat T cells (clone E6; ATCC) and their CD4-knock-out variants (Jurkat CD4-KO cells) were grown in RPMI-1640 medium (Gibco) supplemented with 10% fetal bovine serum (Gibco), Non-essential amino-acids (Gibco) and 10mM HEPES under controlled conditions in a humidified incubator at 37°C, and 5 % CO_2 (Eppendorf). Jurkat CD4-KO cells were derived from wild-type Jurkat T cells (clone E6; ATCC) using CRISPR/Cas9 technology as described.[85] Both cell lines were regularly tested for morphology and mycoplasma infection.

For the expression of exogenous proteins, Jurkat T cells and their CD4 KO variant were transiently transfected with plasmid DNA using Neon® transfection system (Thermo Fisher Scientific) according the manufacturer's instructions. Briefly, 1 µg of vector DNA was used per 200 000 cells in 0.5 ml culture medium. The instrument settings were: 3 pulses, each 1350 V for 10 ms. Transfected cells were used within 36 h since the transfection.

Sample preparation for SR microscopy

Cleaning and handling of coverslips and solutions for microscopy

High precision microscopy coverslips (round, 25 mm in diameter; Marienfeld) in Teflon holders (Wash-N-Dry Coverslip Rack; Diversified Biotech Inc.) were cleaned by incubation at 56°C overnight in 2% Hellmanex III (Hellma Analytics) dissolved in ultrapure Milli-Q® water (Millipore) followed by 30 minutes sonication in a heated sonication bath. Several washes in ultrapure water and one additional sonication step were used to remove all traces of Hellmanex III components. Cleaned coverslips were stored in ultrapure water to avoid drying and contamination with particles of a dust from air.

All other glassware was regularly treated with piranha solution (3 parts of 30% hydrogen peroxide and 7 parts of concentrated sulfuric acid) for 45 minutes followed by several washes with ultrapure water. All solutions were made from concentrated stocks stored in glass containers, diluted with ultrapure water and filtered using syringe filters with 0.22 µm pores (TPP) into piranha-treated glassware.

Glycine coating of coverslips

Ultraclean coverslips were coated by applying 0.5 ml of 2M glycine solution and incubation for 20 min at room temperature in the laminar flow box. Afterwards, the liquid phase was aspirated, and the hydrogel was washed with ultrapure water. Coverslips coated with glycine hydrogel were used immediately for immobilization of cells. The hydrogel-coated coverslips can be stored at 4°C covered with a layer of ultrapure water for several days.

PLL coating of coverslips

Ultraclean coverslips were coated by applying 0.5 ml of 0.01% (w/v) PLL solution in ultrapure water and incubation for 20 min at room temperature in the laminar flow box. Unbound PLL was removed by aspiration of the liquid and a single wash with ultrapure water. Dried, PLL-

coated coverslips can be stored for several weeks. For SR imaging, freshly prepared PLL-coated coverslips were used exclusively.

Immobilization and fixation of cells for SR imaging

Jurkat T cells express varying levels of CD4 which are changing when cells are grown in culture. Therefore, we used transiently transfected Jurkat-CD4KO cells with reintroduced CD4-GFP to study CD4 surface distribution with dTRABI. Cells expressing similar levels of CD4-GFP were selected for imaging and data processing.

For SR imaging, cells were resuspended in pre-warmed PBS (made from 10x stock, Gibco) and seeded on glycine-coated coverslips immediately after the aspiration of a coating liquid. Cells were enabled to land on the coated optical surface for 10 minutes at 37°C in the CO_2 incubator. Afterwards, cells were fixed with pre-warmed 4% paraformaldehyde (Electron Microscopy Sciences) containing 2% saccharose in PBS for 45 minutes at room temperature and the process was stopped with 50 mM NH_4Cl (Sigma-Aldrich) in PBS and three rounds of washing with PBS.

Immunofluorescence

For labeling, cells were first incubated with 5% BSA in PBS (Blocking solution) for 1 hour at the ambient temperature to prevent non-specific binding of antibodies. Immunostaining of specific receptors was performed by incubating cells overnight with Alexa® 647 conjugated primary antibodies (human CD4: OKT4, dilution: 1:100, source: Biolegend; human CD45: MEM-28, dilution: 1:2000, source: ExBio) diluted in Blocking solution. The process was performed at the ambient temperature in a humid chamber to avoid drying of the solutions. After removing of redundant antibodies and 3 times washing with PBS for 5 minutes, the cells were post-fixed with 4% PFA for 5 minutes and washed 5 times with PBS.

The identical protocol was applied for the staining of CD45 on Jurkat CD4 KO cells transfected with pXJ41-CD4-mEOS2 plasmid for 2-color 2D SMLM analysis.

Single-Molecule Localization Microscopy

Three dimensional SMLM experiments for dTRABI analysis were performed on a home-built wide-field setup, which is described elsewhere in detail.[65] Raw image stacks were analyzed with rapidSTORM 3.2 (ref. [86]). Herein, the FWHM was set to 300 nm as an invariant parameter. Furthermore, the lower intensity threshold was set to 500 photons and the fit window radius to 1200 nm. All other fit parameters were kept from the default settings in rapidSTORM 3.2. Linear lateral drift correction was applied manually by spatio-temporally aligning distinct structures to themselves. This was facilitated by color-coding of the temporal coordinate with the built-in tool.

Two-color SMLM experiments were performed on a Nikon Eclipse Ti microscope, which is specified elsewhere in detail.[44] Contrary to the case of dTRABI analysis, the FWHM was set as a free fit parameter, but in the limits of 275 – 750 nm, both for Alexa Fluor 647 antibody and mEOS2 fusion protein localizations. All other parameters were kept consistent to the previous

experiments. Prior to imaging, a glass surface with Tetraspeck beads (Thermo Scientific) was imaged with alternating 561 nm and 647 nm excitation to create a nanometer precise map to allow the correction of chromatic shift. The 561 nm excitation channel was then mapped onto the 647 nm after the localization step.

Prior to acquisition, cells were irradiated in epifluorescence illumination mode to turn emitters, which were out-of-focus in the HILO illumination scheme, into the dark state. In all experiments, the length of the acquisition was set to capture the majority of emitters, i.e. imaging was concluded when only a very minor number of active emitters was detectable. Typical acquisition lengths were 60,000-120,000 frames for Alexa Fluor 647 channel and 30,000-60,000 frames for mEOS2 channel, where integration times were set to 20 ms and 16 ms in the single- and dual-color cases, respectively. Hereby, mEOS2 was excited at 561 nm and activated with 405 nm. The activation power density was increased over the time to create an almost constant signal density.

Intensity based biplane imaging – dTRABI

The principle of dTRABI

We previously reported TRABI-based biplane (BP-TRABI; ref. [65]), where, instead of the axially dependent FWHMs of spots in both optical channels, the photometric ratios *P* of the molecules were used. *P* was calculated as the quotient of the fit intensity (I_{Fit}) and reference intensity (I_R), where only the fixed FWHM PSF fit intensity is used. For BP-TRABI, the photometric ratio of both planes ($P_{1,2}$) is calculated according to

$$( ) = \frac{1 \quad - 2}{1 \quad + 2} \tag{1}$$

with P_1 and P_2 being the photometric ratio of the individual planes.

The quality of the resulting axial coordinate depended on the precision of the TRABI intensity measurement. In order to exclude any interference from neighboring emitters as well as temporal overlap with other fluorophores, a set of rigorous exclusion criteria for spots was employed. As a consequence, many localizations given by the localization software were rejected by TRABI. To compensate, significantly longer image stacks had to be recorded to ensure structural consistency in the reconstructed images regarding the Nyquist-criterion. Though this was already an inconvenience for common SMLM organic fluorophores, which exhibit high repetition counts, it can be a significant obstacle for imaging approaches utilizing photo-activatable or -convertible fluorescent proteins. Furthermore, in cases of sub-optimal photo-switching rates that lead to high spot densities, the TRABI approach is computationally expensive or could even fail to produce an image due to a high rejection rate of fluorescent spots.

For a reasonable large TRABI radii I_R converges for both spots in both planes, thus Eq. (1) can be effectively simplified to

$$( ) = \frac{\text{Fit,1} - \text{Fit,2}}{\text{Fit,1} + \text{Fit,2}} \tag{2}$$

As equation 2 demonstrates, in order to achieve three-dimensional BP imaging, there is no need for an actual photometric TRABI analysis anymore, since I_R is cancelled out. Therefore, dTRABI allows for higher emitter densities, is quicker and requires less input parameters.

Calibration and allocation

Raw calibration curves were generated by linearly moving the focal plane through the sample plane while imaging a single-molecule surface under dSTORM conditions as previously described [65]. For this, a surface of BSA was doped with BSA molecules, attached to a short DNA sequence, labeled with Cy5. Fitting the raw emission pattern by independent Gaussians with equal FWHM yielded axially dependent single-molecule intensity curves. An axially precise raw calibration function γ is derived according to equation 2. The running median (binning width 25 nm) of the raw data is fitted with a high order polynomial to generate the axial lookup table.

After an initial rough alignment between the channels, experimental localizations from both optical channels were assigned by a framewise, linear nearest neighbor analysis. Here, the distance threshold was set to 500 nm, which seemed a reasonable value for the robust allocation between channels in a semi-sparse single-molecule environment. From these sets of localizations, the axially dependent intensity quotient $_{\mathrm{Fit},1,2}$ was calculated and roughly allocated to the look-up table (LUT). The final axial coordinate was determined by a linear interpolation of $_{\mathrm{Fit},1,2}$ between its "left" and "right" nearest neighbor coordinate of the LUT.

Drift and tilt correction

Since the plasma membrane can be seen as flat over the whole-cell scale, we reckoned that it can be used as its own fiducial marker. We traced the spatio-temporal axial footprint of the entire membrane by fitting of the raw localizations by a high-order polynomial in time. This is followed by the straightforward temporal linearization of the localization data, leading to a stable axial mean value over time. In order to instantly assess the quality of three-dimensional SMLM data we suggest the look for white regions in the color-coded image. In our experience, the abundance of these features usually suggests significant axial drift. However, even a subtle axial drift, which cannot be easily recognized by eye, will be detected by the approach described above. Additionally, non-linear drift, commonly occurring due to heating and resting of threads, can be accounted for.

Since we regularly observed a subtle axial tilt in the nanoscopic color-coded images due to the usage of a round coverslip in a magnetic holder, we developed a simple correction workflow (Fig. 3). The axial tilt of the sample is extrapolated by fitting a plane to the raw image data (pixelsize 100 nm). Afterwards, the data is linearized by simply subtracting the precise local plane-value from the raw localization.

Localization precision calculation

Drift and tilt corrected localizations were tracked in time by determining the three-dimensional nearest neighbor distances of localizations in consecutive frames. Localizations

constructing a track with a total inter-localization distance of less than 75 nm were considered to stem from the same fluorophore. For each sample type, we combined the nearest- neighbor tracks from all recorded independent fields of view, calculated the deviation from the mean coordinate of each track for all relevant spatial coordinates and derived a normalized histogram (Supplementary Fig. S5). By fitting these distributions with a Gaussian, we derived the localization precisions as the standard deviation of the mean.

Axial localization distribution analysis

Localization files obtained from rapidSTORM were loaded and processed in Fiji [76] with custom written scripts [77]. First, all localization coordinates in *x, y* and *z* were used to generate a quantitative stack of 2D images with 20 nm pixel size using a separation of 20 nm in *z* (i.e. z-stack). The numeric value in each pixel was equivalent to the number of localizations. Then the z-stack was segmented into defined regions of interest (ROIs). The interior of the cells was manually selected to serve as boundary ROI, in which the edges of the cells were spared. Within this master ROI a set of squared ROIs with 2×2 µm² area was automatically generated. The ROIs were allowed to be confined by the border of the master ROI and only kept when more than 75% of the ROI area, i.e. > 3 µm were preserved (Supplementary Fig. S6).

Afterwards, the localization density of each ROI was analyzed by accumulating the grey values per ROI within the image stack, i.e. stepwise in *z* every 20 nm, and plotted as a function of *z*. The plot was then fitted to a double Gaussian function of the form

with $a_{1,2}$ as amplitudes, $m_{1,2}$ as mean values and $s_{1,2}$ as standard deviations of each Gaussian.

The three parameters that were derived from this fit were the z-distribution width (Fig. 5e-g) calculated according to

$$(m_1 - 1.2s_1) + (m_2 + 1.2s_2), \text{ for } m_2 > m_1 \text{ with } FWHM_{1,2} = s_{1,2} \times 2.355;$$

the peak-to-peak distance (Supplementary Fig. S9) according to $|m_2 - m_1|$;

and the width difference of the two Gaussians (Supplementary Fig. S9) according to $|s_1 - s_2|$. By calculating these fit-derived metrics the axial distribution of localizations of CD4-WT, CD4-CS1 and CD45 was characterized.

Quantifying axial receptor distribution

For quantifying the obtained axial receptor distribution in Fig. 5f, we fitted the z-distribution width of CD4 WT, CD4 CS1 and CD45 with a model of Gaussian functions. CD4 WT was fitted using a mono Gaussian and the range of z-distribution widths was states as x_c FWHM/2, with x_c as the center of the Gaussian and as FWHM as full width at half maximum of the distribution. CD4 CS1 and CD45 data were fitted using a double Gaussian and the resulting ranges were stated as x_{c1} $FWHM_1/2$ and x_{c2} $FWHM_2/2$. The peak-to-peak distributions (Supplementary Fig. S9) were modeled with a mono-exponential decay, and the decay

constant of the fit, i.e. the value at which the amplitude of the distribution is reduced to 36.8%, is stated as mean value in this manuscript.

SOFI

Sample preparation, coverslip coating and image acquisition were performed as described above for SMLM imaging. The raw data were analyzed using balanced SOFI algorithm as described before.[28, 87]

Confocal microscopy

Jurkat CD4-KO T cells were transiently transfected with pXJ41-CD4-mEos2 plasmid 24 hours before the imaging. Cells were immobilized, fixed and immunostained using anti-CD45 antibodies (MEM-28) as described above. Three-dimensional confocal imaging was performed on Leica TCS SP8 WLL SMD-FLIM microscope (Imaging Methods Core Facility of BIOCEV, Vestec, Czech Republic) using two-channel acquisition. The images were processed using standard functions of Fiji/ImageJ software (version 1.52p; ref. [76]).

Calcium measurements

Calcium sensor

Plasmid DNA with the ultrafast, genetically encoded calcium sensor GCaMP6f$_u$ was a kind gift from Katalin Török and Silke Kerruth (St George's, University of London). The coding sequence was amplified using primers AATAGATCTGCCACCATGGGCTGCGTGTGCTCCTC and AATGGATCCTCACTTCGCTGTCATCATTTGTACAAA and subcloned into pXJ41 vector using *BglII* and *BamHI* restriction sites as described before.[88]

Sample preparation

For calcium measurements, the coverslips were coated with 0.01% (w/v) poly-*L*-lysine (Sigma-Aldrich) or 2M glycine as described above. For coating with OKT3 (anti-CD3ε) antibody, clean coverslips were incubated with 0.01 µg/µl OKT3 in PBS for 30 minutes at 37°C. After a brief wash with PBS, the coverslips were used within a day. Coated coverslips were mounted into a ChamLide holder (Live Cell Instruments), filled with 500ul of color-free medium, placed on the microscope and focused to the focal plane prior the acquisition. The measurements were performed twenty hours after transfection of Jukrat T cells with the calcium sensor. For image analysis, cells were washed with PBS, resuspended in phenol red-free RPMI-1640 media (Sigma-Aldrich) supplemented with 2mM *L*-glutamine, 10mM HEPES, 1mM CaCl2 and 1mM $MgCl_2$ and dropped onto the prepared coverslip while running the image acquisition.

The microscope setup and image acquisition

Live cell calcium mobilization imaging was performed on a home built TIRF microscope consisting of the IX73 frame (Olympus), UApo N, 100x 1.49 Oil immersion TIRF objective (Olympus) and OptoSplit II image splitter (CAIRN Optics) mounted on the camera port. Samples were illuminated using 200mW 488 nm laser (Sapphire, Coherent) in a TIRF mode and the intensity was regulated by acousto-optic tunable filter (AOTFnC-400.650-TN, AA

Optoelectronics). Fluorescence emission was detected by an EMCCD camera (iXon ULTRA DU-897U, Andor) with EM gain set to 200. Images were taken in 500ms intervals with the exposure time set to 50 ms.

Data processing

Calcium mobilization was quantified by calculating mean fluorescence in cells immobilized on coated coverslips over the period of 10 minutes. Fiji/ImageJ software was used for the analysis.[76] Graphs in Supplementary Fig. S4 represent a mean fluorescence changes in cells immobilized on PLL-, glycine- or OKT3-coated coverslips. The peak intensity (I(max)) was determined by finding a maximum value using Excel software (Microsoft). The kinetics of fluorescence decay was calculated as a ratio I(max)/I(max+5min) and I(max)/I(max+10min). Higher values indicate a more rapid decay of the fluorescence which indicates stronger response. Values of I(max+5min) and I(max+10min) represent the fluorescence intensity 5 and 10 minutes, respectively, after the maximum calcium response (I(max)) was reached. To avoid the impact of the intensity fluctuations, we calculated I(max), I(max+5min) and I(max+10min) as an average of 10 images (frames).

Characterization of T cell surface in contact with a coated coverslip and cell viability measurements

Microscope setup

For imaging of living T cells forming contact with a coated coverslip and for determining the viability of T cells immobilized on a coated coverslip, a home-build inverted microscope system (IX71, Olympus) equipped with 150 mW 488 nm and 150 mW 561 nm lasers (Sapphire, Coherent) was used. Fluorescence emission for cell surface-contact analysis and viability assay was detected by an EMCCD (iXon DU-897, Andor) and a sCMOS (Zyla-4.2-CL10, Andor) cameras, respectively. Two acousto-optic tunable filters (AOTFnC-400.650-TN, AA Optoelectronics) provided fast switching and synchronization of lasers with a camera. For TIRF imaging, the 488 nm laser beam was focused onto the back focal plane of an objective (UApoN 100x, NA = 1.49, Olympus). TIRF illumination was achieved using a manual micrometer-scale tilting mirror mechanism in the excitation pathway (Thorlabs). For cell viability measurements, the laser light was defocused to achieve a homogenous illumination at the objective sample plane (UPlanSApo 10x, NA = 0.4, Olympus). The system was controlled using the µManager software (version 1.4.22; ref. [89]).

Analysis of the T cell surface in contact with a coated coverslip

For T cell-coverslip contact analysis, Jurkat T CD4-KO cells were transfected with pXJ41-CD4-wt-eGFP plasmid 24-hours prior to the measurement. Cells were then harvested and transferred into color-free RMPI medium (Gibco) supplemented with 2 mM L-glutamine (Lonza) pre-warmed to 37°C. In parallel, cleaned coverslips were mounted into a ChamLide holder for imaging equipped with tubing adaptors (Live Cell Instruments) and covered with a coating solution as described above. After washing with ultrapure water, cells were injected into the ChamLide chamber attached to the microscope stage immediately after coating fluid

removal through the attached tubing. Landing cells were selected under transmitted light and the fluorescence was recorded on EMCCD camera using TIRF illumination for 20 minutes. Images were acquired in one second intervals with 50 ms exposure time. The camera EM gain was set to 100. The experiment was performed at 37°C using the environmental chamber (OKO lab) with controlled temperature. Acquired images were processed using standard functions of Fiji/ImageJ software (version 1.52p; ref. [76]).

T cell viability assay

To evaluate the viability of cells in contact with coated coverslips, Jurkat T cells were transfected with mTurquoise-Farnesyl-5 plasmid (#55551, Addgene bank) 24 hours prior to the assay. This was done to mimic the conditions used for all other experiments in this work but to avoid interference of the protein fluorescence with the dyes used for the assay. For the measurement, cells were washed with PBS, transferred into color-free RPMI (Gibco) medium supplemented with 2 mM *L*-glutamine (Lonza), 10% fetal bovine serum (Gibco), 10 mM HEPES and Non-essential amino-acid mixture (Gibco) containing 25 µg/ml (w/v) calcein-AM viability stain and incubated for 10 minutes at 37°C in the CO_2 incubator. Cells were then transferred into a fresh, color-free RPMI medium supplemented with 2 mM *L*-glutamine and 7AAD (1:20 dilution; 7-Amino-Actinomycine D) viability stain (eBioscience) and incubated for another 5 minutes at 37°C in the CO_2 incubator. After loading with the dyes, cells were injected onto the coated coverslips in ChamLide chamber using attached tubing. Imaging was performed for 30 minutes (with 10 minute acquisition intervals) from the time of the fist cell-coverslip contact detection. Two randomly selected ROIs were selected for each time point to avoid the effect of the fluorophore photo-destruction. Calcein and 7AAD dyes were excited separately by 488 nm and 561 nm lasers, respectively, using defocused light to achieve homogenous illumination. Cells were also imaged under transmitted light to control their morphology. To avoid the impact of fluorescence fluctuations, five frames were collected for each channel, ROI and time point. The frames were then summed to generate a collate image for further quantitative analysis. Data analysis was performed in Fiji/ImageJ (version 1.52p, ref. [76]). Cells were counted by determining local maxima for each channel. The final result was calculated as a percentage of 7AAD positive (dying) cells in all detected cells (calcein positive). The experiment was performed at 37°C using the environmental chamber (OKO lab) with controlled temperature.

Atomic force microscopy

Atomic Force Microscopy (AFM) topography images were collected with Dimension Icon AFM (Bruker Instruments). All images were measured in the Peak Force Tapping mode for fluids, using a probe holder for fluid operation and Scanasyst-Fluid probes (Bruker) with a tip radius of 20 nm and a spring constant of 0.7 N/m.

12 mm diameter coverslips were coated with PLL and glycine as described above. A bare coverslip was prepared as a reference. The AFM probe was submerged in the solution in order to land on the coverslip surface. Due to a delicate nature of the samples and to avoid long

measurement times, setpoint and number of lines were set to 400 pN and 256 x 256 lines respectively, with a scan rate of 1 Hz. Images with scan sizes of 1, 2 and 10 µm were collected.

Acknowledgements

We would like to thank Peter Kapusta, Silke Kerruth and Harsha Mavila for technical assistance and professional advice. We are grateful to Markus Sauer (University of Würzburg) for support of the project. C.F. would like to thank Laure Plantard and Jan Peychl from the MPI-CBG LMF for technical support. M.C. acknowledges funding from Czech Science Foundation (19-0704S), S.vdL. acknowledges funding from Academy of Medical Sciences/the British Heart Foundation/the Government Department of Business, Energy and Industrial Strategy/the Wellcome Trust Springboard Award (SBF003\1163). The measurements at the Imaging Methods Core Facility in BIOCEV, Vestec, Czech Republic were supported by MEYS CR grant Z.02.1.01/0.0/0.0/16_013/0001775.

Contributions

C.F., S.vdL. and M.C. conceived the study. C.F., T.C., Z.K., D.G. and D.H. performed the experiments, C.F., T.C., D.G., S.vdL. and M.C. analyzed the data. A.F. measured and analyzed the AFM data. O.F. and T.B. provided research advice. C.F., S.vdL. and M.C. wrote the paper. All authors reviewed and approved the manuscript.

Corresponding authors

Correspondence to Christian Franke, Sebastian van de Linde and Marek Cebecauer

Additional information

Supplementary Information accompanies this paper at …

Competing interests

The authors declare no competing financial interests.

REFERENCES

1. Cebecauer, M., Spitaler, M., Serge, A. & Magee, A.I. Signalling complexes and clusters: functional advantages and methodological hurdles. *J Cell Science* **123**, 309-320 (2010).

2. Pak, A.J. *et al.* Immature HIV-1 lattice assembly dynamics are regulated by scaffolding from nucleic acid and the plasma membrane. *Proc Natl Acad Sci U S A* **114**, E10056-E10065 (2017).

3. Rossier, O. *et al.* Integrins beta1 and beta3 exhibit distinct dynamic nanoscale organizations inside focal adhesions. *Nat Cell Biol* **14**, 1057-1067 (2012).

4. Barreiro, O. *et al.* Endothelial adhesion receptors are recruited to adherent leukocytes by inclusion in preformed tetraspanin nanoplatforms. *J Cell Biol* **183**, 527-542 (2008).

5. Kellermayer, B. *et al.* Differential Nanoscale Topography and Functional Role of GluN2-NMDA Receptor Subtypes at Glutamatergic Synapses. *Neuron* **100**, 106-119 e107 (2018).

6. Sevcsik, E. & Schutz, G.J. With or without rafts? Alternative views on cell membranes. *Bioessays* **38**, 129-139 (2015).

7. Dustin, M.L. & Davis, S.J. TCR signaling: the barrier within. *Nat Immunol* **15**, 136-137 (2014).

8. Bernardino de la Serna, J., Schutz, G.J., Eggeling, C. & Cebecauer, M. There Is No Simple Model of the Plasma Membrane Organization. *Front Cell Dev Biol* **4**, 106 (2016).

9. Brameshuber, M. *et al.* Monomeric TCRs drive T cell antigen recognition. *Nat Immunol* **19**, 487-496 (2018).

10. James, J.R. *et al.* The T Cell Receptor Triggering Apparatus Is Composed of Monovalent or Monomeric Proteins. *J Biol Chem* **286**, 31993-32001 (2011).

11. Gomes de Castro, M.A. *et al.* Differential organization of tonic and chronic B cell antigen receptors in the plasma membrane. *Nat Commun* **10**, 820 (2019).

12. Campi, G., Varma, R. & Dustin, M.L. Actin and agonist MHC-peptide complex-dependent T cell receptor microclusters as scaffolds for signaling. *J Exp Med* **202**, 1031-1036 (2005).

13. Tolar, P., Hanna, J., Krueger, P.D. & Pierce, S.K. The constant region of the membrane immunoglobulin mediates B cell-receptor clustering and signaling in response to membrane antigens. *Immunity* **30**, 44-55 (2009).

14. Saka, S.K. *et al.* Multi-protein assemblies underlie the mesoscale organization of the plasma membrane. *Nat Commun* **5**, 4509 (2014).

15. Letschert, S. *et al.* Super-resolution imaging of plasma membrane glycans. *Angew Chem Int Ed Engl* **53**, 10921-10924 (2014).

16. Mateos-Gil, P., Letschert, S., Doose, S. & Sauer, M. Super-Resolution Imaging of Plasma Membrane Proteins with Click Chemistry. *Front Cell Dev Biol* **4**, 98 (2016).

17. Puchner, E.M., Walter, J.M., Kasper, R., Huang, B. & Lim, W.A. Counting molecules in single organelles with superresolution microscopy allows tracking of the endosome maturation trajectory. *Proc Natl Acad Sci U S A* **110**, 16015-16020 (2013).

18. Loschberger, A., Franke, C., Krohne, G., van de Linde, S. & Sauer, M. Correlative super-resolution fluorescence and electron microscopy of the nuclear pore complex with molecular resolution. *J Cell Sci* **127**, 4351-4355 (2014).

19. Ehmann, N. *et al.* Quantitative super-resolution imaging of Bruchpilot distinguishes active zone states. *Nat Commun* **5**, 4650 (2014).

20. Jungmann, R. *et al.* Quantitative super-resolution imaging with qPAINT. *Nat Methods* **13**, 439-442 (2016).

21. Lillemeier, B.F. *et al.* TCR and Lat are expressed on separate protein islands on T cell membranes and concatenate during activation. *Nat Immunol* **11**, 90-96 (2010).

22. Rossy, J., Owen, D.M., Williamson, D.J., Yang, Z. & Gaus, K. Conformational states of the kinase Lck regulate clustering in early T cell signaling. *Nat Immunol* **14**, 82-89 (2013).

23. Rossboth, B. *et al.* TCRs are randomly distributed on the plasma membrane of resting antigen-experienced T cells. *Nat Immunol* **19**, 821-827 (2018).

24. Mattila, P.K. *et al.* The actin and tetraspanin networks organize receptor nanoclusters to regulate B cell receptor-mediated signaling. *Immunity* **38**, 461-474 (2013).

25. Balint, S., Lopes, F.B. & Davis, D.M. A nanoscale reorganization of the IL-15 receptor is triggered by NKG2D in a ligand-dependent manner. *Sci Signal* **11**, eaal3606 (2018).

26. Annibale, P., Vanni, S., Scarselli, M., Rothlisberger, U. & Radenovic, A. Identification of clustering artifacts in photoactivated localization microscopy. *Nat Methods* **8**, 527-528 (2011).

27. Burgert, A., Letschert, S., Doose, S. & Sauer, M. Artifacts in single-molecule localization microscopy. *Histochem Cell Biol* **144**, 123-131 (2015).

28. Lukes, T. *et al.* Quantifying protein densities on cell membranes using super-resolution optical fluctuation imaging. *Nat Commun* **8**, 1731 (2017).

29. Levet, F. *et al.* SR-Tesseler: a method to segment and quantify localization-based super-resolution microscopy data. *Nat Methods* **12**, 1065-1071 (2015).

30. Baumgart, F. *et al.* Varying label density allows artifact-free analysis of membrane-protein nanoclusters. *Nat Methods* **13**, 661-664 (2016).

31. Spahn, C., Herrmannsdorfer, F., Kuner, T. & Heilemann, M. Temporal accumulation analysis provides simplified artifact-free analysis of membrane-protein nanoclusters. *Nat Methods* **13**, 963-964 (2016).

32. Vangindertael, J. *et al.* An introduction to optical super-resolution microscopy for the adventurous biologist. *Methods Appl Fluoresc* **6**, 022003 (2018).

33. Raghunathan, K. & Kenworthy, A.K. Dynamic pattern generation in cell membranes: Current insights into membrane organization. *Biochim Biophys Acta Biomembr* **1860**, 2018-2031 (2018).

34. Sezgin, E., Levental, I., Mayor, S. & Eggeling, C. The mystery of membrane organization: composition, regulation and roles of lipid rafts. *Nat Rev Mol Cell Biol* **18**, 361-374 (2017).

35. Jarsch, I.K., Daste, F. & Gallop, J.L. Membrane curvature in cell biology: An integration of molecular mechanisms. *J Cell Biol* **214**, 375-387 (2016).

36. Fisher, P.J., Bulur, P.A., Vuk-Pavlovic, S., Prendergast, F.G. & Dietz, A.B. Dendritic cell microvilli: a novel membrane structure associated with the multifocal synapse and T-cell clustering. *Blood* **112**, 5037-5045 (2008).

37. Kim, H.R. *et al.* T cell microvilli constitute immunological synaptosomes that carry messages to antigen-presenting cells. *Nat Commun* **9**, 3630 (2018).

38. Shalek, A.K. *et al.* Nanowire-mediated delivery enables functional interrogation of primary immune cells: application to the analysis of chronic lymphocytic leukemia. *Nano Lett* **12**, 6498-6504 (2012).

39. Gorelik, J. *et al.* Dynamic assembly of surface structures in living cells. *Proc Natl Acad Sci U S A* **100**, 5819-5822 (2003).

40. Lange, K. Fundamental role of microvilli in the main functions of differentiated cells: Outline of an universal regulating and signaling system at the cell periphery. *J Cell Physiol* **226**, 896-927 (2011).

41. Millington, P.F., Critchley, D.R., Tovell, P.W. & Pearson, R. Scanning electron microscopy of intestinal microvilli. *J Microsc* **89**, 339-344 (1969).

42. Griffiths, G. & Lucocq, J.M. Antibodies for immunolabeling by light and electron microscopy: not for the faint hearted. *Histochem Cell Biol* **142**, 347-360 (2014).

43. Schwarz, H. & Humbel, B.M. Correlative light and electron microscopy using immunolabeled sections. *Methods Mol Biol* **1117**, 559-592 (2014).

44. Franke, C. *et al.* Correlative single-molecule localization microscopy and electron tomography reveals endosome nanoscale domains. *Traffic* **20**, 601-617 (2019).

45. Li, D. *et al.* ADVANCED IMAGING. Extended-resolution structured illumination imaging of endocytic and cytoskeletal dynamics. *Science* **349**, aab3500 (2015).

46. Geissbuehler, S. *et al.* Live-cell multiplane three-dimensional super-resolution optical fluctuation imaging. *Nat Commun* **5**, 5830 (2014).

47. von Diezmann, A., Shechtman, Y. & Moerner, W.E. Three-Dimensional Localization of Single Molecules for Super-Resolution Imaging and Single-Particle Tracking. *Chem Rev* **117**, 7244-7275 (2017).

48. Huang, B., Wang, W., Bates, M. & Zhuang, X. Three-dimensional super-resolution imaging by stochastic optical reconstruction microscopy. *Science* **319**, 810-813 (2008).

49. Juette, M.F. *et al.* Three-dimensional sub-100 nm resolution fluorescence microscopy of thick samples. *Nat Methods* **5**, 527-529 (2008).

50. Ram, S., Prabhat, P., Chao, J., Ward, E.S. & Ober, R.J. High accuracy 3D quantum dot tracking with multifocal plane microscopy for the study of fast intracellular dynamics in live cells. *Biophys J* **95**, 6025-6043 (2008).

51. Pavani, S.R. *et al.* Three-dimensional, single-molecule fluorescence imaging beyond the diffraction limit by using a double-helix point spread function. *Proc Natl Acad Sci U S A* **106**, 2995-2999 (2009).

52. Shtengel, G. *et al.* Interferometric fluorescent super-resolution microscopy resolves 3D cellular ultrastructure. *Proc Natl Acad Sci U S A* **106**, 3125-3130 (2009).

53. Dustin, M.L. & Depoil, D. New insights into the T cell synapse from single molecule techniques. *Nat Rev Immunol* **11**, 672-684 (2011).

54. Smith, C.L. Basic Confocal Microscopy. *Curr. Protoc. Neurosci.*, vol. 56. John Wiley & Sons Inc., 2011, pp 2.2.1-2.2.18.

55. Mazia, D., Schatten, G. & Sale, W. Adhesion of cells to surfaces coated with polylysine. Applications to electron microscopy. *J Cell Biol* **66**, 198-200 (1975).

56. Groves, J.T. & Dustin, M.L. Supported planar bilayers in studies on immune cell adhesion and communication. *J Immunol Methods* **278**, 19-32 (2003).

57. Bunnell, S.C. *et al.* T cell receptor ligation induces the formation of dynamically regulated signaling assemblies. *J Cell Biol* **158**, 1263-1275 (2002).

58. Fritzsche, M. *et al.* Cytoskeletal actin dynamics shape a ramifying actin network underpinning immunological synapse formation. *Sci Adv* **3**, e1603032 (2017).

59. Cavo, M. *et al.* A new cell-laden 3D Alginate-Matrigel hydrogel resembles human breast cancer cell malignant morphology, spread and invasion capability observed "in vivo". *Sci Rep* **8**, 5333 (2018).

60. Chakraborty, A.K. & Weiss, A. Insights into the initiation of TCR signaling. *Nat Immunol* **15**, 798-807 (2014).

61. Glatzova, D. & Cebecauer, M. Dual Role of CD4 in Peripheral T Lymphocytes. *Front Immunol* **10**, 618 (2019).

62. Cordoba, S.P. *et al.* The large ectodomains of CD45 and CD148 regulate their segregation from and inhibition of ligated T-cell receptor. *Blood* **121**, 4295-4302 (2013).

63. Varma, R., Campi, G., Yokosuka, T., Saito, T. & Dustin, M.L. T cell receptor-proximal signals are sustained in peripheral microclusters and terminated in the central supramolecular activation cluster. *Immunity* **25**, 117-127 (2006).

64. van der Merwe, P.A. & Dushek, O. Mechanisms for T cell receptor triggering. *Nat Rev Immunol* **11**, 47-55 (2011).

65. Franke, C., Sauer, M. & van de Linde, S. Photometry unlocks 3D information from 2D localization microscopy data. *Nat Methods* **14**, 41-44 (2017).

66. Sattentau, Q.J., Dalgleish, A.G., Weiss, R.A. & Beverley, P.C. Epitopes of the CD4 antigen and HIV infection. *Science* **234**, 1120-1123 (1986).

67. Bazil, V., Hilgert, I., Kristofova, H., Maurer, D. & Horejsi, V. Sialic acid-dependent epitopes of CD45 molecules of restricted cellular expression. *Immunogenetics* **29**, 202-205 (1989).

68. Schermelleh, L. *et al.* Super-resolution microscopy demystified. *Nat Cell Biol* **21**, 72-84 (2019).

69. de Kruijff, B. & Cullis, P.R. The influence of poly(L-lysine) on phospholipid polymorphism. Evidence that electrostatic polypeptide-phospholipid interactions can modulate bilayer/non-bilayer transitions. *Biochim Biophys Acta* **601**, 235-240 (1980).

70. Pachmann, K. & Leibold, W. Insolubilization of protein antigens on polyacrylic plastic beads using poly-L-lysine. *J Immunol Methods* **12**, 81-89 (1976).

71. van de Linde, S. *et al.* Direct stochastic optical reconstruction microscopy with standard fluorescent probes. *Nat Protoc* **6**, 991-1009 (2011).

72. Klein, T. *et al.* Live-cell dSTORM with SNAP-tag fusion proteins. *Nat Methods* **8**, 7-9 (2011).

73. Santos, A.M. *et al.* Capturing resting T cells: the perils of PLL. *Nat Immunol* **19**, 203-205 (2018).

74. Tokunaga, M., Imamoto, N. & Sakata-Sogawa, K. Highly inclined thin illumination enables clear single-molecule imaging in cells. *Nat Methods* **5**, 159-161 (2008).

75. Franke, C. & van de Linde, S. Reply to 'Impact of optical aberrations on axial position determination by photometry'. *Nat Methods* **15**, 990-992 (2018).

76. Schindelin, J. *et al.* Fiji: an open-source platform for biological-image analysis. *Nat Methods* **9**, 676-682 (2012).

77. van de Linde, S. Single-molecule localization microscopy analysis with ImageJ. *J Phys D Appl Phys* **52** (2019).

78. Hermiston, M.L., Xu, Z. & Weiss, A. CD45: a critical regulator of signaling thresholds in immune cells. *Annu Rev Immunol* **21**, 107-137 (2003).

79. Fernandes, R.A. *et al.* A cell topography-based mechanism for ligand discrimination by the T cell receptor. *Proc Natl Acad Sci U S A* **116**, 14002-14010 (2019).

80. Axelrod, D. Cell-substrate contacts illuminated by total internal reflection fluorescence. *J Cell Biol* **89**, 141-145 (1981).

81. Blaskovic, S., Blanc, M. & van der Goot, F.G. What does S-palmitoylation do to membrane proteins? *FEBS J* **280**, 2766-2774 (2013).

82. Jung, Y. *et al.* Three-dimensional localization of T-cell receptors in relation to microvilli using a combination of superresolution microscopies. *Proc Natl Acad Sci U S A* **113**, E5916-E5924 (2016).

83. Hashimoto-Tane, A. *et al.* Micro-adhesion rings surrounding TCR microclusters are essential for T cell activation. *J Exp Med* **213**, 1609-1625 (2016).

84. Martin, B.R. & Cravatt, B.F. Large-scale profiling of protein palmitoylation in mammalian cells. *Nat Methods* **6**, 135-138 (2009).

85. Kornete, M., Marone, R. & Jeker, L.T. Highly Efficient and Versatile Plasmid-Based Gene Editing in Primary T Cells. *J Immunol* **200**, 2489-2501 (2018).

86. Wolter, S. *et al.* rapidSTORM: accurate, fast open-source software for localization microscopy. *Nat Methods* **9**, 1040-1041 (2012).

87. Geissbuehler, S. *et al.* Mapping molecular statistics with balanced super-resolution optical fluctuation imaging (bSOFI). *Optical Nanoscopy* **1**, 4 (2012).

88. Chum, T. *et al.* The role of palmitoylation and transmembrane domain in sorting of transmembrane adaptor proteins. *J Cell Science* **129**, 95-107 (2016).

89. Edelstein, A.D. *et al.* Advanced methods of microscope control using muManager software. *J Biol Methods* **1** (2014).

FIGURE CAPTIONS

Figure 1. Coating of coverslips with glycine preserves receptor distribution and resting state of imaged T cells. a-b) Schematic illustration of T cell landing on PLL- (left panels) and glycine-coated coverslips (right panels). The arrows indicate forces influencing the cell on the coated coverslip. g-force is the sole force affecting T cells on glycine. T cells on PLL are further stretched due to electrostatic interactions of the surface molecules with PLL. The blue strips represent glass coverslip, the light blue strips above the glycine layer (not in scale). **c-d)** Live cell TIRF microscopy of CD4-GFP in T cells landing on PLL-coated (c) or glycine-coated coverslips (d) measured at 37°C. Blue arrowheads indicate areas of rapid flattening of the cell surface and random distribution of CD4 as indicated by line-profiles in Supplementary Fig. S1. Red arrowheads indicate areas with heterogenous distribution of CD4 on the cell surface as indicated by line-profiles in Supplementary Fig. S1. Selected time-points for the representative cells are shown. In total, 14 cells on glycine-coated and 10 cells on PLL-coated coverslips were analyzed. **e)** Calcium response induced by the interaction of Jurkat T cells with coverslips coated with stimulating antibody (anti-CD3ε; OKT3), PLL or glycine as indicated by the changes in GCaMP3-fast fluorescence over 5 min (black bars) and 10 min (grey bars) since the maximal stimulation of cells. Higher values indicate stronger stimulation of cells (see **Methods** and Supplementary Fig. S4 for more details). **f)** Viability of Jurkat T cells interacting with coverslips coated with PLL- (black bars) or glycine-coated (grey bars) coverslips. Dying cells were defined as a fraction of 7-aminoactinomycin-positive cells within the imaged area using a wide-field microscopy (see **Methods** for more details).

Figure 2. Principle of 3D super-resolution bi-plane imaging using dTRABI. **a**) Overview of the experimental setup applied to perform 3D dTRABI imaging of T cells. HILO illumination of the sample (blue beam; only shown in enlarged box) triggers fluorescence emission (orange), which is split by a 50/50 non-polarizing beamsplitter (50/50 BS) to acquire biplane images on two separate EM-CCD cameras. The respective imaging lenses are shifted along the optical axis to induce a relative defocus of the image detection on synchronized cameras. Spots, apparent in both detection planes are fitted by a Gaussian with identically set FWHM. **b)** Using a piezo stage, the focal plane was linearly moved through the sample plane while imaging a single-molecule surface under dSTORM conditions. Hereby, both cameras were synchronized. Fitting the raw PSFs by independent Gaussians with invariable FWHM yields axially dependent single-molecule intensity curves (upper panel). The relative change of position of the imaging lens in the reflection path is mirrored by the relative shift of the respective intensity curve (indicated by circles). Data points were spline interpolated to guide the eye (solid lines). An axially precise calibration function γ is derived directly from the raw intensities ($I_{Camera1}$, $I_{Camera2}$) of corresponding localizations from both cameras as $\gamma(z)$

$= (I_{Camera2} - I_{Camera1})(I_{Camera2} + I_{Camera1})^{-1}$. The running median of the raw data (grey squares) is fitted with a high order polynomial (black line) to generate the basis of the axial lookup table (lower panel). **c**) A two-dimensional high-resolution data set is generated from both image stacks (transmission and reflection path) to create a three-dimensional dTRABI data

set according to the calibration. Finally, the transmission localization set is used to render a high-resolution, axially color-coded image of the focused target structure. Scale bars, 5 µm.

Figure 3. Fiducial free drift and tilt correction of dTRABI data. CD4 WT on Jurkat T cells are shown, where the membrane was directly labelled by a primary antibody conjugated to Alexa Fluor 647. **a)** Principle of the fiducial free correction of axial drift. *Left:* Representative, color-coded high-resolution dTRABI image of an axially unstable sample. Due to the temporal change of the axial coordinate, the resulting image does not exhibit axially distinct features. *Middle:* By extracting the axial localization distribution of the thin membrane layer per frame and tracking it over the entire stack, a spatio-temporal drift trace can be plotted (top). Fitting of the raw data (grey squares) by a high-order polynomial (red line) allows the temporal linearization of the localization data, leading to a stable axial mean value over time (bottom). *Right:* Re-rendering of the drift-corrected localization data reveals a color-coded dTRABI image, exhibiting distinct, high-density clusters of CD4 below another, disperse, layer. **b)** Principle of the fiducial free correction of axial tilt. *Left:* Representative, color-coded high-resolution dTRABI image of an axially tilted sample. *Middle:* The axial tilt of the sample is extrapolated by a fitting a plane to the raw image. Afterwards, the data is linearized by subtracting the local plane-value from the raw localization. *Right:* The tilt corrected image exhibits a homogeneous color-code in the lowest data layer, indicating no residual axial tilt. Exemplary drift and tilt were simulated based on real data, where the right column represents experimentally corrected real data on which the drift and tilt was projected. Scale bars, 5 µm.

Figure 4. Cell surface receptor nanotopography visualized by 3D TRABI imaging. a) Schematic illustration of a sample preparation for a receptor nanotopography imaging using dTRABI. A cell in suspension is first immobilized on a glycine-coated coverslip and imaged using dTRABI approach. The resulting 3D dTRABI image represents a footprint of a cell on the optical surface with the color-coded axial position of localizations (right panel). **b)** 3D TRABI image of T cell surface receptor CD45 with selected ROIs exhibiting a broad z-distribution of receptor localizations. **c)** Magnified x-z projections of ROIs 1-5 as in a). Blue arrowheads point to microscopic membrane protrusions at the cell edges, magenta arrowheads to folded nanoscopic protrusions under the cell body and green arrowhead membrane invagination. Scale bars represent 5 µm in b) and 500 nm in c).

Figure 5. CD4 clusters represent the receptor accumulation at the tips of membrane protrusions. **a)** Representative 3D dTRABI image of CD4 WT at the surface of T cell immobilized on a glycine-coated coverslip. **b)** The axial distribution of CD4 WT localizations of the 4 µm² region of interest (ROI) of the cell as in a). **c**) Representative 3D dTRABI image of non-palmitoylatable CD4 CS1 mutant at the surface of T cell immobilized on a glycine-coated coverslip. **d**) The axial distribution of CD4 CS1 localizations of the 4 µm² ROI of the cell in c). **e-g)** Quantitative analysis of the receptor axial (z-axis) distribution on the surface of T cells. Receptor z-distribution values were calculated using a double Gaussian fit to the axial distribution of localizations for each ROI as in b, d and i (see Supplementary Fig. S6 for more examples) and the FWHM range of the two Gaussian functions represent the z-distribution

width as depicted in **e**. Black circles in **e** represent the axial distribution of receptor localizations for a selected ROI, black line the double Gaussian fit, which is the sum of two Gaussians as depicted in green and magenta, dashed lines in grey depict z-distribution width and lines in light grey depict mean values of the Gaussian distributions. The graphs in **f** and **g** represent z-distribution widths obtained from 21 CD4 WT cells with 846 ROIs (black), 18 CD4 CS1 cells with 1044 ROIs (green) and 13 CD45 WT cells with 305 ROIs (magenta). The distributions in f) and g) show relative and absolute occurrence, respectively. Data points in b), d), f) and i) were spline interpolated to guide the eye. **h**) Representative 3D dTRABI image of CD45 at the surface of T cell immobilized on a glycine-coated coverslip. Color-bars in the upper right corner a), c) and h) indicate the axial position of the localizations in the image. **i**) The axial distribution of CD45 localizations of the 4 µm² ROI of the cell in h). Scale bars in a), c) and g): 5 µm.

Figure 6. 3D dTRABI image of CD45 on the surface of resting T cells and its axial distribution analysis. **a**) 3D dTRABI image of CD45 on T cell. **b**) Magnified ROI as in a) with indicated areas lacking CD45 localizations (yellow arrowheads). **c)** 2D SOFI image of CD45 on T cell immobilized on a glycine-coated coverslip. CD45 was labelled using Alexa Fluor-647 conjugated MEM-28 antibody. Yellow arrowheads indicate cell surface areas lacking CD45 signal. Scale bar in: a) 5 µm, b) 1 µm and c) 5 µm.

Figure 7. Nanoscopic segregation of CD4 and CD45 on the surface of resting T cells. a) Representative 2D image of T cell surface sequentially analyzed for CD4 (green) and CD45 (magenta) by SMLM. CD4 was visualized as mEos2 fusion protein (PALM) after transient transfection of cells and the surface CD45 was labelled using Alexa Fluor-647 conjugated MEM-28 antibody (dSTORM). ROIs 1-2 were zoomed to indicate details of proteins' distribution (right hand side). **b**) Intensity line-profiles were measured along the transparent grey regions indicated in ROIs 1-2 (as in a). Green line represents CD4 and magenta CD45 signals. **c**) Schematic illustration of microvillus with indicated structural segments: tip, shaft and the basis. The two panels below indicate the predicted organization of CD4 and CD45 on the protrusions in cells expressing native CD4 (WT; middle panel) or its non-palmitoylatable variant (CS1; lower panel) CD4. **d)** 2D SMLM image of a selected T cell associating with the optical surface which was sequentially analyzed for CD4 and CD45 (as in a). The accumulation of CD4 on the tips of large membrane protrusions was observed in 10 out of 32 imaged T cells. ROIs 3-4 were zoomed to indicate the details of membrane protrusions with accumulated CD4 on their tips (right hand side). **e**) Intensity line-profiles were measured along the transparent grey regions indicated in ROIs 3-4. The arrows indicate the onset of line-profiles. Scale bars, 5 µm. Images from three independent experiments are shown (n=32).

Figure 8. Microscopic segregation of CD4 and CD45 on T cells associating with the optical surface. a) Confocal micrographs (x-z section) of CD4 (green) and CD45 (magenta) in T cells landing on a coverslip coated with glycine. Early (upper panel), intermediate (middle panel) and later stage (lower panel) of T cell landing on a coverslip is presented. **b)** X-Y sections of

3D confocal images of CD4 (green) and CD45 (magenta) selected at, or close to, the optical surface. CD4 and CD45 were labelled as in Fig.7. Scale bars, 5 µm. Representative images from two independent experiments are shown (n=29).

Figure 9. T cell surface morphology on glycine-coated coverslips. a) Schematic illustration of a T cell in suspension. The cell is covered with numerous membrane protrusions of different sizes. The size of Jurkat T cells is on average 10 µm in diameter, the protrusions, even though a majority is small (0.5 – 2 µm length), can extend up to 5 µm from the cell body. **b)** After landing on a glycine-coated coverslip, membrane protrusions of T cells are folding under the cell body but are not rapidly removed as on PLL. **c-d)** With the axial penetration depth of dTRABI being ~ 1 µm, we were unable to detect receptors at the plasma membrane basis of T cells exhibiting displacement of the cell body from the contact site (c) or those with the cavity formed between the cell body and the coated coverslip. The footprints of such cells show discontinuous labeling or a hole in the middle of the image (see the inserts). The blue strips represent glass coverslip, the light blue strips above the glycine layer (not in scale).

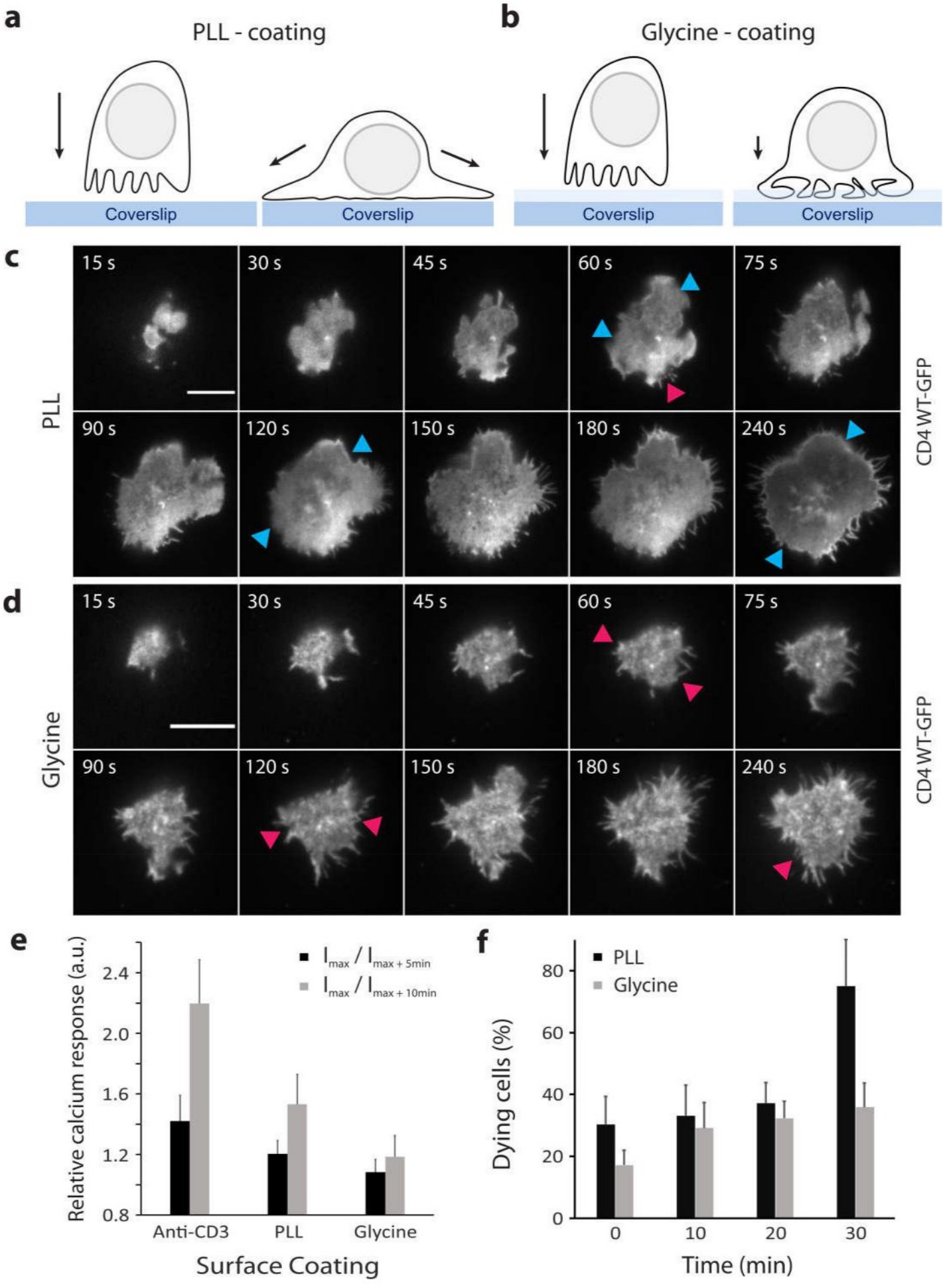

Franke et al. 2020, Fig. 1

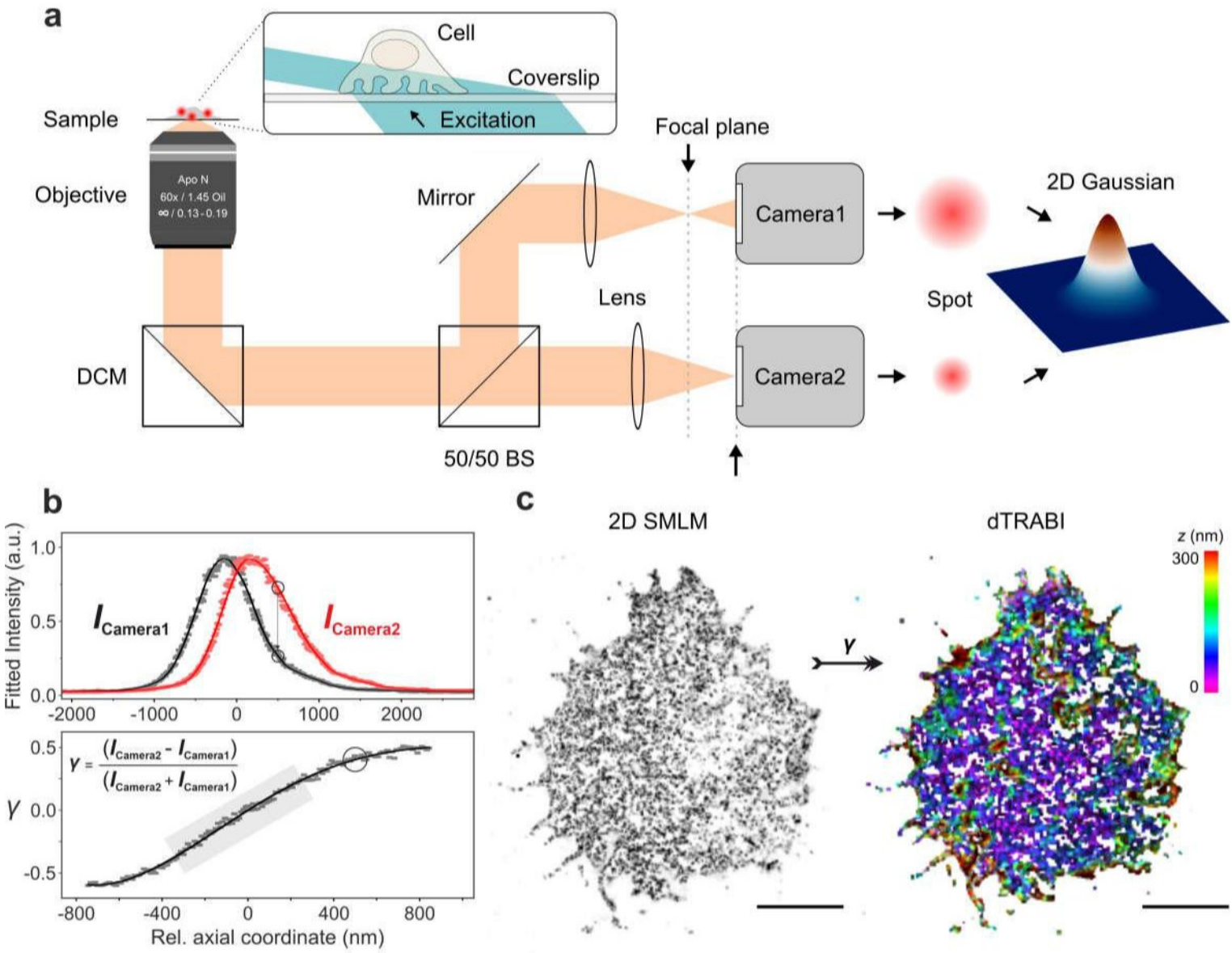

Franke et al. 2020, Fig. 2

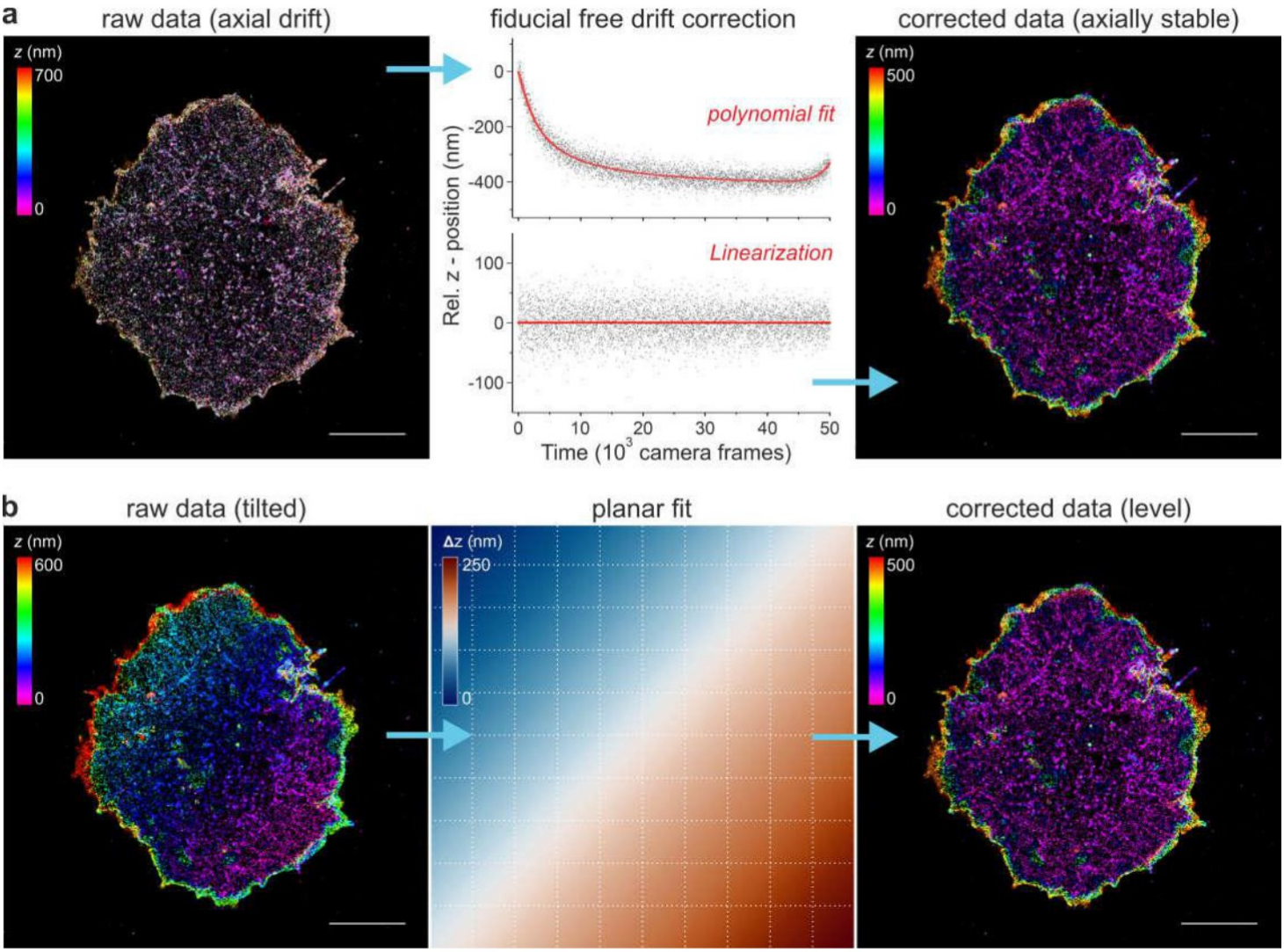

Franke et al. 2020, Fig. 3

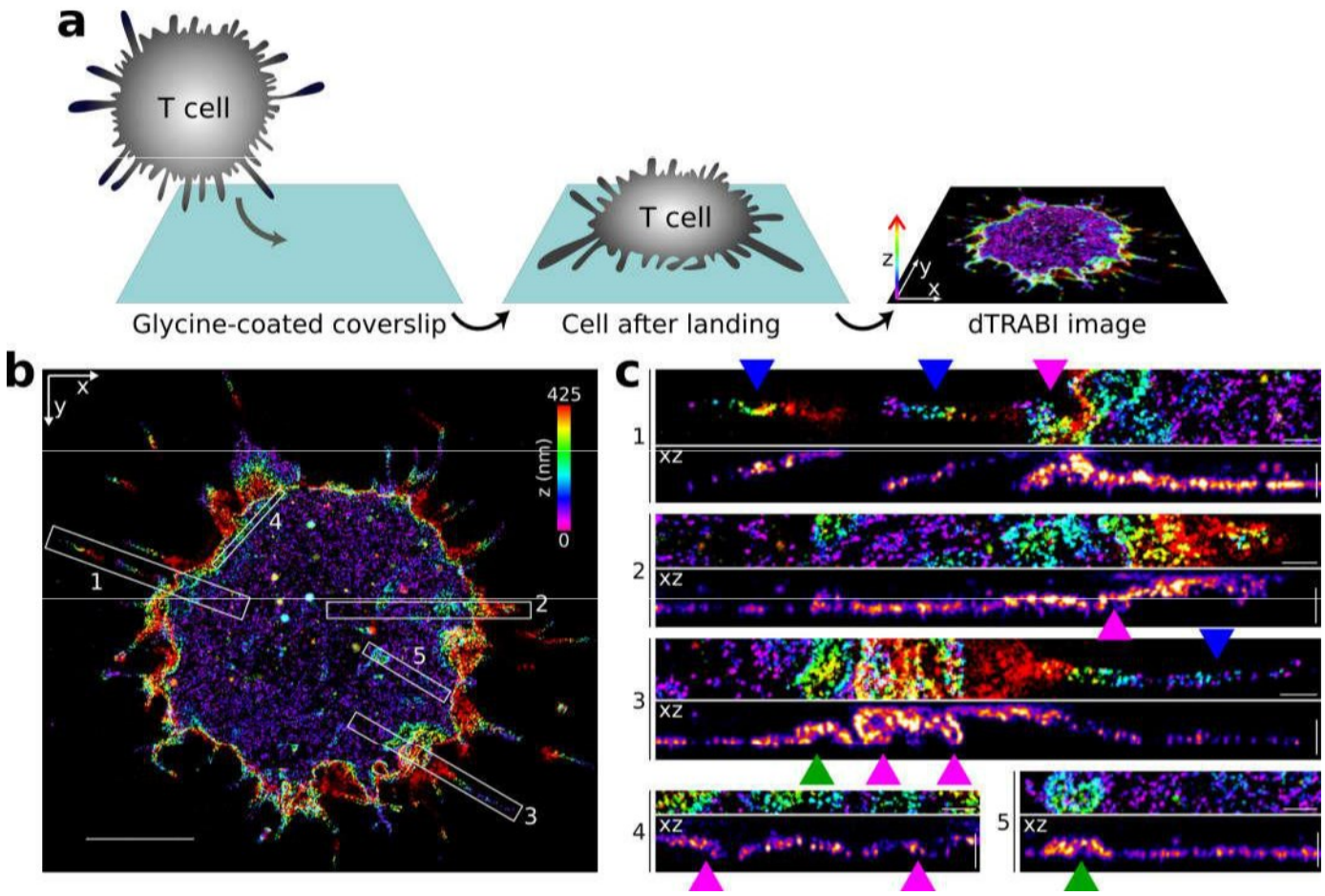

Franke et al. 2020, Fig. 4

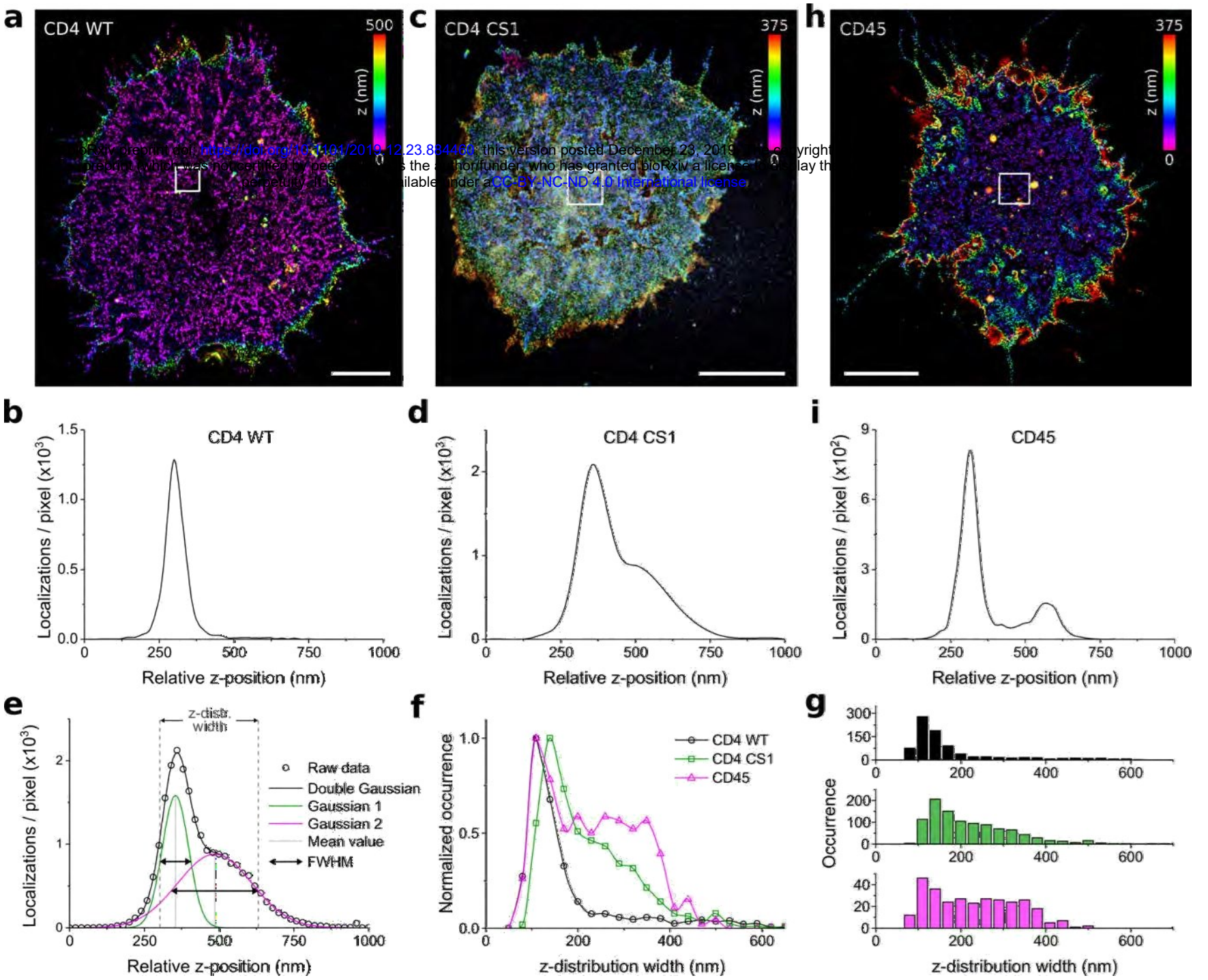

Franke et al. 2020, Fig. 5

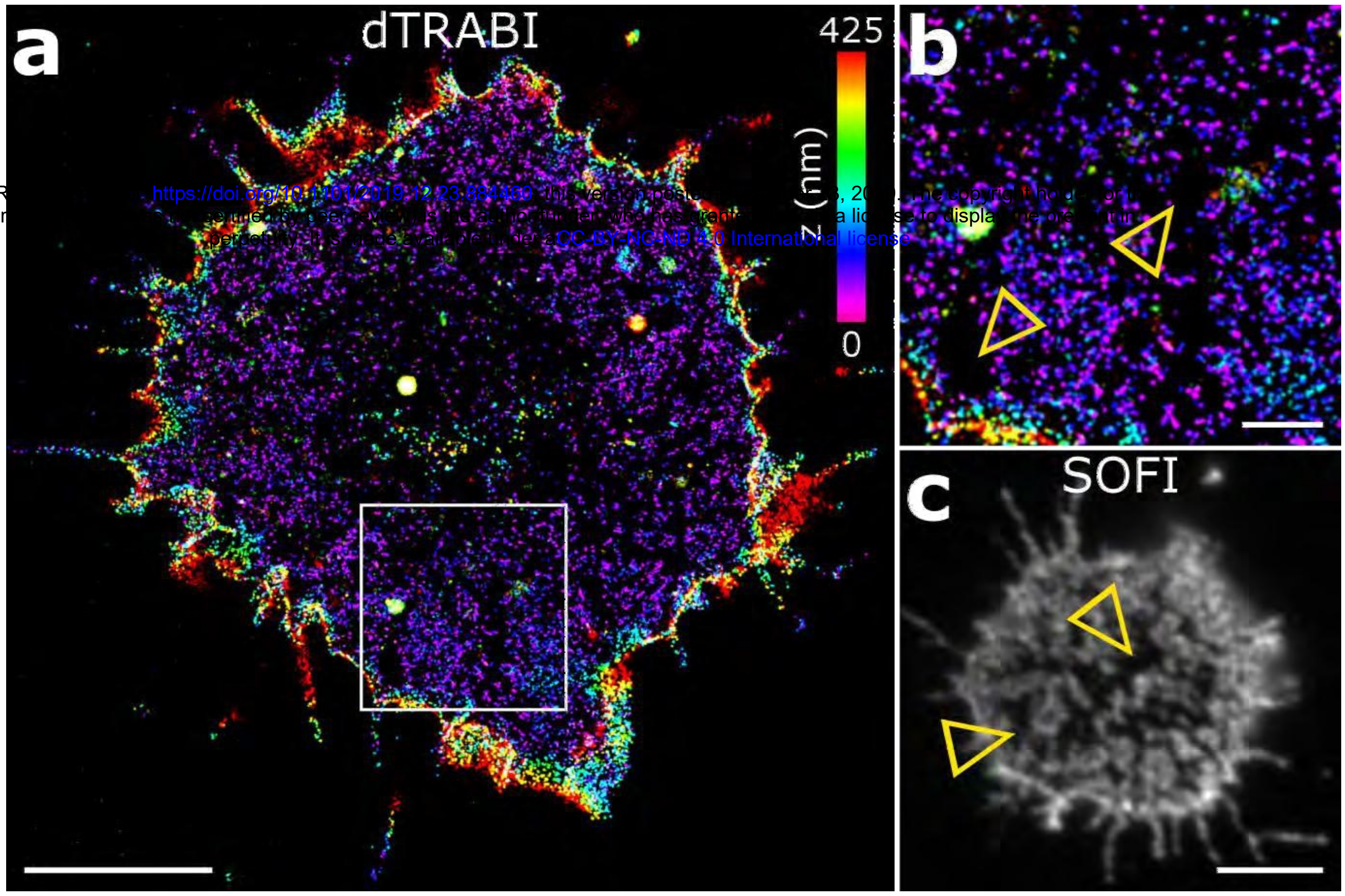

Franke et al. 2020, Fig. 6

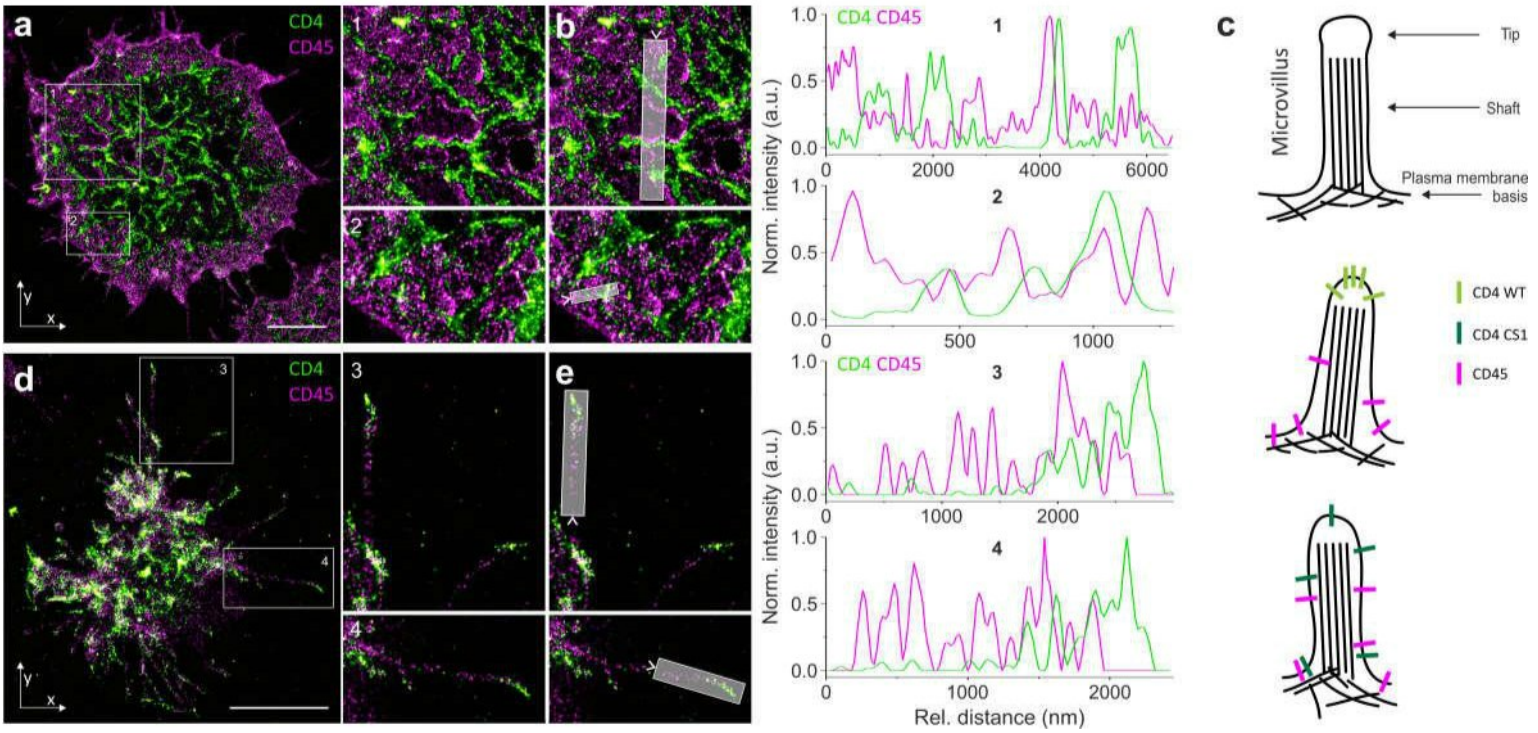

Franke et al. 2020, Fig. 7

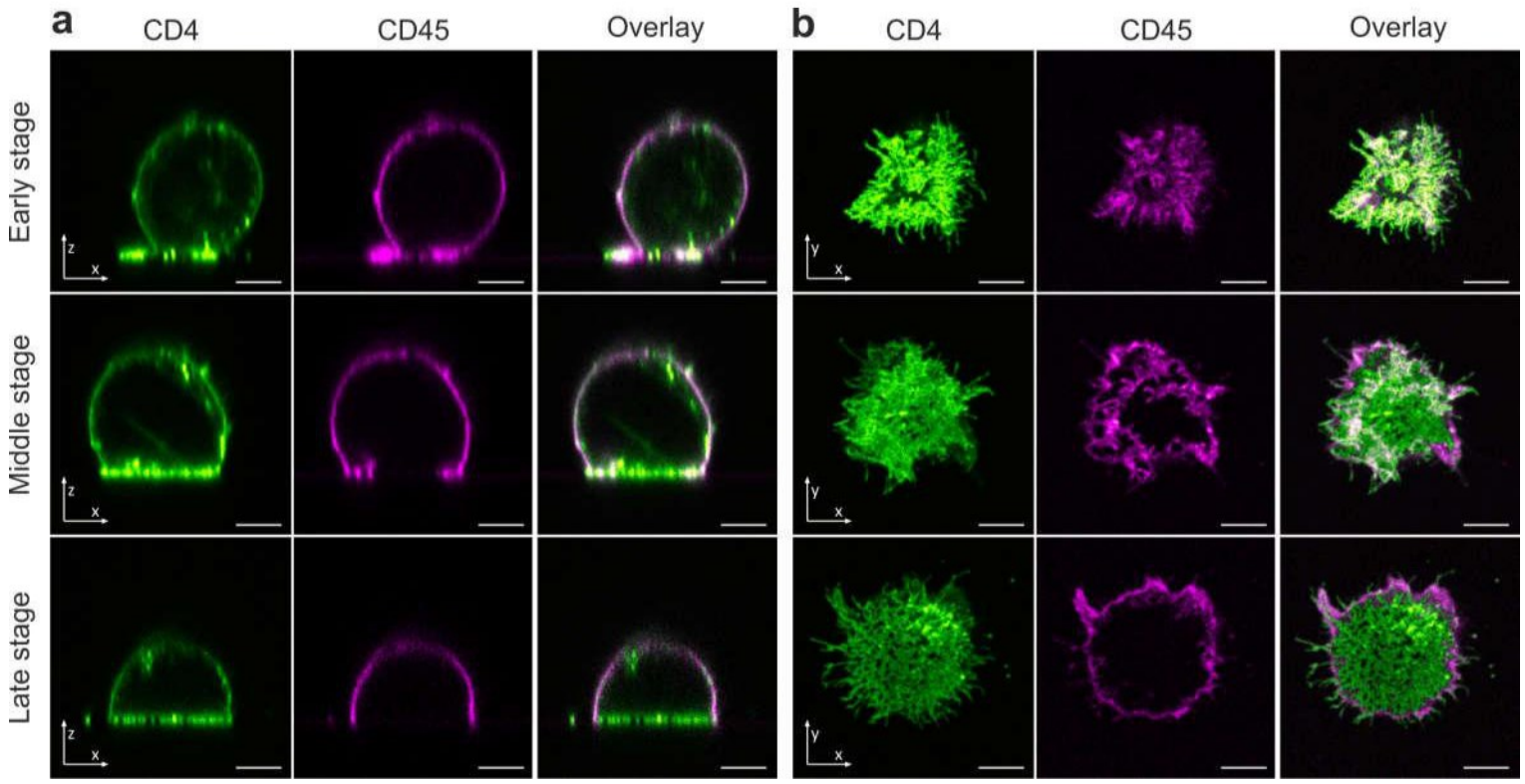

Franke et al. 2020, Fig. 8

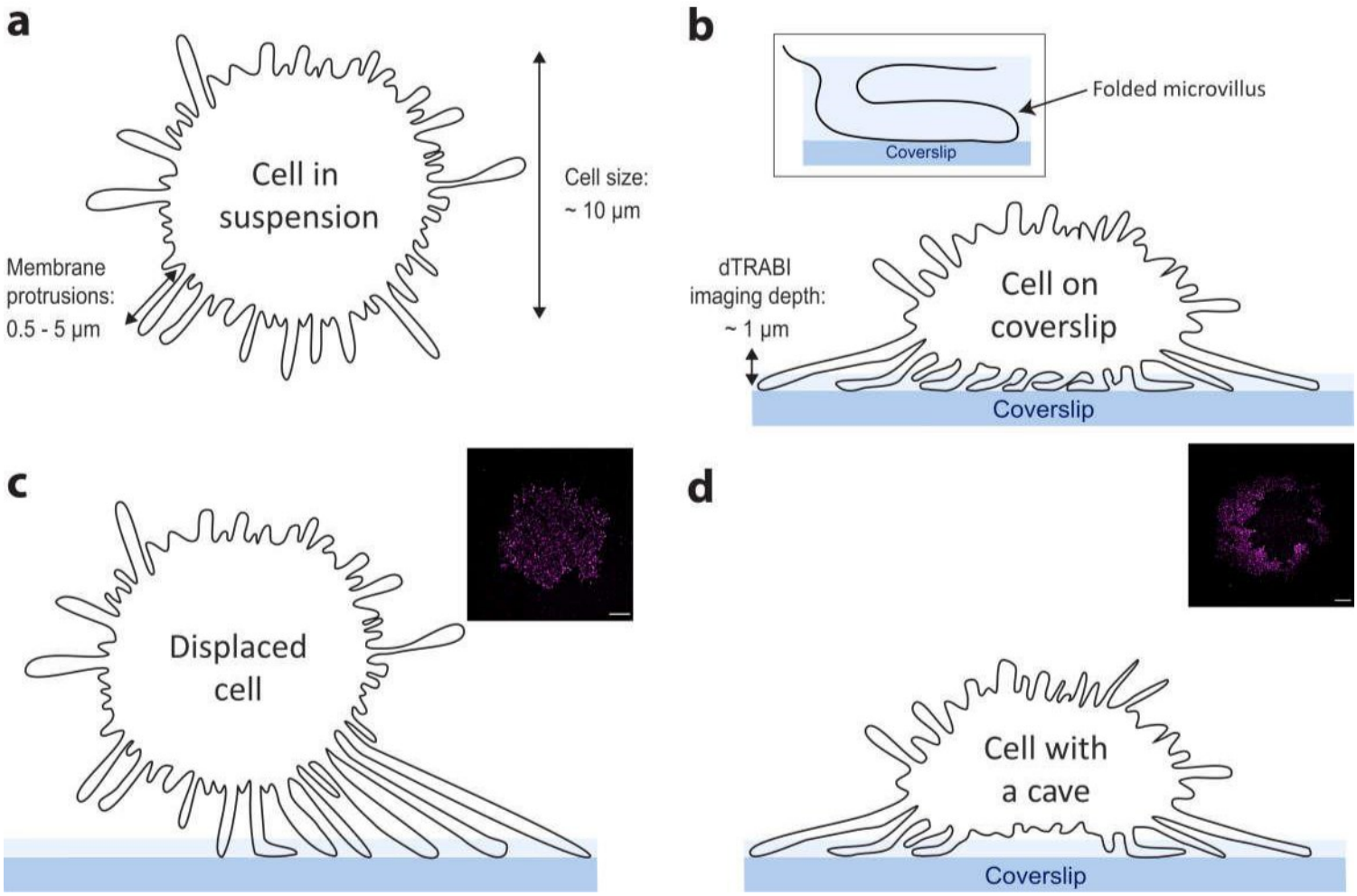

Franke et al. 2020, Fig. 9